Secondary Reactions of Low-Molecular Weight Olefins During Fischer-Tropsch Synthesis

Deborah S. Jordan and Alexis T. Bell
Materials and Molecular Research Division
Lawrence Berkeley Laboratory
and
Department of Chemical Enginereing
University of California, Berkeley, CA 94720

INTRODUCTION

Low molecular weight olefins formed during Fischer-Tropsch synthesis can undergo secondary reactions and thereby influence the distribution of the final products. In the case of Ru catalysts, it has been postulated (1) that the low yields of C_2 and C_3 olefins over these catalysts may be due to the reincorporation of these products into growing chains. Ekerdt and Bell (2) observed that the addition of 2% ethylene to an H_2/CO mixture resulted in an enhanced yield of propylene. Subsequent studies by Kellner and Bell (1) demonstrated that at concentrations above 1% ethylene addition enhanced the rates of C_3 and C_4 formation but suppressed the synthesis of C_{6+} hydrocarbons. Kobori et al. (3) have examined the effects of ethylene, propylene, and 4-octene addition. When ^{12}C-labeled olefins were added to a $^{13}CO/H_2$ mixture, the isotopic distribution of products showed that the carbon from the additives was incorporated randomly into the products. Very recently Morris et al. (4) investigated the effects of ethylene and propylene addition on the hydrogenation of CO over Ru supported on silica, 13x-zeolite, titania, and magnesia. For Ru/SiO_2 and Ru/13x-zeolite, ethylene addition markedly increased the rates of higher hydrocarbon formation without greatly influencing the methanation rate, whereas for Ru/TiO_2 and Ru/MgO, ethylene addition enhanced the rate of higher hydrocarbon formation by a factor of less than two and reduced the methanation rate. With increasing proportion of ethylene in the feed, the yield of methane decreased and the yield of C_{3+} products increased. Propylene addition to CO hydrogenation over Ru/SiO_2 increased the rates of C_2 and C_{4+} hydrocarbon formation, without markedly affecting the methanation rate.

The objectives of this study were to investigate the influence of ethylene addition on the hydrogenation of CO over Ru/SiO_2 and to compare the product distribution obtained with those for CO hydrogenation in the absence of ethylene and ethylene homologation in the absence of CO. To enable identification of the source of carbon in the products, ^{13}C-labeled CO and unlabeled C_2H_4 were used. Products were analyzed by isotope-ratio gas chromatography-mass spectrometry. Among the issues investigated were the influence of ethylene addition on the reactions of CO and the participation of ethylene in processes of hydrocarbon chain initiation and growth. The influence of ethylene addition on methane formation was also examined.

EXPERIMENTAL

A 4.3% Ru/SiO_2 catalyst is used in this investigation. Details concerning its preparation and initial reduction are presented elsewhere (5). The dispersion of the catalyst is 0.27 as determined by H_2 chemisorption at 373 K.

Hydrogen is purified by passage through a Deoxo unit (Engelhard Industries) and 5-Å molecular sieve. Helium (99.999%) and ethylene (99.95%) are used without further purification. Isotopically labeled carbon monoxide (Isotec, Inc.) consisting of 89.3% ^{13}CO, 9.86% $^{13}C^{18}O$, and 0.36% ^{12}CO is used as received.

Reactants are supplied from a gas flow manifold at a pressure of 1 atm to a stainless steel microreactor heated by a fluidized sand bath. The catalyst (0.51 g) is reduced in flowing H_2 for 12 h at 573 K prior to each series of experiments. Reduction is continued at the reaction temperature of 493 K for 2 h before initiating an experiment. The reactant stream is then introduced, and the reaction allowed to continue for 15 min before product samples are taken for analysis. Reduction is resumed and maintained for at least 2 h between experiments. The activity of the catalyst was checked periodically by returning to base case conditions. The activity remained constant to within five percent of its standard activity.

The reactor effluent is analyzed by a combination of gas chromatography and mass spectrometry, to determine the product distribution and the ^{13}C content of each of the products. The products are first separated by gas chromatography and then each eluted product is combusted to CO_2. The ^{13}C content of the CO_2 is determined by mass spectrometry. This analytical approach has been described by Sano et al. (6) and Matthews and Hayes (7), and is termed isotope-ratio gas chromatography-mass spectrometry.

RESULTS AND DISCUSSION

The reaction of C_2H_4 and H_2 over Ru produces, in addition to C_2H_6, CH_4 and C_{3+} olefins and paraffins. A large fraction of the C_{4+} hydrocarbons are branched. As shown in fig. 1, the carbon number distribution of the C_{3+} products does not decrease monotonically, but rather, oscillates so that products with an even number of carbon atoms predominate. The formation of CH_4 is ascribed to the hydrogenolysis of C_2H_4 and the formation of C_{3+} hydrocarbons to homologation of C_2H_4 via chain growth, involving C_1 and C_2 monomer units. An accurate description of the product distribution is achieved using the mechanism illustrated in Fig. 2 (8).

The addition of C_2H_4 to synthesis gas has a strong influence on the hydrogenation of CO. Figures 3 and 4 show that above a C_2H_4/CO ratio of 1.0, the formation of hydrocarbons from CO is completely suppressed and only the hydroformylation of C_2H_4 to form propanal (and some propanol) is observed. The presence of CO suppresses the hydrogenation of C_2H_4 to C_2H_6 but has relatively little effect on C_2H_4 hydrogenolysis and homologation. The selectivities to CH_4 and C_{3+} products are influenced by the partial pressures of C_2H_4, CO, and H_2. High selectivity to C_{3+} products and low selectivity to CH_4 are observed for high C_2H_4, CO, and H_2 partial pressures and low reaction temperatures. The observed distribution of products can be described theoretically using a modified version of the mechanism for C_2H_4 homologation (8).

The results of the present study clearly indicate that ethylene formed via the hydrogenation of CO can undergo extensive secondary reaction. The presence of CO inhibits the hydrogenation of ethylene to ethane, and hence the formation of a stable C_2 hydrocarbon product. A major portion of the readsorbed ethylene will participate in the initiation and propagation of chain growth. A significant fraction will react with adsorbed CO and hydrogen to form propanal (or propanol). Ethylene readsorption will also result in a suppression of CH_4 formation. This would explain why the yield of CH_4 produced over Ru catalyst is observed to decrease as the conversion of CO to products increases.

ACKNOWLEDGMENT

This work was suported by the Division of Chemical Sciences Office of Basic Energy Sciences, United States Department of Energy, under contract DE-AC03-76SF00098.

REFERENCES

1. Kellner, C. S., and Bell, A. T., J. Catal. 70, 418 (1981).
2. Ekerdt, J. G., and Bell, A. T., J. Catal. 62, 19 (1980).
3. Kobori, Y., Yamasaki, H., Naito, S., Onishi, T., and Tamaru, K., Chem. Soc. Faraday Trans. 1 78, 1473 (1982).
4. Morris, S. R., Hayes, R. B., Wells, P. B., and Whyman, R., J. Catal. 96, 23 (1985).
5. Winslow, P., and Bell, A. T., J. Catal. 86, 158 (1984).
6. Sano, M., Yotsui, Y., Abe, H., and Sasaki, S., J. Biomed. Mass Spec. 3, 1 (1976).
7. Matthews, D. E., and Hayes, J. M., Anal. Chem. 50, 1465 (1978).
8. Jordan, D.S., and Bell, A. T., J. Phys. Chem., submitted.

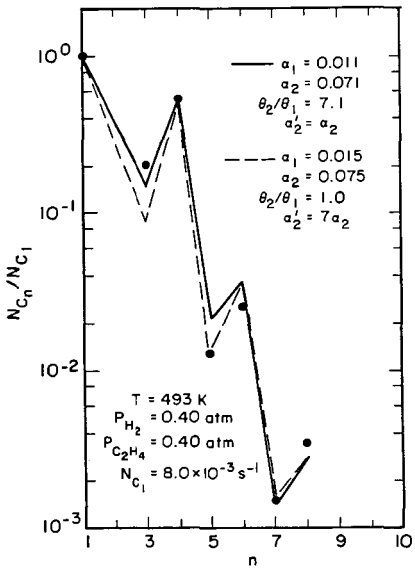

Fig. 1 Distribution of C_1 through C_8 hydrocarbons produced by reaction of H_2 and C_2H_4 at 493K. $P_{H_2} = P_{C_2H_4} = 0.40$ atm. Solid and dashed lines represent a theoretical description of the data for two sets of parameters.

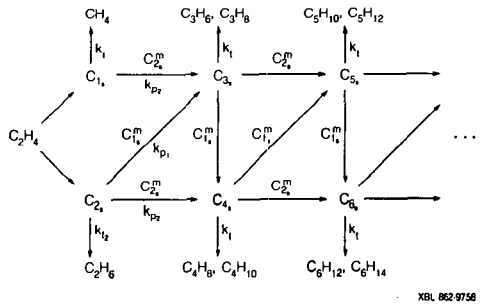

Fig. 2 Proposed scheme of chain growth for the reaction of H_2 and C_2H_4

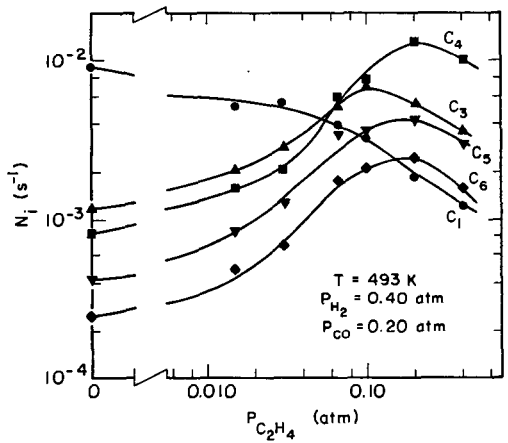

Fig. 3 Influence of $P_{C_2H_4}$ on the rates of production of C_1 through C_6 hydrocarbons. T = 493 K, P_{H_2} = 0.40 atm, P_{CO} = 0.20 atm.

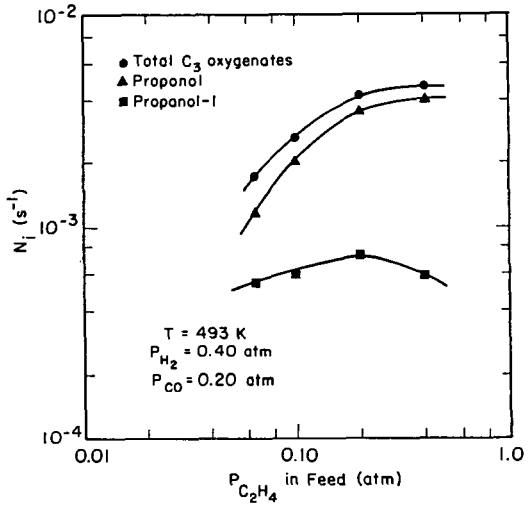

Fig. 4 Influence of $P_{C_2H_4}$ on the rates of production of C_3 oxygenates. T = 493 K, P_{H_2} = 0.40 atm, P_{CO} = 0.20 atm.

CHEMICAL TRAPPING OF CO/H_2 SURFACE SPECIES

John A. Williams, Donna G. Blackmond, and Irving Wender

Department of Chemical & Petroleum Engineering
University of Pittsburgh
Pittsburgh, PA 15261

Introduction

CO hydrogenation reactions over supported metal catalysts can produce a wide spectrum of hydrocarbon and oxygenated compounds depending to a large extent on the type of metal used. Elucidating the nature of the intermediate species formed on metal surfaces may provide the key to understanding the pathways through which these reactions proceed on different metals. The number of different techniques which have been employed in search of this understanding attests not only to the importance of but also to the difficulties inherent in the identification of reactive surface species.

One common method of obtaining evidence of the participation of a postulated reaction intermediate is the use of labelled molecules during reaction (1,2). Other kinds of experiments have involved generating certain labelled or unlabelled species on the catalyst surface and then reacting them to prove their participation in CO hydrogenation reactions (3). Another elegant kind of tracer experiment is carried out by instantaneously switching a CO/H_2 reaction mixture to a stream in which an isotopic analog of one of the reactive components is present (4) and then monitoring the reaction kinetics during the transient period that follows. Other creative experiments have used reactive molecules not part of the reaction scheme to scavenge surface intermediates (5).

Each of these experiments has added greatly to our knowledge of the chemistry of the catalyst surface under reaction conditions. The unanswered questions that remain, however, have emphasized the need for unequivocal surface species identification. This in turn has led us to investigate a novel technique which has recently been developed (6) for chemically trapping adsorbed species. This trapping technique involves introducing an alkylating reagent onto the catalyst surface after it has been contacted with the CO/H_2 reactants. It is postulated that the reagent reacts with the surface intermediate species by alkylating it at each point of former attachment to the catalyst surface. Identification of the products of this alkylation reaction may then lead to back-deduction of the identity of the surface species itself. The schematic in Figure 1 portrays the reaction of alkylating reagents such as CH_3I and $(C_2H_5)_2SO_4$ with some postulated intermediate species. The ideas behind the develop-

ment of this technique draw upon methods used in the determination of mechanisms of organic reactions (7).

Chemical trapping experiments to date have been of limited use in elucidating catalytic reaction mechanisms because they have not been carried out under reaction conditions. Moreover, questions have been raised about whether the trapping reagents actually react quantitatively with surface species in the manner postulated. The purpose of our investigation is to delineate how the trapping reagent reacts with the catalyst surface and to employ the technique to probe the nature of reactive surface intermediates on supported metal catalysts during CO hydrogenation reactions.

Discussion of Experiments

Preliminary chemical trapping experiments were carried out in-situ under CO hydrogenation conditions on a 3% RuKY zeolite catalyst. The addition of CH_3I to a CO/H_2 reaction stream resulted in a profound alteration of the typical ASF product distribution for this catalyst. A dramatic decrease in C_1-C_3 hydrocarbons was observed concomitant with a similarly sharp increase in C_4-C_6 hydrocarbons. The distribution of C_4 products was also significantly altered as shown in Figure 2. These results indicate that addition of the trapping reagent causes perturbations in the observed CO/H_2 products which may be caused by alkylation of surface species by the reagent. However, the complexity of the results make it difficult to clearly identify surface species or to understand the action of the trapping reagent on these surface species.

The complex action of the trapping reagent on metal-adsorbate bonds might be made more clear with the substitution of model organometallic complexes for the catalyst-adsorbate systems under study. These model complexes simulate organic species adsorbed on metal surfaces. The interaction of the organic ligands with chemical trapping reagents may provide important clues about how these reagents interact with species adsorbed on the surface of a metal catalyst. Figure 3 shows the structure of two organometallic complexes now under study using the chemical trapping technique.

The investigations involving model complexes are being coupled with further in-situ trapping experiments on supported Ni and Pd catalysts during CO/H_2 reactions. These two metals yield very different product distributions, but both are generally less complex than those obtained from Ru. Coupled with investigations on model organometallic systems, these trapping studies promise to provide a framework for understanding differences in CO hydrogenation reaction pathways over different metals.

References

(1) Kummer, J. T., DeWitt, T.W., and Emmett, P. H., *J. Am. Chem. Soc.*, 70, 3632 (1948).

(2) Araki, M. and Ponec, V., *J. Catal.*, 49, 439 (1976).

(3) Brady, R. C. and Petit, R., *J. Am. Chem. Soc.*, 102, 6181 (1980).

(4) Biloen, P., Helle, J. N., and Sachtler, W.M.H., *J. Catal.*, 58, 95 (1979).

(5) Eckert, J. G. and Bell, A. T., *J. Catal.*, 62, 19 (1980).

(6) Deluzarche, A., Hindermann, J. P., Kiennemann, A., and Kieffer, R., *J. Mlc. Cat.*, 31, 225 (1985).

(7) Gould, E. S., in *Mechanism and Structure in Organic Chemistry*, Holt, Rinehart and Winston, New York (1959).

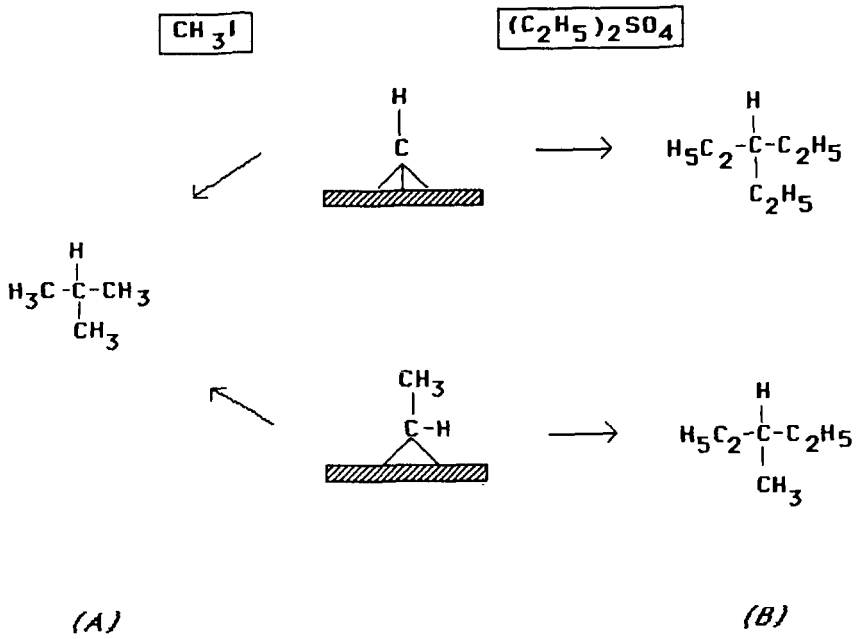

FIGURE 1. Schematic of the reaction of alkylating reagents with some postulated surface intermediate species

(A) products derived from a C_1 alkylating reagent

(B) products derived from a C_2 alkylating reagent

Figure 2A. Total Product Distribution

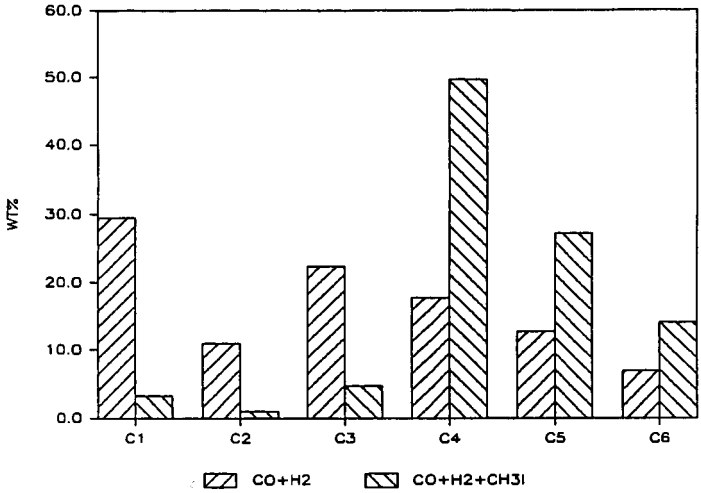

Figure 2B. Composition of C4 Products

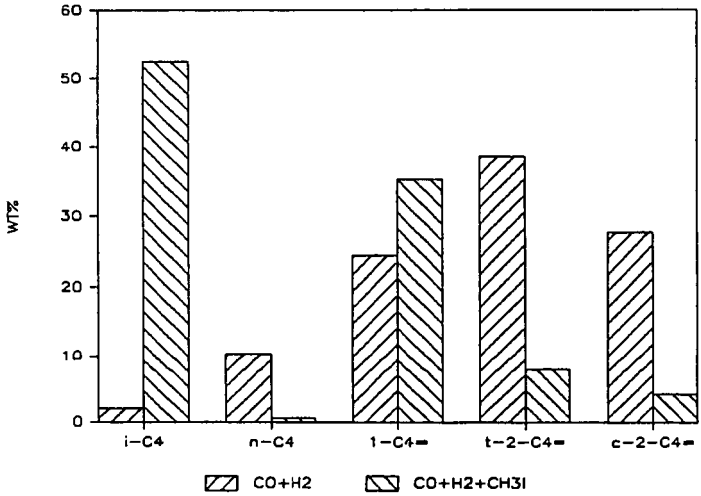

(A)

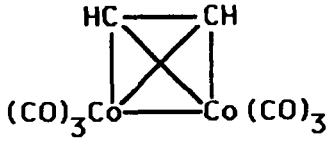

(B)

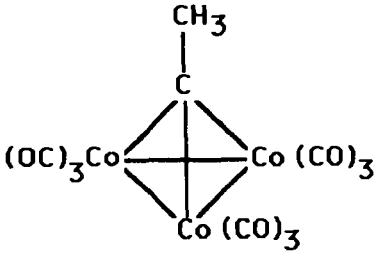

FIGURE 3. Organometallic complexes under study as model metal-adsorbate systems for chemical trapping

(A) acetylene dicobalt hexacarbonyl

(B) ethyl tricobalt enneacarbonyl

Isosynthesis Mechanisms Over Zirconium Dioxide

Ronald G. Silver, Shiaw C. Tseng, and John G. Ekerdt

Department of Chemical Engineering
University of Texas
Austin, Texas 78712

Introduction

The isosynthesis process refers to the selective conversion of synthesis gas into branched aliphatic hydrocarbons over metal oxide catalysts. Thoria and zirconia are the most active oxides that catalyze the formation of hydrocarbons containing four to eight carbon atoms, with isobutane as the major product [1]. The reaction requires high pressures, 30-600 atm, and high temperatures, 375 to 475 C.

The reactions occurring during isosynthesis have not been as thoroughly studied as have the reactions occurring during CO hydrogenation to methanol or during Fischer-Tropsch synthesis. The earliest research was conducted in the 1940's [1]. The effects of oxide composition and synthesis conditions are reported and mechanisms, based on these early studies, have been proposed [1,2,3]. These proposed mechanisms relied on the acid/base nature of the catalytically active oxides and involved acid-catalyzed reactions between methanol or dimethyl ether and olefins. More recently, two additional isosynthesis mechanisms have been proposed [4,5]. Both of the recent mechanisms propose CO insertion into an oxygenated hydrocarbon fragment to explain chain growth and involve aldol condensation as one of the termination reactions. The CO insertion and the aldol condensation reactions differ in that different oxygenated fragments and C_1 fragments are proposed to be involved.

The activation of CO on zirconia has been reported in a series of papers [6,7,8,9]. The activation is proposed to involve the initial formation of a surface formate and its subsequent reduction to a methoxide via an oxymethylene. The oxymethylene carbon is bonded to the Zr cations through two oxygen atoms [7]. This proposed structure was based on limited infrared data and other structures, such as those involving carbon bonded directly to a Zr cation, may be present.

Experimental

The high pressure studies were conducted in a 70 mm section of 6.35 mm OD stainless steel tubing. All of the experiments were conducted at 35 atm and a total flow rate of 100 cc/min. The reactor effluent was analyzed on a gas chromatograph.

A fresh charge (2.0 grams) of zirconia was used for each experiment. The zirconia was pretreated at 425 C in flowing oxygen for 60 min followed by heating at 425 C in flowing hydrogen for 60 min. The treated zirconia was exposed to CO/H_2 at a constant ratio of 1/1 for the data presented in the tables.

Zirconia was prepared by adding concentrated ammonium hydroxide to a 20.3 wt% $Zr(NO_3)_4$ solution (Nyacol). The resulting hydrous ZrO_2 was washed with distilled water and dried in air at 120 C for 24 hr. The ZrO_2 was subsequently calcined in air for 4 hr at 600 C. The ZrO_2 had a BET area ranging from 30-45 m^2/g and was monoclinic. The activity of the ZrO_2 was a strong function of the degree of drying and the calcination conditions. A thorough drying was necessary to achieve high activity to methanol, dimethyl ether and hydrocarbons. (The causes for this are currently under investigation.)

Results

A series of experiments was conducted over the zirconia at temperatures ranging from 250 to 425 C and at varying flow rates. Below 350 C methanol and dimethyl ether were the only products formed in significant quantities. Hydrocarbon production was observed above 350 C. The product distribution trends were similar to those reported over thoria [1].

Experiments were performed to test the mechanisms that have been proposed. These involved adding reactants into the CO/H_2 feed gas that should, on the basis of the different mechanisms, adsorb, transform into a reactive intermediate, and become incorporated into the isosynthesis products. The effect of adding propylene, methanol, formaldehyde, acetone, n-propanol, propionaldehyde and 2-methyl-propionaldehyde has been measured. These were added at low concentrations (50-500 ppm) to minimize their effect on existing surface species and reactions.

Propylene was added at the level it was produced at and it passed through the reactor unreacted and had a negligible effect on the C_4 products. This, and other olefin addition experiments, suggests that olefins are not incorporated into the isosynthesis products and it is unlikely that isosynthesis intermediates can be derived from hydrocarbon products. These results also provide evidence that the early acid-based mechanisms [1,2,3] are not correct.

In many cases, the oxygenated additives did not appear to incorporate, in appreciable amounts, into the next higher synthesis products, but rather underwent self-condensation or underwent reduction. The propionaldehyde and acetone additions have provided the most information. Table 1 presents the effect of adding 200 ppm of propionaldehyde to the feed. (Isosynthesis produced at most 4 ppm of propionaldehyde at the conditions reported here.) Table 2 presents the effect of adding 250 ppm of acetone to the feed. The acetone experiments were conducted over a batch of zirconia that had a lower activity; presumably this was caused by a variation in the preparation of the zirconia.

Methane, methanol and dimethyl ether decreased, while ethylene, propylene, propane, isobutene, and the C_4 alcohols increased in concentration in the presence of added propionaldehyde. Propionaldehyde appeared to react with the methane/methanol precursor to form isobutene. Our atmospheric studies [6,7,8] have demonstrated that the

methane/methanol precursor is a methoxide. The amount of propionaldehyde fed can be accounted for in the increase in ethylene, C_3 hydrocarbons and oxygenates, isobutane and the C_4 alcohols.

The majority of the acetone was reduced to propane and propylene. There was a significant increase in the amount of isobutanol formed and an unexpected decrease in isobutene. The linear butenes were moderately affected. Methanol and dimethyl ether decreased substantially in the presence of acetone. Acetone was expected to form an aldehydic-like species by analogy to previous work with formaldehyde [6,7,8].

Isobutanol was seen to increase and isobutene was seen to decrease in the presence of acetone. Both were expected to increase. The significant drop in isobutene, in parallel with the methanol decrease, may be related to acetone interfering with methanol production. Aldol condensation appears to require the methanol precursor (see next section). The majority of the isobutene loss could be associated with the isobutene formed via aldol condensation.

Discussion

The acetone addition experiments support the CO insertion scheme proposed by Mazanec [4]. This scheme is represented in Figure 1 for a bound aldehyde originating from acetone. This scheme involves CO insertion into a bound aldehyde, I, to form a cyclic acyl, II. The substituents of the cyclic acyl influence subsequent transformations, 1,2-shift of hydrogen (favored over alkyl [4]) through the second valence bond structure, III, or step-wise hydrogenation to the alcohol via the intermediate IV.

The other CO insertion scheme has been proposed by Vedage et al. [5] on the basis of extensive studies of alcohol synthesis over a variety of metal oxide systems. An alkoxide is proposed to undergo CO insertion to form an alkionate which is subsequently reduced to the alcohol. There is an important distinction between the two mechanisms. Secondary alcohols are not observed during isosynthesis; therefore, secondary alkoxides are not formed and the alkoxide-based CO insertion mechanism [5] can only lead to linear products.

Acetone addition led to an increase in isobutanol and a parallel loss of isobutene, which may be related to a suppression of aldol condensation (see below). Isopropanol was not detected, suggesting that acetone did not form the branched alkoxide required, in Vedage et al.'s scheme, to form the increased isobutanol. Additional studies in which n-propanol was added to the feed did not lead to a measurable change in any C_4 product providing additional evidence that alkoxides are unlikely intermediates in CO insertion reactions over zirconia.

Aldol condensation has been proposed as the termination reaction that can account for branching in the synthesis of alcohols [5] and that can account for the non-Flory distribution observed during isosynthesis [4]. The propionaldehyde addition experiments showed a

loss in methanol, methane and dimethyl ether, and an increase in isobutene. These observations suggest that the branching reaction involves the methanol/methane precursor, the methoxide [8,9]. Figure 2 presents the aldol condensation schems that was suggested by Mazanec [4]. Propionaldehyde is proposed to adsorb as structure V and transform into the enolate anion, VI. The enolate reacts with methoxide to form the next higher aldehyde, that is subsequently reduced to the branched hydrocarbon or alcohol. The alternative scheme involves a reaction between the enolate anion, VI, and a formyl [5]. All the previous work over zirconia [6,7,8,9] is consistent with the conversion of CO via a formate rather than a formyl intermediate. This observation along with the effect propionaldehyde had on the mathanol/methane yield supports the aldol condensation scheme represented in Figure 2.

Acknowledgements

This work was supported by the Division of Chemical Sciences, Office of Basic Energy Sciences, U.S. Department of Energy under Contract DE-AS05-80ER10720.

References

1. Pichler, H., and Ziesecke, K-H., Bureau of Mines Bull. 448 (1950).

2. Storch, H. H., Golumbic, N., and Anderson, R. B., "The Fischer-Tropsch and Related Synthesis", Wiley, New York, 1951.

3. Cohn, E. M.,in "Catalysis" (P. H. Emmett, Ed.) Vol. 4, Reinhold, New York, 1956.

4. Mazanec, T. J., J. Catal. 98, 115 (1986).

5. Vedage, G. A., Himelfarb, P. B., Simmons, G. W., and Klier, K. in "Solid State Chemistry in Catalysis", (R. K. Grasselli and J. F. Bradzil) ACS Symposium Series 279, 1985.

6. He, M-Y., and Ekerdt, J. G., J. Catal. 87, 238 (1984).

7. He, M-Y., and Ekerdt, J. G., J. Catal. 87, 381 (1984).

8. He, M-Y., and Ekerdt, J. G., J. Catal. 90, 17 (1984).

9. Jackson, N. B., and Ekerdt, J. G., "Methanol Synthesis Mechanism Over Zirconium Dioxide", J. Catal. (in press).

Table 1 Isosynthesis Products at 425 C and 35 atm over ZrO_2 Made from $Zr(NO_3)_4$

Feed Gas	$H_2/CO/He$	$H_2/CO/He$ with 200 ppm of C_2H_5CHO
CH_4	1312[a]	863
C_2H_4	104	123
C_2H_6	103	103
C_3H_6	67.0	204
C_3H_8	19.0	27.0
$i-C_4H_{10}$	6.1	5.5
$i-C_4H_8$	252	301
$n-C_4H_{10}$	4.0	4.7
$1-C_4H_8$	28.5	30.7
$t-2-C_4H_8$	27.7	27.6
$c-2-C_4H_8$	26.4	26.1
$(CH_3)_2O$	486	455
CH_3OH	171	155
C_2H_5CHO	0	0
$n-C_3H_7OH$	3.1	6.8
$n-C_4H_9OH$	12.3	16.9
$i-C_4H_9OH$	7.9	12.6
$i-C_4H_8/CH_3OH$	1.47	1.94

(a) ppm

Table 2 Isosynthesis Products at 425 C and 35 atm over ZrO_2 Made from $Zr(NO_3)_4$

Feed Gas	$H_2/CO/He$	$H_2/CO/He$ with 250 ppm of acetone
CH_4	1307[a]	834
C_2H_4	155	128
C_2H_6	64.3	34.5
C_3's	93.1	338
$i-C_4H_{10}$	1.2	1.8
$i-C_4H_8$	72.3	37.5
$n-C_4H_{10}$	2.9	11.5
$1-C_4H_8$	20.5	23.2
CH_3OH	665	356
$(CH_3)_2O$	913	25.2
$(CH_3)_2CO$	0	0
$(CH_3)_2CHCHO$	3.9	6.4
$i-C_4H_9OH$	31.9	69.8
$n-C_4H_9OH$	13.3	5.4

(a) ppm

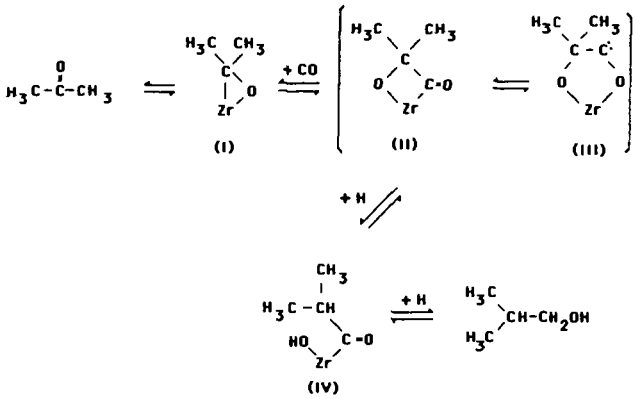

Figure 1. Representative reections for CO insertion during isosynthesis
(adapted from Reference 4)

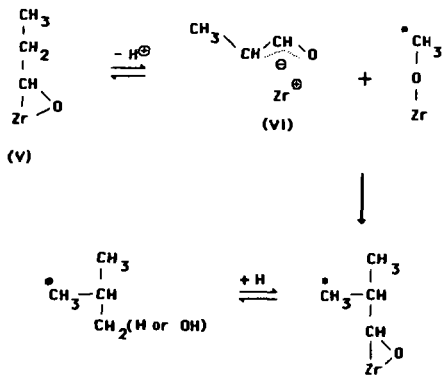

Figure 2. Representative reactions for aldol condensation
involving alkoxide (adapted from Reference 4)

EFFECTS OF H_2O AND CO_2 ON THE ACTIVITY AND COMPOSITION OF IRON FISCHER-TROPSCH CATALYSTS

Mark A. McDonald

U.S. Department of Energy
Pittsburgh Energy Technology Center
P.O. Box 10940
Pittsburgh, Pennsylvania 15236

INTRODUCTION

The composition of an iron Fischer-Tropsch (F-T) catalyst is strongly affected by the % conversion of H_2-CO syngas (1,2). At low % conversion, the strongly reducing syngas mixture tends to convert metallic or oxidic iron species to a bulk iron carbide phase or phases. As % syngas conversion increases, H_2 and CO are converted to organic products, and to H_2O and CO_2. The gas mixture can therefore oxidize an iron catalyst (3). However, the catalyst's synthesis behavior (activity, selectivity, activity and selectivity maintenance) also depends strongly on % syngas conversion (4). Thus, an iron catalyst's composition and synthesis behavior are not easily correlated under typical F-T reaction conditions.

This study was designed to determine how the build-up of H_2O and CO_2 during reaction affect F-T catalyst composition and synthesis behavior. Reaction rate measurements were conducted at differential % syngas conversion using catalyst wafers mounted in an <u>in-situ</u> cell. This cell allowed Mössbauer effect spectroscopy of the used catalyst for determination of the catalyst composition. Additional H_2O and CO_2 were added to syngas to determine the effects on catalyst composition, activity, and selectivity. Furthermore, these experiments were carried out at pressures well above atmospheric, the pressure range required for good iron F-T catalyst behavior (5). Thus, results presented here are more closely related to the state of working F-T catalysts than are previous <u>in-situ</u> Mössbauer studies of iron catalysts, which were done almost exclusively at atmospheric pressure. This paper focuses on initial experiments involving the addition of only H_2O, not CO_2, to a syngas stream.

EXPERIMENTAL METHODS

Flows of 1/1 H_2/CO, H_2, CO_2, CO and He were obtained from cylinders, with purification traps located downstream from each cylinder. Two Brooks 5850 mass flow controllers regulated flows from one or two cylinders at a time. Water was added to the gas streams with an ISCO 314 syringe pump. The water flowing from the pump was vaporized and combined with the gas stream. Gas lines were heated downstream to prevent water condensation. The syringe pump was filled from a distilled water reservoir. The water in this reservoir was sparged 4-10 h with He to remove dissolved gases.

The spectroscopy cell used for reaction experiments was constructed at West Virginia University under the supervision of Dr. Pedro Montano. The cell pressure was regulated with a Tescom back-pressure regulator located downstream. Reaction products were analyzed using a Hewlett-Packard 5730 gas chromatograph. A flame ionization detector analyzed organic products eluted from a capillary column, while a thermal conductivity detector analyzed other gases (CO_2, CO) eluting from a Porapak R column. The Mössbauer spectrometer is an MS-900 manufactured by Ranger Scientific. The source was 100 millicuries of ^{57}Co in Rh, obtained from New England Nuclear.

The iron catalyst was prepared by incipient wetness impregnation of Davison 952 silica with aqueous $Fe(NO_3)_3$ solution, yielding a catalyst precursor of

approximately 12 wt% Fe following drying and calcination. Approximately 0.15 g of this precursor was pressed into a wafer and mounted in the reaction cell for each experiment. The cell was then pressure tested by heating in a He flow to 383 K for 2 h, then given a standard reduction in flowing H_2 at 523 K for 14 h, 623 K for 8 h, and finally 698 K for 14 h. Before exposure to syngas, the catalyst was cooled in H_2 flow to 523 K. All gas treatments reported here were carried out at 2.06 MPa (20.3 atm).

RESULTS

Rates of synthesis of CH_4 and CO_2 obtained after 2 h exposure to 1/1 H_2/CO are shown in Table 1, reported as (moles product)/(mole total Fe · s). Product selectivities to light hydrocarbons are also listed, shown as mole/mole CH_4. The catalyst reached maximum conversion after two hours on stream, and maintained essentially constant activity and selectivity during the entire 24 h of synthesis.

In a separate experiment, a catalyst sample given the same reduction pretreatment and 24 h exposure to syngas was then exposed to syngas containing 12% H_2O. Catalyst activity declined fifty-fold during the first four hours on stream, to a level of activity approaching the accuracy of chromatographic analysis. (Thus, no data are given.) Production of CO_2 declined rapidly over the same period of time.

Mössbauer effect spectra of catalyst samples are shown in the Figure 1. Figure 1a shows the spectrum of the initially reduced catalyst. This spectrum displays the characteristic six-peak spectrum of α-Fe, demonstrating thorough reduction occurred before exposure to syngas. The spectrum may also contain an Fe^{+2} component overlapping with the fourth peak, although no computer fitting of the spectrum has been yet made. Figure 1b shows that during 24 h of syngas exposure, the catalyst was completely converted to iron carbide. The six-peak spectrum is that of ε'-carbide (6,7), although a small amount of χ-carbide may also be present. The sample exposed to an additional 24 h of syngas containing 12% H_2O gave essentially the same spectrum (Figure 1c), even though catalyst activity declined dramatically during this treatment. Thus, the decline in activity upon exposure to syngas + 12% H_2O was not accompanied by any measurable bulk oxidation of iron carbide.

DISCUSSION

At least two processes need to be considered in discussing the effects of adding the oxidant H_2O to syngas: (a) bulk oxidation of the iron catalyst by H_2O, and (b) oxidation of CO by H_2O to form $H_2 + CO_2$, the water-gas shift reaction. The latter reaction is clearly favored thermodynamically under these conditions (8), and is typically equilibrated for K-promoted F-T catalysts operating at non-differential conversions and slightly higher temperatures than used here (9). However, for the experimental conditions reported here, there is little reason to expect the reaction to approach equilibrium. Thus, it is sufficient to consider only the first process and to neglect the water-gas shift reaction. (This statement is equivalent to saying that one need only consider the oxidation of iron by H_2O and need not consider the reverse process, the reduction of iron oxide by CO.)

For the run in which H_2O was added to syngas, the $(H_2O)/(H_2)$ ratio was clearly above that required to oxidize α-Fe to Fe_3O_4 (8). However, ε'-carbide, not α-Fe, was present before exposure to H_2O-containing syngas, and the thermodynamics of the iron carbides are not well-defined (3). The absence of any detectable bulk carbide oxidation during H_2O exposure thus may be due to either the unfavorable thermodynamics or kinetics of bulk oxidation.

Nevertheless, the addition of H_2O to syngas certainly made the gas much more oxidizing. The loss of catalyst activity upon exposure to H_2O-containing syngas suggests that surface oxidation of the catalyst took place. This would be consistent with the idea that reduced iron species are required for hydrocarbon synthesis from syngas (10,11).

The severe loss of catalyst activity upon exposure to $H_2O/H_2/CO$ was larger than the magnitude of effects reported by other workers (9,11,12). In fixed-bed experiments, Karn et al. reported that 10-30% H_2O added to 1/1 H_2/CO had relatively little effect on % CO conversion (12). The main effect was to decrease the % CH_4 in the outlet stream while increasing % CO_2. Thus, the extent of water-gas shift reaction was increased while hydrocarbon synthesis was inhibited. The increase in water-gas shift and inhibition in methane synthesis was most noticeable at low % conversions (high space velocities). At higher % conversions, less inhibition of methane production was observed, attributed to the enhanced H_2/CO ratio resulting from water-gas shift.

In slurry-phase F-T synthesis experiments, Satterfield et al. (9) reported trends similar to those of Karn et al. but of smaller magnitude. Addition of 12% H_2O slightly increased the rate of CO consumption, due to an increase in CO_2 production from water-gas shift. The rate of CO conversion to organic products appears to have declined very slightly. The magnitude of these trends was not much larger even for addition of up to 42% H_2O; the increase in CO_2 production and decrease in CO conversion to organic products still were each only about a factor of two. It should be noted that these runs had H_2 + CO conversions over 50%. Since these authors used a mixed reactor, it is probably most reasonable to compare results presented here with their experiments containing 42% H_2O in the feed, since in each case the reactor concentrations of H_2O were in the same range.

Reymond et al. (13) reported trends somewhat closer to those reported here. In studies at atmospheric pressure and differential % conversion, addition of only 0.6% H_2O to 9/1 H_2/CO produced about a three-fold drop in rates of both CH_4 and CO_2 synthesis.

The difference among these studies are attributable to differences in reactor type and catalyst used. Studies of H_2O addition carried out at high % conversion showed relatively small changes in reaction rates (9,12). Additional CO_2 was produced, synthesis of F-T products was inhibited, but these trends became less pronounced as % conversion increased. In contrast, reactions carried out under differential % conversion (13) showed much larger effects of H_2O addition on catalyst activity but no clear effect on selectivity.

These trends can be rationalized from the following observations. The studies carried out at high % conversion (9,12) had substantial concentrations of H_2O, CO_2, and organic products in the outlet stream, while concentrations of H_2 and CO were well below concentrations in the inlet stream. In addition, K-promoted catalysts were used in both studies. High % conversions and K-promotion both favor equilibration of the water-gas shift reaction (9,14), so this reaction is likely to approach equilibrium under these conditions. Addition of H_2O to the feed perturbs the water-gas shift reaction away from equilibrium and makes the gas mixture more oxidizing. Therefore, the % CO conversion to CO_2 (water-gas shift) increases while F-T activity drops. As % conversion is increased (space velocity is lowered), the water-gas shift reaction approaches equilibrium and the oxidizing effect of H_2O addition is minimized. F-T synthesis is not as strongly inhibited under these conditions.

In contrast, at differential % conversions, the H_2O concentration in the feed is essentially the same as in the outlet. The water-gas shift reaction is not equilibrated, so the increase in H_2O concentration is accompanied by a much larger drop in activity.

DISCLAIMER

Reference in this paper to any specific commercial product, process, or service is to facilitate understanding, and does not necessarily imply its endorsement or favoring by the United States Department of Energy.

REFERENCES

1. Shen, W.M., Dumesic, J.A., and Hill, C.G., Rev. Sci. Instrum. 52, 858 (1981).

2. Madon, R.J., and Taylor, W.F., J. Catal. 69, 32 (1981).

3. Højlund-Nielsen, P.E., and Bøgild-Hansen, J., J. Molec. Catal. 17, 183 (1982).

4. Dry, M.E., in "Catalysis: Science and Technology," Vol. 1 (Anderson, J.R., and Boudart, M., Eds.), Springer-Verlag, Heidelberg, 1981, p. 159.

5. Storch, H.H., Golumbic, N., and Anderson, R.B., "The Fischer-Tropsch and Related Synthesis," Wiley, New York, 1951.

6. Amelse, J.A., Butt, J.B., and Schwartz, L.H., J. Phys. Chem. 82, 588 (1978).

7. Niemantsverdriet, J.W., van der Kraan, A.M., van Dijk, W.L., and van der Baan, H.S., J. Phys. Chem. 84, 3363 (1980).

8. Anderson, R.B., "The Fischer-Tropsch Synthesis," Academic Press, Orlando, Fla., 1984.

9. Satterfield, C.N., Hanlon, R.T., Tung, S.E., Zou, Z.-M., and Papaefthymiou, to be submitted to Ind. Eng. Chem. Proc. Des. Dev.

10. Vogler, G.L., Jiang, X.-Z., Dumesic, J.A., and Madon, R.J., J. Catal. 89, 116 (1984).

11. McDonald, M.A., and Boudart, M., to be submitted to J. Catal.

12. Karn, F.S., Shultz, J.F., and Anderson, R.B., "Actes Congr. Intern. Catalyse, 2e", Vol. 2, Paris, 1961, p. 2439.

13. Reymond, J.P., Meriaudeau, P., Pommier, B., and Bennett, C.O., J. Catal. 64, 163 (1980).

14. Arakawa, H., and Bell, A.T., Ind. Eng. Chem. Proc. Des. Dev. 22, 97 (1983).

TABLE 1. Rates and Selectivities of F-T Synthesis
(523 K, 2.06 MPa, 1/1 H_2/CO, 2 h on stream)

Product		Rate/10^{-4} mol (mol Fe · s)$^{-1}$	
CH_4		3.2	
CO_2		0.75	
Product		**Selectivity/mol (mol CH_4)$^{-1}$**	
CH_4		1.00	
ΣC_2		0.31	
	C_2H_4		.077
	C_2H_6		.235
ΣC_3		0.18	
	C_3H_6		.118
	C_3H_8		.064
ΣC_4		0.095	
ΣC_5		0.050	

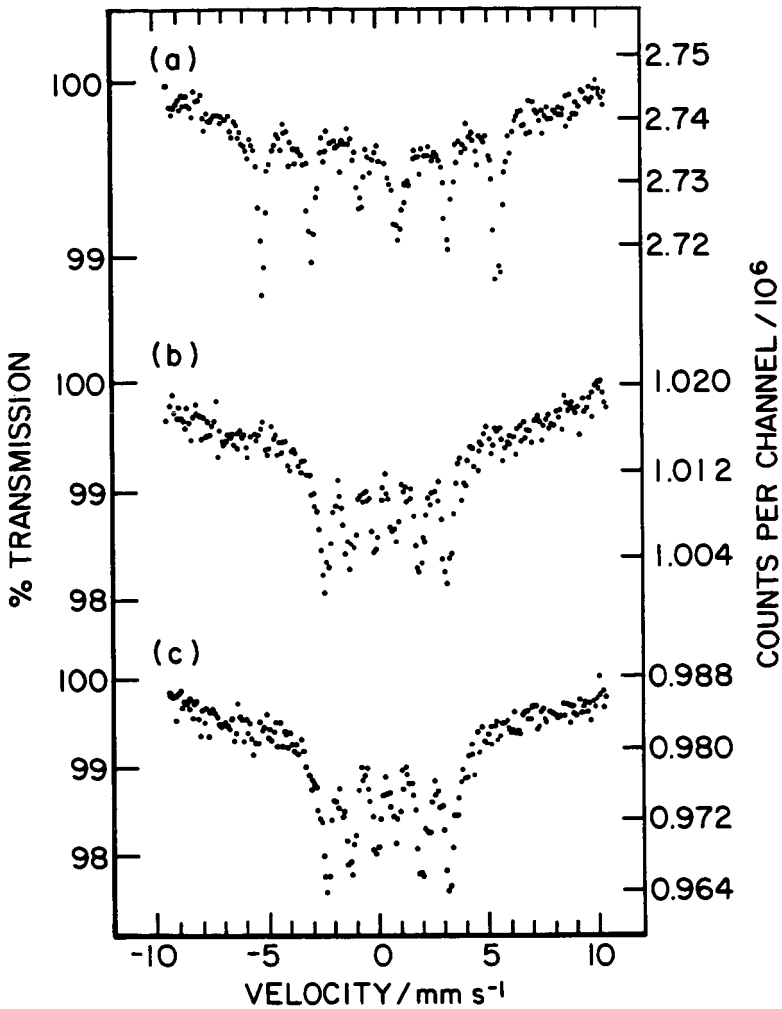

FIGURE 1. Mössbauer Effect Spectra of Fe/SiO_2

(a) Reduced catalyst
(b) Reduced catalyst, reacted 24 h in 1/1 H_2/CO
(c) Reduced catalyst, reacted 24 h in 1/1 H_2/CO, 24 h in 1/1 H_2/CO + 12% H_2O

THE INFLUENCE OF PARTICLE SIZE AND STRUCTURE ON THE MÖSSBAUER SPECTRA OF IRON CARBIDES FORMED DURING FISCHER-TROPSCH SYNTHESIS

R. R. Gatte and J. Phillips

The Pennsylvania State University
133 Fenske Laboratory
University Park, PA 16802

Introduction

Characterization of the active and stable phase of iron-based Fischer-Tropsch catalysts has been a topic of investigation for several years (1-10). Yet, a great deal of controversy still surrounds the identity of the phase(s) present during synthesis. This stems from the fact that neither x-ray nor Mössbauer studies have proven capable of unambiguously characterizing the metastable carbides formed.

Investigations of the metastable, octahedral carbides (as they have been termed (5)) have been going on for many years (11-18), dating back to at least 1949 (12). The iron structure has been assigned as HCP (or 'nearly' HCP) with the carbon atoms occupying the octahedral holes. The most notable of these are the ε and ε' carbides. X-ray results have, however, been rather unsatisfactory for many reasons. For instance, the commercial catalysts studied contained many metallic additives and in most cases the small crystallite sizes gave rise to broad, poorly resolved lines.

In recent years, emphasis has shifted toward the use of Mössbauer spectroscopy for in-situ studies of the carburization behavior (1-10, 13-15, 18). Again, a number of conflicting reports have appeared. Many workers suggest that χ and ε' are the active phases, with ε' being present in smaller particles (4,10). Others have argued that the dominant phases are ε and ε' (2,8,9). Still others have suggested that the identities of ε and ε' are actually the reverse of what has been generally reported (5). It should be clear from a careful review of these studies that the ambiguity arises from the difficult interpretation of the spectra obtained. This may be due to the fact that these phases are present as very small particles (ca. 10 nm diameter), which introduces relaxation effects into the spectra. Further, the characteristic peaks attributed to ε and ε' carbide are, in most cases, present as background lines superimposed on a strong spectral component of α-Fe or Fe-oxide.

It will be shown that if spectra are collected for a single sample over a range of temperatures, and if relaxation effects are properly accounted for, the Mössbauer results <u>can give</u> not only accurate identification of the phase(s) present but also <u>quantitative</u> particle size information and qualitative information regarding particle structure and the nature of particle/support interaction.

Discussion

In this study a Mössbauer modelling routine, described in earlier work (19-21), designed to account for collective magnetic excitations (22,23), superparamagnetic relaxation (24) and quadrupole shift distribution (25,26), was used to generate theoretical iron-carbide spectra which could then be analyzed using a conventional least-squares fitting routine (27). Several parameters (including, temperature, anisotropy energy constant, quadrupole shift distribution, and particle size distribution) were systematically varied to check the effect on the observed spectra. The starting parameters were those of χ-carbide (25).

From the results (shown in Figures 1-4, and Tables I-III) the following conclusions can be drawn:

1.) At least one phase of octahedral carbide forms during Fischer-Tropsch synthesis.

2.) The partially relaxed spectrum of this phase can be reasonably well fit with a single sextuplet with $H_{hf} \cong 170$ kOe and $\delta_{IS} \cong .25$ mm/s (28). However, due to the clear assymetry of the spectrum, more than one sextuplet is probably present.

3.) A wide particle size distribution cannot account for the broadness observed in the peaks attributed to ε'-carbide, and the unrelaxed hyperfine field of this phase is probably larger than 170 kOe.

4.) The particle sizes reported on the basis of x-ray data cannot be correct (i.e., 35Å particle radius), since it is impossible to obtain a defined sextuplet for a particle size this small. Relaxation effects become overwhelming.

All of these conclusions will be discussed in greater detail.

References

1. Amelse, J. A., Butt, J. B., and Schwartz, L. H., J. Phys. Chem. 82, 558 (1978).

2. Raupp, G. B. and Delgass, W. N., J. Catal. 58, 337, 348 (1979).

3. Unmuth, E. E., Schwartz, L. H., and Butt, J. B., J. Catal. 63, 404 (1980).

4. Niemantsverdriet, J. W., Van der Kraan, A. M., Van Dijk, W. L., and Van der Baan, H. S., J. Phys. Chem. 84, 3363 (1980).

5. LeCaër, G., Dubois, J. M., Pijolat, M., Perrichon, V., and Bussiere, P., J. Phys. Chem. 86, 4799 (1982).

6. Van der Kraan, A. M. and Niemantsverdriet, J. W., to appear in "Industrial Applications of the Mössbauer Effect," G. J. Long and J. G. Stevens, eds., Plenum, NY (1986).

7. Loktev, S. M., Makarenkova, L. I., Slivinskii, E. V., and Entin, S. D., Kinet. Katal. 13(4), 1042 (1972).

8. Maksimov, Yu. V., Suzdalev, I. P., Arents, R. A., and Loktev, S. M., Kinet. Katal. 15(5), 1293 (1974).

9. Maksimov, Yu, V., Suzdalev, I. P., Arents, R. A., Goncharov, I. V., Kravtsov, A. V., Loktev, S. M., Kinet. Katal. 13(6), 1600 (1972).

10. Vaishnava, P. P., Ktorides, P. I., Montano, P. A., Mbadcam, K. J., and Melson, G. A., J. Catal. 96, 301 (1985).

11. Barton, G. H. and Gale, B., Acta Cryst. 17, 1460 (1964).

12. Hofer, L.J.E., Cohn, E. M., and Peebles, W. C., J. Am. Chem. Soc. 71, 189 (1949).

13. Arents, R. A., Maksimov, Yu. V., Suzdalev, J. P., Imshennik, V. K., and Krupyanskiy, Yu. F., Fiz. Met. Metalloved. 36(2), 277 (1973).

14. Le Caer, G., Simon, A., Lorenzo, A., and Genin, J. M., Phys. Stat. Sol. A6, K97 (1971).

15. Mathalone, Z., Ron, M., Pipman, J., and Niedzwiedz, S., J. Appl. Phys. 42(2), 687 (1971).

16. Hofer, L.J.E. and Cohn, E. M., J. Am. Chem. Soc. 81, 1576 (1959).

17. Bernas, H., Campbell, J. A., and Fruchart, R., J. Phys. Chem. Solids 28, 17 (1967).

18. Le Caer, G., Dubois, J. M., and Senateur, J. P., J. Solid State Chem. 19, 19 (1976).

19. Phillips, J., Clausen, B., and Dumesic, J. A., J. Phys. Chem. 81, 1814 (1980).

20. Phillips, J., and Dumesic, J. A., Appl. Surf. Sci. 7, 215 (1981).

21. Phillips, J., Chen, Y., and Dumesic, J. A., in New Surface Science in Catalysis (edited by M. L. Deviney and J. Gland) ACS Symposium Series, (1985).

22. Mørup, S. and Topsøe, H., Appl. Phys. 11, 63 (1976).

23. Mørup, S., Topsøe, H., and Lipka, J., J. Phys. (Paris) Colloq. 37, C6-287 (1978).

24. Wickmann, H. H., "Mössbauer Effect Methodology," Vol. 2, edited by I. J. Gruverman (Plenum, NY, 1966) p. 39.

25. Lin, S. C. and Phillips, J., J. Appl. Phys. 58(5), 1943 (1985).

26. Bradford, E. and Marshall, W., Proc. Phys. Soc. London 87, 731 (1966).

27. Sørensen, K., International Report No. 1, Laboratory of Applied Physics II (Technical University of Denver, 1972).

28. Ron, M., "Applications of Mössbauer Spectroscopy," edited by R. L. Cohen (Academic, NY, 1980), Vol. 2, p. 329.

TABLE I: Comparison of input and fitted Mössbauer parameters for a bulk χ-carbide phase.

Parameter	Fe Site	Input Values	Fitted Values
H_{hf}(kOe)	I	196.0	196.5
	II	217.0	217.5
	III	118.0	117.5
δ_{IS}(mm/sec)	I	+0.15	+0.149
	II	+0.17	+0.169
	III	+0.15	+0.143
ΔE_Q(mm/sec)	I	0.00	-0.003
	II	+0.027	+0.025
	III	-0.012	-0.021
Relative Intensity	I	3:2:1	3.9:3.2:1.2
	II	3:2:1	4.0:2.1:1.7
	III	1.5:1:0.5	2.0:1.4:0.4
Linewidths (mm/sec)	I	.25:.23:.23	.5:.43:.35
	II	.25:.23:.23	.48:.48:.46
	III	.25:.23:.23	.61:.68:.79

*Other input parameters were (i) anisotropy energy constant = 1,000,000 erg/cm^3, (ii) average particle size = 200Å, (iii) temperature = 300 K, (iv) σ = 1.20

TABLE II: Mössbauer parameters obtained from a 20-peak fit of the spectra in Figure 1.

Spectrum	Spectral Component	H_{hf}(kOe)	δ_{IS}(mm/s)	ΔE_Q(mm/s)	Linewidths (mm/s)	% Area
1a.	χ-I	192.3	.146	.020	.57:.62:.67	24.7
	χ-II	215.4	.233	.016	.78:.77:.62	24.0
	χ-III	106.7	.241	-.027	.61:.62:.61	10.3
	Doublet	---	.157	.590	.76	41.0
1b.	χ-I	192.6	.140	.009	.61:.50:1.4	35.3
	χ-II	212.3	.178	.023	.55:.55:.44	28.6
	χ-III	110.3	.183	-.019	.72:.88:.51	20.1
	Doublet	---	.152	.533	.60	16.0
1c.	χ-I	192.0	.146	-.002	.49:.69:.62	36.6
	χ-II	212.4	.165	.027	.57:.53:1.0	38.8
	χ-III	113.9	.162	-.020	.52:.64:.63	19.8
	Doublet	---	.181	.879	.75	4.8

TABLE III: Mössbauer parameters obtained from an 8-peak fit of the spectra in Figure 1 and 2.

Spectrum	Spectral Component	H_{hf}(kOe)	δ_{IS}(mm/s)	ΔE_Q(mm/s)	Linewidths (mm/s)	% Area
1a.	Sextuplet	197.7	0.155	0.014	.77:.70:1.6	58.4
	Doublet	---	0.158	0.643	.73	41.6
1b.	Sextuplet	200.4	0.155	0.013	.75:.61:1.7	73.8
	Doublet	---	0.159	0.748	.79	26.2
1c.	Sextuplet	202.0	0.154	0.013	.74:.59:1.0	92.8
	Doublet	---	0.210	1.209	1.40	7.2
2a.	Sextuplet	199.4	0.155	0.013	.75:.69:1.19	55.0
	Doublet	---	0.160	0.681	.73	45.0
2b.	Sextuplet	197.6	0.155	0.014	.78:.61:1.02	79.2
	Doublet	---	0.165	1.594	2.12	20.8
2c.	Sextuplet	198.2	0.157	0.013	.73:.55:.54	91.4
	Doublet	---	0.182	2.300	.692	8.6

FIGURE CAPTIONS

Figure 1. Effect of anisotropy energy constant on spectrum. (a) K = 750,000 erg/cm^3; (b) K = 1,500,000 erg/cm^3; (c) K = 3,000,000 erg/cm^3. Other input parameters were (i) average particle size = 55Å; (ii) σ = 1.20; (iii) T = 300K.

Figure 2. Effect of narrowness of particle size distribution on spectrum. (a) σ - 1.25; (b) σ = 1.10; (c) σ = 1.05; (d) log-normal distribution function for several σ values. Other input parameters were (i) average particle size = 55Å; (ii) T = 300K; (iii) anisotropy energy constant = 1,000,000 erg/cm^3.

Figure 3. Effect of a variation of ε_o (equation (3), Ref. 25). (a) ε_o = 0; (b) $-.5\varepsilon_{curie}<\varepsilon_o<.5\varepsilon_{curie}$; (c) $-.75\varepsilon_{curie}<\varepsilon_o<.75\varepsilon_{curie}$. Other input parameters were (i) average particle size = 80Å; (ii) σ = 1.20; (iii) T = 300K; (iv) anisotropy energy constant = 1,000,000.

Figure 4. Effect of temperature on spectrum. (a) T = 350K; (b) T = 300K; (c) T = 80K. Other parameters were (i) average particle size = 55Å; (ii) σ = 1.20; (iii) anisotrophy energy constant = 1,000,000 erg/cm^3. Values of H_{hf} and δ_{IS} were taken from Ref. 25 at each temperature.

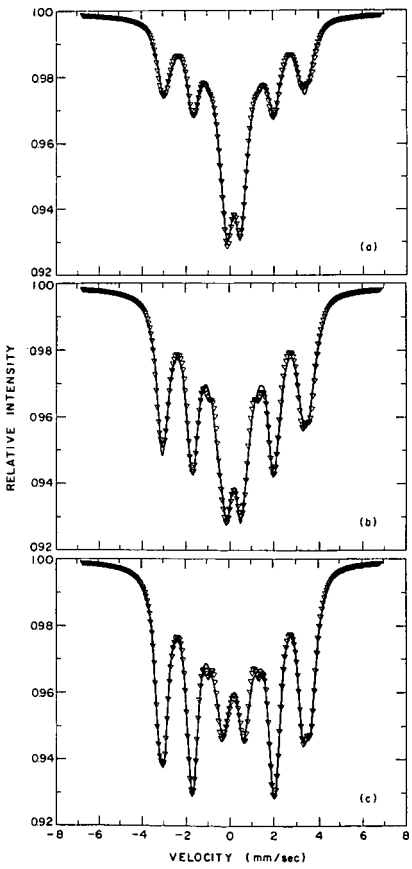

FIGURE 1

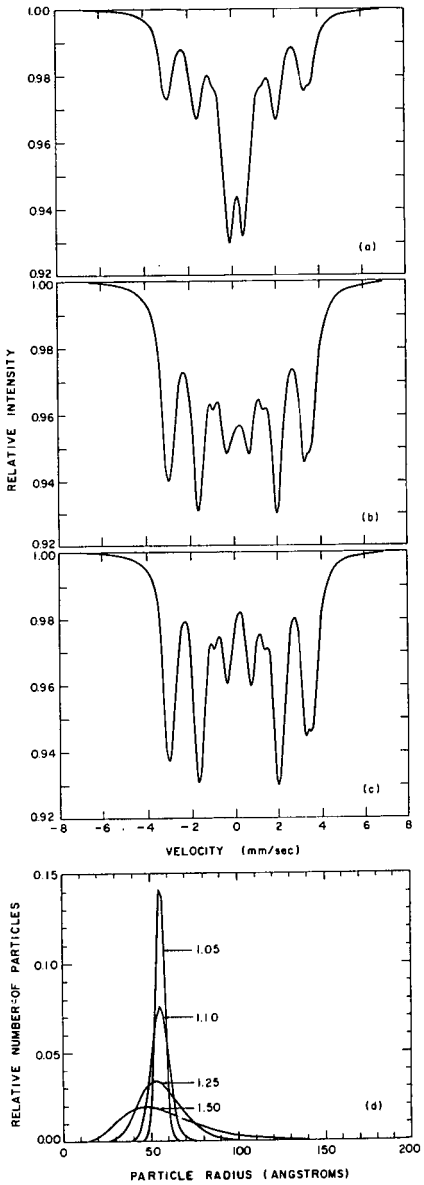

FIGURE 2

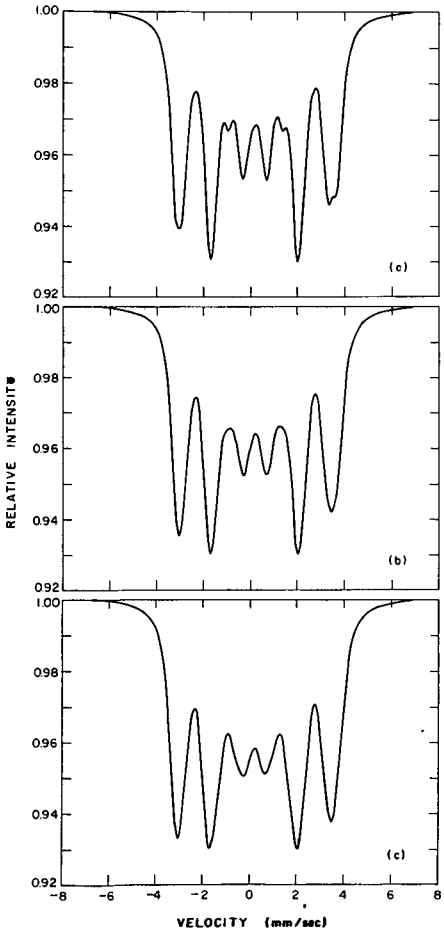

FIGURE 3

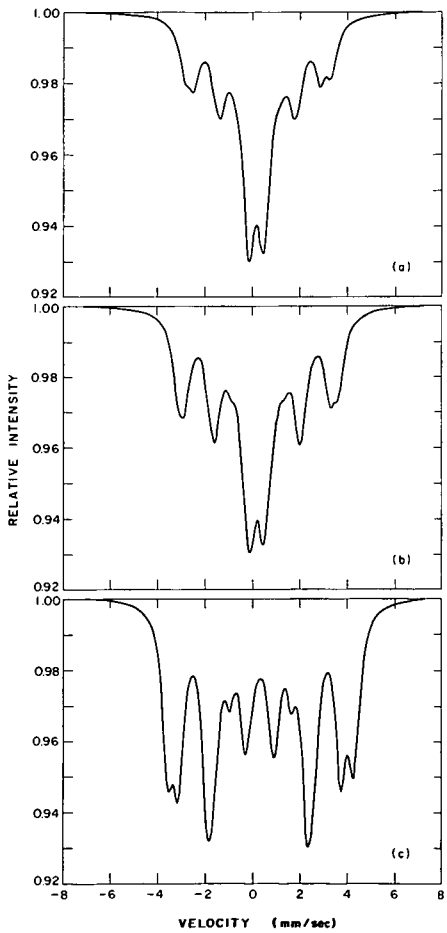

FIGURE 4

NICKEL CRYSTALLITE THERMOMETRY DURING METHANATION

Douglas K. Ludlow and Timothy S. Cale

Chemical & Bio Engineering Department
Arizona State University
Tempe, AZ 85287

ABSTRACT

A magnetic method to measure the average temperature of superparamagnetic nickel crystallites has been applied during CO methanation. The method takes advantage of the temperature dependence of the low field magnetization of such catalysts; however, the adsorption of carbon monoxide and the formation of surface carbon species complicate the interpretation of results. Calibrations to account for temperature change and the adsorption of reactants are described. The calibration for the effects of CO is based on the assumption that the interaction of CO with nickel is the same for methanation and disproportionation. Interphase heat transfer calculations based on the thermometric data compare favorably with previous results from ethane hydrogenolysis, and give no indication of microscopic temperature differences between the nickel crystallites and support.

INTRODUCTION

The temperature of the active sites is of fundamental importance for the proper interpretation of catalytic kinetics. This information is not currently obtainable; however, a magnetic method to determine the bed average nickel crystallite temperature during ethane hydrogenolysis has been developed in this laboratory (1,2). This paper presents some early results of an effort to extend this magnetic crystallite thermometry to carbon monoxide methanation over nickel catalysts. This system is being studied because of its history, practical importance, more complicated magnetochemistry and higher heat of reaction.

The basis of nickel crystallite thermometry is the temperature dependence of the intrinsic magnetization, or magnetic moment per volume, of nickel crystallites in superparamagnetic samples (1,2,3). This can be determined from low field magnetization data. In order to perform the magnetic thermometry during ethane hydrogenolysis, ethane is introduced into a stream of hydrogen and helium which is flowing through a short catalyst bed. This initiates the exothermic ethane hydrogenolysis reaction. The sample moment decreases rapidly as the bed average nickel crystallite temperature increases. The relationship between sample moment and average crystallite temperature, determined by calibration, is then applied. In addition, any change in moment due to changes in surface coverage must be accounted for (1,2). One of the principle reasons that ethane hydrogenolysis over nickel was the system chosen to demonstrate the magnetic thermometry is that ethane does not affect the magnetic moment of nickel crystallites when hydrogen is present (4,5). However, the introduction of ethane reduces the hydrogen partial pressure slightly, which does affect moment. The moment change due to hydrogen partial pressure change is accounted for as explained elsewhere (2).

A principle conclusion of the research on ethane hydrogenolysis performed to date is the absence of microscopic nickel crystallite to support gradients. In contrast, Matyi, et. al. (6) present evidence for microscopic catalytic crystallite to support temperature differences for CO hydrogenation over iron. The higher heat of reaction for CO hydrogenation certainly makes these gradients more likely than during ethane hydrogenolysis. The presence of any microscopic gradients would interfere with the interpretation of kinetic information; therefore, it is of interest to pursue catalytic crystallite thermometry during methanation. If they are found to exist, then much of the experimental information on CO hydrogenation will have to be reviewed.

In contrast to the simple magnetochemistry found for the ethane hydrogenolysis system, thermometry during methanation is complicated by the fact that carbon monoxide affects the sample moment (7,8) of supported nickel catalysts in a complicated manner. In fact, an understanding of the interaction between CO and nickel is the primary hurdle to overcome in order to perform magnetic thermometry during methanation.

Adsorption and formation of surface species, as well as changes in crystallite size, have an affect on the net magnetization of a nickel catalyst in a fixed field. Therefore, these must be considered in order to perform accurate crystallite thermometry. There have been numerous studies concerned with the nature and role of surface carbon species (carbon and carbides) that form during methanation (4,7-18). The formation of nickel carbonyls, which leads to catalyst deactivation through metal loss and crystallite size changes, has also been studied (19,20).

Using gravimetric analyses, Gardner and Bartholomew (15) found that there was an initial rapid weight gain for the first few minutes after initiating methanation, followed by a more gradual uptake. They concluded that three forms of surface species are present during methanation: (1) easily desorbed species such as CO, CH_4, H_2, etc, (2) species reactive with H_2, such as atomic carbon and (3) unreactive species. Their results also suggest that the species adsorbed after the initial rapid weight gain corresponds to a nonreactive surface species, such as a polymeric carbon. In addition, the weight gain during the initial stages of rapid adsorption decreased with increasing temperature. McCarty and Wise (21), using temperature-programmed surface reaction (TPSR) studies, also reported the formation of two carbon species, α and β. These correspond to cases 2 and 3 above, respectively.

The interaction of CO with Ni/SiO_2 catalysts has been studied using saturation magnetization methods by Martin et. al. (13), and Mirodotas, et.al. (17), and by low field magnetization techniques by Kuijpers, et.al. (18). Martin et. al. (13), working with samples containing only small amounts of carbon, concluded that the carbon was interstitially dissolved in the nickel lattice. Mirodotas, et. al. (17) and Kuijpers, et. al. (18), using much higher coverages, concluded that there is bulk carbon dissolution and nickel carbidization during CO disproportionation, whereas mainly surface carbidization dominates during methanation. Kuijpers, et. al. (18) also performed static volumetric adsorption analyses between each magnetic measurement. They noted an initial rapid adsorption, followed by a more gradual and linear drop of pressure in their adsorption manifold. The similarity of this result to the observations of Gardner and Bartholomew (15) during methanation is noteworthy. They also noted that the sample magnetization drops to very low levels (up to 90% loss of magnetization) due to bulk carbide formation during disproportionation, whereas the adsorption of hydrogen onto the same samples reduces the relative magnetization by 26% at most.

Since crystallite growth and metal loss would interfere with the magnetic thermometry, it is important to operate in a region where these are minimized. Shen, Dumesic and Hill (19) established a criteria for "safe" operating conditions for methanation over nickel catalysts, where the catalyst no longer deactivated rapidly due to metal loss or particle growth. The criteria is to maintain the equilibrium nickel tetracarbonyl pressure at less than ca. 7.5×10^{-8} Torr. For this work, all experiments were performed in the "safe" operating region. However, because the AC permeameter design currently used can only operate up to a temperature ca. 510 K, conditions were near the "unsafe" operating region. Thus some changes in nickel crystallite size is to be expected. In addition, van Meerten et. al. (20) found nickel crystallite growth during methanation, even though the catalyst was not deactivating dramatically. This indicates a crystallite size dependence on methanation activity. If microscopic crystallite to support temperature gradients exist, then the more active crystallites will be hotter than the less active crystallites. This would further complicate the interpretation of the thermometric results. Conversely, if these gradients do not exist, then a crystallite size effect on activity has little impact on the magnetic thermometry. In that case, the measured temperature is the local temperature of the support and crystallites of all sizes.

EXPERIMENTAL

A one half gram sample of a 25% nickel on silica catalyst, with an average equivalent spherical diameter of 0.018 cm, was packed into a quartz reactor (22,23) to a bed length of 0.6 cm. The catalyst was from the same batch as the catalysts used in previous crystallite thermometry experiments (1,2). The catalyst sample was reduced in flowing hydrogen at 673 K for 5 hrs and "cleaned" (23) in flowing helium at 723 K for 1/2 hr. Before beginning thermometric experiments, the catalyst was "aged" under reaction conditions until the magnetization no longer changed much. To perform the thermometry, the catalyst sample is initially brought to equilibrium with a flowing stream of hydrogen and helium. The average crystallite temperature is then that of the bulk stream. Reaction is initiated by introducing carbon monoxide at essentially constant total pressure.

An AC permeameter (3,22) is used to follow the changes in magnetic moment of the nickel catalyst sample upon initiation of reaction. The output voltage of the permeameter is related to average catalyst bed temperature via a calibration. Corrections for the change in sample moment due to adsorption and surface species formation are taken into account as described elsewhere in this paper. Reaction products are analyzed using a Carle Analytical gas chromatograph to determine the extent of reaction. Details of the equipment are presented elsewhere (1,2,22). Modifications of the gas handling system which was used for ethane hydrogenolysis were required in order to perform CO methanation. Ultra high purity hydrogen (99.999%, Alphagaz) passes through a palladium Deoxo purifier (Engelhard), a Linde gas purifier column (Model 120: indicating silica gel and molecular sieve), and a 7 micron filter (Nupro) before passing through a Linde mass flowmeter (Model FM 4570). The hydrogen is then mixed with ultra high purity helium (99.999%, Alphagaz) which has similarly passed through a Linde gas purifier column, 7 micron filter, and mass flowmeter. In order to remove remaining components that react with nickel, the hydrogen/helium mixture passes through a Ni/SiO_2 "guard" reactor at 600 K, as well as another silica gel trap. The gas mixture then flows to a manifold were carbon monoxide can be added to the mixture before entering the reactor. The carbon monoxide (99.3%, Air Products) passes through a 7 micron filter and mass flowmeter before passing through a carbonyl trap, which consists of a column of copper turnings (19,20) heated to 500 K. The carbon monoxide is further purified by passing through an Oxy-Trap (Alltech Associates, Inc., Model 4002) heated at 400 K and an Alltech gas purifier column (Model 8125: indicating silica gel and molecular seive). The carbon monoxide then passes through a needle valve. A ball valve is used to introduce the carbon monoxide into the hydrogen/helium stream just before the sample reactor.

RESULTS AND DISCUSSION

An example of the rapid decrease in AC permeameter voltage which occurs upon introducing carbon monoxide into the flowing stream of hydrogen and helium is shown in Figure 1. This corresponds to the decrease in sample moment due the average crystallite temperature rise as well as to the adsorption of carbon monoxide. After this rapid decrease, the sample signal remains relatively constant. When the reaction is terminated by stopping the carbon monoxide flow, there is a rapid increase in sample moment followed by a more gradual increase in moment which levels off within 5 to 10 minutes. This is also shown in Figure 1.

As with ethane hydrogenolysis, the temperature and adsorption calibrations were performed after an initial aging period, in order to minimize any post calibration changes. In order to monitor catalyst aging, a series of methanation experiments was performed with the H_2/CO ratio kept at 7. Figure 2 shows the decrease in conversion relative to that of the fresh catalyst. The catalyst was left in flowing hydrogen for a period of 16 hours between samples 10 and 11, and for a period of 17 hours between samples 26 and 27. This is taken to account for the higher conversion in run 11; however, there is no corresponding increase between samples 26 and 27. Nevertheless, the activity of the catalyst seems to level off and remain comparatively constant.

The temperature calibration is performed by perturbing the average bed temperature by temporarily removing the catalyst bed from the AC permeameter/oven while flowing hydrogen and helium over the catalyst. After allowing the sample to cool 5 to 10 K, as measured by a thermocouple at the bed exit, the catalyst sample is returned to the optimal sensing location within one of the secondary coils. The AC permeameter signal and exit fluid temperatures are then monitored as the catalyst bed heats. This is repeated several times. The sensitivity (mV/K), determined using least squares regression is assumed constant over the small temperature range considered. As mentioned, this calibration will be affected by changes in crystallite size and by the formation of "permanent" nonmagnetic nickel compounds. Thus, it is important that these do not change significantly between a calibration and the corresponding thermometry experiments.

The calibration procedure used in this study to account for changes in magnetization due to changes in CO uptake takes advantage of the similarity between the uptake results reported during methanation (15) and disproportionation (17,18), discussed previously. The formation of bulk carbide during the CO disproportionation calibration would result in large magnetization decreases and invalidate the procedure; therefore, the possibility of its formation was investigated. Previous studies (17,18) found the formation of bulk carbide during CO disproportionation. However, Mirodatos et. al. (17) using both static and flow experiments, only found bulk carbidization at times greater than 30 minutes for their flow conditions. For experiments in this laboratory, when carbon monoxide is introduced into a helium stream flowing through the catalyst bed, there is a rapid decrease in sample moment, followed by a more gradual decrease in moment, as shown in Figure 3. When disproportionation is allowed to run for longer periods of time, the moment decrease approaches a limiting value after 10 to 15 minutes with a final moment loss of only 6 to 8% of the total sample moment. This relatively small moment loss indicates that no significant amount of bulk carbidization has occurred. When the reaction is terminated, leaving only helium flowing through the catalyst bed, there is a gradual increase in moment which reaches a limiting value after 15 to 20 minutes with a recovery of greater than 90% of the lost moment.

If hydrogen flow is initiated through a catalyst that has previously been exposed to CO disproportionation, there is a rapid increase in sample moment, indicating the removal of a hydrogen reactive surface species. This is in agreement with the results of other laboratories (15,17). There is no discernible change in the sample moment when the hydrogen flow is terminated, leaving only helium flowing. With repeated cycles of 10 minutes of a H_2/He mixture followed by 20 minutes of pure He flow through the catalyst bed, there is a rapid increase in sample moment after each hydrogen introduction. However, the magnitude of the moment increase declines somewhat with each sucessive initiation of hydrogen flow. Analysis of the effluent shows that methane is evolved after each hydrogen introduction. Similar results are also obtained for the catalyst after methanation with an H_2/CO ratio of at least seven. There is no marked difference in the response of the sample moment to the initiation of hydrogen flow after either the methanation or disproportionation experiments. These results indicate the formation of carbon species, during both methanation and disproportionation, all forms of which are not available for reaction with hydrogen, but with which they become available for reaction. This corresponds to the interstitially dissolved carbon reported by other researchers (13,17,18), where the surface carbon is removed by the hydrogen, and is replaced by the migration of the interstitially dissolved carbon.

The use of CO disproportionation for a calibration to account for carbon monoxide adsorption effects is substantiated by these results because: (1) they indicate no significant formation of bulk carbide, at least not in the short time required for the calibrations, and (2) they indicate that there is no significant difference in the carbon formed during both methanation and disproportionation. The results do not preclude the possibility of the formation of the filamentous carbon species reported by other researchers (24-26) during the CO disproportionation calibration. Such filamentous carbon species can deactivate the catalyst, but have no effect on the sample moment (18).

Baseline drift is usual when using an AC permeameter. Therefore for thermometry, we rely on the rapid change in sample moment which occurs within the first 1/2 to 1 minute after introducing carbon monoxide into the hydrogen and helium stream. As mentioned, there is also a rapid decrease in sample moment when carbon monoxide is introduced into a helium stream (see Figure 3). The magnitude of the rapid decrease depends upon the carbon monoxide partial pressure, and is reproducible. This is in apparent agreement with the results of Gardner and Bartholomew (15) and Kuijpers et.al. (18). For calibration purposes, this magnitude is assumed to correspond to the adsorption of carbon monoxide which occurs upon the initiation of methanation. The calibration is performed by introducing carbon monoxide at various partial pressures into helium. The carbon monoxide is allowed to flow only long enough to record the initial rapid decrease in sample moment (2 to 3 minutes). The results were fit to the following equation using least squares regression:

$$\Delta\text{Signal(mV)} = 0.00462*(P_{CO}(\text{Torr}))^{0.662} \qquad 1)$$

As indicated, with the termination of methanation there is a rapid increase in moment within the first minute after the carbon monoxide flow is stopped, which is followed by a more gradual increase. However, when the carbon monoxide flow is stopped during CO disproportionation there is only a gradual increase in sample moment, as shown in Figure 3. In the absence of a rapid moment change, a time of 60 seconds was arbitarily chosen to represent the signal increase corresponding to desorption upon reaction termination. Again, the change is reproducible, and dependent upon the carbon monoxide partial pressure present before reaction termination. The results with this choice of time scale is represented by the equation

$$\Delta\text{Signal(mV)} = 0.00071*(P_{CO}(\text{Torr}))^{1.05} \qquad 2)$$

obtained using least squares regression.

The introduction of carbon monoxide in order to initiate methanation slightly decreases the hydrogen partial pressure, which effects the sample moment. A calibration for the moment change due to hydrogen partial pressure changes is performed by slightly changing the hydrogen partial pressure during reaction. Hydrogen partial pressure affects the reaction rate, however for the small changes that are required for the calibration, the extent of conversion changes at most only 2 to 5%. A small decrease in signal results from a decrease in hydrogen partial pressure. Just the opposite was observed if the hydrogen partial pressure was changed during ethane hydrogenolysis (2). Thus, it seems that the decrease in hydrogen partial pressure leads to an increase in the crystallite surface coverage by carbon, instead of a decrease in surface coverage by hydrogen. The moment change is reproducible and dependent upon the change in hydrogen partial pressure. There is no significant difference in the magnitude of the moment decrease with decreasing partial pressure and the moment increase with an equivalent increase in hydrogen partial pressure. The results are correlated using least squares regression and fit to the equation

$$\Delta\text{Signal(mV)} = 0.00003(\Delta P_{H_2}(\text{Torr}))^{1.27} \qquad 3)$$

It is important to note that this effect is one to two orders of magnitude less than that for changes in carbon monoxide partial pressure, and seldom has significance in the thermometry experiments since the hydrogen partial pressure changes only slightly.

The average crystallite temperature rise due to the initiation of methanation is determined by first measuring the magnitude of the signal change upon the initiation of reaction. Signal changes due the increase in CO partial pressure and decrease in hydrogen partial pressure are then subtracted. The result is then divided by the temperature sensitivity (mV/K) to determine the temperature rise.

The validity of the calibration technique was tested by camparing the results of this study with the those for ethane hydrogenolysis. Assuming that no microscopic crystallite to support gradients exist, it is possible to determine the interphase Nusselt number using the described thermometry (1,2,27,28). The average crystallite temperature rise determined from crystallite thermometry is used to calculate the average solid temperature. This information, along with the average bulk fluid temperature rise, and the conversion (heat release) allows the direct

calculation of interphase Nusselt number within the differential reactor assumption. The flow conditions ($0.3<Re<0.6$) were not varied enough in this study to determine the functional dependence of the interphase Nusselt number (Nu) on Reynolds number (Re). The interphase Nu was determined for runs for which the catalyst bed was operated under differential conditions, taken as less than 5% conversion. The resulting Nu are scattered uniformly around the results from the previous study using ethane hydrogenolysis (2,27,28). The average Nu determined from the methanation data matches the previously determined relationship. If the results obtained during ethane hydrogenolysis are accepted, then the calibration method used in this work seems valid. Due to the limited Re range covered, these preliminary results are inconclusive, but also indicate the absence of microscopic temperature differences between the crystallite and support. A significantly smaller interphase Nu would be expected if these microscopic temperature differences existed. If this conclusion is correct, then any crystallite size dependence of activity does not interfere with the thermometry.

The possibility of crystallite growth during the initial aging period was investigated. This is not critical to this work, but it is of interest. Samples with larger nickel crystallites exhibit a larger magnetization than those with smaller crystallites, at a fixed field (3). As discussed, the calibrations were performed on the "aged" catalyst. Therefore, the sample moment would be larger than that for the fresh sample, at a given field, if crystallite growth occurred. This assumes that there is no significant loss of nickel. Thus, the fresh catalyst would show smaller magnetization changes than the aged sample for a given temperature change. Therefore, if the temperature calibration performed on the aged sample is applied, a smaller "measured" solid temperature rise is indicated from crystallite thermometry. The average solid temperature rise expected for given flow and conversion data can be estimated using the interphase heat transfer data from the ethane hydrogenolysis study (2,27,28). As discussed above, the interphase heat transfer results using data gathered on the aged catalyst have already been shown to agree with these previous results. Figure 4 shows a plot of the difference between the "measured" solid temperature and the "predicted" temperature during the initial aging period. The results show that initially, the "measured" solid temperatures were much smaller than that predicted. The difference between the measured and predicted temperatures decreased as the catalyst aged. Subsequent data reflects scatter. The crystallite growth inferred from these results is in agreement with the results of van Meerten et. al. (20). Those researchers performed crystallite size estimates as the catalyst aged and found crystallite growth. However, contrary to the results of that laboratory, a significant loss of activity was found in this work. A strong size dependence of activity is not apparent.

CONCLUSIONS

Nickel crystallite thermometry has been performed during CO methanation. The analysis and calibrations are more complicated than for ethane hydrogenolysis, because of the more complicated magnetochemistry involved. The calibration scheme used to account for CO adsorption and the formation of surface species seems to work satisfactorily. The scheme used is based on results that show no significant formation of bulk carbide during the disproportionation calibration and no significant difference in the carbon species formed during methanation and disproportionation. In addition, interphase Nusselt number estimates are in good agreement with those obtained during ethane hydrogenolysis. However, it would be more satisfying to have a calibration based on methanation, rather than disproportionation.

An alternate calibration scheme in which the methanation rate is decreased while maintaining the same CO adsorption conditions is under development. The approach is to decrease the reaction rate while holding the adsorption/surface carbon species formation effects constant. The effect due to the temperature rise will decrease. Thus, it should be possible to extrapolate to zero rate in order to isolate the moment change due only to adsorption. Preliminary results following

this line of reasoning are inconclusive, and further work is necessary to determine whether such a calibration scheme can be developed.

ACKNOWLEDGEMENTS

Financial assistance from the Petroleum Research Fund and the National Science Foundation is gratefully acknowledged.

REFERENCES

1. Cale, T. S., and Ludlow, D. K., J. Catal. 86, 450 (1984).
2. Cale, T. S., J. Catal. 90, 40 (1984).
3. Selwood, P. W., "Chemisorption and Magnetization" Academic Press, New York, 1975.
4. Martin, G. A., and Imelik, B., Surf. Sci. 42, 157 (1974).
5. Martin, G. A., Dutarte, R., and Dalmon, J. A., in "Growth of Properties of Metal Clusters", Bourdon, J. (ed.) p. 467, Elesevier, Amsterdam, 1980.
6. Matyi, R. J., Butt, J. B., and Schwartz, L. H., J. Catal. 91, 185 (1985).
7. Geus, J. W., Nobel, A. P. P., and Zwietering, P., J. Catal. 1, 8 (1962).
8. Primet, M., Dalmon, J. A., and Martin, G. A., J. Catal. 46, 25 (1977).
9. Mulay, L. N., Everson, R. C., Mahajan, O. P., and Walker, P. L., Jr., AIP Conf. Proc., 29 (Magn. Magn. Mater., Annu. Conf., 21st), 536 (1975).
10. Farrauto, R. J., J. Catal. 41, 482 (1976).
11. Wentrcek, P. R., Wood, B. J., and Wise, H., J. Catal. 43, 363 (1976).
12. Martin, G. A., Dalmon, J. A., and Primet, M., C. R. Hebd. Seances. Acad. Sci. SerC. 284(4), 163 (1977).
13. Martin, G. A., Primet, M., and Dalmon, J. A., J. Catal. 53, 321 (1978).
14. Falconer, J. L., and Zagli, A. E., J. Catal. 62, 280 (1980).
15. Gardner, D. C., and Bartholomew, C. H., Ind. Eng. Chem. Fundam. 20, 229 (1981).
16. Kuijpers, E. G. M., Breedjik, A. K., van der Wal, W. J. J., and Geus, J. W., J. Catal. 81, 429 (1983).
17. Mirodatos, C., Dalmon, J. A., and Martin, G. A., Stud. Surf. Sci. Catal. 19, 505 (1984).
18. Kuijpers, E. G. M., Kock, A. J. H. M., Nieuwesteeg, M. W. C. M. A., and Geus, J. W., J. Catal. 95, 13 (1985).
19. Shen, W. M., Dumesic, J. A., and Hill, C. G., Jr., J. Catal. 68, 152 (1981).
20. van Meerten, R. Z. C., Beaumont, A. H. G. M., van Nisselrooij, P. F. M. T., and Coenen, J. W. E., Surf. Sci. 135, 565 (1983).
21. McCarty, J. C., and Wise, H., J. Catal. 57, 406 (1979).
22. Cale, T. S., and Ludlow, D. K., Anal. Instrum. 13(2), 183 (1984).
23. Cale, T. S., and Richardson, J. T., J. Catal. 79, 378 (1983).
24. Rostrup-Nielsen, J. R., J. Catal. 27, 343 (1972).
25. Tøttrup, P. B., J. Catal. 29, (1976).
26. Gardner, D. C., and Bartholomew, C. H., Ind. Eng. Chem. Prod. Res. Dev. 20, 80 (1981).
27. Lawson, J. M., Ludlow, D. K., and Cale, T. S., Proceedings IASTED International Conference, AIMS '84, 26 (1984).
28. Cale, T. S., and Lawson, J. M., Chem. Eng. Commun. 39, 241 (1985).

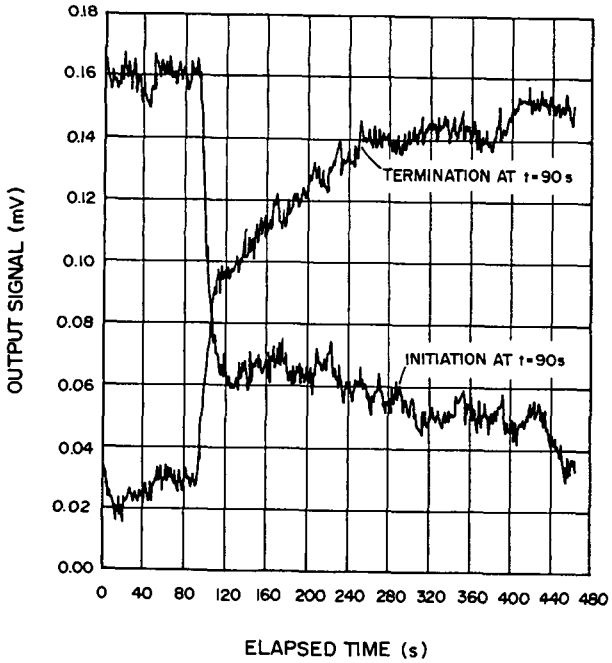

Figure 1. Examples of the changes in AC permeameter output voltage that occur upon the initiation and termination of CO methanation.

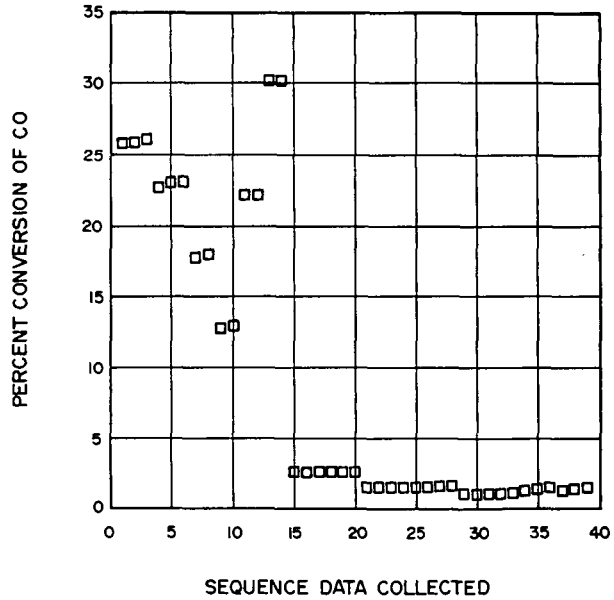

Figure 2. Conversion data during initial aging period. The H_2/CO ratio is seven. The catalyst was left in flowing hydrogen for 16 and 17 hours between samples 10-11 and 26-27, respectively.

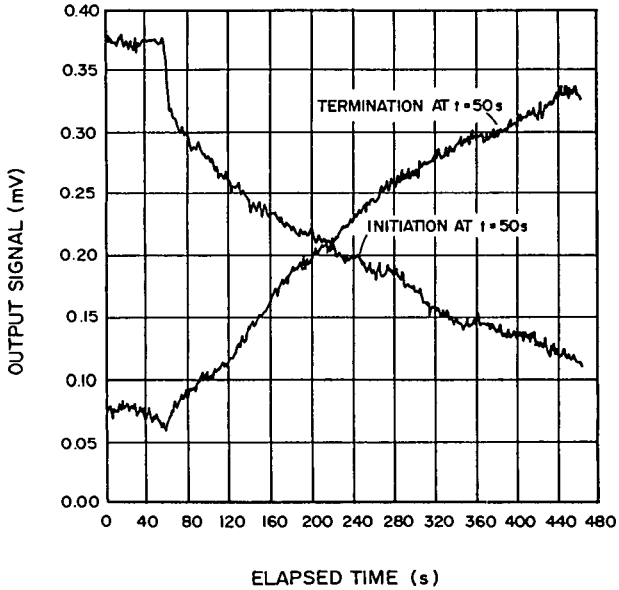

Figure 3. Examples of the changes in AC permeameter output voltage that occur upon the initiation and termination of CO disproportionation. (See text for explanation.)

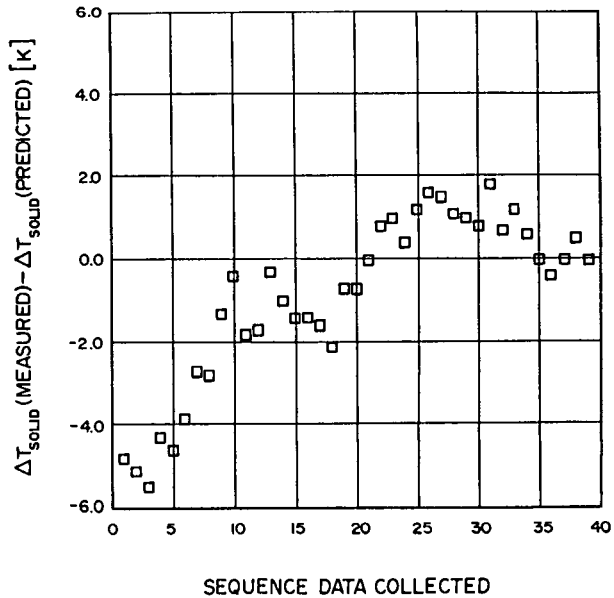

Figure 4. Difference in the "predicted" and "measured" solid temperature rise during initial aging period. (See text for explanation.)

SUPPORTED MOLECULAR CATALYSTS FOR CO HYDROGENATION

H. Henry Lamb and B. C. Gates

Center for Catalytic Science and Technology
Department of Chemical Engineering
University of Delaware
Newark, DE 19711

INTRODUCTION

The metal-oxide support is known to exert a strong influence on the activity and selectivity of heterogeneous CO hydrogenation catalysts (1). Ichikawa demonstrated that catalysts derived from $[Rh_4(CO)_{12}]$ deposited on basic MgO produced methanol from CO + H_2 with >95% selectivity, whereas $[Rh_4(CO)_{12}]$-derived catalysts supported on more acidic metal oxides such as γ-Al_2O_3 and SiO_2 produced chiefly methane with only traces of oxygenated products being formed (2). Only limited data is currently available relating these differences in catalytic performance to differences in catalyst structure (3). However, it was recently demonstrated that under high-temperature CO hydrogenation conditions (275°C, 10 atm) anionic osmium carbonyl clusters (e.g., $[Os_{10}C(CO)_{24}]^{2-}$) are formed on MgO from adsorbed $[H_2Os(CO)_4]$ (4). This finding is in contrast to the cluster fragmentation and Os(II) subcarbonyl formation observed under similar conditions for osmium clusters adsorbed on γ-Al_2O_3 and SiO_2 (5); the nature of the support dictates the surface organometallic chemistry.

Here we present the results of an investigation confirming the presence of $[Os_{10}C(CO)_{24}]^{2-}$ on the surfaces of conventional MgO-supported CO hydrogenation catalysts prepared by aqueous impregnation with $[H_2OsCl_6]$ (6). The carbido carbonyl cluster is synthesized in high yield from Os(IV) on MgO exposed to CO hydrogenation conditions.

EXPERIMENTAL

The MgO support (MX-65-1 powder, MCB reagents) was contacted with an aqueous solution of $[H_2OsCl_6]$ having sufficient volume (~2 ml/g) to yield a heavy paste. The material was dried at 70°C in vacuum, and the resultant light-blue powder was analyzed by X-ray fluorescence (XRF) spectroscopy and found to contain 1.3 wt % Os.

Samples (0.30 g) of MgO impregnated with $[H_2OsCl_6]$ were treated with H_2 or a H_2 + CO mixture in a tubular flow reactor. The samples were thoroughly dried by pretreatment in flowing He for 1 h at 150°C. Conventional Os/MgO catalysts (7) resulted from reduction with H_2 at 275°C and 1 atm for 10 h. These catalysts were subsequently exposed <u>in-situ</u> to H_2 + CO (equimolar) at 275°C and 1 or 10 atm for 8 h. A sample of $[H_2OsCl_6]$ and MgO was treated directly with H_2 + CO (equimolar) at 275°C and 1 atm for 5 h. In each case the sealed reactor tube was unloaded in a dry box. The H_2-reduced materials were metallic gray after exposure to CO hydrogenation conditions; the sample exposed directly to H_2 + CO was reddish-pink. The gases employed were Matheson UHP grade and were further purified by passage over activated 5A molecular sieve and supported Cu_2O (H_2 and He only).

$[Et_4N]_2[Os_{10}C(CO)_{24}]$ was synthesized following the procedure of Hayward and Shapley (8). The metal cluster was adsorbed on MgO (pretreated in vacuum at 400°C) from dry tetrahydrofuran (THF) solution. The resultant reddish-pink solid was recovered by filtration, washed with fresh THF, and dried in flowing nitrogen.

Acetone solutions of [PPN][Cl] ($PPN^+ = N(PPh_3)_2^+$) were used to extract $[Os_{10}C(CO)_{24}]^{2-}$ from the catalyst surfaces by ion exchange. $[PPN]_2[Os_{10}C(CO)_{24}]$ in the extract solutions was detected by infrared spectroscopy.

Infrared spectra were obtained with a Nicolet 7199 Fourier transform spectrometer. Powders were pressed, forming self-supporting wafers which were loaded (without exposure to air) into a leak-tight glass cell fitted with NaCl windows. The thermostated cell could be connected to a manifold for evacuation or gas treatments.

Ultraviolet-visible spectra of powders under N_2 were recorded with a Cary 219 spectrophotometer equipped with a diffuse reflectance attachment.

Extended X-ray absorption fine structure (EXAFS) measurements were conducted at the Cornell High Energy Synchrotron Source (CHESS). $[Os_{10}C(CO)_{24}]^{2-}$/MgO formed by the H_2 + CO reduction of Os(IV) on MgO and a sample of $[Et_4N]_2[Os_{10}C(CO)_{24}]$ and MgO were examined.

RESULTS AND DISCUSSION

In the presence of CO or an equimolar mixture of H_2 + CO at 275°C and 1 atm, Os(IV) on MgO is reduced and carbonylated to yield $[Os_{10}C(CO)_{24}]^{2-}$ ionically bound to the MgO surface. The formation of $[Os_{10}C(CO)_{24}]^{2-}$ under these conditions has been confirmed by IR, UV-Vis, and EXAFS spectroscopies, in addition to the isolation of $[PPN]_2[Os_{10}C(CO)_{24}]$ from the surface by cation metathesis with [PPN][Cl] in acetone.

Treatment of MgO impregnated with $[H_2OsCl_6]$ in H_2 + CO (equimolar) at 275°C and 1 atm for 5 h in a flow reactor, resulted in a change in color of the solid from light blue to reddish pink, indicative of the formation of $[Os_{10}C(CO)_{24}]^{2-}$. The UV-Vis diffuse reflectance spectrum (200-800 nm) of the product is in excellent agreement with that of $[Et_4N]_2[Os_{10}C(CO)_{24}]$ deposited on MgO from THF. Extraction of a portion of the material with [PPN][Cl] in acetone resulted in a white solid and a brownish-red solution. The infrared spectrum of the solution contains only strong bands assigned to $[PPN]_2[Os_{10}C(CO)_{24}]$ (Table 1).

The synthesis of $[Os_{10}C(CO)_{24}]^{2-}$ on the MgO surface was also monitored by <u>in-situ</u> infrared spectroscopy. Slowly heating a wafer of $[H_2OsCl_6]$ and MgO to 275°C in flowing H_2 + CO at atmospheric pressure, first produced Os(II) subcarbonyls (ν_{CO} = 2105(m), 2030(s), 1936(s) cm^{-1}) on MgO (9). However, near 275°C there was a dramatic increase in absorption in the carbonyl stretching region, and after 1.5 h under these conditions strong bands assigned to $[Os_{10}C(CO)_{24}]^{2-}$/MgO (Table 1) were present. A similar experiment conducted using pure CO instead of H_2 + CO also resulted in the formation of the carbido carbonyl cluster in high yield.

TABLE 1

Molecular Cluster	ν_{CO} (cm^{-1})	Ref.
$[PPN]_2[Os_{10}C(CO)_{24}]$	2034(s), 1992(s) (acetone)	(8)
$[Et_4N]_2[Os_{10}C(CO)_{24}]$ and MgO	2079(vw), 2062(w), 2030(s), 1998(sh), 1986(sh), 1975(vs), 1966(sh)	This work
$[Os_{10}C(CO)_{24}]^{2-}$ from Os(IV) on MgO	2104(vw), 2080(w), 2040(s), 1998(sh) 1989(s), 1979(sh), 1963(sh)	This work

Confirmation of the identity of the surface species was obtained from EXAFS spectroscopy. The reduction and carbonylation were again effected <u>in-situ</u> and comparison made to the spectrum of $[Et_4N]_2[Os_{10}C(CO)_{24}]$ deposited on MgO. Close agreement was found for the EXAFS oscillations above the Os L_{III} edge over the range of the wavevector from k = 3 to 12 $Å^{-1}$. A final structure determination awaits detailed analysis of the data.

Even reduction of MgO impregnated with $[H_2OsCl_6]$ with H_2 to yield supported Os aggregates (7) did not completely inhibit the formation of $[Os_{10}C(CO)_{24}]^{2-}$. The highly stable molecular cluster was isolated in low yields by ion exchange of H_2-reduced samples exposed to H_2 + CO at 275°C and 1 or 10 atm for 8 h. The presence of the cluster in the lightly colored extract solutions was confirmed by infrared spectroscopy. In addition, Deeba et al. have reported that MgO-supported catalysts derived from the decomposition of adsorbed $Os_3(CO)_{12}$ gave evidence for the presence of molecular clusters following use in CO hydrogenation to produce C_1-C_4 hydrocarbons at 300°C and 7 atm (10). Comparing the infrared data reported for their used catalysts (ν_{CO} = 2080(m), 2048(sh), 2039(s), 2010(sh), 1986(vs), 1950(sh) cm^{-1}), with those of $[Os_{10}C(CO)_{24}]^{2-}$/MgO, we infer that this molecular cluster was formed on these catalysts as well.

In summary, $[Os_{10}C(CO)_{24}]^{2-}$ represents an extremely stable molecular structure on the surfaces of Os/MgO CO hydrogenation catalysts. The basicity of the MgO support appears to be essential; analogous structures do not form on the more acidic γ-Al_2O_3 and SiO_2 surfaces (4), and the surface-mediated synthesis of $[Os_{10}C(CO)_{24}]^{2-}$ parallels the syntheses of high-nuclearity Group VIII - metal clusters in basic solution (11). What direct role this metal cluster has in the catalysis remains to be elucidated.

ACKNOWLEDGEMENT

The authors wisb to acknowledge Dr. D. C. Koningsberger for his valuable assistance in the EXAFS measurements. This work was supported by the National Science Foundation (grant CPE8218311) and the Exxon Education Foundation.

REFERENCES

(1) Katzer, J. R., Sleight, A. W., Gajardo, P., Michel, J. P., Gleason, E. F., and McMillan, S., Fara. Disc., 72, 121 (1981).
(2) Ichikawa, M., Bull. Chem. Soc. Jpn., 51, 2268 (1978).
(3) (a) Solymosi, F., Tombácz, I., and Kocsis, M., J. Catal., 75, 78 (1982); (b) Erdöhelyi, A. and Solymosi, F., J. Catal., 84, 446 (1983).
(4) Lamb, H. H. and Gates, B. C. J. Am. Chem. Soc., 108, 81 (1986).
(5) Eds., Gates, B. C., Guczi, L., and Knözinger, H., "Metal Clusters in Catalysis," Elsevier, Amsterdam, in press.
(6) Lamb, H. H., Krause, T. R., and Gates, B. C., J. Chem. Soc., Chem. Commun., in press.
(7) Odebunmi, E. O., Matrana, B. A., Datye, A. K., Allard, L. F., Jr., Schwank, J., Manogue, W. H., Hayman, A., Onuferko, J. H., Knözinger, H., and Gates, B. C., J. Catal., 95, 370 (1985).
(8) Hayward, T. C. and Shapley, J. R., Inorg. Chem., 21, 3816 (1982).
(9) Psaro, R., Dossi, C., and Ugo, R., J. Mol. Catal., 21, 331 (1983).
(10) Deeba, M., Scott, J. P., Barth, R., and Gates, B. C., J. Catal., 71, 373 (1981).
(11) Chini, P., Longoni, G., and Albano, V. G., Adv. Organomet. Chem., 14, 285 (1976).

Methanation and HDS Catalysts Based on Sulfided, Bimetallic Clusters

M. David Curtis, Johannes Schwank, Levi Thompson,
P. Douglas Williams, and Oswaldo Baralt

Departments of Chemistry and Chemical Engineering,
The University of Michigan, Ann Arbor, MI 48109

INTRODUCTION

Environmental concerns have led to an increased interest in hydrotreating catalysts, i.e. catalysts for hydrodesulfurization (HDS) or hydrodenitrogenation (HDN) (1-3). Although HDS may be catalyzed by bulk or supported MoS_2 and related sulfides, the most effective catalysts are those derived from "sulfided cobalt molybdate" supported on Al_2O_3. These catalysts are prepared conventionally by impregnating the alumina support with solutions of molybdate ions and cobaltous ions. The impregnated support is then calcined to convert the adsorbed species to their respective oxides. The supported metal oxides are then converted to sulfides ("sulfided") with a mixture of H_2 and H_2S (or the feed stream itself) at temperatures in the range 300-400°C. Alternate promoters, e.g. Ni and Fe, may be used in the place of Co, but the resulting catalysts usually show a lower activity.

Despite intensive study, the exact nature of the active "CoMoS" phase is still uncertain, and hence the role of the Co promotor and the exact mechanism of HDS remain obscure. XPS and Mössbauer Emission Spectroscopy has been used to show that a "CoMoS" phase, distinct from Co_9S_8 or MoS_2, is present and that the activity of the catalyst parallels the amount of this CoMoS phase present (4).

More recently, EXAFS has been used to study these cobalt molybdate catalysts in both the oxidized and sulfided states (5-11). The most popular model has Co-atoms coordinated to sulfur at the edges of basal planes of small (10-30Å) crystallites of MoS_2 (see Figure 1). The EXAFS results also are best fit by assuming the MoS_2 rafts are essentially two dimensional.

The promotor metal, Co or Ni, is intimately involved in the active site. The activities of the promoted MoS_2 can be 10^2 that of unpromoted MoS_2, usually with the Co/Mo ratio $\simeq$1.0 (12). It is therefore surprising that Co-Mo vectors have never been identified in the EXAFS studies of these catalysts. Therefore, the location of the Co relative to the Mo in these CoMoS catalysts is still uncertain. New approaches are necessary to probe the nature of the active site of these sulfided catalysts.

MOLECULAR MODELS OF PROMOTED MoS_2 PHASES

We have prepared discrete, molecular clusters which may serve as models for the active sites in promoted molybdenum sulfide catalysts (13-15). These clusters are composed of one metal each from the sets, {Mo,W} and {Fe,Co,Ni}; they contain sulfur in the cluster framework and organic ligands, e.g. carbonyls, cyclopentadienyls (Cp), etc. on the periphery of the cluster. The structures of representative clusters are shown in Figure 2.

These clusters have been deposited on oxide supports by dissolving the molecular cluster in an appropriate solvent, e.g. CH_2Cl_2, and then adding the calcined support. With the low loadings (1% total

metal) employed in this study, the clusters are quantitatively adsorbed onto the support from solution. The solvent is then removed and the solid dried under vacuum. The supported clusters are then subjected to temperature-programmed decomposition (TPDE) in a stream of H_2 or He. The exit gas stream is analyzed for CO,CO_2, hydrocarbons, etc. by GC and GC/MS. Figure 3 shows a typical TPDE curve for the MoFeS cluster, 1, (Figure 2).

In the TPDE of cluster 1 on γ-Al_2O_3, ca. 5 CO per cluster are lost at 100°C, and heating to 400°C causes gradual loss of one additional CO/cluster. In addition, small quantities of Me_2S, CH_4, and CO_2 are lost between 150°C and 400°C. The average composition of the remaining surface species is found to be $C_5Mo_2Fe_2S_{1.8}O_xH_y$ (the oxygen and hydrogen are uncertain since surface OH groups may contribute to the formation of CO_2, CH_4, etc.). Similar results are obtained for all the clusters investigated. The high carbon retention observed even with TPDE in flowing H_2 is attributed to carbide formation.

The facile loss of CO by the supported cluster stands in contrast to the thermal stability of the pure compound which is stable to >250°C. Therefore, there must be a strong support-cluster interaction which facilitates loss of CO from the adsorbed cluster.

Figure 4 shows the IR spectrum of pure cluster 1 and spectra of the cluster adsorbed on γ-Al_2O_3. The bridging CO band at 1795 cm^{-1} is most strongly perturbed, suggesting that the cluster is bound to a Lewis acid site (e.g. Al^{+3}) on the surface through the bridging CO, normally the most basic CO on the cluster (16). As the adsorbed cluster is heated to 110°C, the intensities of the CO bands diminish and finally disappear as the CO is lost. No new CO peaks are observed during the TPDE and no new CO bands appear if the decarbonylated cluster is placed in an atm. of CO at 25°C. Since the TPDE shows the loss of only 5 of the 8 CO-groups under these conditions, the remaining 3 CO's must be either dissociatively adsorbed or must be bonded in a multi-hapto manner with very low frequency CO-stretching vibrations.

The Mössbauer parameters (Table 1) suggest that the Fe in the cluster is oxidized during TPDE from Fe^o to Fe^{+3}.

Table 1. Mössbauer Spectral Parameters (mms^{-1})

	Pure 1	MoFeSA-01*	Used Cat.
I.S.	-0.01	0.38	0.43
ΔE_Q	0.78	0.84	0.84

*1% loading of cluster 1 on γ-Al_2O_3

METHANATION CATALYSIS

Clusters 1 and 3 (1% total metal loading) on γ-Al_2O_3 were pretreated in flowing H_2 (1 atm.) at 400°C for 6-12 hr. The resulting catalysts are labelled MoFeSA-01 and MoCoSA-01. The methanation activity of these catalysts was determined in the temperature range 250°-500°C with total pressures from 30 psi to 300 psi. The feed stream composition was 3:1 or 1:1 H_2:CO. A differential flow reactor

with GHSV $\approx$ 2500 hr^{-1} and CO conversions $\leq$ 2% was employed for kinetic measurements.

A break-in period of several hours was observed during which time the methanation activity was nearly zero. Methane then appears and the activity goes through a peak and then reaches steady state behavior which remains constant for days if the temperature is $\geq$ 300°C. At lower temperatures, a very gradual decrease in activity, presumably due to coking, was observed.

Arrhenius plots of the formal turnover frequency, N_f, vs. 1/T are shown in Figure 5 (N_f is defined as moles of CH_4/mole of cluster precursor/sec). Apparent activation energies are approximately 22 kcal/mol for MoCoSA-01 and 26 kcal/mol for MoFeSA-01.

The methanation reaction over MoFeSA-01 seems to follow Langmuir-Hinshelwood kinetics with the rate expression (T = 300°C, P in psi.):

$$N_f(s^{-1}) = \frac{(4.0 \times 10^{-6}) P_{H_2} P_{CO}}{\{1 + (0.018\ P_{H_2})^{1/2} + 0.143\ P_{CO}\}^2}$$

This rate law is consistent with a CO dissociative mechanism in which CH(ads.) + H(ads.) $\rightarrow$ CH_2(ads.) is the rate limiting step and all previous steps are in steady-state equilibrium.

The product distributions are plotted in Figure 6 for MoFeSA-01 and MoCoSA-01 under typical conditions. Selectivity for methane ranges from 90-98% depending on the temperature and pressure. Higher temperatures and lower pressures favor methane formation. Small amounts of C_2 and C_3 alkanes and olefins are formed, the latter are in greater abundance with the MoCoSA-01 catalyst. At higher pressures, dimethyl ether constitutes 2-4 mole % of the product stream, but methanol has never been detected.

It should be pointed out that the selectivities of MoFeSA-01 and MoCoSA-01 differ from Mo/Al_2O_3, MoS_2, Fe/Al_2O_3 or Co/Al_2O_3 which all produce less CH_4 and more C_2-C_5 hydrocarbons in a Schultz-Flory distribution. This result suggests that the clusters are not fragmenting and re-aggregating into larger metal (or metal sulfide) crystallites. After reaction, SEM and STEM also failed to reveal any particles >10Å, the resolving power of the microscope under the conditions used. The Fe I.S. (Table 1) increases somewhat after time on stream, possibly indicating that Fe(III) is being reduced somewhat.

HDS CATALYSIS

The activity of MoFeSA-01 and MoCoSA-01 toward catalysis of thiophene HDS has been determined in a differential flow reactor at GHSV $\approx$ 3000 hr^{-1} and thiophene conversions of 1-2% (conditions: 2.8 mol % thiophene in 1 atm. H_2 at 250°C-350°C). The catalysts were reduced in H_2 at 400°C and then presulfided with H_2S/H_2 or directly with the thiophene/H_2 feed stream. No difference in catalytic behavior due to the different pretreatments was observed. Catalytic activity was immediately established, in contrast to the methanation activity. Steady state selectivity was observed after 1 hr. on stream and no diminution of catalytic activity was observed after 3-4 days of operation.

Figure 7 is an Arrhenius plot of the formal turnover frequencies (moles converted/mole cluster/sec) for total thiophene conversion and for C_4 and C_3 products. Table 2 compares turnover frequencies and product slates of a clean Mo (100) surface, several cobalt molybdate catalysts with high metal loading, and the MoFeSA-01 and MoCoSA-01 (1% total metal loading) catalysts described above.

Table 2. Comparison of Activities and Selectivities of Various Catalysts for Thiophene HDS.

catalyst	$N_f(sec^{-1})$	T°C	BuH				
Mo(100)[a]	.02-.12	340	8	53	14	19	-
Mo14-Co4[b,c]	0.05	420	-	NOT GIVEN -			-
Mo8-Co3[d]	0.03	?		"butenes"			
Mo13-Co7[e]	0.05	290	10	-	29	62	-
MoCoSA-01	0.04	340	1	14	17	26	41
MoFeSA-01	0.01	340	2	13	18	25	41
				(11)	(19)	(27)[f]	

a) J. Catal. 1984, 88, 546. Butadiene (6%) also formed.
b) numbers refer to %Mo and %Co on γ-Al_2O_3.
c) J. Catal. 1984, 87, 292.
d) ibid. 1984, 85, 44.
e) ibid. 1984, 86, 55.
f) equilibrium ratios of butenes.

Two features are especially noteworthy. First, the activity of the MoCoSA-01 catalyst is comparable to catalysts with much higher metal loadings when compared on a per mol of Mo basis. This is unusual for HDS catalysts because the first few % of metal occupies tetrahedral holes in the Al_2O_3 lattice and is not converted to sulfides during the sulfiding step in conventional HDS catalysts.

Second, the cluster catalysts produce a large fraction of propene. Thus a carbon-carbon bond has been totally cleaved by hydrogenolysis. To our knowledge, C-C bond hydrogenolysis without C=C bond hydrogenation is unprecedented. Methane and 1-5% C_2 hydrocarbons (mostly C_2H_4) are also produced, but technical difficulties have precluded our quantifying the methane. Presumably, the amount of methane is equal to the amount of propene.

CONCLUSIONS

Sulfided bimetallic clusters of early and late transition metals have been shown to be precursors for methanation and HDS catalysts when supported on Al_2O_3. The activities and selectivites in CO hydrogenation closely resembles other metals in very highly dispersed states on Al_2O_3. Thus, stable metal clusters are not likely to be useful Fischer-Tropsch catalyst precursors.

However, these cluster species are exceptionally active in thiophene HDS and exhibit an unprecedented selectivity. Catalysts capable of simultaneously removing sulfur and cracking large molecules into smaller unsaturated fragments at relatively low temperatures could be especially useful for producing clean, low viscosity fluids from still bottoms and heavy coal liquids.

References

1. Wen, C.-Y.; Lee, E. S. "Coal Conversion Technology", Addison-Wesley, Reading, MA, 1979.

2. Cusumano, J. A.; Dalla Betta, R. A.; Levy, R. B. "Catalysts in Coal Conversion", Academic Press, New York, NY, 1978.

3. Grange, P. Catal. Rev. 1980, 21, 135.

4. Alstrup, I.; Chorkendorff, I.; Candia, R.; Clausen, B. S.; Topsoe, H. J. Catal. 1982, 77, 397.

5. Boudart, M.; Arrieta, J. S.; Dalla Betta, R. A. J. Am. Chem. Soc. 1983, 105, 6501.

6. Clausen, B. S.; Topsoe, H.; Candia, R.; Villadsen, J.; Langeler, B.; Als-Nielsen, J.; Christensen, F. J. Phys. Chem. 1981, 85, 3868.

7. Clausen, B. S.; Langeler, B.; Candia, R.; Als-Nielsen, J.; Topsoe, H. Bull. Soc. Chim. Belg. 1981, 90, 1249.

8. Parham, T. G.; Merrill, R. P. J. Catal. 1984, 85, 295.

9. Chiu, N.-S.; Bauer, S. H.; Johnson, M. F. L. J. Catal. 1984, 89, 226.

10. Clausen, B.; Topsoe, H.; Candia, R.; Langeler, B. Springer Proc. Phys. 1984, 2, 181.

11. Boudart, M.; Dalla Betta, R. A.; Foger, K.; Loffler, D. G. Springer Proc. Phys. 1984, 2, 187.

12. Chianelli, R. R.; Pecoraro, T. A.; Halbert, T. R.; Pan, W.-H.; Stiefel, E. I. J. Catal. 1984, 86, 226.

13. Curtis, M. D.; Williams, P. D. Inorg. Chem. 1983, 19, 2661.

14. Williams, P. D.; Curtis, M. D.; Duffy, D. N.; Butler, W. M. Organometallics 1983, 2, 165.

15. Curtis, M. D.; LaBarge, W. Unpublished results, 1985.

16. Horwitz, C. P.; Shriver, F. D. Adv. Organometal. Chem. 1984, 23, 219.

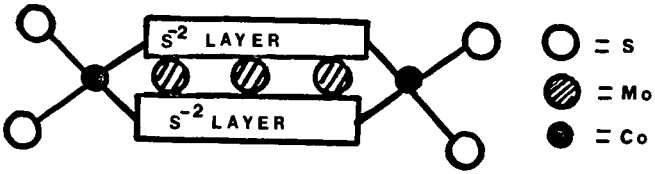

Figure 1. Proposed structure of "CoMoS" phase in promoted MoS_2 HDS catalysts.

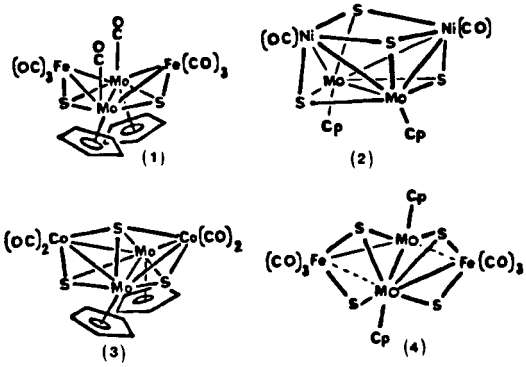

Figure 2. Structures of molecular models of promoted Mo-sulfide phases.

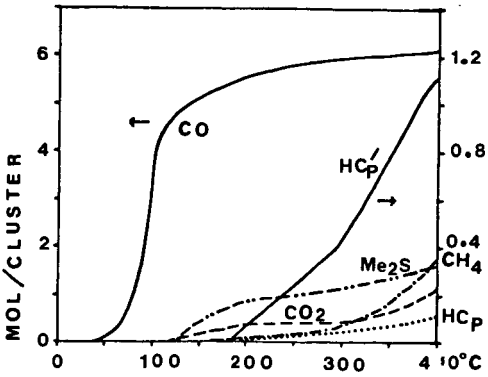

Figure 3. TPDE curves for cluster 1.

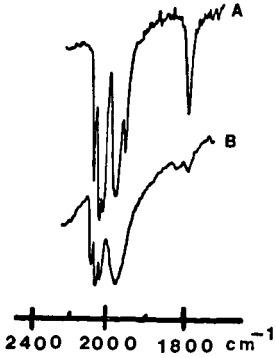

Figure 4. IR spectra of 1 in CH_2Cl_2 solution (A) and on Al_2O_3 (B).

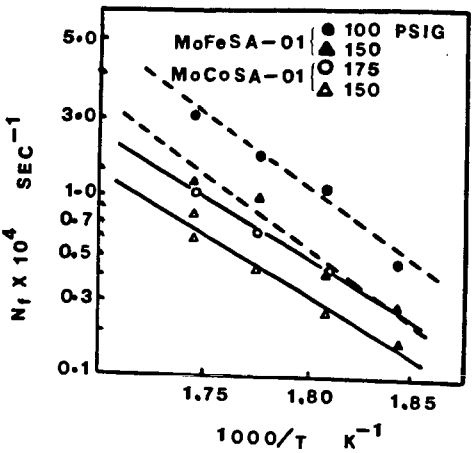

Figure 5. Arrhenius plots for CO hydrogenation with cluster catalysts.

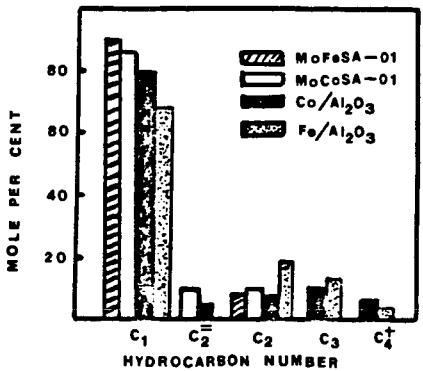

Figure 6. Product distribution in CO hydrogenation with various catalysts.

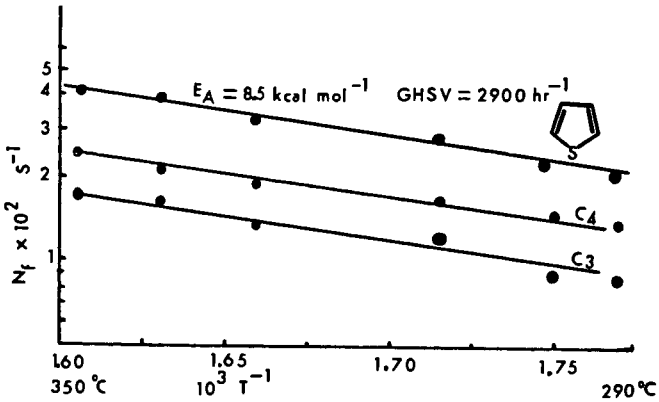

Figure 7. Arrhenius plots for thiophene HDS catalyzed by MoCoSA-01.

PHYSICAL AND CHEMICAL PROPERTIES OF $Fe(CO)_5/Al_2O_3$ CO-HYDROGENATION CATALYSTS.

M. Rameswaran and C. H. Bartholomew.

BYU Catalysis Laboratory, Department of Chemical Engineering, Brigham Young University, Provo, UT 84602.

Introduction

Carbonyl-derived catalysts (CDCs), ie catalysts prepared by the decomposition of metal carbonyls on catalyst carriers, have attracted recent attention because of their unusually high dispersions (fractions exposed to the surface) and high extents of reduction [1,2] . While conventional preparation methods may lead to metal contamination with S or Cl or may result in support decoration [3,4], it may be possible to produce "clean" particles by decomposing carbonyl complexes on carefully dehydroxylated supports. Thus, effects of metal loading, and crystallite size may be investigated in the absence of these contaminants using this class of catalysts.

The objective of this study was to investigate the effects of metal loading and support dehydroxylation temperature on the physical and chemical properties of Fe CDCs.

Experimental

Alumina (DISPAL M,) was dehydroxylated under vacuum at 473-1073 K for 16 hours and stored in a dry box. A dehydroxylation temperature of 923 K was used in the preparation of most of the catalysts in this study. About a two fold excess of $Fe(CO)_5$ to achieve a given Fe loading was mixed with pentane. The dehydroxylated alumina was then impregnated to incipient wetness using this solution. The pentane solvent was removed by evacuation at room temperature. About 10 g of the catalyst thus prepared was reduced in flowing hydrogen and stored in a dry box and the remainder was sealed and stored in a refrigerator. Total hydrogen adsorption capacities and oxygen titration uptakes (upon oxidizing the reduced catalyst at 723 K) were measured using a volumetric apparatus and procedures described elsewhere [5]. The reactor system used for obtaining the activity/selectivity properties are described elsewhere[6].

Results and Discussion

Figure 1 depicts the effect of reduction temperature on the dispersion and the extent of reduction of a 4.6 %Fe/alumina catalyst. The dispersion goes through a maximum while the extent of reduction reaches 100% as the temperature of reduction is increased from 473-773 K. Garten [7] reported that in the case of Fe/alumina catalysts prepared by aqueous impregnation, up to 1.5% Fe (300

μmoles per gram catalyst) was irreducible even at very high reduction temperatures due to strong interaction of iron oxide with the support. However, the results from this study indicate that the Fe/alumina prepared via carbonyl decomposition can be easily reduced to the Fe(0) state at relatively mild reduction conditions. The significant decrease in dispersion at higher reduction temperatures suggests that the carbonyl-derived species are mobile at higher temperatures in reducing atmosphere. Since the maximum dispersion was obtained at 573 K, this temperature was used for reducing all the catalysts in this study.

Data showing the effects of metal loading on the physical properties of carbonyl-derived Fe/alumina reduced at 573 K are tabulated in Table 1. Although dispersion decreases with increasing metal loading, neither the hydrogen uptake nor the extent of reduction follow any clear trends. Nevertheless, the dispersions and extents of reduction for these catalysts are much higher than obtainable for catalysts prepared by other method with similar metal loadings.

Table 2 illustrates effects of support-dehydroxylation temperature on the physical properties of Fe/alumina CDS's. All the catalysts listed in Table 2 contain 4.0-4.8 wt.% iron. However the amount of hydrogen adsorbed per gram of catalysts varies significantly with dehydroxylation temperature. The extent of reduction and the %D for the catalyst with the support dehydroxylated at 473 K were not obtained due to the inability to measure any significant oxygen uptake by the conventional methods. Hence it can be safely assumed that the impregnated carbonyl was fully oxidized. However, the catalyst with the support dehydroxylated at 1023 K was easily reduced. Thus, it is seen that the extent of reduction (or the ease of reduction) increases with decreasing surface OH concentration. This observation is consistent with that of Brenner and Burwell [8], who proposed that the surface OH groups act as anchors for the carbonyls by causing their partial oxidation.

The activity of iron/alumina dehydroxylated at 923 K increases with decreasing metal loading or increasing dispersion. This observation is opposite to that observed for Co/alumina prepared by aqueous impregnation [9] and Ru/alumina prepared from carbonyls on partially dehydroxylated alumina [10]. However, the selectivities of these Fe/alumina CDC catalysts were independent of metal loading or dispersion (Table 3). The 1 and 1.5% Fe/alumina catalysts deactivated rapidly at temperatures above 473 K, hence accurate measurement of activation energies was not possible. Although Fu and Bartholomew [9] observed a trend of decreasing activity with decreasing metal loading or increasing dispersion for Co catalysts prepared by aqueous impregnation with cobalt nitrate, they also observed that a 3% Co/alumina CDC catalyst was at least twice as active as 3% Co/alumina prepared by impregnation. Their results suggest that the conventional impregnation method leads to crystallite decoration and thus lower activity. Hence the results

TABLE 1.
Effects of Metal Loading on the Physical Properties of Fe/ Alumina[a] Catalysts.

Wt % Fe	H_2 uptake (μmoles/g)	% Dispersion[b]	Extent[c] of Reduction
1.0	45.1	75	33.6
1.5	31.5	40	58.6
4.6	72.6	31	55.1

a. Support dehydroxylated at 923 K under vacuum, catalyst reduced at 573 K.

b. $\%D = \frac{\text{\#of exposed atoms of Fe measured by hydrogen adsorption}}{\text{Total \# of reduced Fe atoms.(From oxygen titration and AA)}} \times 100$

c. Measured by O_2 titration at 673 K.

Table 2
Effects of Support Dehydroxylation Temperature on the Physical Properties of ~4.5 Fe/Alumina[a].

Dehydroxy-lation Temp. (K)	H_2 uptake (μmoles/g)	% Dispersion[b]	Extent[c] of Reduction
473	8.9	--[d]	--[d]
923	72.6	31	55.1
1073	55.9	16	95.4

a. Catalyst reduced at 573 K.

b. $\%D = \frac{\text{\#of exposed atoms of Fe measured by hydrogen adsorption}}{\text{Total \# of reduced Fe atoms.(From oxygen titration and AA)}} \times 100$

c. Measured by O_2 titration at 673 K.

d. Unable to measure oxygen uptakes.

TABLE 3.

Effects of Metal Loading on Activity/Selectivity Properties.
(H_2/CO = 2, 1 atm, 473 K)

Wt % Fe	TOF[a] x10^{-3} (sec^{-1})	% HC in[b] product Stream	HC Selectivity[c]				O/P[d]
			CH_4	C_2-C_4	C_5-C_{11}	C_{12+}	
1.0	0.36	87.2	26.2	40.8	33.0	0	1.6
1.5	0.13	83.8	28.3	42.4	29.3	0	2.5
4.6	0.05	87.2	21.7	40.1	38.1	0	2.5

a. Based on total H_2 adsorption.

b. Mole percent based on carbon balance; the remainder of the C apppeared as CO_2.

c. Wt.% hydrocarbon in product.

d. $O/P = \sum_{n=3}^{7} C_n^{=} / C_n$

observed for catalysts prepared by conventional methods [9] are probably due to a secondary structure-sensitivity [ie. decoration of the crystallites by support species] while the results in this study reflect either a primary structure sensitivity or changes in the electronic properties of the small metal clusters in the well-dispersed Fe/alumina. In a study by Kellner and Bell [10] of highly dispersed Ru/alumina prepared from the carbonyl, their observation of a decreasing activity with increasing dispersion may be a result of incomplete dehydroxylation of the support leading to crystallite contamination in the more highly dispersed catalysts.

The results of this study show that the support dehydroxylation temperature has a greater influence on the activity/selectivity properties than does dispersion (Table 4). The activity, selectivity for CH_4 and C_2-C_4 hydrocarbons, and the O/P ratio decrease with increasing dehydroxylation temperature, while the C_5-C_{11} fraction increases. Figure 2 indicates that the activation energy also increases with increasing dehydroxylation temperature. These effects of dehydroxylation temperature may be due to changes in the concentration of surface OH groups.

Conclusions

1. It is possible to produce highly dispersed and highly reduced catalysts by decomposing $Fe(CO)_5$ on dehydroxylated alumina.

2. The specific activity decreases with increasing metal loading (or decreasing dispersion). This effect may be due to a primary structure sensitivity on "clean" metal crystallites. The independence of selectivity with metal loading supports this hypothesis.

3. The significant changes in activity/selectivity with support dehydroxylation temperature may be a function of support hydroxyl group concentration, a significant concentration leading to support contamination of the metal surface and oxidation of the metal.

Acknowledgments

The authors wish to acknowledge the financial support of Atlantic Richfield Company for this project. M.R. also wishes to thank ASBYU for a research grant which enabled the construction of bulk pretreatment cell.

References.

1. Phillips, J. and Dumesic, J. A., Appl. Catal., 9(1981), 1.

TABLE 4.

Effects of Dehydroxylation Temperature on Activity/Selectivity Properties of ~4.5 % Fe on Al_2O_3.
(H_2/CO = 2, 1 atm, 473 K)

Dehydro-xylation Temp.(K)	TOF[a] $\times 10^{-3}$ (sec^{-1})	% HC in[b] product Stream	HC Selectivity[c] CH_4	C_2-C_4	C_5-C_{11}	C_{12+}	O/P[c]
473	0.2	77.0	43.0	56.0[e]	0	0	∞[f]
923	0.05	87.2	21.7	40.1	38.1	0	2.5
1073	0.02	87.4	21.7	39.0	39.7	0	2.3

a. Based on total H_2 adsorption.

b. Mole percent based on carbon balance; the remainder of the C apppeared as CO_2.

c. Wt.% hydrocarbon in product.

d. $O/P = \sum_{n=3}^{7} C_n^{=} / C_n$

e. C_2 and C_3 only

f. C_2: no parafins; C_3: O/P=1.54

2. Zwart, J. and Snell, R. J. Mol. Catal., 30(1985), 305.

3. Raupp, G. B. and Dumesic J. A., J. Catal.,95(1985), 587.

4. Bartholomew, C. H., (ed. Paal, Z. and Menon, P. G.) in press.

5. Weatherbee G.D., Rankin, J. L. and Bartholomew, C. H., Appl. Catal., 11(1984), 73.

6. Rameswaran, M. et al., paper in preparation, (1986).

7. Garten, R. L, J. Catal, 43 (1976), 18.

8. Brenner, A. and Burwell, R. L., J. Catal., 52(1978), 353.

9. Fu, L. and Bartholomew, C. H., J. Catal., 92(1985), 376..

10. Kellner, C. S. and Bell, A. T., J. Catal., 71(1981), 296.

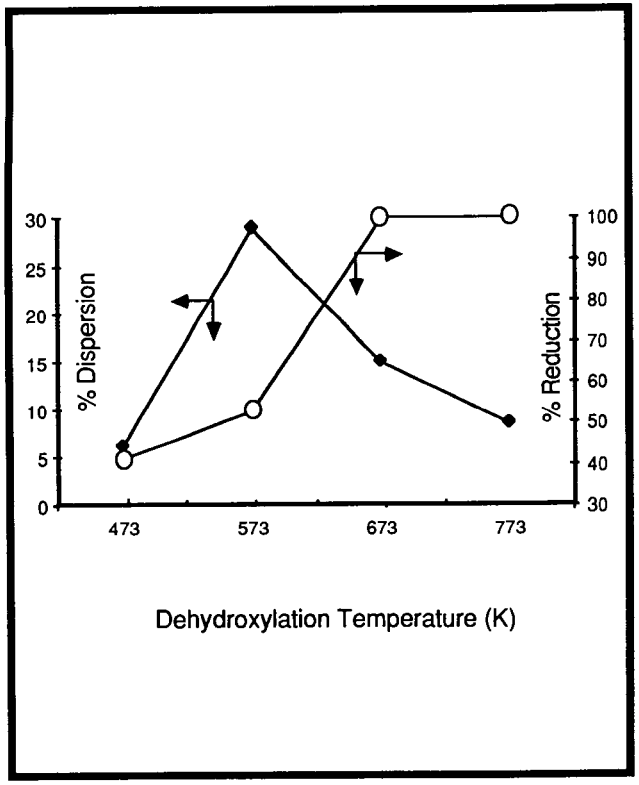

Figure 1. Reduction Temperature vs % Reduction and % Dispersion

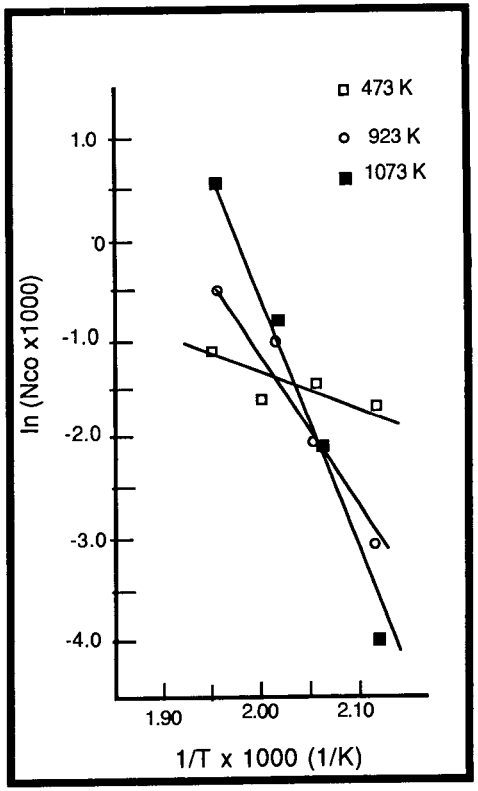

Figure 2. Effect of Dehydroxylation Temperature on Activation Energy for CO Hydrogenation

ZSM-5 SUPPORTED Fe AND Ru FROM $Fe_3(CO)_{12}$ AND $Ru_3(CO)_{12}$: STRUCTURE-ACTIVITY CORRELATIONS FOR SYNTHESIS GAS CONVERSION

Ellis B. Zuckerman and Gordon A. Melson

Department of Chemistry, Virginia Commonwealth University, Richmond, VA 23284.

INTRODUCTION

The goal of improving the efficiency and product selectivity in the conversion of synthesis gas ($CO + H_2$) to liquid hydrocarbons has resulted in efforts to develop bifunctional catalysts which combine a transition metal Fischer-Tropsch component with a zeolite support. This combination utilizes the carbon monoxide reduction and carbon chain propagation functions of the metal as well as the shape selectivity and dispersive effects of the zeolite. During the 1970's, workers at Mobil introduced the new synthetic zeolite ZSM-5 which possesses a unique channel structure. In its acid form H^+-ZSM-5 is capable of isomerizing hydrocarbons and converting reactive species to alkylbenzenes in the gasoline range. The combination of metal oxides with ZSM-5 and the impregnation of metal salts into ZSM-5 have resulted in catalysts which produce gasoline range hydrocarbons containing a high percentage of aromatics from synthesis gas (1-4). Metal particle size and metal-support interaction also affect product selectivity. It has been argued (5) that the former, in particular, is an important factor in controlling the molecular weight distribution of hydrocarbon products from synthesis gas conversion.

During the past decade, there has been considerable interest in the development of supported metal catalysts by the incorporation of metal carbonyls (6,7). It has been demonstrated that this approach, depending on the method of preparation, is a means of rendering the metal component in the form of highly dispersed, small particles on oxide and zeolite supports (8). It thus provides an alternative to conventional aqueous impregnation of metal salts which usually results in the formation of large metal particles and low dispersion. Furthermore, the method of preparation of zeolite-supported metal catalysts affects the interaction of the metal with the Brönsted acid sites of the zeolite. It has been demonstrated (9,10) that the introduction of transition metals by aqueous methods leads to ion-exchange between metal ions and protons and results in a partial depletion of the catalytically active Brönsted acid sites. It also seems reasonable to suspect that physical blockage of the zeolite channels causes an apparent loss of acidity after calcination or reduction if the metal species initially penetrates the zeolite channels.

The present goal of the research effort is to develop supported metal catalysts which are both efficient for synthesis gas conversion and selective for the production of aromatic and branched aliphatic hydrocarbons in the gasoline range. If the metal component can be introduced onto the zeolite particle without extensive penetration of the channel structure and subsequent ion-exchange at the Brönsted acid sites, an efficient bifunctional catalyst should be produced. Such a catalyst would convert reactive intermediates and high molecular weight hydrocarbons produced by the metal component directly on the particle. This would eliminate the necessity for physical transfer of the organic products from the metal site to the zeolite site that is necessary in a mixed metal-zeolite system. Additionally, the products of synthesis gas conversion may be different by using a bifunctional catalyst from those obtained with the mixed system. In order to achieve this goal, we have

prepared bifunctional ZSM-5 supported Fe and Ru in which the catalytic functions of the metal and the support are retained. This was accomplished by using an extraction method reported earlier (8) with $Fe_3(CO)_{12}$ and $Ru_3(CO)_{12}$ as the source of the metals. It was anticipated that this method would lead initially to a high degree of dispersion of the metal and that the metal would be restricted to the external surface of the zeolite. It was also anticipated that changes in the metal particle size could be induced by subsequent pre-treatment, e.g. calcination. We report here evaluation of some Fe/ZSM-5 and Ru/ZSM-5 catalysts for their activity and product selectivity in the conversion of synthesis gas, and draw conclusions concerning catalyst structure-activity relationships.

EXPERIMENTAL

ZSM-5 (SiO_2/Al_2O_3 = 32) was received in the NH_4^+ form and was calcined under vacuum at 400°C for 3 h to obtain the acid form. Ru/ZSM-5 and Fe/ZSM-5 materials were prepared by an extraction technique (8) using $Ru_3(CO)_{12}$ (Strem Chemical) and $Fe_3(CO)_{12}$ (Alfa, Ventron Division) with cyclohexane as the solvent. All of the catalysts discussed in this report have metal loadings of approximately 3% by weight. Portions of the as-prepared (AP) catalysts were calcined in air at 400°C (H-400) in order to induce an increase in the particle size of the metal component.

The materials have been characterized by infrared spectroscopy (IR), X-ray powder diffractometry (XRPD), X-ray photoelectron spectroscopy (XPS), ion scattering spectrometry (ISS), Mossbauer spectroscopy (for Fe), and pyridine chemisorption studies.

For catalytic evaluation, the catalysts were dispersed in silica (200-300 mesh), and reduced under flowing H_2 at 20.4 atm. Fe catalysts were reduced at 450°C for 20 h whereas Ru catalysts were reduced at 400°C for 12-15 h. Following reduction, Fe catalysts underwent a carbiding step in flowing synthesis gas (H_2/CO = 1) at 6.8 atm and 250°C for 20 h. Evaluation was carried out by using a fixed-bed, continuous flow microreactor. The reaction conditions consisted of a pressure of 20.4 atm of synthesis gas (H_2/CO = 1) and reactor temperatures of 280°C and 300°C. For studies designed to determine the effects of space velocity, the flow rate was adjusted so that the WHSV was established at 990, 2085, and 3135 cc/g.h. In studies which did not involve space velocity comparisons, the WHSV was set to 2090 cc/g.h. Each evaluation at a given set of conditions was allowed to proceed for a period of 48 h during which the liquid products were collected in an ice-cooled trap which followed a heated trap (180°C) for the collection of high molecular weight products. The gaseous effluent was analyzed by using a gas chromatograph which is an integral part of the reactor system. The liquid product was separated into oil and aqueous fractions; the analysis of the oil was accomplished primarily by a quantitative infrared method described earlier (11). Additional supporting information such as the carbon number distribution and the degree of paraffin branching were obtained by capillary GC and ^1H NMR spectroscopy respectively.

RESULTS AND DISCUSSION

Characterization

The results of characterization studies have been reported earlier (12); however, because our objective is to enable correlations between the nature of the

catalysts and the results of catalytic evaluation to be drawn, some conclusions are presented here.

In XRPD studies of both Fe/ZSM-5/AP and Ru/ZSM-5/AP, no evidence for the presence of the metal component was detected. This suggests that the metals are highly dispersed with a particle size of <50 Å and/or that the metal species are non-crystalline. Calcination of the AP materials induces the formation of bulk α-Fe_2O_3 and RuO_2, which have been detected by XRPD. Depth profile studies of both Fe/ZSM-5/AP and Ru/ZSM-5/AP, by ISS, reveal a rather large initial M/Si ratio which rapidly decreases with sputtering. We have interpreted this observation to indicate that the metal component is restricted to the external surface of the zeolite particles (by virtue of the relative sizes of the metal clusters and the diameter of the ZSM-5 channels) and is highly dispersed, perhaps monodispersed at low loadings, on that surface. The ISS depth profiles of calcined materials consist of small initial M/Si ratios which increase slightly with sputtering time and suggest the formation of large metal oxide particles. XPS studies of Fe/ZSM-5/AP and Ru/ZSM-5/AP reveal the presence of metal oxides, but are inconclusive regarding the exact nature of the species. Calcined materials clearly contain the metals in the form of Fe_2O_3 and RuO_2, and the trends observed with sputtering of AP and calcined samples parallel those observed in ISS studies. Infrared studies of chemisorbed pyridine were conducted as a probe to determine whether channel blockage and/or chemical interaction between the metal and Brönsted acid sites in the zeolite channels had occurred as a result of metal loading or subsequent calcination or reduction. No indication of such interactions was observed.

We have concluded from the results of characterization of Fe/ZSM-5 and Ru/ZSM-5 materials that both contain the metal component in a highly dispersed state on the external surface of the zeolite particles. Calcination, and to a lesser extent reduction, both induce the formation of large particles of the oxides or metals which remain excluded from the zeolite channels. The restriction of the metal to the external surface of the of the ZSM-5 particles should result in the retention of Bronsted acidity and permit access of reactants to the interior of the zeolite.

Catalytic Evaluation

Fe/ZSM-5/AP, Ru/ZSM-5/AP and Ru/ZSM-5/H-400 catalysts have been evaluated for their efficiency and selectivity in synthesis gas conversion. The three catalysts discussed here have been compared in order to investigate effects of the choice of transition metal and the effects which result from calcination of the Ru/ZSM-5 catalyst prior to evaluation. Furthermore, the effect of varying the space velocity at different temperatures for Fe/ZSM-5/AP and Ru/ZSM-5/AP was examined.

Comparison of the data in Tables 1 and 2 reveals a number of similarities regarding the effects of space velocity and temperature on the two catalysts. For both as-prepared catalysts, the percentages of H_2 and CO conversion generally decrease at higher space velocities while increasing at higher temperature. The two catalysts exhibit a decreasing activity for the water gas shift reaction at higher space velocity and an increasing activity for the shift reaction at higher temperature. Analysis of the liquid products by a quantitative IR technique reveals an enhanced selectivity for aromatic hydrocarbons coupled with an apparent consumption of olefins and oxygenated species at higher temperature and lower space velocity. The efficiencies of synthesis gas conversion, the shift reaction, and the conversion of Fischer-Tropsch products and intermediates by the acidic and shape selective

TABLE 1. RESULTS FROM CATALYTIC EVALUATION OF A 3% Ru/ZSM-5/AP CATALYST

WHSV ($\frac{cc}{g \cdot h}$)	CATALYST TEMP. (°C)	% CONVERSION		REACTOR EFFLUENT DISTRIBUTION (wt. %)					HYDROCARBON PRODUCT DISTRIBUTION (wt. %)						LIQUID PRODUCT DISTRIBUTION (wt. %)			
		H_2	CO	CO	H_2	CO_2	H_2O	HC	CH_4	C_2	C_3	C_4	C_5^+	WAX	AR	OL	SAT	OX
990	280	92	51	54	1	4	21	20	23	5	7	13	52	0	27	7	63	3
2085		70	31	64	2	2	18	14	27	5	10	17	41	0	21	11	64	4
3135		49	23	71	3	2	14	10	33	7	12	13	35	0	18	12	65	5
990	300	89	55	47	1	15	17	20	49	11	13	10	18	0	30	3	65	2
2085		75	37	60	2	6	17	16	40	8	11	17	23	0	26	5	66	3
3135		69	35	62	2	4	17	15	43	8	11	10	28	0	21	6	70	3

TABLE 2. RESULTS FROM CATALYTIC EVALUATION OF A 3% Fe/ZSM-5/AP CATALYST

WHSV ($\frac{cc}{g \cdot h}$)	CATALYST TEMP. (°C)	% CONVERSION		REACTOR EFFLUENT DISTRIBUTION (wt. %)					HYDROCARBON PRODUCT DISTRIBUTION (wt. %)						LIQUID PRODUCT DISTRIBUTION (wt. %)			
		H_2	CO	CO	H_2	CO_2	H_2O	HC	CH_4	C_2	C_3	C_4	C_5^+	WAX	AR	OL	SAT	OX
990	280	37	37	64	5	12	12	7	37	19	16	16	12	0	47	<1	51	<1
2085		28	17	75	5	6	7	7	33	17	21	12	17	0	26	1	72	1
3135		26	16	75	5	7	7	6	32	17	12	15	24	0	19	3	77	1
990	300	46	49	51	4	26	6	13	55	20	11	7	7	0	47	0	53	0
2085		41	31	64	4	15	6	11	43	17	9	18	13	0	48	<1	51	0
3135		42	32	62	4	16	7	11	35	17	15	12	21	0	33	1	66	0

zeolite are known to be influenced by temperature and the residence time of the reactants and products in the catalyst bed. In this respect, the trends mentioned above are not surprising.

Of greater interest is the effect of the choice of metal on the overall behavior of the catalysts. Inspection of Tables 1 and 2 reveals a number of differences in the efficiencies and product selectivities. These serve to distinguish the two catalysts on the basis of the metal component in spite of the presence of the ZSM-5 which is certainly a factor in controlling the nature of the product distribution and may also exert an influence on the properties of the metals. For example, the Ru/ZSM-5/AP catalyst showed higher activity than Fe/ZSM-5/AP for synthesis gas conversion. This observation is consistent with the results reported by Vannice (13) who demonstrated that Ru has the greatest specific activity among Group VIII metals for the conversion of CO/H_2 mixtures to hydrocarbons. Furthermore, Ru is well known to be the most selective of the Group VIII metals for higher molecular weight hydrocarbons, and this is also evident in the present study when the relative quantities of C_{5+} hydrocarbons are compared. This same selectivity, on the part of Ru, for species of higher carbon number may also account for the smaller aromatic content of the oil from Ru/ZSM-5/AP compared to that from Fe/ZSM-5/AP. The higher molecular weight products are more likely to be cracked and isomerized by the zeolite whereas lighter products such as C_3 and C_4 olefins are more favorable for conversion to aromatics. If this is the case, then the greater selectivity of Fe for lighter hydrocarbons could explain the greater aromaticity of the oil product from Fe/ZSM-5/AP. Consistent with this explanation is the fact that the normalized ratio of methyl to methylene hydrogen in the aliphatic fraction, obtained from ^1H NMR spectra, is large and is indicative of a significant degree of branching. This suggestion is not meant to preclude other factors which may influence the liquid product distribution. For example, we have considered the possibility that Fe might be more favorable for the formation of the correct chemical species (olefins and alcohols) for conversion to alkylbenzenes.

It should also be noted that the oil product from Ru/ZSM-5/AP contains a substantially larger fraction of olefins and oxygenates than that from Fe/ZSM-5/AP. At first glance this would appear to refute the statement above concerning correct chemical species for aromatization. However, it must be mentioned that the olefins detected in all of these oils are trans and branched α olefins which, unlike normal α olefins, are not considered to be primary products of synthesis gas conversion. The presence of these species may result from the activity of the zeolite. The oxygenated fraction consists of aldehydes and acids but no alcohols. Kellner and Bell (14) have reported that acetaldehyde was the only oxygenate produced over a Ru/SiO_2 catalyst.

Finally, it is apparent that the Fe catalyst is more active for the water gas shift reaction than the Ru catalyst. This is in agreement with the fact that the shift reaction is faster over Fe than over Ru, Co or Ni (15).

Comparison of the results of evaluation of the Ru/ZSM-5/AP and the Ru/ZSM-5-/H-400 catalysts reveals some striking differences in activity and product selectivity. It should be mentioned, before further discussion, that while the activity and selectivity of the AP catalyst were stable for the 48 h duration of each evaluation period, the H-400 catalyst exhibited significant deactivation over the first 24 h at 280°C. Consequently it is unreasonable to treat the results of the

H-400 evaluation as if they were representative of a behavior which persisted for 48 h; nevertheless, some general comparisons of the two catalysts can be made.

At 280°C and a space velocity of 2090 cc/g.h the percentage conversion of CO and H_2 was much lower over the H-400 catalyst than over the AP catalyst. Furthermore, the selectivity for higher molecular weight hydrocarbons is greater with the H-400 catalyst. Both of these observations may be related to a metal particle size effect as a result of prior calcination. The liquid hydrocarbon product, like that produced over the AP catalyst, contained substantial aromatic and branched aliphatic fractions.

CONCLUSIONS

Bifunctional catalysts consisting of Fe and Ru supported on ZSM-5 have been prepared by an extraction technique using metal cluster carbonyls. As anticipated, these precursors of the supported metal component were excluded from the ZSM-5 channels which have a diameter significantly smaller than that of the metal clusters. Evidence for this restriction was obtained from studies of the catalysts by ISS, XPS and pyridine chemisorption. These studies revealed that the metal was present as highly dispersed metal particles on the external surface of the ZSM-5 particles and that obstruction of the zeolite channels and extensive interaction with Bronsted acid sites did not occur. As a result, these materials were found to be efficient bifunctional catalysts for synthesis gas conversion. The metal component produces hydrocarbon and oxygenated products and intermediates which are further converted by the zeolite to mixtures containing substantial fractions of aromatic and branched hydrocarbons.

Calcination of a Ru/ZSM-5 catalyst prior to evaluation results in an increase in the average metal particle size. When evaluated, this catalyst exhibits less activity, but greater selectivity for higher molecular weight products when compared to the as-prepared catalyst. However, rapid deactivation of the calcined catalyst occurred. Although the reason for this is not clear at the time of writing, this behavior is being investigated.

The product distributions obtained by synthesis gas conversion over the above bifunctional catalysts will be compared with those obtained from catalysts consisting of the metal component dispersed on a conventional oxide support as well as from these catalysts physically mixed with ZSM-5. Correlations concerning the nature of the catalysts and differences observed among the various product distributions will be drawn, and mechanistic considerations will be presented.

ACKNOWLEDGEMENTS

The authors wish to thank J.M. Stencel and J.R. Diehl of the U.S. Department of Energy, Pittsburgh Energy Technology Center, for assistance in obtaining some of the characterization data (XPS and ISS) and the Department of Energy for financial support.

REFERENCES

1. Chang, C.D., Lang, W.H. and Silvestri, A.J., J. Catal., 56, 268 (1979).

2. Caesar, P.D., Brennan, J.A., Garwood, W.E. Ciric, J., J. Catal., 56, 274 (1979).

3. Rao, V.U.S., Gormley, R.J., Hydrocarbon Process., 59 (11), 139 (1980).

4. Huang, T.J., Haag, W.O., in "Catalytic Activation of Carbon Monoxide", ACS Symposium Series, Vol. 152, Peter C. Ford (ed.), American Chemical Society, Washington, D.C., 1980.

5. Nijs, H.H. and Jacobs, P.A., J. Catal., 65, 328 (1980).

6. Zwart, J. and Snel, R., J. Mol. Catal., 30, 305 (1985), and references therein.

7. Phillips, J. and Dumesic, J.A., Applied Catal., 9, 1 (1984), and references therein.

8. Crawford, J.E., Melson, G.A., Makovsky, L.E., Brown, F.R., J. Catal., 83, 454 (1983).

9. Rhee, K.H., Brown, F.R., Finseth, D.H., Stencel, J.M., Zeolites, 3, 344 (1983).

10. Shamsi, A., Rao, V.U.S., Gormley, R.J., Obermeyer, R.T., Schehl, R.R., Stencel, J.M., Ind. Eng. Chem., Prod. Res. Dev., 23, 513 (1984).

11. Zuckerman, E.B., Melson, G.A., Finseth, D.H., 35th Southeastern Regional Meeting of the American Chemical Society, Charlotte, NC (1983).

12. Zuckerman, E.B. and Melson, G.A., Abstracts, 191st Annual Meeting of the American Chemical Society, New York, NY (1986).

13. Vannice, M.A., J. Catal., 37, 449 (1975).

14. Kellner, C.S. and Bell, A.T., J. Catal., 71, 288 (1981).

15. Anderson, R.B., "The Fischer-Tropsch Synthesis," Chapter 5. Academic Press, Orlando, 1984.

CO HYDROGENATION ON ZEOLITE-SUPPORTED Ru: EFFECT OF NEUTRALIZING CATIONS

Rachid Oukaci, Jeffrey C.S. Wu, James G.Goodwin,Jr.

Department of Chemical & Petroleum Engineering,
University of Pittsburgh, Pittsburgh, PA 15261

INTRODUCTION

Previous results for zeolite-supported Ru prepared by ion exchange suggested a possible effect of the nature and concentration of the neutralizing cations in the zeolite on the catalytic properties of the metal (1). However, the interpretation of these results was complicated by the fact that a series of zeolites with different Si/Al ratios was used.

The present study was undertaken to investigate systematically the influence of the nature of alkali neutralizing cations on CO hydrogenation over ion-exchanged Y- zeolite-supported ruthenium catalysts.

EXPERIMENTAL

A series of RuY catalysts was prepared from NH_4Y, LiY, NaY, KY, RbY, and CsY zeolites by ion-exchange with $Ru(NH_3)_6Cl_3$. After decomposition under vacuum and reduction in hydrogen at 673 K, the resulting Ru catalysts were characterized by atomic absorption and chemisorption of hydrogen and carbon monoxide.

CO hydrogenation was carried out in a tubular microreactor where the prereduced catalyst (0.25 g) was first rereduced in a hydrogen stream at 673 K for two hours before cooling to reaction temperature. The reaction was carried out at atmospheric pressure and 483-573 K using 1:1 mixture of H_2 and CO. A sample of the effluent gas was analyzed on-line by gas chromatography after five minutes of reaction. The hydrogen bracketing technique was used to maintain a clean metallic surface.

RESULTS AND DISCUSSION

Catalytic Activity and Product Distribution

Hydrogen chemisorption measurements were used to calculate the Ru dispersion (Table I) as described in (2). Based on both H_2 and CO chemisorption results it was concluded that the metal dispersions were high and similar in the various Y-zeolites, except for RuHY.

Table I compares the turnover frequencies (TOF) at 523 K for CO conversion on the various catalysts, as well as the product distributions. No significant effect of the nature of the neutralizing alkali cations on TOF nor on the selectivity for CH_4 and the chain growth probability were observed. Having similar metal loadings, the concentrations of the structural hydroxyl groups, formed during the reduction of the ruthenium ions in LiY NaY, KY, RbY, and CsY, should be comparable in all these catalysts.

TABLE I

CATALYTIC PROPERTIES OF ZEOLITE-SUPPORTED RU CATALYSTS AT 523 K

Catal.	Load. (wt%)	Disp. (%)	TOF ($s^{-1}x10^3$)	Selectivity (wt%) C_1	C_2	C_3	C_4	C_5	C_6
RuHY	3.8	30	40.5	34.3	13.7	19.1	17.1	12.3	3.5
RuLiY	3.4	53	10.7	33.4	14.3	21.8	17.6	11.8	1.1
RuNaY	3.8	67	6.9	32.7	14.0	21.5	17.0	10.9	3.9
RuKY	3.2	52	8.0	30.7	13.7	23.5	15.8	11.0	5.2
RuRbY	3.6	49	14.1	33.5	14.4	22.0	15.3	9.7	5.1
RuCsY	3.7	56	12.4	36.1	13.2	21.6	15.1	9.8	4.2

It is generally accepted that for alkali cation zeolites, exchange of sodium ions for smaller or larger cations produces a change in the electostatic field inside the zeolites, and hence a change in the strength of their acid sites (3-4). However one possible reason why these different acid sites have no significant effect on the catalytic properties of the metal is the "neutralization" of these sites by olefins adsorbed on them (5) , thus interrupting any possible interactions that these acid sites might have with the metal particles. Such interactions have been often suggested to be responsible for the observed changes in adsorption properties of zeolite-supported metals (6-7). The higher activity observed for RuHY is probably due in large part to the fact that the Ru particles were significantly larger in this catalyst.

The apparent activation energy for CO conversion, E_a, varied with the neutralizing cation employed. A plot of E_a versus the crystal ionic radius of the initial charge balancing cations suggests that Ru is more uniformly distributed throughout the zeolite crystallites for the small cation zeolites. In the larger cation zeolites, Ru is probably preferentially distributed in the external shell of the zeolite crystallites. Although this uniform versus shell distribution, if true, does not seem to affect the % dispersion of the reduced Ru, but it affects the activation energy of reaction by introducing diffusion limitations on reactants and products for the zeolite catalysts having smaller neutralizing cations. This is further confirmed by the non-linearity of the Arrhenius plots for these catalysts.

Secondary Olefin Transformations

The nature of the neutralizing cations in Y-zeolites was found to have a strong influence on the olefin-to-paraffin ratios ($C_3^=/C_3^-$), regardless of whether the comparison was made at constant temperature (Figure 2) or constant CO conversion .The $C_3^=/C_3^-$ ratio was highest where the larger alkali cations had been exchanged into the zeolite and followed the sequence: Cs ~

Rb > K > Na > Li ~ H. The variation in the amount of isobutane in the C_4-fraction is also included in Figure 2 as this reflects the secondary acid-catalyzed reactions which were enhanced in the order: Cs ~ Rb < K << Na < Li << H. The results listed in Table II show that at 523 K RuHY gave 53% isobutane (based on the total amount of C_4). When this catalyst was exchanged after reduction with a dilute solution of K_2CO_3, in order to replace H^+ by K^+, the isobutane was no longer obtained and the propene-to-propane ratio increased to 16.9. On the other hand, RuRbY yielded only very small quantities of isobutane, but, when 0.2 g of HY was added at the tail end of the reactor bed in a separate layer, the isobutane content of the C_4-fraction increased to 30%, and the $C_3^=/C_3^-$ ratio dropped from 6.4 to 4.1.

These results provide strong evidence that the hydrocarbon products of CO hydrogenation over supported ruthenium catalysts are mainly, if not totally, desorbed as olefins which can then undergo secondary reactions on the acid sites or to a lesser extent hydrogenation on the metal sites.

TABLE II

EFFECT OF ACIDITY ON OLEFIN AND ISOBUTANE SELECTIVITIES

Catalyst	Propene/Propene Ratio	Isobutane (wt% in C_4)
RuHY	1.1	53.0
RuHY(K)[a]	16.9	0.0
RuRbY	6.4	1.4
RuRbY+HY[b]	4.1	30.6

(a) RuHY treated in 0.1 N K_2CO_3 solution after reduction.
(b) RuRbY and HY in separate layers.

The most important acid-catalyzed reactions of olefins are isomerization, oligomerization, disproportionation, hydrogenation by hydride transfer, and coke formation. The rate of these reactions are influenced by the concentration and the acid strength of the hydroxyl groups present in the zeolite (8). The decrease of the olefin-to-paraffin ratio with decreasing cation radius, paralleled by an an increasing acidity strength, may be partly explained by the enhancement of hydrogen transfer reactions catalyzed by acid sites. Several studies (8-10) of acid-catalyzed olefin reactions have demonstrated that the interaction of acidic hydroxyl groups with adsorbed olefins is accompanied by olefin oligomerization. At temperatures higher than 370 K, the olefin oligomers decompose by a disproportionation mechanism to produce gaseous paraffins and some polyene species which remain on the zeolite (8). The primary olefinic products may be hydrogenated on the acid sites, not only by hydrogen resulting from the oligomer decomposition, but also by hydrogen supplied by spillover from the metal to the support. However, the effect of mass transfer

limitations on the propene-to-propane ratio due to a uniform versus shell distribution of Ru in the zeolite cannot be ruled out. The increase in residence time of olefins following their formation may result in an increased probability for readsorption on the metal sites and hydrogenation.

It has also been shown that the higher the concentration and strength of the acid sites in a zeolite, the more branched the olefin oligomers (8). Thus, decomposition of the oligomers formed on the more acidic zeolites would result in the formation of more isoparaffins. The trend in selectivity for isobutane suggests that the nature of the alkali cations modify the strength of the acid sites. A possible effect of diffusion and steric factors may also account for this trend in selectivity for isobutane.

CONCLUSION

The nature of the charge balancing cations in zeolites can have a marked effect on the catalytic properties of ruthenium for CO hydrogenation in ion-exchanged zeolite-supported Ru catalysts. Although it has hardly any influence on the specific activity of the catalysts or on the overall chain growth probability, the nature of the neutralizing cations has a pronounced effect on the selectivities for olefins and branched hydrocarbons. Variations in the strength of the acid sites with the nature of these cations as well as mass transfer limitations apparently play a major role in shaping the olefin and isoparaffin selectivities.

LITERATURE CITED

(1) Chen, Y.W., Wang, H.T., and Goodwin, J.G., Jr., J. Catal. 85, 499 (1984).
(2) Goodwin, J.G., Jr., J. Catal. 68, 227 (1981).
(3) Barthomeuf, D., in "Catalysis by Zeolites", (B. Imelik et al. eds.), p.55, Elsevier Sci. Publ. Co., Amsterdam, 1980.
(4) Ward, J.W., J. Catal. 10, 34 (1968).
(5) Romannikov, V.N., Ione, K.G., and Pedersen, L.A., J. Catal. 66, 121 (1980).
(6) Arai, H., Nippon Kagaku Kaishi 192 (1982), Chem. Abstr. 96, 125964f (1982).
(7) Blackmond, D.G., and Goodwin, J.G., Jr., J. Chem. Soc., Chem. Comm., 125 1981).
(8) Datka, J., in "Catalysis by Zeolites", (B. Imelik et al. eds.) p. 121, Elsevier Sci. Publ. Co., Amsterdam, 1980.
(9) Venuto, P.B., Hamilton, L.A., and Landis, P.S., J.Catal. 5, 484, (1966).
(10) Langner, B.E. J. Catal. 65, 416 (1980).

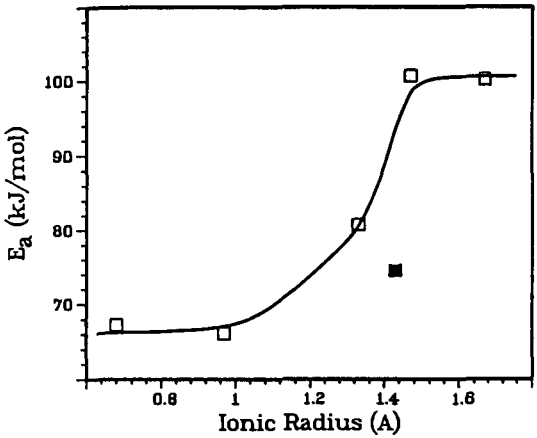

Figure 1. Variation in E_a with neutralizing cation radius; (■) RuHY.

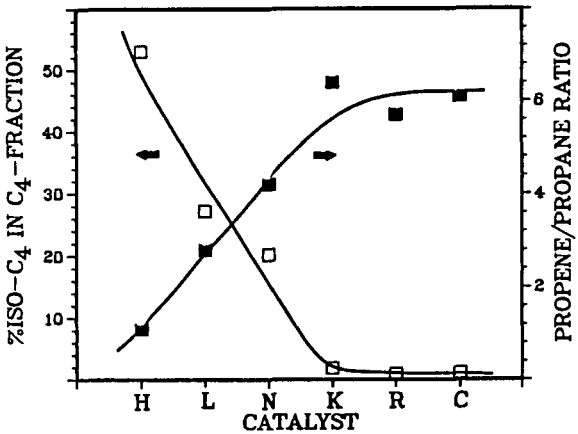

Figure 2. Effect of neutralizing cation on olefin fraction and isobutane formation; Catalysts: (H) RuHY, (L) RuLiY, (N) RuNaY, (K) RuKY, (R) RuRbY, (C) RuCsY.

Synthesis and CO Hydrogenation Activity of
Ruthenium Zeolite A

Joseph A. Rossin and Mark E. Davis

Department of Chemical Engineering
Virginia Polytechnic Institute and State University
Blacksburg, Virginia 24061

Ruthenium zeolite A was synthesized by several techniques from either $RuCl_3$ or $[Ru(NH_3)_5Cl]Cl_2$. An example of our synthesis procedure with $RuCl_3$ is described below. First, zeolite A is synthesized in the presence of $RuCl_3$ by simple addition of the ruthenium salt to a standard zeolite A synthesis gel. The resulting ruthenium-zeolite A was crystallized in approximately 2 hours under autogeneous pressure at 95°C. Next, a portion of the ruthenium-zeolite A was added to another zeolite A synthesis gel to serve as a "carrier" of ruthenium and as a "seed" for the synthesis. Ruthenium-zeolite A was recovered from the "seeded" synthesis and exchanged with $CaCl_2$ for the two reasons: (1) to remove exchangeable ruthenium from the surface of the zeolite (intrazeolitic ruthenium will be too large to exchange out of the α-cage), and (2) to place the zeolite A in its most stable form (the calcium form of zeolite A is more stable than NaA to attack by water at elevated temperatures). This RuCaA will be denoted catalyst B. For comparison, a CaA was ion exchanged with aqueous $RuCl_3$ and this RuCaA will be denoted catalyst A.

Table 1 shows the X.P.S. and bulk chemical analysis (C.A.) data for catalysts A and B. Notice that the X.P.S./C.A. ratio for ion exchanged RuCaA is 14.7 while that of our synthesized RuCaA is 0.22. Since the X.P.S./C.A. ratio gives an indication of the amount of ruthenium in the superficial region relative to that in the bulk, it is obvious that catalyst B contains intrazeolitic ruthenium.

Catalyst B was tested for CO hydrogenation activity. The catalyst was heated to 150°C in flowing He for several hours to partially dehydrate the zeolite before reduction. Next, this material was exposed to flowing H_2 at 275°C, 2.25 atm. in order to reduce the ruthenium. Finally, 1:1 $CO:H_2$ was contacted with the catalyst at 255°C, 2 atm. (2.1 g catalyst, F = 6.5 ml/min).

Figure 1 shows the start-up behavior of catalyst B. Notice that the production of all hydrocarbons other than C_5 proceeds through a maximum. Also, these maxima do not occur at the same time. Figure 2 illustrates the hydrocarbon product distribution for over 10 hours of contact with syngas. In no case were branched hydrocarbons or hydrocarbons of C_8 (only traces of C_6 and C_7) or greater observed in the product stream (see Table 2 for an example of an exact product distribution).

X-ray diffraction analysis of catalyst B following reaction showed no loss in crystallinity, however, a 22% loss in pore volume (by O_2 adsorption) was observed. The loss in pore volume could be due to adsorbed hydrocarbons, structural rearrangements of the zeolite, or a combination of both factors. The FTIR spectrum of catalyst B after exposure to reaction conditions did show new bands in the zeolite framework region. These alterations suggest that changes in the zeolite have occurred over the course of the reaction. X.P.S. analyses of catalyst B: (i) as synthesized, (ii) after H_2 exposure, and (iii) after reaction show that the ruthenium was reduced by the H_2 and that during the course of the reaction the ruthenium did not migrate to the surface of the zeolite.

Table 1

XPS and Chemical Analysis Data for RuCaA

Catalyst	wt.%Ru	Ru/Si			Preparation
		XPS	CA	XPS/CA	
A	1.98	0.534	0.0363	14.7	exchange
B	1.53	0.006	0.0276	0.22	synthesis

Table 2

Product Distribution for RuCaA (Catalyst B).

T = 255°C, P = 2 atm, $CO:H_2$ (1:1), t = 3.5 h

Hydrocarbon	Mole Percent	Weight Percent
Methane	66.09	36.17
Ethane	2.00	2.19
Ethylene	2.00	2.19
Propane/Propylene	13.30	21.84
1-Butene	0.43	0.95
n-Butane	2.98	6.52
t-2-Butene	7.08	15.15
c-2-Butene	3.65	7.80
n-Pentane	2.48	6.80

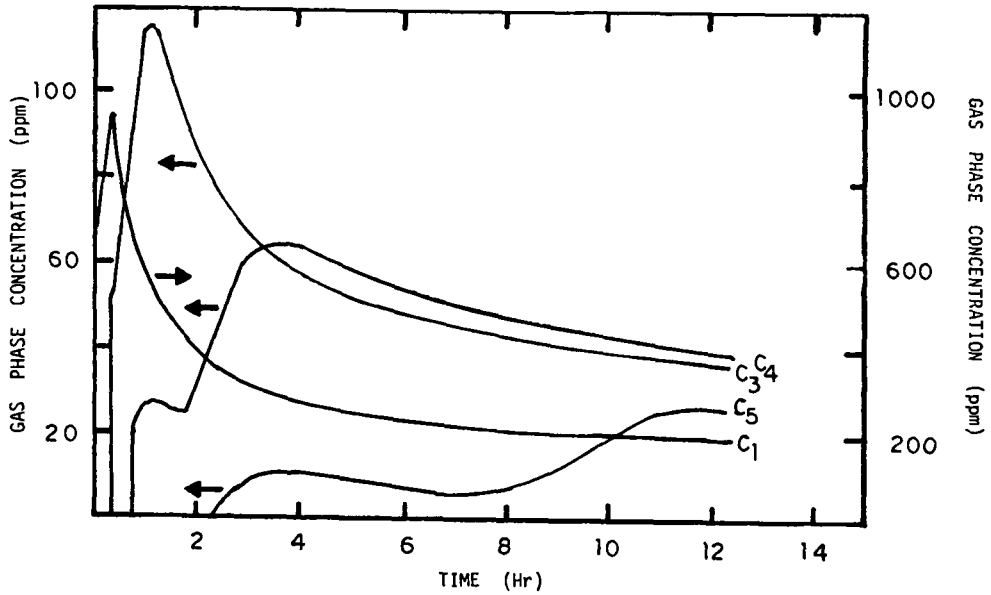

Figure 1: Hydrocarbon Product Start-up Behavior for Catalyst B at 255 C. All hydrocarbons were linear.

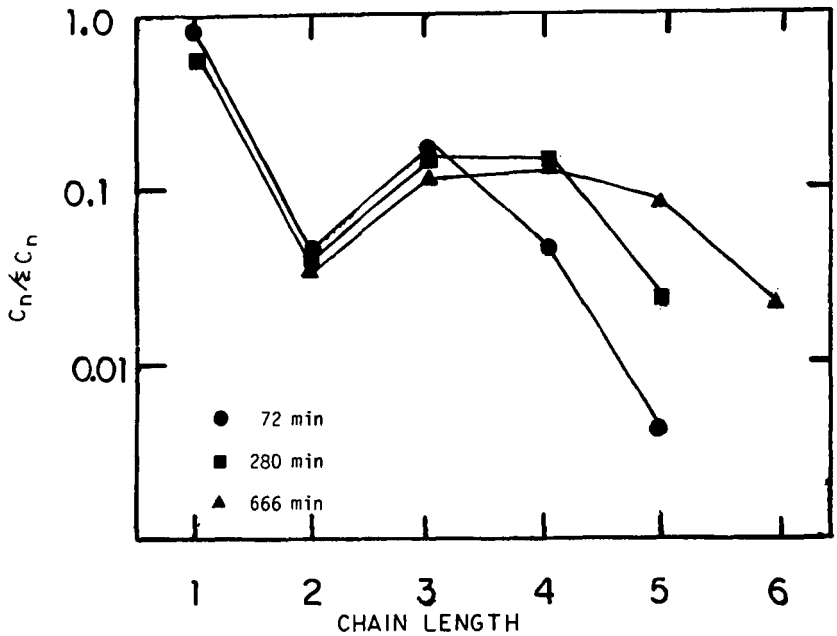

Figure 2: Hydrocarbon Product Distribution for Catalyst B at 255 C. All hydrocarbons were linear.

CATALYTIC CONVERSION OF SYN GAS WITH PEROVSKITES

J. A. Broussard and L. E. Wade

Celanese Research Company, Summit, NJ, 07901

INTRODUCTION

Perovskites, mixed metal oxides of the general formula ABO_3, have been examined as catalysts for conversion of syn gas to oxygenated organic chemicals. Several of these perovskites have been found to provide moderate to high selectivities to oxygenated organics, particularly methanol and C2OX (acetic acid, acetaldehyde, and ethanol).

RESULTS AND DISCUSSION

CATALYST EVALUATIONS

The perovskites were prepared by co-precipitation with subsequent calcination in air to form pure crystalline phases. The resulting powders (pelleted with SiO_2) were evaluated in a U-tube vapor phase reactor. Catalysts were evaluated with 2:1 H_2:CO at 1000 psig. Conclusions are based on results obtained in the CO conversion range of 1-20% (usually 1-10%). Results of catalyst evaluations are presented in Tables I-III.

Perovskites of La with late transition metals and other closely related perovskites were evaluated as syn gas conversion catalysts. The maximum oxygenate selectivities obtained with $LaCoO_3$, $LaNiO_3$, and $LaFeO_3$ were in the range of 24-33%. No oxygenated products were observed with $LaMnO_3$. $LaCoO_3$ and $LaNiO_3$ underwent runaway methanation, but $LaFeO_3$ and $LaMnO_3$ did not. Co, Ni, and Fe are best known as catalysts for producing hydrocarbons (1, 2).

Six substituted derivatives of the above ternary perovskites were evaluated in hopes of finding positive synergism. $LaNi_{0.5}Fe_{0.5}O_3$ and $LaMn_{0.5}Ni_{0.5}O_3$ exhibited positive synergism (i. e. higher oxygenate selectivity than the average for the related ternary perovskites). $LaNi_{0.5}Co_{0.5}O_3$, $LaFe_{0.5}Co_{0.5}O_3$, $LaMn_{0.5}Co_{0.5}O_3$, and $LaMn_{0.5}Fe_{0.5}O_3$ exhibited either no synergism or negative synergism when compared to the related ternary perovskites.

Partial substitution of La with Ce and Sr was examined as a means of modifying the catalytic behavior of $LaCoO_3$. The maximum oxygenate selectivities obtained with $La_{0.8}Ce_{0.2}CoO_3$ and $La_{0.8}Sr_{0.2}CoO_3$ (7-8%) were much lower than the results obtained with the parent system.

$LaCo_{0.5}Ru_{0.5}O_3$, $LaNi_{0.5}Ru_{0.5}O_3$, and $LaFe_{0.5}Ru_{0.5}O_3$ were evaluated to determine the effect of partial substitution of Ru for Co, Ni, and Fe and the selectivity patterns typical of Ru in these perovskite lattices. The maximum oxygenate selectivities obtained with these materials (3-14%) are much lower than those obtained with related ternary perovskites. Ru is apparently a poor catalyst for converting syn gas to oxygenates which is consistent with reports that Ru is used in Fischer Tropsch synthesis for producing higher hydrocarbons (2).

$LaNi_{0.5}Ti_{0.5}O_3$ and $LaFe_{0.5}Ti_{0.5}O_3$ were evaluated to determine the catalytic effects of partial substitution of the B cations by Ti(IV). Both of these materials provided significantly lower oxygenate

selectivities than the related ternary perovskites.

$LaCu_{0.5}Ti_{0.5}O_3$ and $LaCu_{0.5}Mn_{0.5}O_3$ were evaluated to determine the catalytic behavior of Cu in a perovskite lattice. Both materials exhibited high methanol selectivities (37-38%, maximum). These results suggest that Cu is the catalytic metal in these systems, probably in reduced form. Cu is used in commercial methanol synthesis catalysts.

$NdNiO_3$, $NdFeO_3$, and $NdCoO_3$ were evaluated to determine the catalytic effects of replacing La with closely related Nd. The maximum oxygenate selectivities obtained with these perovskites (0-10%) are much lower than those obtained with the analogous La perovskites (24-33%).

Perovskites of barium with platinum group metals were also evaluated as catalysts for syn gas conversion. These materials were prepared by Professor B. L. Chamberland (U. Conn.). Materials prepared by low temperature calcination (< 400°C) were amorphous by XRPD. Materials prepared by re-calcination at higher temperatures (≥ 600°C) were pure crystalline phases by XRPD.

High oxygenate selectivities (almost exclusively methanol) were obtained with $BaRhO_3$ and $BaPtO_3$ (maximum, 62% and 54%, respectively). Maximum oxygenate selectivities obtained with $BaIrO_3$ and $BaRuO_3$ were 39% and 14%, respectively. High methanol selectivities have been reported for the related $LaRhO_3$ by Bartley (3) and by Watson and Samorjai (4). Supported Pt catalysts have been reported to be selective catalysts for methanol synthesis (2). Supported Ir has been reported as catalysts for both methanol and hydrocarbon synthesis (2). Ru Fischer Tropsch catalysts (2) and our own La-Ru perovskites are mainly hydrocarbon producing catalysts.

CATALYST CHARACTERIZATION

Catalysts were characterized to determine the crystalline phase purity of starting materials, to determine if perovskite phases were preserved or decomposed (by reduction) under reaction conditions, and to determine the nature of catalytic sites in these materials. Catalyst samples were characterized by XRPD, EXAFS, XANES, AND ESCA. Results are presented in Table IV.

The "A" cations in these perovskites (La(III), Nd(III), and Ba(II)) are stable to reduction and catalytically inactive under these conditions. Therefore, the stability of these crystalline lattices to reductive decomposition and the catalytic activity of these materials depends on the late transition metal "B" cations.

The ternary perovskites of La with Co, Ni, Fe, and Mn were pure crystalline phases prior to catalyst testing. EXAFS and XANES results indicated the expected +3 bulk oxidation state for the "B" metals. ESCA analysis of surface "B" atoms indicated oxidation states > 0, but specific oxidation state (i. e. +2 or +3) could not be assigned.

Recovered materials exhibited a consistent trend. Perovskite lattices of materials not exposed to runaway methanation were preserved. Ni and Co perovskites not exposed to runaway methanation appeared to have been partially reduced (ca. one electron) to form oxide deficient perovskite lattices. Fe and Mn perovskites were unaffected. The oxidation state of surface "B" cations in all of these recovered

catalysts was > 0 .

Perovskite lattices of materials exposed to runaway methanation were destroyed by reduction. During runaway methanation catalyst bed temperatures exceed 500°C. After exposure to runaway methanation the perovskite lattices of $LaCoO_3$ and $LaNiO_3$ were destroyed. Ni was reduced from +3 to a mixture of +1 and 0, and Co was probably comparably reduced. These results parallel those of Hall and coworkers who reported that hydrogen reduces $LaCoO_3$ by one electron at 400°C and by three electrons at 500°C (5). The Fe and Mn perovskites did not undergo runaway methanation under the conditions employed.

Based on these data it appears that the catalytic sites for these materials are higher valent (> 0), late transition metal, surface "B" cations in a perovskite or perovskite-like lattices, so long as runaway methanation does not occur. This conclusion applies also to substituted perovskites of La and Nd with Mn, Fe, Co, and Ni.

Six perovskites of the general formula $LaM_{0.5}M'_{0.5}O_3$ ($M \neq M'$ = Mn, Fe, Co, and Ni) were characterized after catalyst testing. $LaNi_{0.5}Co_{0.5}O_3$ was exposed to runaway methanation and its crystalline lattice was decomposed. The other materials were not exposed to runaway methanation, and their crystalline lattices were preserved.

$La_{0.8}Ce_{0.2}CoO_3$ and $La_{0.8}Sr_{0.2}CoO_3$ were exposed to runaway methanation, and the crystalline lattices of both materials were destroyed.

$LaCo_{0.5}Ru_{0.5}O_3$ was not exposed to runaway methanation, but $LaNi_{0.5}Ru_{0.5}O_3$ and $LaFe_{0.5}Ru_{0.5}O_3$ were. Yet, the perovskite lattices of all three materials were preserved. This contrasts with the behavior of $LaNiO_3$ which underwent lattice decomposition under these conditions. Ru apparently confers added stability to these lattices.

$LaNi_{0.5}Ti_{0.5}O_3$ and $LaFe_{0.5}Ti_{0.5}O_3$ were not exposed to runaway methanation. As expected, the perovskite lattices were preserved. The catalytic sites for these materials appear to be higher valent surface cations of Ni and Fe in perovskite lattices.

Neither of the Cu containing perovskites were exposed to runaway methanation. The perovskite structures of both materials were preserved, albeit, with partial reduction. The stability of these lattices is probably due to the reductive stability of Ti(IV) and Mn(IV). The catalytic sites for these materials appear to be lower valent surface atoms of Cu in a perovskite or perovskite-like lattice.

$NdNiO_3$, $NdCoO_3$, and $NdFeO_3$ all underwent runaway methanation. Like the analogous La compounds, the Ni and Co perovskite structures were destroyed , but the perovskite structure of $NdFeO_3$ was preserved.

The crystalline barium platinum metal perovskites were all pure crystalline phases prior to catalyst testing. The bulk oxidation states of the platinum metals were the expected +4. However, all of these materials except $BaRuO_3$ contained surface platinum metal cations in lower oxidation states instead of, or in addition to the +4 state.

Both crystalline and amorphous barium platinum metal perovskites are unstable to syn gas and its products. Platinum metals were reduced to the elemental state, and Ba was converted to $BaCO_3$. It appears that these materials after an induction period are transformed to zero valent platinum metal crystallites on $BaCO_3$.

CONCLUSIONS

Seven base metal lanthanum perovskites that provide 20-40% selectivity to oxygenates have been found. All of the lanthanum metal perovskites are stable to reductive decomposition if not exposed to runaway methanation and some are stable even if exposed to runaway conditions. The catalytic sites in these materials are thought to be late transition metal surface "B" atoms in higher oxidation states (> 0) and in perovskite or perovskite-like lattices. Two platinum metal barium perovskites that provide > 50% selectivity to oxygenates (mainly methanol) have also been found. These materials are unstable under reaction conditions and are converted to elemental platinum metals and $BaCO_3$. After an induction period, the catalytic sites for these materials are thought to be the mainly zero valent platinum metal crystallites on $BaCO_3$.

ACKNOWLEDGMENTS

The authors wish to acknowledge the contributions of several of their co-workers to this study. Messrs. R. Sgrignoli and G. Abaskaron prepared catalysts and performed catalyst evaluation experiments. Dr. D. Karim performed and interpreted EXAFS and XANES experiments. Dr. E. Prack performed and interpreted ESCA experiments. Dr. J. Stamatoff and Dr. C. Saw performed and interpreted XRPD experiments. The authors also want to thank the Celanese Research Company for supporting this research and permitting presentation of this paper.

REFERENCES

1. Kalfadelis, C. D., and H. Shaw, in "Encyclopedia of Chemical Technology", John Wiley and Sons, New York, NY, 1980.
2. Anderson, R. B., "The Fischer-Tropsch Synthesis", Academic Press, New York, NY, 1984.
3. Bartley, W. J. (Union Carbide), United States Patent 4,312,955, January 26, 1982.
4. Watson, P. R. and G. A. Samorjai, J. Catal. 74, 282-95, 1982.
5. Crespin, M. and W. K. Hall, J. Catal. 69, 359-70, 1

TABLE I

CATALYTIC EVALUATION OF PEROVSKITES FOR SYN GAS CONVERSION (a)

PEROVSKITE	GHSV	TEMP	CO CONV	CO SELECTIVITY, %					STY, G/L.HR	
	1/HR	°C	%	MeOH	C2OX	HiOX	HC	CO2	OXY	TOTAL
LaCoO3	3944	280	2.3	12.5	10.0	10.6	62.4	4.4	2.1	14.6
		300	9.2	10.3	15.7	0.7	37.9	35.4	9.4	21.5
		320	100.	3.7	3.3		64.5	28.4	91.5	1120.
LaNiO3	2471	320	4.1	20.8	4.7	1.6	55.6	17.3	8.2	24.9
	2434	340	8.7	10.6	2.9	0.9	62.2	23.5	10.1	59.1
		360	100.				67.4	32.6		748.
LaFeO3	3000	280	3.9	6.4	15.0	2.5	66.5	9.6	7.8	25.0
		300	10.4	4.5	14.0	2.3	66.3	12.8	16.7	63.6
		320	22.8	3.7	8.2	2.1	70.3	15.6	24.7	142.5
LaMnO3	3054	340	4.3				64.3	35.7		33.2
		360	6.2				61.9	38.1		50.0
		380	8.3				62.4	37.6		74.6
LaNi0.5Fe0.5O3	3487	340	9.5	0.9	31.3		54.6	13.1	33.1	55.1
		360	15.2	0.6	16.0		66.7	16.8	28.6	111.7
		380	26.4		8.7		73.3	17.9	26.1	212.8
LaMn0.5Ni0.5O3	3504	320	2.6		26.6		61.5	11.9	6.5	15.8
		340	4.5	0.8	15.6		69.3	14.4	6.9	31.3
		360	6.5	0.6	10.8		71.5	17.1	6.9	48.8
LaNi0.5Co0.5O3	3529	280	2.72		1.0	0.4	93.6	5.0	0.3	18.3
		300	7.4	1.4	13.9	0.4	73.1	11.3	11.6	50.1
		320	100.				73.2	26.8		1013.
LaFe0.5Co0.5O3	3529	320	13.6		19.0		73.5	7.5	28.4	80.0
		340	30.2	0.5	8.1		79.4	12.0	26.4	213.2
		360	34.0		6.8		77.6	15.5	26.0	266.5
		380	40.6		5.1	0.1	76.3	18.4	24.5	346.9
LaMn0.5Co0.5O3	2958	320	3.3		0.3	3.0	76.3	20.4	0.6	20.8
		340	19.3	3.4	0.3	0.2	82.8	13.3	4.2	71.8
		360	22.6	2.0	0.3	0.1	79.9	17.6	4.6	137.
LaMn0.5Fe0.5O3	3769	340	10.4	5.3	4.6	4.0	69.5	16.7	18.6	115.
		360	15.9	3.9	3.7	2.0	69.4	20.9	18.6	170.
		380	19.1	3.3	3.2	1.3	68.8	23.4	19.8	223.

a. Pressure = 970-1000 psig, GHSV = gas hourly space velocity, TEMP = temperature, CO CONV = CO conversion, STY = space time yield, MeOH = methanol, C2OX = ethanol + acetaldehyde + acetic acid, HiOX = C3-C6 alcohols, HC = hydrocarbons, OXY = oxygenated organics.

TABLE II

CATALYTIC EVALUATION OF PEROVSKITES FOR SYN GAS CONVERSION (a)

PEROVSKITE	GHSV	TEMP	CO CONV	CO SELECTIVITY, %					STY, G/L.HR	
	1/HR	°C	%	MeOH	C2OX	HiOX	HC	CO2	OXY	TOTAL
La0.8Ce0.2CoO3	3250	280	2.9		1.3	1.6	88.5	8.6	0.7	22.
		300	7.8	4.1	1.2	2.7	83.1	8.9	6.9	62.
		320	40.2	0.7	1.2	1.6	84.5	12.0	12.7	308.
La0.8Sr0.2CoO3	3803	280	2.8		6.9		80.9	12.2	2.1	27.
		300	95.9		0.7	1.0	74.9	23.5	14.1	966.
LaCo0.5Ru0.5O3	2615	320	1.7				94.0	6.0		9.4
		340	5.2				96.9	3.1		26.9
		360	28.3		2.6	0.3	83.7	13.4	5.8	171.4
LaNi0.5Ru0.5O3	3015	320	10.0		6.9	.5	87.6	5.0	6.0	57.
		340	19.6	6.7	3.7	.4	82.6	6.7	6.6	130.
		360	52.1		1.3	.5	89.5	8.6	7.9	355.
LaFe0.5Ru0.5O3	2658	300	5.7		12.6	0.9	81.3	5.2	5.5	26.1
		320	11.0		8.5	0.7	79.1	11.7	7.0	59.6
		340	21.7		4.5	1.0	81.9	9.7	8.5	123.
		360	60.7	0.1	1.5	8.5	67.4	22.6	14.7	132.
LaNi0.5Ti0.5O3	3337	360	1.2				69.7	30.3		9.6
		380	1.9				69.7	30.3		15.5
LaFe0.5Ti0.5O3	3189	340	11.4	6.9	10.1	1.3	60.2	21.5		95.5
		360	16.5	4.9	4.7	0.6	64.0	26.9	15.9	143.
		380	20.3	3.1	3.3	0.2	60.5	32.8	12.9	189.
LaCu0.5Ti0.5O3	3323	320	2.9	38.0		0.9	28.7	32.4	13.8	35.6
		340	5.0	32.3		1.6	32.6	33.6	20.7	60.6
		360	7.6	24.1		2.0	35.4	36.8	23.3	88.3
LaCu0.5Mn0.5O3	3361	320	3.4	37.0			29.0	34.0	14.2	38.2
		340	6.5	28.9		.6	36.3	34.2	21.2	69.4
		360	12.4	20.5		1.3	48.8	29.4	30.0	121.5
NdNiO3	3561	260	2.4				92.8	7.2		15.1
		280	7.0		9.8		90.2		6.0	43.3
		300	73.		0.7		79.6	19.7	3.8	549.
NdFeO3	3060	300	3.3				70.6	29.4		29.6
		320	36.8		2.1	0.7	68.4	28.8	8.3	335
NdCoO3	3494	260	.68				86.2	13.8		5.6
		280	6.1				95.8	4.2		39.7
		300	92.1		0.3		77.3	22.3	3.2	892.

a. Pressure = 970-1000 psig, GHSV = gas hourly space velocity, TEMP = temperature, CO CONV = CO conversion, STY = space time yield, MeOH = methanol, C2OX = ethanol + acetaldehyde + acetic acid, HiOX = C3-C6 alcohols, HC = hydrocarbons, OXY = oxygenated organics.

TABLE III

CATALYTIC EVALUATION OF PEROVSKITES FOR SYN GAS CONVERSION (a)

PEROVSKITE	GHSV	TEMP	CO CONV	CO SELECTIVITY, %					STY, G/L.HR	
	1/HR	°C	%	MeOH	C2OX	HiOX	HC	CO2	OXY	TOTAL
BaRuO3, Amorph	2381	280	3.5		2.6	3.6	83	10.9	1.2	17.4
		300	9.6		4.3	3.8	81.5	10.4	4.6	46.3
		320	34.4		3.2	3.5	83.1	10.2	12.8	158.4
		340	80.9	0.2	0.3	0.2	79.9	19.4	4.1	550.2
BaRuO3, Cryst	3564	260	6.6	1.5	12.1	0.6	66.6	19.2	7.5	49.2
		280	13.4		8.7	1.1	66.9	23.3	8.9	91.9
		300	100.		0.4		71.4	28.2	3.9	1055.
BaRhO3, Amorph	2556	240	1.1	54.3	2.4	0.9	27.5	14.9	6.9	10.3
		260	2.5	36.6	8.4	1.5	29.8	23.6	11.7	24.8
		280	6.7	22.6	10.2	3.1	38.8	25.4	22.2	60.6
		300	16.7	13.4	10.3	3.2	44.3	28.9	39.2	147
BaRhO3, Cryst	2483	260	1.7	62.3	2.2	0.5	22.2	12.8	11.6	16.8
		280	3.9	46.8	5.0	1.0	28.2	19	19.9	35.9
		300	7.9	29.7	5.9	1.3	36.9	26.2	28.3	73.3
		320	19.0	15.5	6.4	1.6	43.2	33.2	40.8	174.
		340	49.6	4.7	5.3	1.5	51.5	37	49.1	455.
BaIrO3, Amorph	2576	280	2.9	29.3	7.7	2.2	43.1	17.6	10.8	24.1
		300	8.7	20.4	5.8	2.1	51.0	20.6	23.1	71.4
		320	21.4	17.1	5.1	1.4	47.6	28.7	43.7	173.
		340	22.0	8.8	6.2	1.0	61.2	22.8	30.7	162.
		360	34.0	5.1	3	0.9	61.4	29.5	25.6	260.
BaIrO3, Cryst	2550	360	4.3	0.2	1.2	0.9	59.8	37.9	0.8	41.
		380	10.0	4.6	0.9	0.9	56.3	37.6	5.9	90.
BaPtO3, Amorph	2540	280	5.7	38.6	4.8	2.2	26.4	28	25	55.3
		300	8.4	48.1	3.4	6.2	19.6	22.6	44.5	78.7
		320	10.6	53.8	4.3	0.4	19.8	21.6	59.5	102.
		340	12.7	49.6	1.9	0.2	25.2	23	63.1	119.
		360	13.3	39.8	1.9	0.2	31.5	26.6	52.2	120.
BaPtO3, Cryst	2860	320	2.6	46	1.5		24.2	28.4	14.6	16.3
		340	4.4	49.1	1.2	0.2	23.6	25.9	25.5	23.5
		360	6.7	43.8	8.1	0.3	24.2	23.6	38.7	34.7
		380	6.5	37.1	1.8	0.3	32.0	28.9	30.6	45.5

a. Pressure = 970-1000 psig, GHSV = gas hourly space velocity, TEMP = temperature, CO CONV = CO conversion, STY = space time yield, MeOH = methanol, C2OX = ethanol + acetaldehyde + acetic acid, HiOX = C3-C6 alcohols, HC = hydrocarbons, OXY = oxygenated organics, Amorph = amorphous by XRPD, Cryst = crystalline by XRPD.

TABLE IV

CHARACTERIZATION OF PEROVSKITES RECOVERED AFTER CATALYST EVALUATION

PEROVSKITE (a)	MAX RXN TEMP, °C (b)	XRPD(c) STRUCTURE PRESERVED	XRPD(c) OTHER PHASES	EXAFS/XANES, BULK OXID STATE FRESH	EXAFS/XANES, BULK OXID STATE USED	ESCA, SURFACE OXID STATE FRESH	ESCA, SURFACE OXID STATE USED
LaCoO3	RUNAWAY	NO					
LaCoO3	300	YES, (PR)		+ 3	+ 2	> 0	> 0
LaNiO3	RUNAWAY	NO		+ 3	+ 1, 0		
LaNiO3	340	YES, (PR)					
LaFeO3	320	YES		+ 3	+ 3	> 0	> 0
LaFeO3	360	YES					
LaMnO3	380	YES		+ 3	+ 3	> 0	> 0
LaFe0.5Co0.5O3	380	YES					
LaNi0.5Co0.5O3	RUNAWAY	NO					
LaNi0.5Fe0.5O3	380	YES					
LaMn0.5Co0.5O3	380	YES					
LaMn0.5Ni0.5O3	380	YES					
LaMn0.5Fe0.5O3	380	YES					
La0.8Ce0.2CoO3	RUNAWAY	NO					
La0.8Sr0.2CoO3	RUNAWAY	NO					
LaCo0.5Ru0.5O3	360	YES					
LaNi0.5Ruo.5O3	RUNAWAY	YES					
LaFe0.5Ru0.5O3	RUNAWAY	YES					
LaNi0.5Ti0.5O3	380	YES					
LaFe0.5Ti0.5O3	380	YES					
LaCu0.5Ti0.5O3	380	YES, (PR)					
LaCu0.5Mn0.5O3	380	YES, (PR)					
NdNiO3	RUNAWAY	NO					
NdFeO3	RUNAWAY	YES					
NdCoO3	RUNAWAY	NO					
BaRuO3, Amorph	360	NO	BaCO3, Ru(0)				
BaRuO3, Cryst	RUNAWAY	NO	BaCO3, Ru(0)	+ 4	0	+ 4	+ 4, 0
BaRhO3, Amorph	RUNAWAY	NO	BaCO3, Rh(0)				
BaRhO3, Cryst	RUNAWAY	NO	BaCO3, Rh(0)	+ 4	0	+ 3	0
BaIrO3, Amorph	380	NO	BaCO3, Ir(0)				
BaIrO3, Cryst	380	NO	BaCO3, Ir(0)	+ 4	0	+ 4, + 3	+ 3
BaPtO3, Amorph	380	NO	BaCO3, Pt(0)				
BaPtO3, Cryst	380	NO	BaCO3, Pt(0)	+ 4	0	+ 4, + 2	+ 2, 0

(a) Amorph = amorphous by XRPD, Cryst = crystalline by XRPD.
(b) Runaway indicates that the catalyst bed temperature has exceeded 500°C.
(c) PR indicates that the perovskite structure has apparently been partially reduced through the formation of oxide vacancies, but the lattice has been essentially preserved.

FISCHER-TROPSCH SLURRY CATALYSTS FOR SELECTIVE TRANSPORTATION FUEL PRODUCTION

W. E. Carroll, N. Cilen, H. P. Withers, Jr.

AIR PRODUCTS AND CHEMICALS, INC.
P. O. Box 538, Allentown, PA 18105

©Air Products and Chemicals, Inc., 1986

Introduction

The future use of coal as a source of conventional transportation fuel will depend on the development of an economical and energy efficient liquefaction process. Technologies that have been commercially proven or that are close to commercialization include the fixed- and fluidized-bed Fischer-Tropsch (FT) synthesis, methanol synthesis (fixed-bed and slurry-phase) and the Mobil methanol-to-gasoline process. Of these technologies, the Fischer-Tropsch hydrocarbon synthesis produces the widest slate of products and has been in operation for the longest period.

The FT reaction produces hydrocarbons with a broad spectrum of molecular weights ranging from methane to paraffin waxes. This broad product distribution significantly limits the maximum yield of transportation fuel fraction and creates the need for further downstream processing such as hydrocracking and light olefin oligomerization to increase such yields. Research has shown that selectivity is controlled mainly by catalyst composition and process conditions. In order to improve the economics of the FT process, a catalyst should display high activity and minimize the formation of both light hydrocarbons (C_1-C_4) and waxes (C_{24}+), while producing the bulk of the product fraction in either the gasoline (C_5-C_{11}) or diesel (C_{12}-C_{18}) ranges. Product selectivity, however, has been more successfully controlled by manipulating process conditions. Since the FT reaction is exothermic, control of the reaction heat plays a major role in controlling product selectivity. The slurry-phase process offers the best means of heat transfer and temperature control and has been shown to improve liquid product selectivity mainly by lowering the light gas yield(1). The amount of data from slurry-phase operation, however, is limited to only a few studies and significant differences have been reported in yields, catalyst life and ease of operation(1-4). More research is needed to fully determine the potential of slurry-phase FT processing, and we will describe our efforts in developing new slurry-phase FT catalyst systems.

Under an earlier contract with the Department of Energy, Air Products and Chemicals, Inc. developed several new slurry-phase FT catalysts that enhanced selectivity to liquid fuel products(5). One group of catalysts included supported metal carbonyl clusters modified by promoters. To further develop and improve these catalyst systems, Air Products has begun a program to thoroughly investigate the preparation, characterization and performance of metal carbonyl cluster-based catalysts for use in slurry phase FT technology. Our overall objectives focused predominately on increasing catalyst activity, improving product selectivity for liquid fuels, reducing the yield of methane, developing catalyst systems active at high CO/H_2 ratios and incorporating water-gas shift activity. Catalysts were evaluated by a combination of tests in stirred and fixed-bed reactors. In addition, catalysts were characterized by surface techniques and bulk analyses.

Experimental

Catalyst Preparation: Catalyst precursors and supports were purchased from commercial sources. The following supports were used after a calcining treatment at 500°C for 3 hr in air: γ-Al_2O_3 (Catapal® SB, 217 m^2/g), SiO_2 (Davison 952, 339

m^2/g), $MgO \cdot 3.6\ SiO_2$ (Florisil®, 298 m^2/g) and TiO_2 (Degussa P-25, 50 m^2/g). The catalysts and precursors were protected from air and moisture using standard Schlenk techniques(6) and a Vacuum Atmospheres dry box. All solvents were reagent grade and distilled from sodium benzophenone ketyl in a nitrogen atmosphere. Immediately prior to use, the supports were further dried in vacuo at 110°C for 1-2 hr. Catalysts were prepared by impregnation (to incipient wetness) of the supports with separate solutions containing the promoter and metal carbonyl. Several promoters were evaluated, with one being particularly effective. All catalysts discussed in this report made use of this promoter (designated "Prom"). This method was used for the following catalysts that were prepared from metal carbonyls:

- 3.8% Co/6.8% Prom on Al_2O_3 } basecase catalysts
- 2.8% Ru/4.9% Prom on Al_2O_3 } basecase catalysts
- 4.7 Co on Al_2O_3 (no promoter) } basecase catalysts
- 5.1% Co/4.4% Prom on Al_2O_3
- 4.0% Co/6.4% Prom on Al_2O_3
- 10.8% Co/8.5% Prom on Al_2O_3
- 3.5% Co/6.6% Prom on SiO_2
- 3.7% Co/7.2% Prom on $MgO \cdot 3.6\ SiO_2$
- 3.5% Co on TiO_2 (no promoter)

Two catalysts were also prepared using $Co(NO_3)_2$ as the cobalt source. The method was slightly modified, in that after addition of the promoter and removal of the solvent, the material was exposed to air. An aqueous solution of $Co(NO_3)_2$ was then used to impregnate the support, the material was dried at 110°C and calcined at 300°C in air for 5-6 hr. The two catalysts and their analyses are as follows:

- 4.2% Co/7.1% Prom on γ-Al_2O_3
- 4.6% Co/7.5% Prom on SiO_2

Gas Phase Tests: Prior to slurry-phase testing, gas-phase tests were conducted to screen catalyst activity. Those catalysts with gas-phase activities greater than 20 mol of syngas converted/kg of catalyst/hr were selected for further slurry-phase testing.

The gas phase reactor was a fixed-bed, 316 SS tubular unit with downflow configuration and 10 cc bed volume. All gas-phase tests used a CO/H_2 feed ratio of 1 at 300 psig and nearly all were conducted at 1000 GHSV (v/v). Temperature was varied in the range of 220 to 280°C. For the gas-phase tests, the catalyst was activated with H_2.

Slurry Phase Tests: Two continuous, stirred, 1 liter autoclave reactors were used for slurry tests. Figure 1 shows a schematic diagram of one of these units. For the slurry phase tests, catalysts were activated in a separate, 150 cc fixed bed tubular unit using either pure H_2 or 20% syngas in N_2. Activated catalyst was slurried in deoxygenated paraffin oil (Fisher #0-122) in the dry box and transferred to the slurry autoclave reactor under a N_2 blanket.

Slurry tests were performed continuously for up to 21 days, except for the test of basecase Co on promoted alumina, which was run for 55 days. Inlet CO/H_2 ratios were 2, 1.5, and 0.5, with emphasis on CO-rich feeds. Space velocities were 1 and 2 NL/g of catalyst/hr. Operating pressures and temperatures ranged from 300 to 600 psig and 220 to 280°C, respectively. The solids content of the slurry was 15 to 25 wt%.

Because of the complexity of the Fischer-Tropsch product, equilibration of the reactor and the product collection systems, and a flexible quantitative analysis scheme incorporating all products including waxes were required to produce good carbon and hydrogen material balances, which were in the range of 95-105%. The details of the analytical and data handling system have been published(7). The method, illustrated schematically in Figure 2, consisted of four separate gas

chromatographs linked via a Perkin-Elmer Sigma 15 computing integrator/controller to a Tektronix 4052 microcomputer equipped with a 1.9-megabyte disk system.

Catalyst Characterization: Catalyst supports were characterized by B.E.T. surface area measurements, mercury intrusion porosimetry, helium pycnometry, and particle size distribution. Freshly prepared catalysts and reduced catalysts were characterized by B.E.T. surface area measurements and hydrogen chemisorption. Metal loadings were determined in-house and at Schwarzkopf Microanalytical Laboratories. Some of the catalysts were also studied using X-ray photoelectron spectroscopy and X-ray diffraction.

Results and Discussion

The type of activation used for "conventional" FT catalysts has been shown by several researchers to affect performance(8). Dry detailed the effects of activation on the performance of precipitated and fused iron catalysts(9) and indicated that pure H_2 was preferred. Another recent study of catalyst performance vs. degree of reduction for $Co(NO_3)_2$ on alumina used only H_2 reduction(10). The activation of supported metal carbonyl catalysts has generally been done by thermal decomposition under vacuum or inert atmosphere(11). The effect of reducing gases such as H_2 and syngas on supported metal carbonyls has not been well established, but these gases should improve the degree of metal reduction since the metals are initially oxidized by the support.

Our study of activation conditions compared pure H_2 activation with syngas (CO/H_2 = 1) activation using the 4% Co on promoted alumina catalyst. Hydrogen activation significantly improved both activity and liquid fuel selectivity in the slurry tests. Figure 3 compares syngas conversion following both types of activation as a function of temperature and space velocity. At comparable reaction conditions, H_2 activation converted 30 to 40% more syngas in the 220 to 260°C range, but at 280°C, the difference was less. For H_2-activated catalyst at lower space velocity, the syngas conversion appeared to be independent of temperature between 240 and 280°C.

Table 1 shows that H_2 activation increased the C_{5-23} selectivity by 25 relative percent, from 57 to 71 wt% and decreased both the CH_4 and wax selectivity. The increased activity probably resulted from a higher degree of Co reduction but the reason for the enhanced liquid fuel selectivity is less clear. Perhaps the degree of reduction and metal particle sizes which both depend on activition conditions together affect chain growth probability. However, we did not examine or compare the catalysts from different activation procedures for these two properties. Since a major objective of our research was to study the use of metal carbonyls as catalyst

Table 1. Effect of syngas vs. hydrogen activation on hydrocarbon selectivity.

4% Co ON PROMOTED - Al_2O_3

	SYNGAS	H_2
SPACE VELOCITY, NL/g cat/hr.	1.6	2.0
CO/H_2	1.5	1.5
PRESSURE, PSIG	300	300
TEMPERATURE, °C	250	255
WT%		
C_1	11.5	7.2
C_{2-4}	10.4	10.6
C_{5-11}	29.2	34.1
C_{12-18}	15.3	27.9
C_{19-23}	12.5	8.5
C_{24+}	21.1	11.4
C_{5-23}	57.0	70.6

precursors, a comparison to conventionally prepared catalysts was necessary. This was done by examining catalysts prepared from cobalt nitrate using the same support and promoter as the cobalt carbonyl-based catalysts. The activity and selectivity of the two catalysts in the slurry-phase reactor are compared in Table 2. Both

catalysts had similar cobalt and promoter loadings. Again, performance differences were larger at lower temperatures. At 240°C, bulk activity of the carbonyl catalyst was more than twice that of the nitrate catalyst, while specific activity was three times higher. At 260°C, the carbonyl catalyst still outperformed the nitrate catalyst in both bulk activity (29% increase) and specific activity (52% increase). The carbonyl-prepared catalyst also provided better liquid fuel selectivity at both temperatures, producing less methane but more light hydrocarbons (C_{2-4}). The major difference was in the production of heavier hydrocarbons, with the nitrate-derived catalyst giving significantly higher $C_{24}+$ selectivity. These differences are likely related to metal particle sizes and work is in progress toward characterizing and comparing these catalysts.

Table 2. Effect of Co source on activity and selectivity.

4% Co ON PROMOTED Al_2O_3
(CO/H_2 = 1.0, 2.0 NL/hr·g cat, 300 psig)

COBALT SOURCE	CARBONYL		NITRATE	
	240°C	260°C	240°C	260°C
BULK ACTIVITY, mol SYNGAS/kg cat/hr	35.3	38.5	15.8	29.9
SPECIFIC ACTIVITY, mol CO/mol Co/min	0.29	0.32	0.09	0.21
SELECTIVITY, WT%				
C_1	7.9	10.4	10.9	16.5
C_{2-4}	13.7	15.0	6.5	11.1
C_{5-11}	37.0	44.5	12.9	26.5
C_{12-18}	23.4	25.8	19.6	23.8
C_{19-23}	8.9	2.0	21.9	10.6
C_{24+}	9.1	2.3	28.0	11.5
TOTAL FUELS C_{5-23}	69.3	72.3	54.6	60.9

Several other parameters were examined using the carbonyl-based catalysts. The effect of cobalt to promoter ratio on activity was examined with alumina-supported catalysts. Figure 4 plots specific activity vs. cobalt/promoter ratio for slurry-phase tests at similar reaction conditions and different activation procedures. Catalyst that had undergone syngas activation showed a decrease in specific activity as the Co/promoter ratio increased. The specific activity of the H_2-activated catalyst, however, was independent of this ratio. One possible explanation involves the interaction of cobalt with the support and its subsequent reducibility. As the amount of promoter decreases, the cobalt interacts more strongly with the support and becomes more difficult to reduce. This decreased reducibility is especially evident when the catalyst is activated with syngas; the cobalt is not sufficiently reduced, resulting in lower activity. Hydrogen, on the other hand, provides sufficient reducing power to activate cobalt that is more strongly associated with the support.

The effect of cobalt loading on bulk activity of the cobalt carbonyl-promoted alumina catalyst was examined in the slurry reactor at 240 and 260°C (Figure 5). Higher loading gave lower bulk activities at both temperatures. Since the catalyst having the higher cobalt loading also had a higher metal dispersion, these results agree with the general trend of increasing activity with decreasing dispersion reported in the literature.

The type of support also had a major influence on catalyst activity, as shown in Figure 6. These catalysts all had similar cobalt and promoter loadings, except for the TiO_2-supported catalyst, which had no promoter. The silica-supported catalyst was approximately twice as active as all the others. This may be due to the low reactivity between cobalt carbonyl and silica as opposed to the high reactivity of the other supports towards metal carbonyls. A surface area effect is being checked by using a lower surface area silica.

We also studied the effects of operating parameters such as temperature and CO/H_2 feed ratio on catalyst performance. As expected, increasing the reaction temperature increased the bulk activity of both Al_2O_3- and SiO_2-supported Co catalysts, as shown

in Figure 7. The SiO_2-supported catalyst activity was independent of temperature at 240°C and 260°C, but increased at 280°C. The activity of the Al_2O_3-supported catalyst began to level off at higher temperatures.

The ratio of carbon monoxide to hydrogen in the feed strongly affected catalyst activity, as shown in Figure 8 for promoted cobalt on silica. The catalyst performed best with H_2-rich feed; when the feed was stoichiometric with respect to hydrocarbon ($-CH_2-$) formation (CO/H_2 = 0.5), the syngas converison was highest at 60%. Conversion dropped dramatically to only 25% when the CO/H_2 ratio was increased to 1.5.

This poor performance with CO-rich feeds reflects the low activity for the water-gas shift reaction. Figure 9 further illustrates this by comparing CO/H_2 usage ratios with feed ratios for the supported cobalt and ruthenium catalysts, as well as, a precipitated iron catalyst, all in the slurry reactor. The cobalt catalyst showed the poorest CO usage at all feed levels, usage ratios never exceeded 0.60. The ruthenium catalyst offered some improvement with a usage ratio nearly matched to a CO/H_2 feed ratio of 1.0. The usage ratio, however, never improved above 1.0 as the feed ratio was increased. The slight improvement in shift activity for ruthenium correlates with its observed shift activity in homogeneous systems(12). Neither catalyst showed the excellent shift activity that is exhibited by precipitated or fused iron catalysts.

In an effort to improve the shift activity of the promoted Co on alumina catalyst, a commercially available, low temperature shift catalyst ($Cu/Zn/Al_2O_3$) was physically mixed with it and tested in the gas phase reactor. The results are summarized in Table 3 along with results in which no shift catalyst was added. The added shift catalyst caused a drop in activity with no indication of enhanced shift activity. There was an increase in oxygenate production, especially of ethanol and higher alcohols. A second gas-phase test of the mixed catalysts, this time using preactivated shift catalyst, still gave lower activity than without shift catalyst, but shift activity increased slightly. Upon increasing the feed ratio from 1.0 to 1.9, however, shift activity declined as the usage ratio dropped to 0.35.

Table 3. Addition of Cu/Zn/Al water-gas shift catalyst to $Co/Prom/Al_2O_3$ FT catalyst.

Catalyst[1]	CO/H_2	Usage Ratio (CO/H_2)	% Conversion, $CO + H_2$	Bulk Activity, (mol syngas/kg cat/hr)
90% F-T + 10% SHIFT	1.0	0.53	36	16.8
90% F-T + 10% SHIFT	1.0	0.65	44	21.6
(Preactivated)	1.9	0.35	16	8.6
BASECASE F-T	1.0	0.59	56	27.0

[1]CONDITIONS: 240°C, 300 psig, 1000 GHSV

Another important objective of this study was catalyst characterization and its correlation to catalyst performance. X-ray photoelectron spectroscopy (XPS) was used to examine cobalt oxidation states; three spectra are shown in Figure 10. The lower spectrum is that for oxidized Co on promoted Al_2O_3 prepared from $Co(NO_3)_2$. The binding energy for Co 2p electrons of 781 eV corresponds to established values for Co(II) and Co(III). The strong interaction of cobalt with alumina was evident from the XPS data on fresh catalyst prepared from zero-oxidation-state $Co_2(CO)_8$. This data, shown as the middle spectrum, indicates that most of the cobalt is oxidized to 2+ and 3+. Only a shoulder corresponding to a binding energy less than 780 eV suggests the presence of a small amount of zero valent cobalt. Finally, upon activation in pure H_2 at 300°C, the top spectrum was obtained, indicating the presence of a only oxidized cobalt. This is further evidence for a strong

metal-support interaction. That supported cobalt is difficult to reduce, especially at low loadings, is well established(10). Hall and coworkers have used XPS to show that after H_2 reduction at 250°C, alumina-supported $Co_4(CO)_{12}$ had only 25% of its cobalt as zero valence(13).

Hydrogen chemisorption was used to determine active cobalt surface area and percent dispersion. These results, presented in Table 4, are consistent with the XPS data, showing only small amounts of metallic cobalt. Hydrogen chemisorption was low, especially at room temperature and low loadings. This activated adsorption has been reported by Reuel and Bartholomew(14) and is possibly due to some metal support

Table 4. Catalyst properties.

Catalyst	B.E.T. Surface Area	Total H_2 Uptake	Active Metal Surface Area	% Dispersion
4% Co/Prom/Al_2O_3	209 m^2/g	5.0 μmol/g at 35°C	0.4 m^2/g	1.2
10.8% Co/Prom/Al_2O_3	N.A.	101.2 at 100°C	5.4	9.7
3.5% Co/Prom/SiO_2	316	39.8 at 100°C	3.0	10
3% Co/SiO_2 [1]	N.A.	20	N.A.	11
3% Co/Al_2O_3 [1]	N.A.	5.6	N.A.	10
32% Co/0.5% Ru/Th/Al_2O_3 [2]	150-225	150-200	N.A.	N.A.

[1] C. H. Bartholomew (1985) [2] U.S. Patent 4,413,064 to Gulf (11/1/83).

interaction. Comparison shows our data are consistent with those of Bartholomew. Furthermore, a 22% Co/0.5% Ru/Th/Al_2O_3 catalyst described in a U.S. Patent to Gulf showed high H_2 chemisorption, probably because reduction occurs more readily as metal loading is increased.

Finally, we compared the activity of our supported cobalt catalysts with other supported cobalt catalysts (see Table 5). All of the data, except one, are from fixed-bed reactors. Our bulk activities fall near that of the Gulf catalyst, but are somewhat lower than that of the Shell catalyst. Note though that our data were not obtained at the optimum H_2/CO feed ratio of 2.0, at which the other catalysts were tested. Turnover frequencies, based on H_2 chemisorption data, are quite good for our catalysts.

Table 5. Catalyst activity comparisons, fixed-bed reactors.

Catalyst	Temp. (°C)	Press. (psig)	Feed H_2/CO	Bulk Activity (mol syngas/kg cat/hr)	Turnover Frequency (molecules CO / site-sec) x 10^3
3.5% Co/Prom/SiO_2	220	300	1.0	31	50
3.5% Co/Prom/SiO_2 (Slurry)	240	300	1.0	36	41
10.8% Co/Prom/Al_2O_3	220	300	1.0	18	14
17% Co/Zr/SiO_2 (Shell)	220	300	2.0	91	N.D.
22% Co/0.5% Ru/Th/Al_2O_3 (Gulf)	215	15	2.0	34	8
3% Co/SiO_2 (Bartholomew)	225	15	2.0	N.D.	6

Acknowledgments

We would like to acknowledge the U.S. Department of Energy (Contract No. DE-AC22-84PC70030) and Air Products and Chemicals, Inc. for supporting this work. The skilled technical assistance of P. A. Dotta, G. W. Long, M. Louie, V. A. Monk and L. E. Schaffer, is greatly appreciated, as well as the contributions of S. A. Motika and D. A. Bohling.

References

1. H. Kolbel and M. Ralek, Catal. Rev. Sci. Eng., 21, 225 (1980).

2. M. L. Poutsma, "Assessment of Advanced Process Concepts for the Liquefaction of Low H_2/CO Ratio Synthesis Gas", ORNL-5635 (1980).

3. W.-D. Deckwer, Y. Serpeman, M. Ralek and B. Schmidt, Ind. Eng. Chem. Proc. Des. Dev., 21, 222 and 231 (1982).

4. C. N. Satterfield, G. A. Huff and J. P. Longwell, Ind. Eng. Chem. Proc. Des. Dev., 21, 465 (1982).

5. (a) R. Pierantozzi, E. G. Valagene, A. F. Nordquist and P. N. Dyer J. Mol. Catal., 21, 189 (1983).

   (b) J. V. Bauer, B. W. Brian, S. A. Butter, P. N. Dyer, R. L. Parsons, and R. Pierantozzi in "Catalytic Conversions of Synthesis Gas and Alcohols to Chemicals", R. G. herman, ed., Plenum, New York (1984), pp. 129-149.

6. "The Manipulation of Air-Sensitive Compounds", D. F. Shriver, McGraw-Hill, New York (1969).

7. J. V. Bauer and P. N. Dyer, Chem. Eng. Prog., 78 (9), 51 (1982).

8. C. N. Satterfield and H. G. Stenger, Ind. Eng. Chem. Proc. Des. Dev., 23, 849 (1984).

9. M. E. Dry in "Catalysis - Science and Technology", J. R. Anderson and M. Boudart, eds., Vol. 1, Springer-Verlag, New York (1981) p. 159.

10. S. H. Moon and K. E. Yoon, Applied Catalysis, 16, 289 (1985).

11. J. Zwart and R. Snel, J. Mol. Catal., 30, 305 (1985).

12. P. C. Ford, C. Ungermann, V. Landis, S. A. Moya, R. C. Rinker and R. M. Laine, "Advances in Chemistry Series, No. 173: Inorganic Compounds with Unusual Properties-II", R. B. King, ed., American Chem. Soc. (1979).

13. G. F. Meyers and M. B. Hall, Inorg. Chem., 23, 124 (1984).

14. (a) R. C. Reuel and C. H. Bartholomew, J. Catal., 85, 78 (1984).

    (b) R. C. Reuel and C. H. Bartholomew, J. Catal., 85, 63 (1984).

FIGURE 1

CONTINUOUS, AUTOMATED FISCHER-TROPSCH SLURRY REACTOR

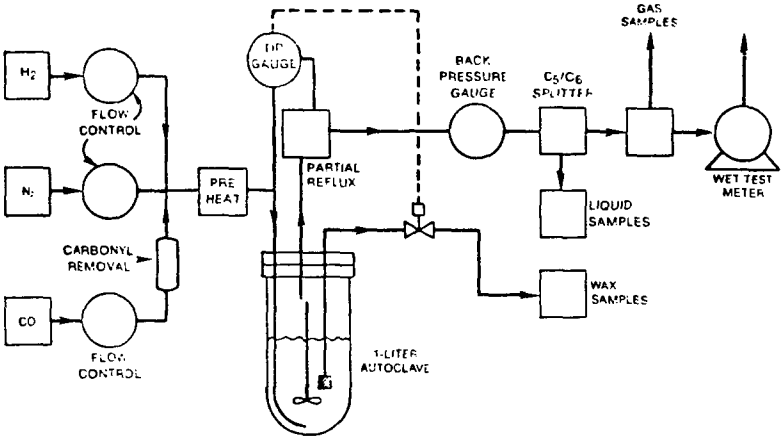

FIGURE 2

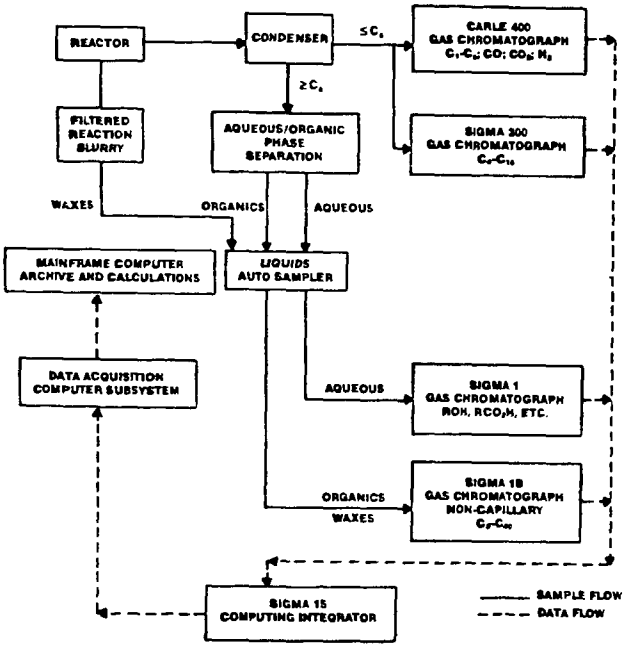

FIGURE 3

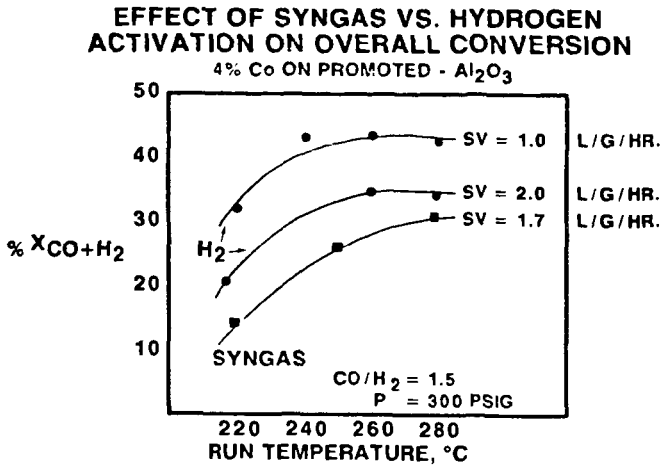

FIGURE 4

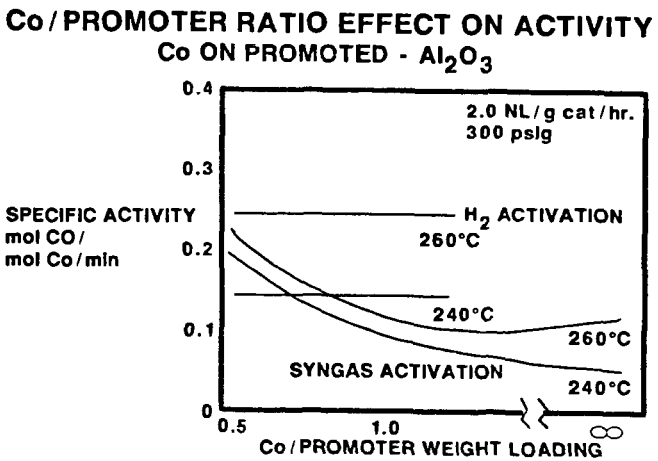

FIGURE 5

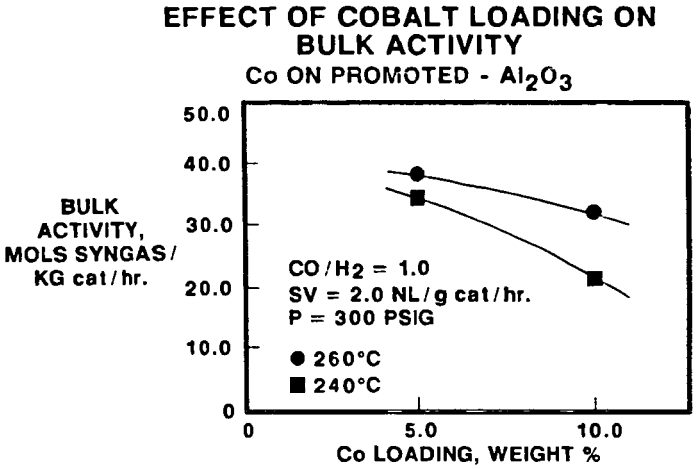

FIGURE 6

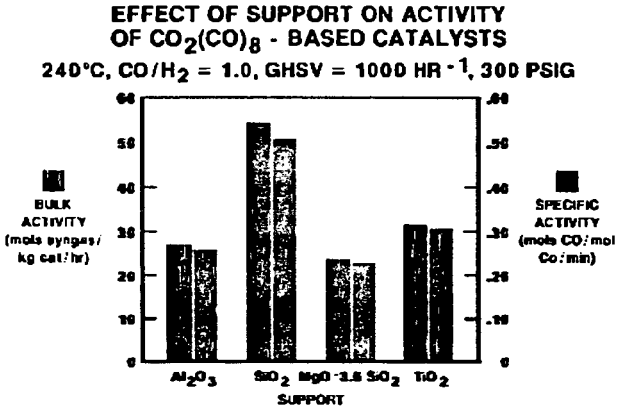

FIGURE 7

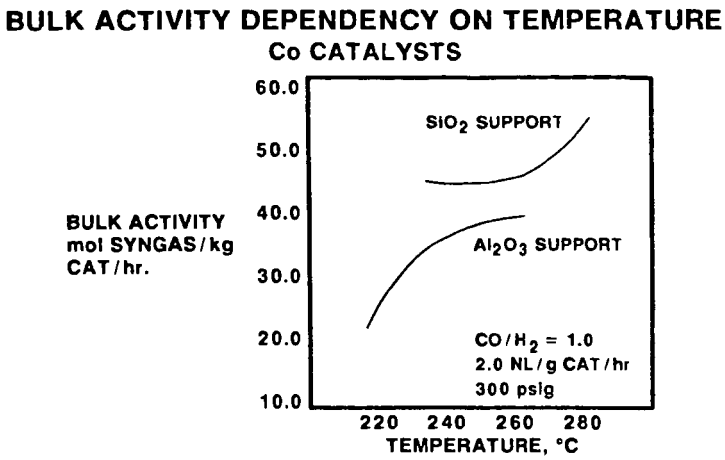

FIGURE 8

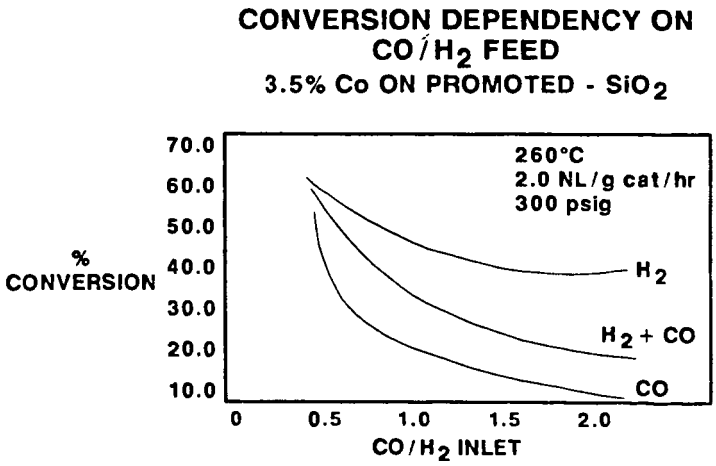

FIGURE 9

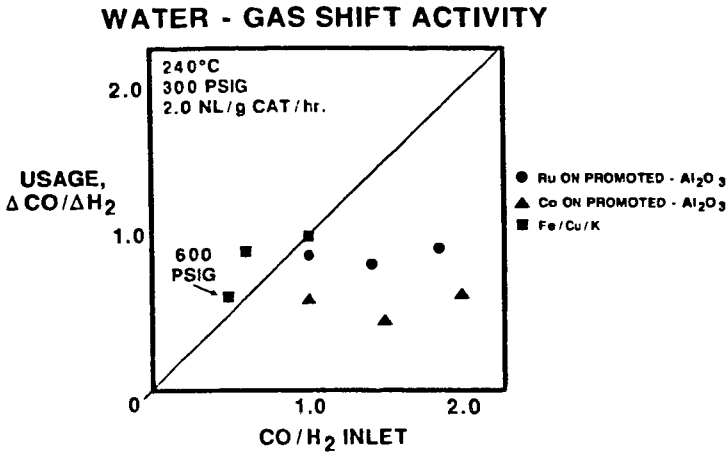

FIGURE 10

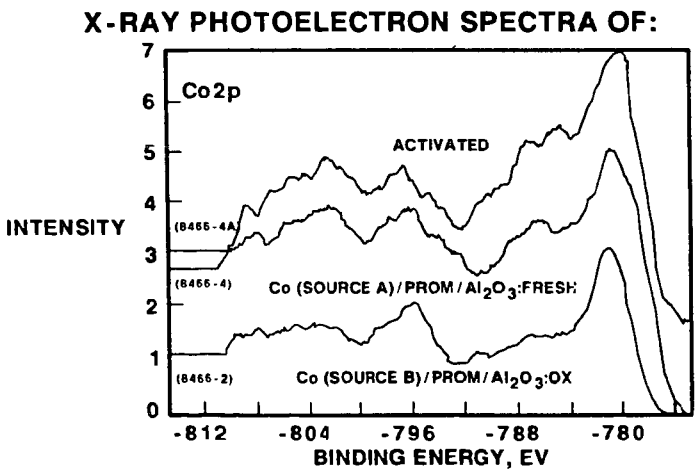

THE HYDROGENATION OF CARBON MONOXIDE OVER RANEY IRON-MANGANESE CATALYSTS

K. R. Chen, F. V. Hanson, N. K. Nag and A. G. Oblad

Department of Fuels Engineering
University of Utah
Salt Lake City, UT 84112-1183

INTRODUCTION

The hydrogenation of carbon monoxide for the synthesis of hydrocarbons was extensively investigated in Germany beginning in the 1920s[1] and in the United States during the 1950s.[2] These early studies focused on the production of liquid hydrocarbons and methane and very little attention was paid to the synthesis of low-molecular weight hydrocarbons such as ethane, ethylene, propane, butane and butylenes.

Coprecipitated iron-manganese catalysts[3] gave favorable selectivity for low molecular weight olefins. This preliminary investigation[3] was extended to include process variable and reactor studies using coprecipitated iron-manganese catalysts.[4-6]

Raney alloy catalysts, first developed by Raney[7], have been used in applications where high activity and selectivity were required in hydrogenation reactions.[7] Raney iron-manganese catalysts have recently been studied to determine their selectivity towards low molecular weight C_2-C_4 olefins.[8]

The objective of this investigation was to determine the optimum operating conditions for the production of low-molecular weight olefins over Raney iron-manganese catalysts.

EXPERIMENTAL APPARATUS AND PROCEDURES

Raney Alloy Preparation

The individual metal components; aluminum, iron and manganese were weighed in the appropriate proportions: Al/Fe/Mn = 59/38/3 parts by weight, were thoroughly mixed and transferred to a carbon crucible, which was placed inside a ceramic crucible and heated by an electric furnace at 1523 K for 24 hours in flowing argon. The resulting melt was quenched to room temperature. Specific details regarding the preparation procedures have been reported elsewhere.[8,9]

Raney Catalyst Activation

Fifty grams of the alloy (25-50 mesh) were added in 5 gram aliquots to a well-stirred tank reactor which contained a 25-weight percent solution of sodium hydroxide at 3-minute intervals to avoid a significant temperature rise in the solution. The reaction temperature was controlled at 363 ± 5 K. After all the alloy had been added to the reactor it was maintained at the leaching temperature for an additional 90 minutes in order to complete the leaching of the aluminum. The catalyst was washed with distilled

water until the pH of the decanted solution was 7.0 ± 0.3. It was then washed three times with 95% alcohol, followed by three times with 100% alcohol. The catalyst was stored under 100% ethyl alcohol in a refrigerator for subsequent characterization and evaluation.

Catalyst Evaluation Apparatus

A fixed-bed flow reactor was used to evaluate the catalysts. The flow rates of H_2 and CO gases were controlled by mass flow meters (Union Carbide Model FM 4550) which were calibrated at different operating pressures for a variety of flow rates. A Grove loader was used as a back pressure control valve to maintain the reactor system pressure constant. Downstream from the Grove loader, the pressure dropped to the ambient pressure. A condenser at the ambient temperature and pressure was used to collect the liquid products. The condensable vapor-free product gas flow was measured with a wet test meter.

Catalyst Evaluation Unit and Operating Procedure

Approximately, 2 grams of dried catalyst was mixed with an appropriate amount of inert Denstone, wetted with water and loaded into the reactor. A hydrogen flow (600 cm^3/min) was established through the catalyst bed at the ambient temperature and pressure and was maintained for 1 hour to evaporate any water from the catalyst surface. The temperature of the system was then raised to 648 K in flowing hydrogen and the catalyst was reduced for 6 hours. At the desired temperature, the reactant gas (a mixture of H_2/CO) was passed through the system and the pressure was slowly increased to the desired value. The stabilization period for a typical experiment with the Raney iron-manganese catalyst was 6 to 15 hours. When necessary, the system operating variables were changed and after the system stabilized at the new conditions (30 to 45 minutes) the product stream was sampled after an additional 10 minutes. The gas products were analyzed by a gas chromatograph (HP 5830A). A thermal conductivity detector (TCD) was used for carbon dioxide, carbon monoxide and water and a flame ionization detector (FID) was used for the hydrocarbon products up to heptanes. A Chromosorb 102 (80-100 mesh 6.1 meters) column which was capable of resolving methane through the heptanes (saturates and unsaturates), was used.

Catalyst Stability Test

The stability of Raney iron-manganese catalyst was determined in an experiment which lasted 36-40 hours. The global heat transfer problem associated with exothermic reactions in fixed-bed reactors was alleviated by loading inert Denstone with the catalyst. The density of Raney catalyst is approximately equal to 2 g/cm^3, and 2 grams of it were used in each experiment. The amounts of Denstone diluent loaded with the catalyst in the three experiments were 1, 2, and 4 cm^3, respectively. Thus, the volume ratios used in the stability tests were 1, 2 and 4.

Process Variable Investigation

A statistical design[9] method was used in the process variable investigation with the Raney iron-manganese catalyst system. Four variables, namely, temperature, pressure, H_2/CO ratio and space velocity were selected for study. Each process operating variable was assigned five different levels: -2, -1,0, 1 and 2. The selection of the range of operating variables was based on preliminary experimental data and on experimental design theory. The process operating conditions are listed in Table 1.

RESULTS AND DISCUSSION

Catalyst Loading and Stability Tests

The loading and stability tests were conducted to determine the range of operating conditions for the process variable investigation and to determine the effect of on-stream time on the activity, selectivity and stability of Raney iron-manganese catalysts. The carbon monoxide conversion as a function of run time at different inert diluent to catalyst ratios at 1470 KPa, 443 K, sv of 4.2 $cm^3g^{-1}s^{-1}$ and H_2/CO ratio of two is presented in Figure 1. It was determined that the induction period for the catalysts at three different diluent/catalyst ratios was about 15 hours. The two diluted bed experiments gave the same carbon monoxide conversions 2.8%, after 15 hours on stream. The effect of reaction temperature on the product selectivity for two different diluent/catalyst ratios at 1470 KPa, sv of 4.2 $cm^3g^{-1}s^{-1}$ and H_2/CO ratio of two are presented inFigures 2 and 3. The temperature had almost no effect on the yields of all products except carbon dioxide in both cases. The carbon dioxide selectivity increased as the temperature increased and the rate of increase was almost the same for both the dense and the diluted bed modes of operation; however, at a given temperature, the carbon dioxide yield for the diluted bed mode was lower than that for the dense bed mode. It was concluded from the higher operating temperature and lower carbon dioxide yields in the diluted bed mode that the surface temperature of the catalyst in dense bed mode was higher than the catalyst surface temperature in the diluted bed. Poor heat transfer in the dense bed caused a higher temperature gradient. The results of the loading and the stability test indicated that the preferred diluent to catalyst ratio was four to one.

Process Variable Investigation: C_2-C_4 Olefin Yield Response Equation

A statistical design model was used to optimize the C_2-C_4 olefin production. The second order response equation for a four variable system is written as follows:

$$Y_1 = B_0 + B_1X_1 + B_2X_2 + B_3X_3 + B_4X_4 + B_{11}X_1^2 + B_{22}X_2^2 + B_{33}X_3^2 + B_{44}X_4^2 + B_{12}X_1X_2 + B_{13}X_1X_3 + B_{14}X_1X_4 + B_{23}X_2X_3 + B_{24}X_2X_4 + B_{34}X_3X_4$$

where Y_1 is the C_2-C_4 olefin to paraffin ratio response factor, X_1 is the pressure, X_2 is the temperature, X_3 is the reactant gas space velocity,and X_4 is the H_2/CO molar ratio.

The operating variables, carbon monoxide conversions and the product distributions for 25 design experiments are listed in Table 2. The carbon dioxide yield, the carbon monoxide conversion, the C_2-C_4 hydrocarbon yield, the olefin to paraffin ratio in the C_2-C_4 hydrocarbon fraction and the C_5^+ hydrocarbon yield were used as independent variables in the statistical design computations. The selectivities, as reflected by the olefin to paraffin ratios for the C_2, C_3, C_4 and C_2-C_4 hydrocarbon fractions, are listed in Table 3. The computed response surface correlation coefficients are listed in in Table 4. The F-test technique was used to determine the significance of each coefficient. Those coefficients which were determined not to be significant were eliminated. The reduced set of response surface correlation coefficients from the process variable study are listed in Table 5. The C_2-C_4 olefin to paraffin ratio, Y_1, can be expressed as a response surface equation from the data as follows:

$$Y_1 = 3.406-0.243\ X_1 + 0.319\ X_2-0.884\ X_4 + 0.026\ X_1^2 - 0.003\ X_2^2+$$

$$0.111\ X_4^2 + 0.164X_1X_4-0.233\ X_2X_4$$

where Y_1, X_1, X_2, X_3 and X_4 have been defined previously.

This equation can be used to quantitatively predict the C_2-C_4 olefin to paraffin ratio for the range of operating variables investigated. The response surface equations for other independent variables can also be constructed using the same technique and the coefficients are presented in Table 5. In this study, the H_2/CO ratio appeared to be the most significant operating variable. The response factor for the C_2-C_4 olefin to paraffin ratio changed by a factor of unity when the H_2/CO ratio was changed by a factor of -0.884 and thus the H_2/CO ratio was judged to be the most significant operating variable while the space velocity was the least significant operating variable influencing the olefin to paraffin ratio. Thus, the space velocity (X_3) was eliminated from the response surface equation. The first-order coefficients for the pressure and temperature terms (X_1 and X_2, respectively) were B_1=-0.243 and B_2 = 0.319, respectively. Since the magnitude of each is less than the magnitude of the first order coefficient for the H_2/CO ratio (X_4), B_4 =-0.884, the temperature and pressure are less significant with regard to the C_2-C_4 olefin-to-paraffin ratio than the H_2/CO ratio. The first and second order coefficients for the C_2-C_4 and C_5^+ hydrocarbon yields are considerably smaller than their respective zero order coefficients, which indicates that the yield of C_2-C_4 and C_5^+ hydrocarbons is somewhat insensitive to the operating conditions in the range of process variables investigated.

Effect of Pressure on Product Distribution and Olefin Selectivity

The carbon monoxide conversion decreased as the pressure decreased. At a temperature of 463 K, a space velocity of 9 $cm^3g^{-1}s^{-1}$ and a H_2/CO ratio of one, the carbon monoxide conversion decreased from 4% at 4230 KPa to 2.8% at 1470 KPa. At a temperature of 473 K, a space velocity of 12 $cm^3g^{-1}s^{-1}$ and H_2/CO ratio of two, the carbon monoxide conversion decreased from 6.3% at 3540 KPa to 5.7% at 2160 KPa. This decrease may be due to a change in the carbon monoxide surface coverage brought about by the pressure

decrease. The C_2-C_4 olefin to paraffin ratio decreased from 3.8 at 1470 KPa to 2.7 at 4230 KPa. The carbon dioxide, C_2-C_4 hydrocarbons, and C_5^+ hydrocarbon yields remained almost constant in the pressure range from 1470 to 4230 KPa. The olefin to paraffin ratios for the C_2, C_3, C_4 and C_2-C_4 hydrocarbon fractions also decreased as the pressure increased. The olefin to paraffin ratios for the C_2 and C_3 hydrocarbon fractions were consistently higher than that of the C_4 hydrocarbon fraction in the pressure range investigated: 1470 KPa to 4230 KPa. At a reaction temperature of 453 K, a space velocity of 9 $cm^3g^{-1}s^{-1}$ and a H_2/CO ratio of 1, the olefin to paraffin ratios for the C_2, C_3, C_4 fraction increased from 3.7, 2.8 and 2.1 at 4230 KKPa to 4.2, 3.7 and 3.8 at 1470 KPa, respectively. It is obvious from the stoichiometric equation for the olefin hydrogenation reaction:

$$C_nH_{2n} + H_2 = C_nH_{2n+2}$$

that the olefinic products are favored at lower pressure.

Effect of Temperature on Product Distribution and Olefin Selectivity

The carbon monoxide conversion increased as the temperature increased at a reaction pressure of 3540 KPa, a space velocity of 12 $cm^3g^{-1}s^{-1}$ and a H_2/CO of two; that is, the carbon monoxide conversion increased from 5.4% at 453 K to 6.3% at 473 K. The C_2-C_4 olefin to paraffin ratio increased from 2.8 to 3.7 as the temperatures increased from 443 to 483 K. The olefin to paraffin ratios of the C_3 and C_4 fraction increased as the temperature increased, whereas the olefin to paraffin ratio of the C_2 to C_3 hydrocarbon fractions was consistently higher than that of the C_4 hydrocarbon fraction in the temperature range investigated, 443 to 483 K. At a pressure of 2850 KPa, a space velocity of 9 $cm^3g^{-1}s^{-1}$ and a H_2/CO ratio of 1, the olefin to paraffin ratios of C_2, C_3 and C_4 increased from 4.1, 2.5 and 1.9 at 443 K to 4.3, 3.8 and 3.3 at 483 K, respectively. The carbon dioxide selectivity increased as the temperature increased. This is consistent with the observations made in connection with the catalyst loading and stability tests.

Effect of Reactant Gas Space Velocity on Product Distribution and Olefin Selectivity

The carbon monoxide conversion decreased as the space velocity increased (Table 2). At higher space velocities, the contact time between reactant species and the catalyst surface was reduced. The shorter contact time resulted in lower carbon monoxide conversion. At a pressure of 3540 KPa, a temperature of 453 K and a H_2/CO ratio of two, the carbon monoxide conversion increased from 3.6% to 5.4% as the space velocity decreased from 12 $cm^3g^{-1}s^{-1}$ to 6 $cm^3g^{-1}s^{-1}$. The olefin to paraffin ratios of C_2, C_3, C_4, and C_2-C_4 hydrocarbon fractions remained constant in the range of space velocities from 3 to 15 $cm^3g^{-1}s^{-1}$. The olefin to paraffin ratios of the C_2 and C_3 hydrocarbon fractions were consistently higher than that of the C_4 hydrocarbon fraction in the range of space velocities from 3 to 15 $cm^3g^{-1}s^{-1}$. At other operating conditions, the olefin to paraffin ratios were the same at space velocities of 6 and 12 $cm^3g^{-1}s^{-1}$. The yields of the C_2-C_4 and C_5^+ hydrocarbon yields were independent of space velocity. The carbon dioxide yield decreased from 50% at a

space velocity of 3 $cm^3g^{-1}s^{-1}$ to 27% at a space velocity of 15 $cm^3g^{-1}s^{-1}$. As mentioned in the stability test section, the high space velocity suppresses the Boudouard and water gas shift reactions, thus leading to a decrease in carbon dioxide production.

Effect of Hydrogen to Carbon Monoxide Ratio on Product Distribution and Olefin Selectivity

The carbon monoxide conversion decreased as the H_2/CO ratio decreased (Table 2). At a pressure of 2850 KPa, a temperature of 463 K and a space velocity of 9 $cm^3g^{-1}s^{-1}$ the carbon monoxide conversion decreased sharply from 14.5 % at a H_2/CO ratio of 5 to 0.9 % at a H_2/CO ratio of 0.2. The olefin to paraffin ratios of the C_2, C_3, C_4, and C_2-C_4 hydrocarbon fractions were very sensitive to the H_2/CO ratio (Table 3). At a constant total pressure a reduction in the hydrogen to carbon monoxide ratio reduces the hydrogen partial pressure in the reactor thus favoring the formation of olefins. The carbon dioxide yield also increased to some extent at the hydrogen to carbon monoxide ratio decreased indicating the rate of the Boudouard reaction increased with lower hydrogen to carbon monoxide ratio.

Interaction of Process Variable

The C_2-C_4 olefin to paraffin ratios were influenced by the process variables: temperature, pressure and H_2/CO ratio. The coefficient B_{14} represents the interaction between the pressure and the H_2/CO ratio and was equal to 0.164. Thus, whenever the total pressure or the H_2/CO ratio was changed by one level, the olefin to paraffin ratio in the C_2-C_4 hydrocarbon fraction changed by an amount corresponding to a value of 0.164. The coefficient B_{24} represents the interaction between temperature and the H_2/CO ratio and was equal to -0.223. Thus, whenever the reactor temperature or the H_2/CO ratio is changed one level, the olefin to paraffin ratio in the C_2-C_4 hydrocarbon fraction changes by an amount corresponding to a value of 0.223. The retention of interactive terms B_{14} and B_{24}, after the analysis of the coefficients is probably related to the influence of pressure, temperature and H_2/CO ratio on the fraction of the surface covered by the reacting species, hydrogen and carbon monoxide and on the ratio of the fraction of the surface covered by each.

Statistical Model

The C_2-C_4 olefin to paraffin ratio, displayed as a function of process variables, taken two at a time, predicted from the statistical design are presented in Figures 4 and 5. These figures were prepared using a commercial (Golden Graphics) software package[11] on an IBM PC AT. The inverse distance squared algorithm was selected for the grid calculation.[12] the calculation conditions: grid size 21, smooth factor 0.95, view angle 60 degrees, rotation angle 225 degrees, and height/width ratio of one were selected to better display the response surfaces. The variable dependence can be understood by comparing the slopes of the two lines AB and AC in Figure 4. The rate of change of AC as a function of the H_2/CO ratio is greater than that of AB as a function of pressure. The smooth response surface obtained from the correlation

at least indicates that the reaction conditions used in this investigation are reasonable and the predicted model can be extended to other process variables.

Optimum Process Operating Conditions

The process operating conditions required to produce the optimal C_2-C_4 hydrocarbon fraction, olefin to paraffin ratio, were computed using the calculated coefficients for the response surface as the input data. As discussed, a lower H_2/CO ratio, a higher temperature and a lower pressure would be expected to produce a higher olefin to paraffin ratio in the C_2-C_4 hydrocarbon fraction. The H_2/CO ratio is limited to a minimum value of 0.5 in the experiment to avoid excessive carbon deposition on the catalyst. The optimal operating conditions and the C_2-C_4 olefin to paraffin ratios predicted from the response surface equation were: a pressure of 1470 KPa, a temperature of 473 K, a space velocity of 12 $cm^3g^{-1}s^{-1}$, a H_2/CO ratio of 0.5 and an olefin to paraffin ratio of 5.4. At the predicted optimal operating conditions, an olefin to paraffin ratio of 6.4 was obtained, which was higher than expected. At the optimal operating conditions, the olefin to paraffin ratios for the C_2, C_3 and C_4 hydrocarbon fractions were as follows: the ethylene to ethane ratio was 5, the propylene to propane ratio of 9.3 and the butylenes to butanes was 5.2

CONCLUSIONS

1. The activity as reflected by carbon monoxide conversion and the selectivity as reflected by the C_2-C_4 olefin to paraffin ratio of the Raney iron-manganese catalyst were constant up to 40 hours on stream.

2. The most influential operating variable in determining the olefin selectivity is the H_2/CO ratio.

3. The optimal operating conditions for the maximization of low molecular weight olefins were: a temperature of 473 K, a sv of 12 $cm^3g^{-1}s^{-1}$, a H_2/CO ratio of 0.5 and a pressure of 1470 KPa. The olefin to paraffin ratio at these conditions is 6.4.

ACKNOWLEDGEMENT

The financial assistance provided by the Mobil Research and Deveopment Corporation through the Industrial Affiliates Program of the Laboratory of Coal Science, Synthetic Fuels and Catalysis is gratefully acknowledged.

REFERENCES

1. Storch, H. H., Gouloumbic, N. and Anderson, R. B., The Fischer-Tropsch and Related Synthesis, Wiley, New York, 1951.

2. Gryson, M., Demeter, J. J., Schkesinger, M. D., Johnson, G. E., and Myers, J. W., Synthesis of Methane," Report of Investigations 5137, Bureau of Mines, 1955.

3. Yang, C. H., "Catalytic Synthesis of Light Hydrocarbons from Carbon Monoxide and Hydrogen over Metal Catalysts," Ph.D. Dissertation, University of Utah, Department of Mining and Fuels Engineering, 1979.

4. Tsai, Y. S., "The Hydrogenation of Carbon Monoxide over Unsupported Iron/Manganese Catalysts to Produce Low Molecular Weight Olefins," Master Thesis, University of Utah, Department of Mining and Fuels Engineering, 1980.

5. Tai, W. P., "The Hydrogenation of Carbon Monoxide over Coprecipitated Iron/Manganese Catalyst in a Pseudo Slurry Reactor, " Ph.D. Dissertation, University of Utah, Department of Mining and Fuels Engineering, 1983.

6. Tsai, Y.S., "The Synthesis of Low Molecular Weight Olefins over Co-Precipitated Iron/Manganese Catalysts", Ph.D. Dissertation, Univ. of Utah, Dept. of Fuels Engineering (1985).

7. Raney, M., "Catalysts from Alloys," Ind. Eng. Chem., 1940, 32, 1199.

8. Kim, C. S., "The Hydrogenation of Carbon Monoxide over Raney Iron-Manganese Catalysts," Ph.D. Dissertation, University of Utah, Department of Fuels Engineering, 1983.

9. Chen, K. R., "The Hydrogenation of Carbon MOnoxide over Raney Iron/Manganese Catalysts: Process Variable Investiation", M.S. Thesis, University of Utah, Department of Fuels Engineering (1985).

10. Box, G. E. P. and Wilson, K. B., "On the Experimental Attainment of Optimum Conditions," J. of the Royal Stat. Soc. (series B), 1951, 13, 1.

11. Golden Graphics System Version 2. Golden Software, Inc., Colorado, 1985.

12. Ripley, B. D., Spatial Statistics, Wiley, New York, 1981.

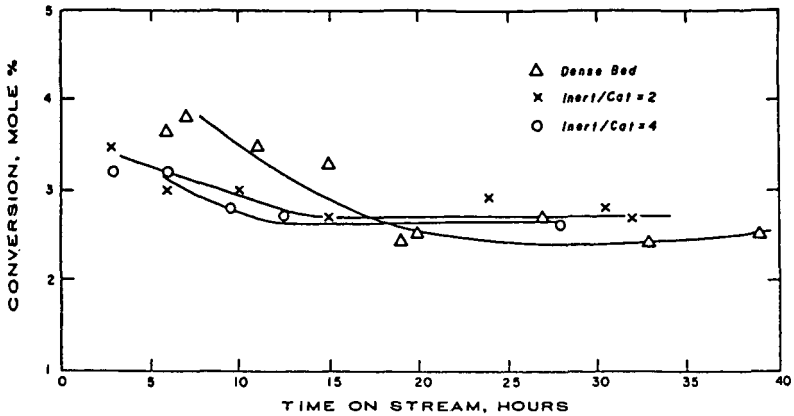

Figure 1 Catalyst Stability Test: Carbon Monoxide Conversion
Raney Fe/Mn Catalyst; T = 443 K; P = 1470 KPa;
H_2/CO = 2/1; Space Velocity = 4.2 $cm^3\ g^{-1}\ s^{-1}$

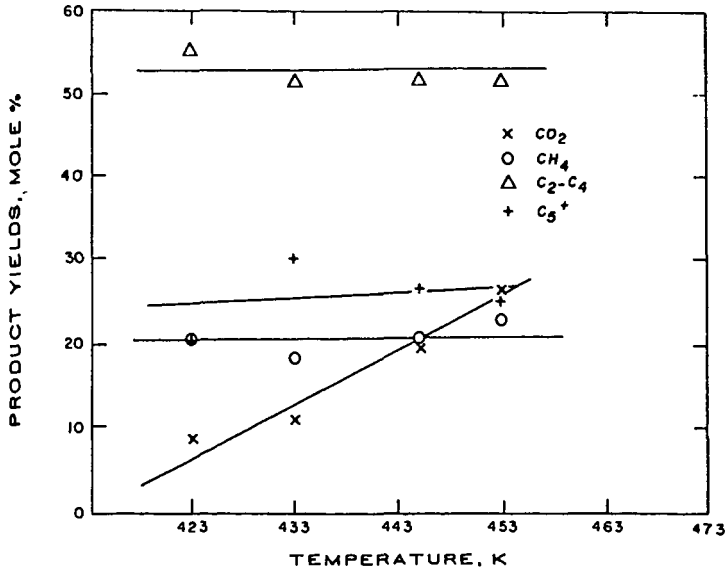

Figure 2 Effect of Temperature on Product Distribution
Raney Fe/Mn Catalyst; P = 1470 KPa, H_2/CO = 2/1
Space Velocity = 4.2 $cm^3\ g^{-1}\ s^{-1}$; Diluent/Catalyst
Ratio = 0/1

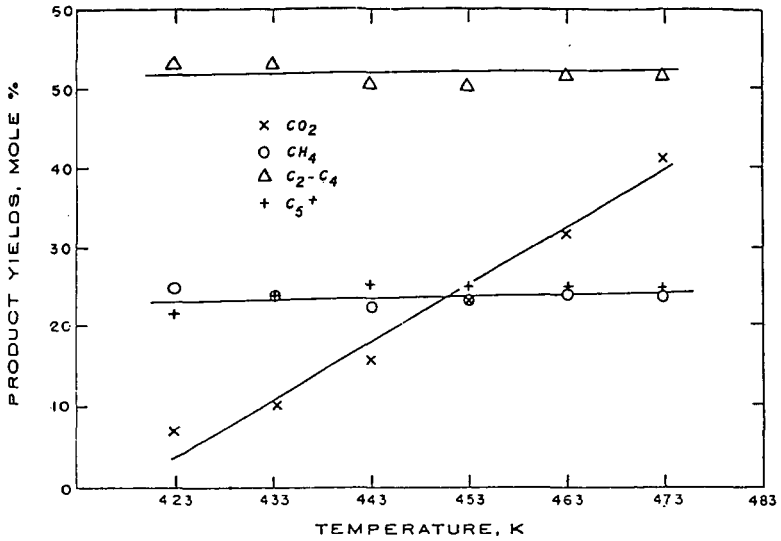

Figure 3 Effect of Temperature on Product Distribution
Raney Fe/Mn Catalyst, P = 1470 KPa, H_2/CO = 2/1
Space Velocity = 4.2 cm^3 g^{-1} s^{-1}; Diluent/Catalyst Ratio = 4/1

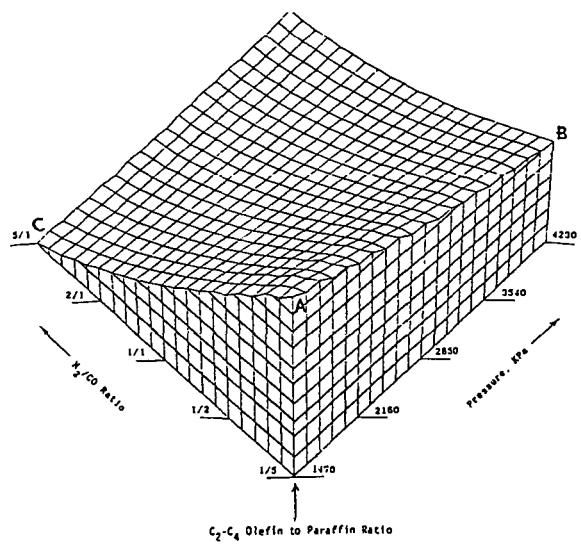

Figure 4 C_2-C_4 Olefin to Paraffin Ratio as a Function of H_2/CO Ratio and Pressure at 463 K

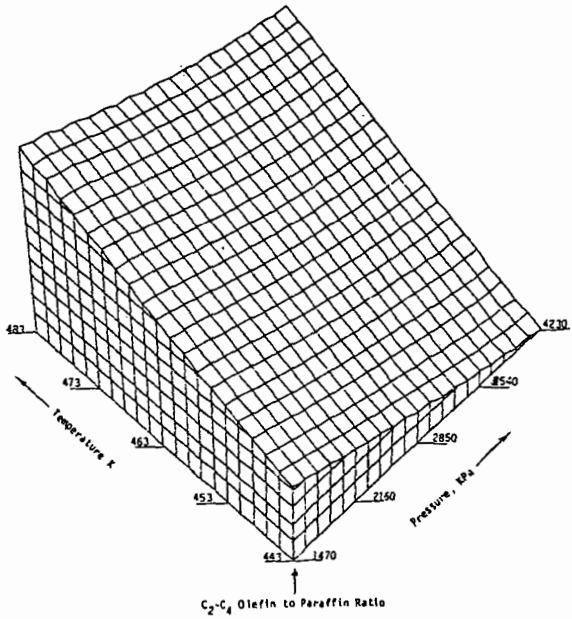

Figure 5 C_2-C_4 Olefin to Paraffin Ratio as a Function of Temperature and Pressure at a H_2/CO Ratio of Unity

Table 1

Range of Process Operating Conditions for Process Variable Study

Variable Level	-2	-1	0	1	2	Range(1)
Temperature, K	443	453	463	473	483	10
Pressure, KPa	1470	2160	2850	3540	4230	690
Hydrogen to Carbon Monoxide Ratio	5/1	2/1	1/1	1/2	1/5	1/2
Space Velocity, $cm^3\ g^{-1}\ s^{-1}$	3	6	9	12	15	3

(1) $$\text{Range} = \frac{\text{Condition(2)} - \text{Condition(1)}}{4}$$

Table 2

Carbon Monoxide Conversion and Product Distribution
Process Variable Investigation

Raney Iron/Manganese (16/1) Catalyst

Run No.	Pressure (KPa)	Temperature (K)	Space Velocity ($cm^3g^{-1}s^{-1}$)	Hydrogen/Carbon Monoxide Ratio	Carbon Monoxide Conversion (mol %)	Product Distribution (mol %) C_1	C_2-C_4	C_5^+	CO_2
1	3540	473	12	2/1	6.3	0.19	0.53	0.27	0.18
2	3540	473	12	1/2	2.2	0.15	0.54	0.31	0.27
3	3540	473	6	2/1	13.3	0.18	0.53	0.28	0.22
4	3540	473	6	1/2	5.7	0.14	0.55	0.30	0.51
5	3540	453	12	2/1	3.6	0.19	0.55	0.26	0.15
6	3540	453	12	1/2	1.2	0.17	0.49	0.29	0.38
7	3540	453	6	2/1	5.4	0.20	0.53	0.26	0.11
8	3540	453	6	1/2	1.8	0.15	0.50	0.31	0.30
9	2160	473	12	2/1	5.8	0.22	0.52	0.26	0.24
10	2160	473	12	1/2	1.8	0.17	0.51	0.32	0.32
11	2160	473	6	2/1	11.2	0.21	0.52	0.26	0.29
12	2160	473	6	1/2	2.5	0.16	0.53	0.31	0.23
13	2160	453	12	2/1	2.7	0.23	0.53	0.24	0.12
14	2160	453	12	1/2	1.1	0.19	0.45	0.31	0.44
15	2160	453	6	2/1	4.6	0.22	0.52	0.26	0.15
16	2160	453	6	1/2	1.5	0.17	0.49	0.29	0.29
17	4230	463	9	1/1	4.0	0.16	0.56	0.27	0.32
18	1470	463	9	1/1	2.8	0.20	0.50	0.29	0.31
19	2850	483	9	1/1	11.9	0.17	0.55	0.28	0.52
20	2840	443	9	1/1	0.9	0.20	0.49	0.25	0.09
21	2850	463	15	1/1	2.5	0.18	0.49	0.29	0.27
22	2850	453	3	1/1	13.6	0.16	0.56	0.27	0.51
23	2050	463	9	5/1	14.5	0.27	0.50	0.22	0.15
24	2850	463	9	1/5	0.9	0.19	0.53	0.28	0.61
25	2850	463	9	1/1	3.0	0.18	0.53	0.30	0.33

Table 3

C_2, C_3, C_4 and C_2-C_4 Olefin Selectivity
Process Variable Investigation

Raney Iron/Manganese (16/1) Catalyst

Run No.	Pressure (KPa)	Temperature (K)	Space Velocity ($cm^3g^{-1}s^{-1}$)	Hydrogen/Carbon Monoxide Ratio	Carbon Monoxide Conversion (mol %)	Olefin to Paraffin Ratio			
						C_2	C_3	C_4	C_2-C_4
1	3540	473	12	2/1	6.3	1.9	2.8	2.1	2.3
2	3540	473	12	1/2	2.2	5.0	4.3	3.5	4.0
3	3540	473	6	2/1	13.3	1.9	2.9	2.7	2.5
4	3540	473	6	1/2	5.7	5.0	4.3	3.2	4.0
5	3540	453	12	2/1	3.6	2.4	2.3	1.8	2.1
6	3540	453	12	1/2	1.2	4.8	3.2	2.3	3.1
7	3540	453	6	2/1	5.4	2.1	2.3	1.7	2.0
8	3540	453	6	1/2	1.8	4.6	3.1	2.3	3.1
9	2160	473	12	2/1	5.8	1.5	3.4	2.5	2.4
10	2160	473	12	1/2	1.8	5.4	5.6	4.3	5.1
11	2160	473	6	2/1	11.2	1.5	3.5	2.6	2.5
12	2160	473	6	1/2	2.5	5.2	5.6	4.1	4.9
13	2160	453	12	2/1	2.7	2.2	2.8	2.1	2.4
14	2160	453	12	1/2	1.1	5.6	3.8	2.8	3.7
15	2160	453	6	2/1	4.7	2.0	2.7	2.0	2.4
16	2160	453	6	1/2	1.5	5.4	3.8	2.8	3.7
17	4230	463	9	1/1	4.0	3.7	2.8	2.1	2.7
18	1470	463	9	1/1	2.8	4.1	4.2	3.7	3.8
19	2850	483	9	1/1	11.9	4.3	3.8	3.3	3.8
20	2840	443	9	1/1	0.9	4.1	2.5	1.9	2.6
21	2850	463	15	1/1	2.5	3.9	3.1	2.4	3.0
22	2850	453	3	1/1	13.6	3.3	3.4	2.3	3.0
23	2850	463	9	5/1	14.5	0.9	2.3	1.7	1.6
24	2850	463	9	1/5	0.9	7.1	5.9	4.4	5.6
25	2850	463	9	1/1	3.3	3.5	3.6	2.8	3.3

Table 4

Correlation Coefficients from the Process Variable Investigaion

β_i (1)	C_2-C_4 Olefin/Paraffin Ratio	Product Yields			
		C_1	C_2-C_4	C_5^+ Hydrocarbons	Carbon Dioxide
β_0	3.310	0.180	0.530	0.300	0.380
β_1	-2.43	-0.012	0.011	-0.001	0.003
β_2	0.319	-0.007	0.012	0.006	0.049
β_3	-0.007	0.006	-0.010	0.001	-0.023
β_4	-0.884	0.021	0.004	-0.019	-0.092
β_{11}	-0.034	-0.001	-0.001	-0.002	-0.030
β_{22}	-0.057	0.000	-0.003	-0.006	-0.033
β_{33}	-0.093	-0.004	-0.002	-0.002	-0.002
β_{44}	0.051	0.011	-0.004	-0.010	-0.014
β_{12}	-0.019	0.000	0.001	0.000	0.010
β_{13}	-0.033	0.000	0.001	-0.001	-0.025
β_{14}	0.164	-0.003	-0.002	0.004	-0.020
β_{23}	-0.223	0.001	-0.014	0.000	0.030
β_{34}	-0.031	-0.001	0.005	0.004	-0.015

(1) β_1: pressure, β_2: temperature, β_3: space velocity
β_4: hydrogen to carbon monoxide ratio

Table 5

Reduced Correlation Coefficients from the Process Variable Investigation

β_i (1)	C_2-C_4 Olefin/Paraffin Ratio	Product Yields			
		C_1	C_2-C_4	C_5^+ Hydrocarbons	Carbon Dioxide
β_0	3.047	0.180	0.520	2.910	0.308
β_1	-0.243	-0.012	0.011	.....	
β_2	0.319	0.07	0.012	0.006	0.048
β_3	.....	0.006	-0.010	.....	-0.023
β_4	-0.884	0.021	.....	-0.019	-0.092
β_{11}	0.026	.....	.....	.....	.....
β_{22}	0.003	.....	.....	-0.004	-0.016
β_{33}	.....	.....	.....	.....	.....
β_{44}	0.111	0.011	.....	-0.008	0.002
β_{12}	.....	.....	.....	.....	.....
β_{13}	.....	.....	.....	.....	.....
β_{14}	0.164	.....	.....	.....	.....
β_{23}	.....	.....	.....	.....	.....
β_{24}	-0.223	-0.014	.....	.....	.....
β_{34}	.....	.....	.....	.....	.....

(1) β_1: pressure, β_2 : temperature, β_3: space velocity
β_4: hydrogen to carbon monoxide ratio

SELECTIVE PRODUCTION OF ALPHA OLEFINS FROM SYNTHESIS GAS OVER ZnO SUPPORTED Pd-Fe BIMETALLICS

Bruce L. Gustafson and Paul S. Wehner

Research Laboratories, Eastman Chemicals Division,
Eastman Kodak Company, Kingsport, Tennessee 37662

INTRODUCTION

Olefins are basic raw materials for a wide variety of commercial processes within the chemical industry. A synthesis-gas-based route to low molecular weight α-olefins would provide the chemical industry with an alternative route to raw materials in the advent of future petroleum shortages or price increases.

The catalytic production of α-olefins from synthesis gas has been the subject of many investigations over the past 50 years.(1,2) It has been established that, in some systems, olefin selectivity can be enhanced through the addition of various promoters such as K, Mn, Ti, or Zn.(1,3-7) Olefin selectivity can also be dependent on process parameters such as temperature, pressure, conversion levels, or feed compositions.

Recent reports in the literature indicate that supported Fe-containing bimetallics may also be selective for the production of olefins from synthesis gas.(8) This study reports the use of Pd-FE bimetallics supported on ZnO for the selective production of olefins from synthesis gas.

EXPERIMENTAL

Catalyst Preparation

The majority of catalysts used in this study were prepared by using aqueous co-impregnation with excess solvent. The nitrate salts of the desired metals ($Pd(NO_3)_2$, Alpha Products or $Fe(NO_3)_3$, Mallinckrodt) were dissolved in excess H_2O at room temperature. It was noted that if acetate salts were used for the metal source or if acetate impurites were present on the support material, the samples which resulted were totally inactive under the conditions employed in this study. For Mössbauer studies, isotopically enriched ^{57}Fe was obtained from Oak Ridge National Laboratory as Fe_2O_3. This material was added to a HNO_3 solution, the solution was evaporated to near dryness twice, and then the residue was dissolved in H_2O. A sufficient amount of this solution was added to the impregnation solution to achieve approximately 50% enrichment in ^{57}Fe.

The solution containing the metals for impregnation was added to the ZnO support (Alpha Products, BET S.A. 7 m^2g^{-1}) at ambient temperature, and then the excess H_2O was removed by gentle heating in air. The samples were frequently stirred to ensure uniform impregnation. Following impregnation, the samples were calcined at 200-300°C for 3 hours to decompose residual nitrates. Metal loading levels were determined by using atomic absorption spectroscopy.

XPS measurements were made by using a PHI Model 550 ESCA/SAM spectrometer with a base pressure of 2×10^{-10} torr. All data were obtained at room temperature by utilizing unmonochromatized Mg Kα radiation ($h\nu = 1253.6$ eV) and an analyzer resolution of 0.3 eV. The Zn $2p_{3/2}$ peak was used as an internal standard for the determination of binding energies. In previous studies, this peak was found to have a binding energy of 1021.8 eV.(9)

Mössbauer spectra were obtained by using a Ranger Scientific MS-900 spectrometer equipped with a ^{57}Co-Rh source. All isomer shifts were measured relative to this source. The spectrometer was operated in the constant acceleration-flyback

mode so that only a single spectrum was recorded per scan. The velocity scale was calibrated by using an NBS-calibrated Fe foil absorber.

Catalyst Evaluation

All catalyst evaluations were conducted in a high-pressure-plug-flow reactor system. For a typical run, 1 mL of sample (14X40 standard mesh) was loaded into a reactor tube that was constructed from standard 1/4" stainless steel, high-pressure tubing. Prior to catalytic evaluation, the samples were reduced at 100 psig and at 300°C for 1 hour in a flow of H_2 or H_2/CO (Matheson Gas Ultra High Purity H_2, Matheson Purity CO). The feed gas was passed through an activated carbon bed at 130°C to remove metal-carbonyl impurities. Feed compositions were controlled by using Brooks mass flow controllers capable of operation up to 1500 psig. Reaction products were analyzed by using an on-line gas chromatograph fitted with a Chromosorb 102 (TM) column. Periodically, samples were analyzed off-line by GC-MS to verify product assignments. To ensure accurate rate measurements, space velocities were adjusted to keep CO conversion levels below 5%.

RESULTS AND DISCUSSION

Following an initial prereduction, the Fe/ZnO and Pd, Fe/ZnO samples were active catalysts at 300°C and at 100 psig for the conversion of synthesis gas to hydrocarbons in the C_1-C_5 range. The olefin fraction was typically in excess of 50 wt% of the observed products for the unpromoted catalysts. In the C_2-C_5 range, propene was the major component, with typical propene/propane ratios of 8-10. The influence of pretreatment conditions, metal loading levels, temperature, and H_2/CO ratio on catalytic activity and selectivity to olefins was investigated. The results of these studied are summarized below.

Catalyst Pretreatment

The catalytic activity of a 1% Pd, 0.3% Fe/ZnO sample was dependent on the nature of the pretreatment procedure. Samples reduced in a 1:1 H_2/CO feed at 100 psig and at 220°C for 1 hour were inactive for the conversion of synthesis gas. However, reduction in H_2/CO at 100 psig and at 260°C for 1 hour was sufficient for catalyst activation. Furthermore, after reduction at 260°C, the catalysts were active for the conversion of synthesis gas at 220°C.

Reduction at 220°C and at 100 psig in H_2 was comparable to reduction in H_2/CO at 260°C. Pretreatment above 300°C resulted in irreversible catalyst deactivation.

XPS spectra were obtained following reduction at various pretreatment temperatures. The results of this study are summarized in Table 1. Following reduction, the Pd $3d_{5/2}$ peak shifted to 336.0 eV, a value approximately 1 eV higher in binding energy than that of Pd metal.(10) This shift in Pd binding energy has been observed in the absence of Fe and can be attributed to a strong interaction between Pd and reduced ZnO. (10). As in a previous study on Pd,/ZnO (ref. 10), a shoulder was observed on the Zn Auger peak which indicated that some reduction of the ZnO surface occurred with the possible formation of a Pd-Zn bimetallic particle. Similar shifts in the Pd and Zn peaks were observed following reduction under the various conditions.

In contrast to the Pd spectra, shifts in the Fe $2p_{3/2}$ peak were sensitive to the pretreatment conditions. At reduction temperatures above 250°C, a significant level of zero-valent Fe (Fe°) was observed by XPS.

Preliminary Mössbauer studies were conducted with the Pd, Fe/ZnO system to determine if the oxidation state of Fe could be correlated with catalytic

activity. The spectrum obtained for the 1% Pd, 0.3% Fe/ZnO catalyst following reduction at 350°C is given in Figure 1. The best fit obtained for this data indicated the presence of two forms of iron (Fe^0 and Fe^{3+}). At lower reduction temperatures (200°C), Fe^{2+} and Fe^{3+} were the only Mössbauer observable forms of Fe present. Given the low loading levels of Fe and low transmission levels encountered with ZnO in the Mössbauer experiment, the presence of Fe^0 at lower temperatures is not precluded. The absence of observable Fe^0 may be a qualitative indication as to the relative amount of Fe^0 formed at 350°C compared to the amount formed at a lower reduction temperature. In contrast to other Pd-Fe systems, no significant amount of Pd-Fe bimetallic was observed by Mössbauer spectroscopy under any of the reduction conditions employed in this study.

STEM studies on these samples indicate that the average particle size increased from approximately 40 Å to more than 120 Å when pretreatment temperature was raised from 260 to 350°C. Coupled with the observations discussed previously, the decrease in activity observed following reduction above 300°C may be due to a decrease in the amount of Fe^{2+} present in these samples and a sintering of the metallic components.

Pd, Fe Ratio

Whereas a variety of metal loadings levels were employed for this study, the results reported here were all obtained by using a constant 1 wt% Pd loading level. As shown in Table II, increasing the Fe loading resulted in a corresponding increase in catalytic activity. In all cases, the olefin/paraffin ratio was greater than unity. It is also apparent from Table II that the addition of 1 wt% Pd to the supported Fe catalysts did not significantly alter the product distribution, but did result in increased catalytic activity. This behavior is in contrast to Pd, Fe/SiO_2 samples evaluated in our laboratory where Pd addition resulted in a tremendous decrease in olefin to paraffin ratio.

Although Pd/ZnO is a good methanol synthesis catalyst (Table II), it should be noted that very little methanol was observed over the Pd, Fe/ZnO samples. The only apparent effect of Pd addition is to increase the overall catalytic activity of the Fe-based catalyst.

The promotional effect of Pd exhibited in this system may involve increasing the Fe dispersion. High Fe dispersions are difficult to obtain on most supports.(11) In some supported Fe-containing bimetallic systems, the metal particle surface is thought to be enriched in Fe.(12,13) It is conceivable that, in the Pd, Fe/ZnO samples, the bimetallic particles consist of a Pd-rich center covered by an Fe-rich coating. Such a model would explain the apparent lack of methanol production by the Pd component.

Because the product distribution was essentially identical for the Fe/ZnO and Pd, Fe/ZnO catalysts, significant changes in oxidation state of the Fe component were probably not responsible for the increased activity following Pd addition. In fact, the XPS and Mössbauer studies mentioned previously indicate that an increase in the Fe reduction was accompanied by catalyst deactivation.

Chemisorption and microscopy experiments were undertaken in an attempt to further characterize the Pd, Fe/ZnO catalyst. Unfortunately, because of the strong Pd-Zn interaction discussed above, chemisorption results were ambiguous and are not reported here. STEM experiments were also inconclusive, primarily due to difficulties in observing Fe on ZnO.

Temperature and H_2/CO ratio

The apparent activation energies which were measured for the 1% Pd, 0.3% Fe/ZnO

sample between 250-300°C are shown in Table III. For comparison, the activation energies for the 0.3% Fe/ZnO are also given. While the olefin/paraffin ratio decreased slightly with increasing temperature, the olefinic fraction remained above 50 mol% of all products over this temperature range.

The fact that the apparent activation energies for the C_1, C_2, C_3, and C_4 fractions are equivalent implies that formation of a common intermediate, such as CH_2, is the rate-determining step for both CH_4 formation and chain growth to higher molecular weight products.

It is also evident from Table III that the apparent activation energies for the 0.3% Fe/ZnO catalyst were 5-6 Kcal/Mol higher than those measured for the Pd-containing catalyst. If hydrogenation is involved in the rate-determining step, this result indicates that Pd may assist in the activation of H_2 in this catalyst system. This conclusion is supported by the observed H_2 partial pressure dependency (Table IV) for the two separate systems. Addition of Pd to the Fe catalyst resulted in a decrease in reaction order with respect to H_2.

CONCLUSIONS

The addition of Pd to Fe supported on ZnO results in a significant increase in catalytic activity for the conversion of synthesis gas. At the same time, selectivity to olefins remains high over these catalysts. One possible role of Pd addition is to increase the dispersion of the Fe component. Kinetic studies indicate that Pd may also assist in the activation of H_2.

REFERENCES

1. (a) Storch, H. H., Galombic, N., and Anderson, R. B., "The Fischer Tröspch Synthesis," John Wiley & Sons, 1951.
   (b) Anderson, R. B., "The Fischer Tröspch Synthesis", Academic Press, Inc., 1984.
2. Caldwell, L., Council for Scientific and Industrial Research Report CENG 330, Pretoria, South Africa, June, 1980.
3. Kobel, H., Tillmetz, K. D., U. S. Patent #4,177,203, 1979.
4. McVicher, G. B., Vannice, M. A., U. S. Patent #4,192,777, 1980 and references therein.
5. Papadopoulos, M., Kieffer, R., and Deluz Arche, A., Bull. Soc. Chim., Fr., 1(3), 109, 1982.
6. Yang, C. H., Oblad, A. G., Preprints, Div. Pet. Chem., ACS Meeting, Anaheim, CA, 1978.
7. Yang, C. H., Ph.D. Dissertation, University of Utah, 1979.
8. Vannice, M. A., Lam, Y. L., Garten, R. L., Adv. Chem. Ser., 178, 25, 1979.
9. Wehner, P. S., Apai, G. A., Mercer, P. N., J. Catal., 84, 244, 1983.
10. Wehner, P. S., Tustin, G. C., Gustafson, B. L., J. Catal., 88, 246, 1984.
11. Brenner, A., J.C.S., Chem. Comm., 251, 1979.
12. Ott, G. L., Delgass, N. N., Winograd, N., Baitinger, W. E., J. Catal., 56, 174, 1979.
13. Schay, Z., Guczi, L., J.C.S. Faraday Trans. I, 78, 1911, 1982.

Table I

XPS Results For 1% Pd, 0.3% Fe/ZnO

Reduction Conditions	Binding Energy, eV* Pd $3d_{5/2}$	Fe $2p_{3/2}$
Fresh	336.9 ±0.1	710.7 ±0.3
H_2, 250°C	335.9	710.1
H_2, 350°C	336.0	710.3/ 707.0
H_2/CO, 260°C	336.0	710.3/ 707.0
CO, 260°C	336.0	710.5

*- Referenced to the Zn $2p_{3/2}$ peak assigned to be 1021.8 eV

Table II

Effect Of Fe Loading Level On Catalytic Performance
For ZnO Supported Samples

T= 300°C, P= 100 psig, H_2/CO = 1

Metal Loading		Rate (Umoles G^{-1} S^{-1}) X 10^2									
% Pd	% Fe	CH_4	$C_2^=$	C_2^-	$C_3^=$	C_3^-	$C_4^=$	C_4^-	$C_5^=$	C_5^-	CH_3OH
0.0	0.3	2.5	.65	.42	.78	.10	.37	.11	.23	.15	.31
1.0	0.3	11.	2.9	1.5	3.3	.43	1.7	.48	.93	.45	.86
0.0	1.0	13.	3.3	1.8	4.8	.48	2.5	.66	1.7	.87	
1.0	1.0	46.	7.4	12.	15.	3.4	6.6	4.0	3.8	4.8	
0.0	2.5	16.	4.9	2.4	6.9	.67	3.9	.83	2.5	1.1	1.2
1.0	2.5	48.	9.0	11.	16.	3.0	7.1	3.3	4.3	4.1	
1.0	0.0	---	.01	---	---	---	---	---	---	---	7.18

$C_n^=$ denotes olefin fraction, C_n^- denotes paraffin fraction

Table III

Apparent Activation Energies For ZnO Supported Catalysts

Rate= $Ae^{-Ea/RT}$

($P_{CO}=P_{H_2}=50$ psig, T=250-300°C)

	Ea, Kcal/Mol	
Carbon No.	1% Pd, 0.3% Fe	0.3% Fe
1	25	30
2	25	31
3	25	31
4	25	30

Table IV

Reaction Orders For ZnO Supported Catalysts

Rate= $k\ P_{CO}^{N}\ P_{H_2}^{M}$

(T=300°C)

	1 % Pd, 0.3 % Fe		0.3% Fe	
Carbon No.	N	M	N	M
1	0.1	0.7	0.8	1.5
2	0.1	0.5	0.9	1.1
3	0.1	0.0	---	---
4	-0.6	-1.5	---	---

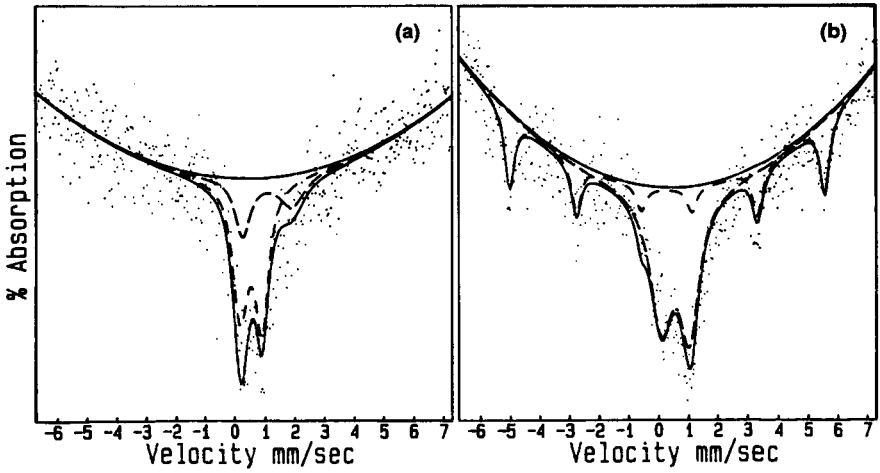

Figure 1. (a) 1% Pd, 0.3% Fe/ZnO Treated in H_2 at 200°C
(b) 1% Pd, 0.3% Fe/ZnO Treated in H_2 at 350°C

CATALYTIC CONVERSION OF BIOMASS DERIVED SYNTHESIS GAS TO DIESEL FUEL IN A SLURRY REACTOR

William H. Zimmerman
Charles N. Campbell
James L. Kuester

Dept. of Chemical Engineering
Arizona State University
Tempe, Arizona 85287

INTRODUCTION

A project has been under investigation for several years at Arizona State University (ASU) with the objective of producing transportation grade liquid hydrocarbon fuel from a wide variety of biomass type feedstocks. The intended product is the equivalent of that derived from petroleum. Thus a renewable and/or waste feedstock is to be utilized to produce a high quality product that is compatible with the existing distribution system and engine designs.

The fundamental characteristics of biomass (as compared with coal) are given in Table 1. As indicated, biomass contains a higher hydrogen/carbon and oxygen/carbon ratio but lower sulfur and ash content. The heating value for biomass is lower (due to the oxygen content) but the volatile matter content is higher. Thus, except for the oxygen content, biomass exhibits more attractive characteristics than coal for producing a liquid hydrocarbon fuel (less hydrogen source addition, less sulfur and ash removal, milder operating conditions). To address the oxygen problem, an indirect liquefaction approach was chosen for study at ASU. The basic steps are:(1) gasification of the biomass in a circulating solid fluidized bed system to a synthesis gas containing primarily hydrogen, carbon monoxide, ethylene, methane and carbon dioxide, and (2) conversion of the synthesis gas to a liquid hydrocarbon fuel in a catalytic reactor. The oxygen in the biomass is thus converted to carbon monoxide, carbon dioxide and some water in the gasification step. In the liquefaction step, the carbon monoxide is converted to paraffinic hydrocarbons, water and normal propanol via the following possible reactions:

$$C_2H_4 + (n-2)CO + (2n-4)H_2 \rightleftharpoons C_nH_{2n+2} + (n-2)H_2O$$

$$1/2(n-1)C_2H_4 + CO + 3H_2 \rightleftharpoons C_nH_{2n+2} + H_2O$$

$$C_2H_4 + CO + H_2 \rightleftharpoons C_2H_5CHO$$

$$C_2H_5CHO + H_2 \rightleftharpoons C_3H_7OH$$

Table 1. COAL AND BIOMASS COMPOSITION (WEIGHT %)

	Coal	Biomass
C	70-80	35-55
H	4-6	4-6
O	5-20	25-50
N	0.5-2	<0.5
S	1-5	<0.5
ash	5-30	0-10
Heating values (Btu/lb) (dry basis)	9500-15000	6500-9500
Volatile matter, wt. %	30-50	60-90

With proper manipulation of the above reactions, the oxygen in the biomass will end up in water, carbon dioxide and normal propanol. Carbon dioxide and water will be vented from the gasification system regenerator and an immiscible alcohol-water phase will be separated from an oxygen free paraffinic hydrocarbon phase. Past and present efforts on the project have been aimed at optimizing the implementation of this scheme via feedstock assessment, factor studies and operational reliability/control improvements. The individual steps have been studied as well as the integrated system. This paper will address recent studies on the liquefaction system. A range of synthesis gas composition produced in the laboratory in the gasification step (for approximately 100 different feedstocks and a range of operating conditions) is as follows (mole%):

hydrogen	10-45
carbon monoxide	15-60
ethylene	5-40
methane	10-45
ethane	1-5
carbon dioxide	0-15

To a certain extent, the synthesis gas composition is feedstock dependent. However control is possible with operating condition manipulation in the gasification step with the major factors being temperature, steam/biomass ratio and choice of solid in the fluidized bed system. Details on the gasification step can be found elsewhere (1,2).

LIQUEFACTION SYSTEM

The catalyst candidates chosen for study fall into two categories: (1) iron, and (2) cobalt. Iron is the traditional active ingredient when performing conversion studies with a synthesis gas dominated by carbon monoxide and hydrogen (3). However biomass offers the opportunity to produce a significant amount of unsaturated gases (primarily ethylene). For this case, cobalt based catalysts are attractive candidates due to the relatively high activity for olefin conversion (as opposed to the relatively inert behavior of iron). Initial liquefaction studies at ASU were performed in a fluidized bed mode. However, primarily motivated by the control complexity of operating fluidized beds in series, a slurry phase system was selected for study as an alternative. In addition to residence time (velocity control) flexibility, the slurry reactor offered the following potential advantages:

- superior temperature control
- longer catalyst life
- catalyst configuration flexibility
- superior gas distribution

The potential disadvantages were increased process complexity (slurry liquid storage and distribution) and possible slurry liquid composition stability problems.

The catalyst and liquid candidates selected for study are listed in Tables 2 and 3. Selection was based on literature guidance, physical and chemical property considerations and system compatibility. All work was performed in a bubble column reactor configuration. Reaction system details and operating procedures are described elsewhere (4,5). The experimental strategy is depicted in Figure 1.

RESULTS

Base operating condition screening runs resulted in the selection of following catalyst/slurry liquid combinations for additional study: (1) 25 Co/175 Al_2O_3 in Fisher paraffin oil, and (2) 48 Fe/4.8 Cu/47.2 kieselguhr in Chevron Refined Wax 143.

Results of fractional factorial experiments to study the effect of reactor operating conditions on product yields for the cobalt study are given in Table 4. Iron catalyst factorial experiment results are shown in Table 5. Note that the feed composition did not include ethylene for the iron study since olefins are essentially inert in the presence of iron. Factor choice and levels were guided by the literature and ASU laboratory experience. Example product compositions for the two studies are shown in Figures 2 & 3. Data was obtained over a sufficient period of time (>8hrs) to insure steady state operation. Base point replication indicated an experimental error[1] of 2% for the cobalt study and 5% for the iron study. Mass balance closures (mass out/mass in x 100) were in the 95-105% range for the two studies.

Table 2
Catalyst Candidates

Cobalt/Alumina
Cobalt Oxide Powder
Cobalt Oxide Precipitate
Cobalt-Potassium/Alumina
Iron-Copper-Potassium Precipitate
Girdler C-73-1 (Iron Based Ammonia Synthesis Catalyst)
Iron-Copper/Kieselguhr
Iron-Copper/Alumina
Iron-Copper-Potassium/Alumina
Iron-Copper Precipitate

Table 3
Slurry Liquid Candidates

Product Liquid
Commercial No. 2 Diesel
Mineral Oil/Paraffin Oil
Chevron 143 Refined Wax
Synthetic Motor Oil (Mobil One)
Tetralin
Tetraethylene Glycol
Dimethyl Napthalene
Hexadecane
Triethylene Glycol
1-Octadecene
Diethyl Phthalate
Dow 210H
Dow Syltherm 800
Alpha Eicosane
Revco Mineral Motor Oil

Mathematical models were fitted to the experimental data for each study, optimized and experimentally verified. Verification of predicted optimums were mixed, dependent on the particular problem posed. Thus close agreement was achieved in some cases while other problems resulted in deviations in both high and low directions. Additional product analyses were performed (eg, heating value, cetane index, API gravity, average molecular weight, most abundant carbon number, grouped composition, Shulz-Flory analysis). Also equilibrium calculations were performed. Composition analysis on the slurry liquids did not indicate any appreciable degradation in the presence of the catalysts although total operating time length was not extensive. Catalyst activity was also stable for the prescribed run lengths.

[1] $\text{exp. error} = \frac{\text{base point product yield range}}{\text{factorial product yield range}} \times 100$

Table 4
Cobalt Study Results[1]

Factors		Feed Gas Comp(mole%)[2]			Responses			
					Gas Conversions			Product Yield
T, °C	P, psia	H_2	C_2H_4	CO	H_2	C_2H_4	CO	(mg/gcat/hr)
Factorial Pts:								
310	95	20	5	20	55.8	87.2	36.1	9.7
210	95	40	5	40	28.6	46.6	7.6	2.9
210	95	20	25	40	22.7	13.6	3.4	3.7
310	95	40	25	20	61.7	89.0	37.6	27.0
210	295	40	25	20	28.2	39.6	12.8	82.0
310	295	20	25	40	75.9	80.6	6.4	166.0
310	295	40	5	40	68.8	87.9	39.3	85.0
210	295	20	5	20	13.0	38.6	5.2	11.0
Base Pt.								
260	195	30	15	30	42.0	62.6	13.7	53.0
260	195	30	15	30	50.1	68.0	15.8	50.0
260	195	30	15	30	51.3	69.5	18.3	53.0

[1] experiment: 2^{5-2} (2 level, 5 factor)
fractional factorial with base point replication.
Superficial gas velocity = ~ 1.0 cm/sec st T,P
[2] balance of gas = carbon dioxide + methane

Table 5
Iron Study Results[1]

Factors				Responses		
				Gas Conversions		Product Yield
T, °C	P, psia	H_2/CO (molar)	Catalyst Amount (wt. frac.)	H_2	CO	(mg/gcat)/hr
Factorial Pts:						
220	120	0.5	0.05	5.2	0.10	0.9
300	120	0.5	0.05	66.4	44.4	31.7
220	200	0.5	0.05	1.1	1.1	2.2
300	200	0.5	0.05	71.0	46.9	118.0
220	120	2.5	0.05	1.2	3.6	1.4
300	120	2.5	0.05	32.2	76.7	8.5
220	200	2.5	0.05	1.5	5.1	0.7
300	200	2.5	0.05	43.3	88.5	5.0
220	120	0.5	0.20	2.4	10.0	6.6
300	120	0.5	0.20	68.4	24.2	8.9
220	200	0.5	0.20	5.4	1.0	2.8
300	200	0.5	0.20	54.1	54.9	28.8
220	120	2.5	0.20	11.3	18.7	5.2
300	120	2.5	0.20	26.6	50.5	11.5
220	200	2.5	0.20	9.0	19.7	3.8
300	200	2.5	0.20	45.7	49.8	5.7
Base Pts:						
260	160	1.5	0.125	41.0	77.0	30.3
260	160	1.5	0.125	56.0	81.0	31.6
260	160	1.5	0.125	38.1	87.9	26.2

[1] experiment: 2^4 (2 level, 4 factor)
full factorial with base point replication.
Superficial gas velocity = ~ 1.0 cm/sec at T,P
[2] balance of gas = CO_2 + methane (H_2 + CO = 50 mole %)

SUMMARY AND CONCLUSIONS

The following assessment of the results presented in the preceeding section is offered:

(1) For the cobalt study, the order of importance of the factors studied with regard to effect on product yield is as follows (via analysis of variance): temperature, pressure, ethylene, hydrogen, carbon monoxide. For the iron study, the order of importance of the factors is as follows: temperature, H_2/CO, catalyst amount, pressure.

(2) Product compositions and properties are attractive and potentially competitive with commercial fuels such as No. 2 diesel and aviation fuels. Product composition is relatively insensitive to operating condition changes with a fixed catalyst.

(3) Cobalt based catalysts are preferred if a significant amount of olefins are present in the synthesis gas. Without significant olefins, iron catalysts should be considered.

(4) Product yield improvement potential is considerable via adjustment of catalyst, slurry liquid and reactor operating variable factors via optimization studies.

(5) The slurry reactor is an advantageous system with regard to temperature control, residence time flexibility and possibly catalyst life. A major disadvantage is the complexity of an additional ingredient in the system (if the product liquid is not utilized).

(6) Catalyst and liquid life endurance testing need to be performed on the catalyst/liquid systems reported in this paper.

ACKNOWLEDGEMENTS

The work reported in this paper received support from the U.S. Department of Energy (Division of Industrial Programs) and the U.S. Department of Agriculture (Science and Education Administration)

REFERENCES

1. Kuester, J. L., "Diesel Fuel via Indirect Liquefaction", Chapter 24 in Energy Applications of Biomass (M. Lowenstein ed.)., Elsevier Applied Science Publishers Ltd (1985).
2. Kuester, J. L. "Diesel Fuel from Biomass, in Energy from Biomass and Wastes VIII, Institute of Gas Technology (1984).
3. Anderson, R. B. The Fischer-Tropsch Synthesis, Academic Press (1984).
4. Campbell, C. Synthesis of Liquid Hydrocarbon Fuels from Biomass in a Slurry Reactor, MSE Thesis, Arizona State University (December, 1983).
5. Zimmerman, W. Slurry Phase Synthesis of Liquid Hydrocarbon Fuels from Biomass Pyrolysis Gas Using Iron Catalysts, MS Thesis, Arizona State University (May, 1985).

Figure 1

EXPERIMENTAL PLAN

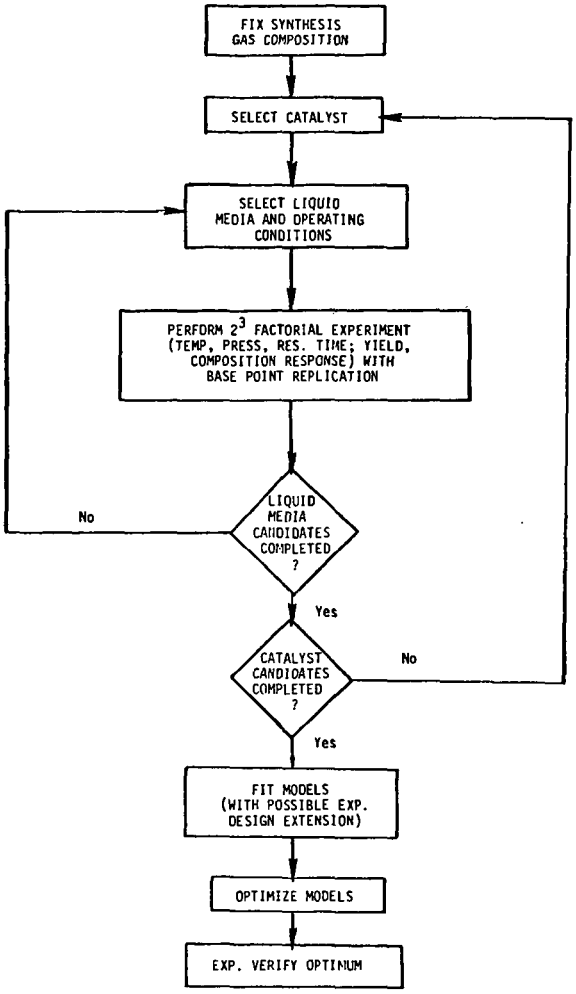

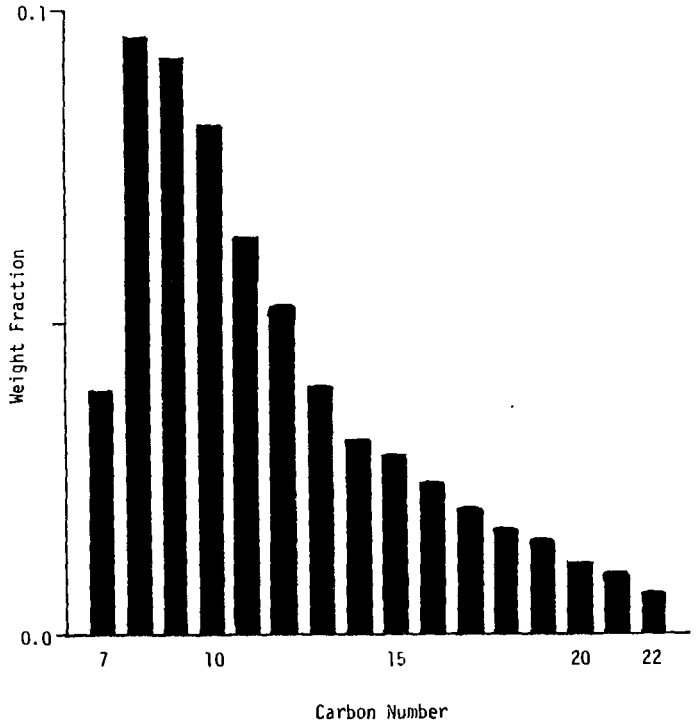

Figure 2
Organic Product Distribution--Iron Catalyst
Feed Composition: 26% H_2, 32% CO, 16% CO_2, 13% CH_4, 13% C_2H_4 (mole %)
Temperature: 260 ^oC
Pressure: 160 psig
Superficial velocity: 1 cm/sec at T,P

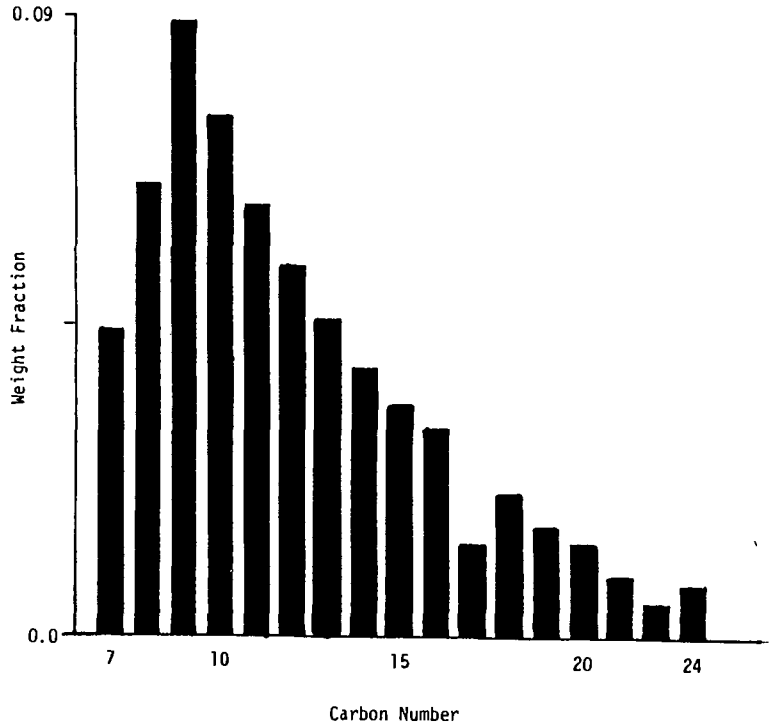

Figure 3
Organic Product Distribution--Cobalt Catalyst
Feed Composition: 26% H_2, 32% CO, 16% CO_2, 13% CH_4, 13% C_2H_4 (mole %)
Temperature: 260 °C
Pressure: 160 psig
Superficial velocity: 1 cm/sec at T,P

THE CATALYTIC DECOMPOSITION OF METHANOL INTO SYNGAS FOR USE AS AN AUTOMOTIVE FUEL

David T. Wickham, Boyce W. Logsdon, and Scott W. Cowley

Department of Chemistry and Geochemistry
Colorado School of Mines, Golden, CO 80401.

ABSTRACT

Although methanol is thought to be an excellent automotive fuel, it has a smaller volumetric fuel value than gasoline. The catalytic decomposition of methanol into syngas, prior to its combustion in the engine, improves its fuel value by approximately 14%. Palladium and platinum on modified alumina supports demonstrate the necessary qualities for this process. The catalytic activity and thermal stability of palladium is strongly affected by the nature of the catalyst support used. A gamma-alumina support was modified with the oxides of Li, Mg, Cs, and La. The effect of the modified support on the activity, selectivity, and thermal stability of the palladium metal was studied during exposure to a thermal cycle of 300, 500, and 300°C. The profound difference in catalyst behavior may be due to strong metal-support interactions, to variations in metal dispersion, or to chemical alteration of the palladium. In order to determine the chemical state of the palladium metal and the modified support before and after testing, the catalysts were characterized by TPD, XRD, XPS, and volumetric chemisorption techniques.

INTRODUCTION

Methanol is available from renewable sources, such as biomass, or from non-petroleum sources, such as coal. For this reason it is considered an attractive alternative to gasoline as an automotive fuel. However, it suffers the disadvantage of having a lower enthalpy content than gasoline, which translates into less mileage per gallon of fuel(1). The potential fuel value of methanol can be improved by catalytically decomposing it into syngas prior to it's combustion in an internal combustion engine. Syngas, which is also referred to as dissociated methanol, has approximately a 14% higher enthalpy content than methanol. The combustion enthalpies for methanol, syngas ($2CO + 4H_2$), and dimethyl ether (a side product of methanol decomposition) is given in Table I. A Chevrolet Citation and a Ford Escort have been retrofitted with catalytic converters in order to demonstrate the feasibility of this process. A schematic of the automotive system is shown in Figure 1. The design and testing of this system was carried out at the Solar Energy Research Institute (SERI). A more

detailed description of the automotive system employed in these studies is available in the literature(2).

At the time this study was initiated, no catalyst had been designed specifically for the decomposition of methanol into syngas in an automotive converter. In order to find an effective catalyst for this process, the following catalyst requirements were defined. First, the catalyst must demostrate good selectivity for syngas over a large temperature range. Second, the catalyst should be able to withstand high temperatures without deactivating. Third, the catalyst should show significant activity at low temperatures. Forth, the catalyst should be mechanically strong. Fifth, the catalyst cost should be reasonable. Several catalysts were prepared by placing active metals (Cu, Ni, Pd, and Pd) on a variety of supports (magnesia, silica, alumina) were tested and the results were compared with those obtained from several commercial formulations(3). All of the commercial formulations failed either the first, second or fourth requirements or a combination of those requirements. Palladium and platinum were found to be the best metals for the decomposition of methanol and alumina was found to be the best support, however, the alumina support is also active for the dehydration of methanol into dimethyl ether, which is an undesirable side reaction. Therefore, several catalysts were prepared in our laboratory in which active metals were impregnated onto a variety of modified gamma-alumina supports. The modified supports have a marked effect on the activity, selectivity, and thermal stability of some metals and little effect on others.

The objective of this study is to establish the function of these modified supports in controlling the behavior of the active metal. Many of the initial test and characterization results have been reported in the literature(3,4). However, some of the more interesting catalysts have been studied and characterized in more detail and are discussed below.

EXPERIMENTAL

The catalysts were tested under the same temperature and flow conditions that would be experienced in the automotive system. The tests were conducted in a microcatalytic plug-flow reactor. Methanol was pumped into a heated inlet and vaporized. The catalyst was mounted on a fritted disk in a quartz tube. The methanol vapor was passed over the catalyst bed and the decomposition products were introduced by a gas sampling valve into a gas chromatograph. The gas chromatograph was equipped with a thermal conductivity detector and a 9 ft. x 1/8 inch stainless steel column packed with Poropack Q. Hydrogen analysis was accomplished by using a 5% hydrogen in helium carrier gas and a subambient program.

The modified supports were prepared by impregnating a gamma-alumina support with a solution containing the nitrate salt of the desired modifying agent. Subsequently, the modified supports were dried at 150°C, calcined at 550°C, and

impregnated with a solution containing either the nitrate or chloride salts of palladium or platinum. The drying and calcining steps were repeated for the finished catalyst. The catalysts were activated in the reactor under a flow of hydrogen at 300°C for 1 hour and at 400°C for 1 hour prior to testing.

Approximately 0.4 grams of 14-20 mesh catalyst particals were tested in each run, using a methanol flow rate of 0.19 g MeOH/g cat.-hr. The methanol was distilled over magnesium turnings and stored over 5A molecular sieve before use. Ultra high purity hydrogen was passed over a Matheson Model 450 purifer.

The total catalyst surface areas were obtained using conventional BET methods. The active metal surface areas were obtained with a volumetric apparatus using hydrogen chemisorption, carbon monoxide chemisorption, and hydrogen-oxygen titration techniques.

For the temperature programmed desorption studies, 0.4 grams of the catalyst were reduced in hydrogen at 400 or 500 °C for 2 hours. The hydrogen was stripped from the catalyst surface in a helium for 15 min. and then cooled in helium to 0°C. Subsequently, several pulses of carbon monoxide were introduced until the surface was saturated. The temperature desorption profile was obtained by increasing the temperature at a rate of 25°C/min. and analyzing the desorption products in a quadrapole mass spectrometer. The temperature programmed desorption apparatus is very similar to that used by other researchers(5). All the gases used during the characterization studies were of Ultra High Purity grade and they were further purified to remove traces of oxygen, water and other impurities.

The catalysts were also characterized before and after testing using a Rigaku x-ray diffractometer, a Perkin Elmer 5000 atomic absorption spectrometer, and a Surface Science SSX-100 x-ray photoelectron spectrometer.

RESULTS AND DISCUSSION

Catalyst Testing

All catalysts were tested at 300°C, the average operating temperature of the converter, and at 500 or 550°C to simulate a high temperature excursion. Subsequently, the temperature was lowered to 300°C to check for possible catalyst deactivation. The results of these tests are given in Table II. Each catalyst contains approximately 5 wt.% of the metal oxide modifying agent and a 0.5 wt% Pd or Pt. The modifying agents Li_2O, MgO, Cs_2O, and La_2O_3 are represented in Table II as Li, Mg, and La. The gamma-Al_2O_3 support is represented as Al. The products observed in these tests were hydrogen, carbon monoxide, methane, carbon dioxide, water, dimethyl ether, and unconverted methanol. The mole % products in Table II are reported on a hydrogen free basis.

To begin with we will only consider the initial activity

of the catalysts at 300°C prior to a high temperature excursion at 550°C. The alumina support (Al) shows almost no activity for the formation of the desired CO decomposition product, but is very active for the formation of dimethyl ether. The formation of dimethyl ether is an exothermic reaction and should be avoided. In the case of the Pd-Al and Pt-Al catalysts, it is obvious that the metal plays the primary role in the production of CO, however, the dehydration activity of the support is still apparent. For those catalysts using the modified supports, Pd-Li-Al, Pd-Mg-Al, Pd-La-Al, Pt-Li-Al, Pt-Mg-Al, and Pt-La-Al the dehydration activity of the catalysts has been eliminated or reduced to an acceptable level. It is interesting to note that the modified supports have a pronounced effect on the initial activity of the Pd metal as indicated by the production of CO, with the Pd-Li-Al showing the lowest activity and the Pd-La-Al showing the highest activity. On the other hand, the initial activity of the Pt metal does not appear to be influenced by the nature of the modifier used.

At 550°C, the modified supports have a pronounced effect on the catalyst selectivity. All the Pt catalysts and the Pd-La-Al catalyst produce substantial amounts of methane, carbon dioxide, and water, while the Pd-Al, Pd-Li-Al, and Pd-Mg-Al catalysts are quite selective for the desired CO product. These results suggest that the latter catalysts have thermally deactivated and the resultant activity and selectivity is really due to the support and not the metal.

The final activity at 300°C, after testing at 550°C, shows all of the Pd catalysts (with exception of the 3% Pd catalyst) have thermally deactivated, while the Pt catalysts show no deactivation or an increase in activity.

The catalyst testing was extended to modified catalysts containing approximately 3 wt% Pd, and the results are shown in Table III. In these tests the hydrogen analysis was included. The effects of the modified supports on the initial and final activities of the catalysts is obvious, with the Pd-La-Al catalyst representing the best case and the Pd-Li-Al catalyst the worst case. The Pd-La-Al catalyst appears to experience a slight loss in activity after a thermal cycle. However, exposing the Pd-La-Al catalyst to repeated thermal cycling over a three day period resulted in no further deactivation. This catalyst was selected for use in the "dissociated methanol car" and has fullfilled all the catalyst requirements with exception of the cost of the material. In any case, it has allowed the feasiblity of the process to be demonstrated in an automobile.

Catalyst Characterization

The modified supports have a marked influence on the catalyst activity, selectivity and thermal stability. Modified alumina supports may have an important impact on the behavior of metals other than Pd and Pt. The effects of these modified supports may extend to other important chemical reactions which involve hydrogenolysis, dissociation, or hydrogenation steps,

such as, Fischer Tropsch, and methanol synthesis. In order to understand the role of the modified support in controlling the behavior of the active metal component, selected catalysts were characterized using both bulk and surface techniques. Since the Pd-Li-Al and the Pd-La-Al catalysts represent the most extreme cases in activity, selectivity and thermal stability, they were selected for futher detailed studies.

The complete thermal deactivation of the Pd-Li-Al catalyst could result from one of the following processes:

1) Loss of total surface area due to support sintering.
2) Loss of total surface area due to pore blockage.
3) Loss of the active Pd metal from the catalyst.
4) Sintering of the metal crystallites.
5) Migration of the metal into the support.
6) Covering the active metal with an inactive material.
7) Formation of a new inactive Pd compound.

The first two possiblities were eliminated by measuring the total surface area of the fresh and reduced Pd-Li-Al catalyst using the BET method. There was no significant change in the total surface area and the results are given in Table IV.

The metal content of the fresh, reduced and tested catalysts were determined using atomic adsorption and the results are also given in Table IV. It is apparent that the active metal does indeed remain with the catalyst.

Broadening of the Pd lines in x-ray diffraction would suggest sintering of the metal crystallites was involved. The XRD spectra for both the reduced and tested Pd-Li-Al catalyst is shown in Figure 2. There is no evidence of line broadening, however, all the palladium lines of the tested catalyst have shifted to lower 2θ values. This suggests that either a new compound has been formed or that the Pd lattice has expanded, possibly due to the palladium forming a solution with another element. These results would also arque against the migration of the Pd metal into the support as a cause for the themal deactivation.

The catalyst deactivation was also found to be reversible, as shown in Figure 3. Although the catalyst was deactivated at high temperatures, its activity could be restored by recalcining the catlyst in air and reducing in hydrogen. The catalyst demonstrated an activity almost identical to its initial activity. However, the catalyst was again deactivated after a thermal cycle. This result strongly arques against migration of the Pd metal into the support, which should be an irreversible process. It also suggests that the element which is causing the deactivation is easily removed by treatment with oxygen, an example of such an element would be carbon.

XPS analysis of the fresh, reduced, and tested Pd-Li-Al and Pd-La-Al catalysts is shown in Figure 4. These survey scans provided information about the elemental composition of the catalyst surfaces before and after testing. The peaks of most interest are the Pd 3d peaks. For the Pd-La-Al catalyst the Pd is present at the surface of the fresh, reduced, and tested catalyst. In fact, the Pd signal is inhanced after

testing. On the other hand, the Pd-Li-Al catalyst shows that the Pd signal has almost disapeared on the tested catalyst. This would suggest that the catalyst is being covered by some other element. The carbon signal, just to the right of the Pd peak, appears to increase on the Pd-Li-Al catalyst but not for the Pd-La-Al catalyst. A depth profile of the surface was obtained by sputtering the surface with argon ions. The results are shown in Figures 6 and 7. The Pd signal for the Pd-Li-Al catalyst increased as the surface was sputtered away, while the carbon signal disappeared at the same time. The Pd-La-Al catalyst showed little effect with sputtering of the surface.

Finally, temperature programmed desorption/reaction of carbon monoxide from the surface was conducted to study the ability of the two catalysts to disproportionate carbon monoxide into carbon dioxide and carbon. The disproportionation reaction may be the primary source of the carbon for the deactivation of the Pd-Li-Al catalyst, see Figure 5. It is apparent that much more carbon dioxide is produced over the Pd-Li-Al catalyst and the reaction takes place at a much lower temperature. This suggests that the modified supports have a pronounced effect on the surface activity of the Pd metal.

SUMMARY

The activity, selectivity, and thermal stability of Pd metal is strongly influenced by the use of the modified supports. This suggests that either the modified support is influencing the behavior of the metal by either controlling the dispersion of the metal crystallites or by exhibiting a strong metal-support interaction.

REFERENCES

1) J. Finegold, J.T. McKinnon, and M. Karpuk, "Reformed Methanol", Non-petroleum Fuels Symposium III, October 1980.

2) J. Finegold, G.P. Glinsky, and G.E. Voecks, "Dissociated Methanol Citation: Final Report", SERI/TR-235-2083, August 1984.

3) S.W. Cowley and S.C. Gebhard, "The Catalytic Decomposition of Methanol into Synthesis Gas for Use as an Automotive Fuel", CSM Quarterly, 7(3), 41 (1983).

4) S.C. Gebhard, B.W. Logsdon, and S.W. Cowley, "The Decomposition of Methanol Over Supported Palladium and Platinum Catalysts", manuscript in preparation.

5) J.M. Zowtiak and C.H. Bartholomew, J. Catal., 83, 107 (1983).

TABLE I. Combustion Enthalpies for Methanol, Dimethyl Ether, Methane, and Synthesis Gas.

Combustion Reactions	H_r (kcal/mole) 400°K	800°K
1. $2CH_3OH + 3O_2 \longrightarrow 2CO_2 + 4H_2O$	-322.4	-321.5
2. $CH_3OCH_3 + 3O_2 \longrightarrow 2CO_2 + 3H_2O$	-317.1	-316.8
3. $2CH_4 + 4O_2 \longrightarrow 2CO_2 + 4H_2O$	-365.0	-341.4
4. $2CO + 4H_2 + 3O_2 \longrightarrow 2CO_2 + 4H_2O$	-367.7	-371.0

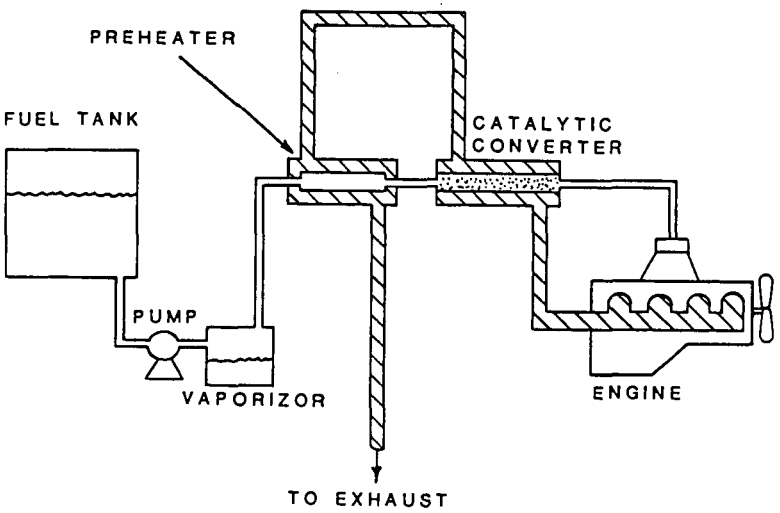

Figure 1. Automotive system for methanol decomposition. The unhatched pathway delineates the transport of fuel toward and into the engine; the hatched pathway illustrates the discharge of exhaust gases from the engine.

TABLE II. Methanol Decomposition Over Pd and Pt Catalysts.

CATALYST*	TEMP. (°C)	%Pd or %Pt	MOLE % PRODUCTS					
			CO	CH_4	CO_2	H_2O	CH_3OH	DME
Al	300	0	0.9	0	0	25.1	47.5	26.6
	550		78.9	7.5	6.7	5.8	0	0
	300		0.9	0	0	25.5	46.7	27.0
Pd-Al	300	0.5	60.8	0.9	0.8	13.5	12.2	21.3
	550		72.5	10.3	6.7	8.1	0.8	0
	300**		0.4	0	0	2.5	95.0	0
Pd-Li-Al	300	0.5	36.5	0	0	1.5	62.0	0
	550		94.3	0	1.3	2.7	1.0	0.8
	300**		1.0	0	0	0.8	98.0	0
Pd-Mg-Al	300	0.5	36.6	0	0	1.5	61.9	0
	550		92.9	1.2	1.3	3.5	0.7	0.5
	300**		0.7	0	0	2.5	95.0	1.8
Pd-La-Al	300	0.5	85.6	0.8	0.7	3.2	9.2	1.5
	500		61.7	2.0	2.6	13.6	7.1	12.9
	300**		-	-	-	-	-	-
Pd-La-Al	300	3.0	85.4	2.4	1.0	5.8	2.7	2.4
	550		18.0	41.8	17.7	22.1	0	0
	300**		83.5	2.0	0.7	7.6	2.5	2.6
Pt-Al	300	0.5	25.2	2.7	1.8	25.4	23.3	21.1
	550		40.9	28.4	13.0	16.4	0.6	0
	300**		35.8	1.5	0.7	22.0	19.3	20.0
Pt-Li-Al	300	0.5	46.8	0.8	0.8	1.0	49.5	0
	550		65.2	16.0	8.1	9.7	0	0
	300**		45.0	0.9	0.6	1.2	51.2	0
Pt-Mg-Al	300	0.5	45.8	0.6	0.5	1.6	51.8	0
	550		52.7	22.0	11.4	12.3	0	0
	300**		50.1	1.0	0.4	2.5	44.5	0
Pt-La-Al	300	0.5	48.3	0	2.0	4.6	42.1	0
	550		26.6	35.5	16.8	19.8	0.6	0
	300**		69.6	0	1.2	2.9	23.0	0

* Catalyst Wt. = 0.400 g, approx. 5% metal oxide modifier present
Space Velocity = 1.9 g MeOH/g cat.-hr.
Pressure = 608.0 mm Hg

** After testing at 500°C

TABLE III. Methanol Decomposition Over Modified 3% Pd Catalysts. Hydrogen Analysis Included in Product Analysis

CATALYST*	TEMP. (°C)	MOLE % PRODUCTS						
		H_2	CO	CH_4	CO_2	H_2O	CH_3OH	DME
Pd-Al	300	57.8	31.0	0.7	0.3	6.5	1.1	2.5
	550	25.6	5.4	31.0	15.8	22.3	0	0
	300**	59.2	32.2	0.8	0.3	5.0	0	0
Pd-Li-Al	300	53.4	29.2	0	0	1.1	16.3	0
	550	60.8	30.2	0.8	2.3	3.0	0.2	2.7
	300**	1.4	0.5	0	0	2.3	96.8	0
Pd-Cs-Al	300	34.8	19.9	0.5	0	4.1	40.6	0
	550	56.7	27.9	6.4	4.2	4.9	0	0
	300**	34.2	18.2	0.3	0	2.5	44.8	0
Pd-La-Al	300	56.7	30.4	0	0	0	13.0	0
	500	33.9	10.5	25.0	14.2	16.1	0	0
	300**	51.6	28.0	0	0	1.7	18.6	0

* Catalyst Wt. = 0.400 g, approx. 5% metal oxide modifier present
Space Velocity = 1.9 g MeOH/g cat.-hr.
Pressure = 612-622 mm Hg
** After testing at 500°C

TABLE IV. Elemental Composition and Surface Analysis of Pd Catalysts.

Catalyst	Catalyst History	Pd Metal* (wt.%)	Metal Oxide** (wt.%)	BET (m^2/g)	Chemisorp. (mole Pd/g)		
					H_2	CO	H_2-O_2
Pd-Al	fresh	2.6	0	-	-	-	-
	reduced	2.6	-	-	115.1	102.8	107.4
	tested	2.6	-	-	-	-	-
Pd-Li-Al	fresh	2.9	5.0	75.6	-	-	-
	reduced	2.9	-	-	45.7	37.0	-
	tested	2.9	-	75.6	-	-	-
Pd-Cs-Al	fresh	2.8	5.0	-	-	-	-
	reduced	2.8	-	-	67.7	64.5	57.0
	tested	2.9	-	-	-	-	-
Pd-La-Al	fresh	3.4	5.0	-	-	-	-
	reduced	3.3	-	-	66.0	53.8	48.7
	tested	3.4	-	-	-	-	-

* Wt. % metal was determined by atomic absorption
** Estimated from preparation

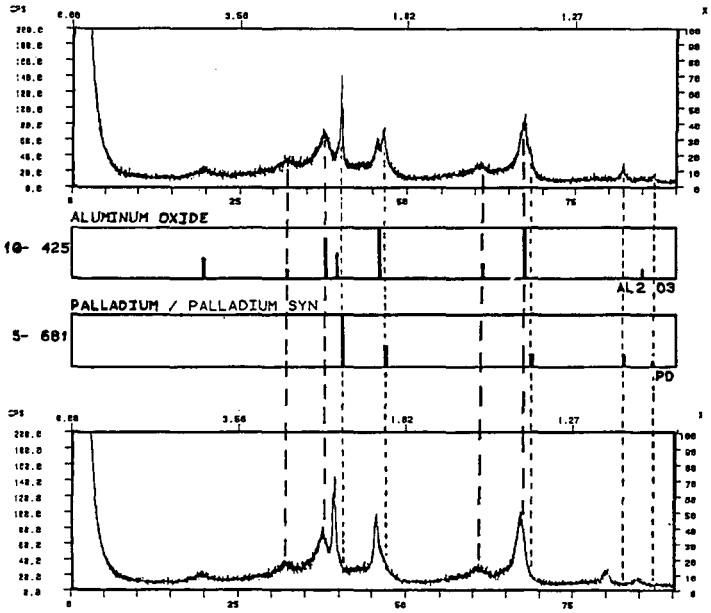

Figure 2. The XRD specta of a reduced (top) and a tested (bottom) Pd/alumina catalyst modified with lithia.

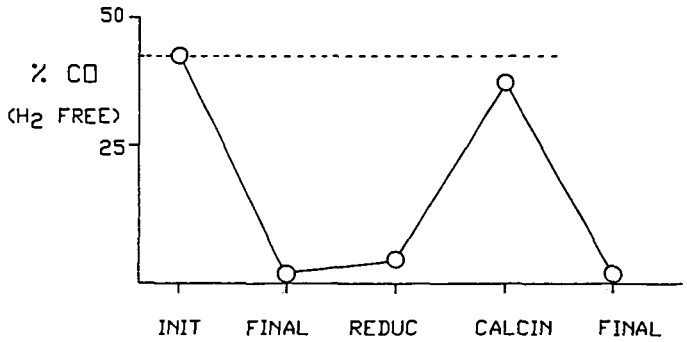

Figure 3. The lithia modified Pd/alumina catalyst always shows severe deactivation (final) after exposure to high temperature, but its activity can be restored after calcining in air and reducing the catalyst (calcin).

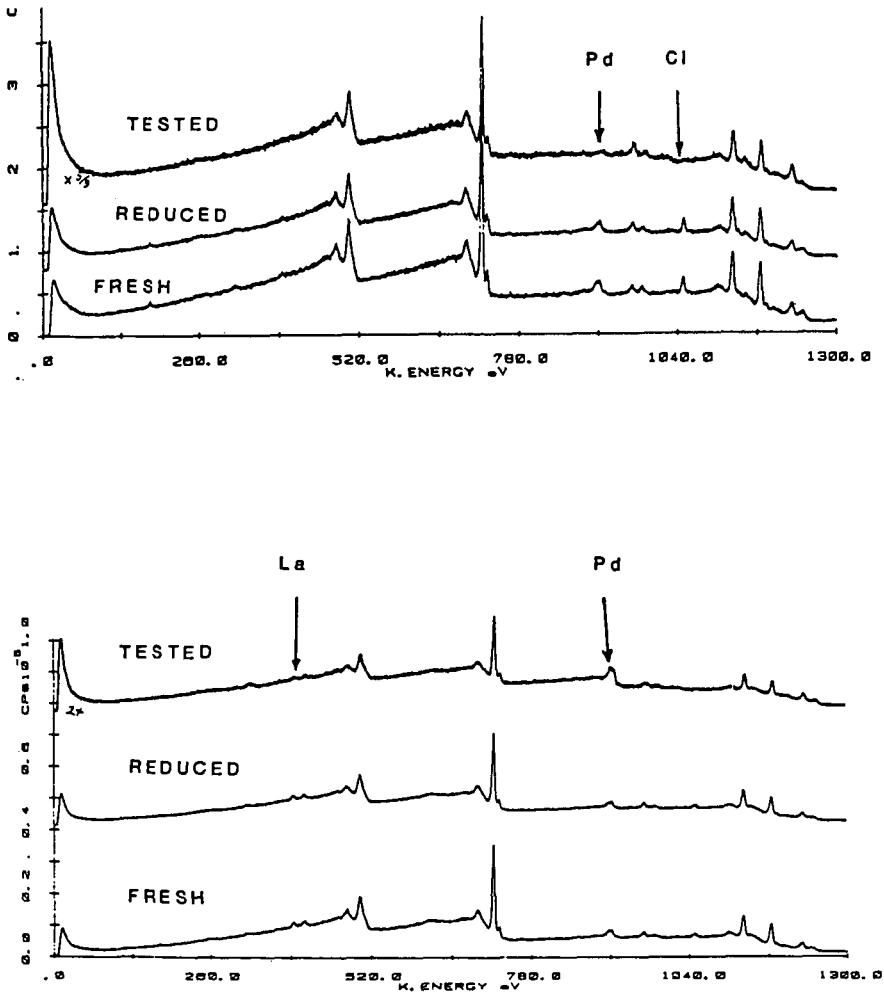

Figure 4. XPS survey scan of a lithia (top) and a lanthana (bottom) modified Pd/alumina catalyst which has been either freshly calcined, reduced, or tested.

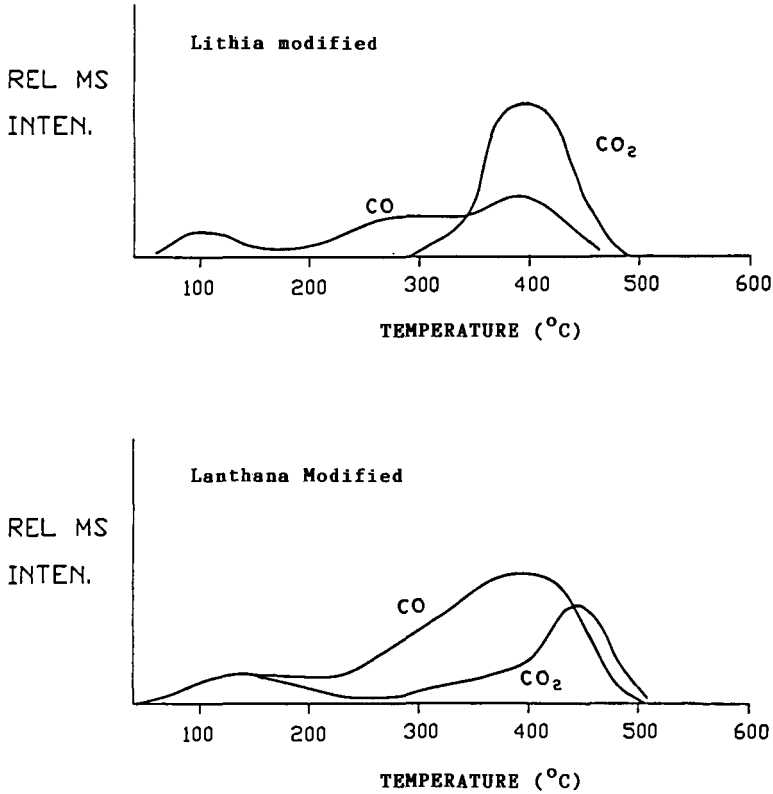

Figure 5. TPD profile of CO from a lithia (top) and a lanthana (bottom) modified Pd/alumina catalyst.

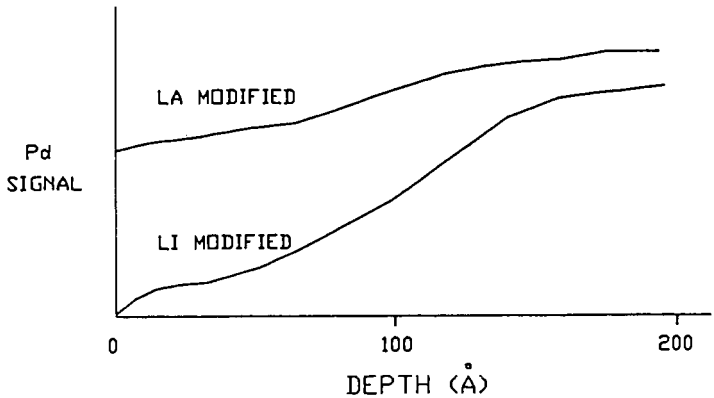

Figure 6. The depth profiles of the XPS Pd_{3d} signal for Pd/alumina catalysts modified with lanthana or lithia.

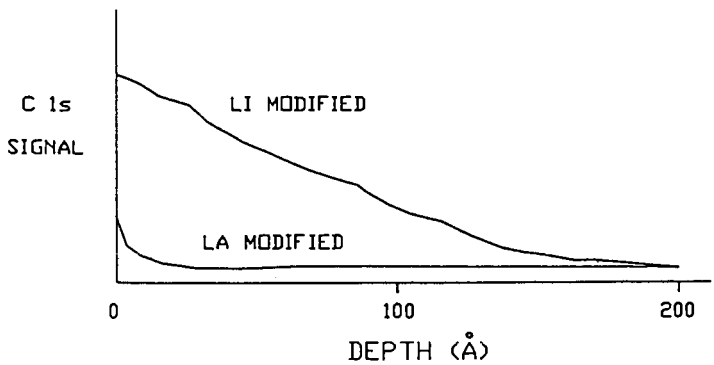

Figure 7. The depth profiles of the XPS C_{1s} signal for Pd/alumina catalysts modified with lanthana or lithia.

TESTING OF A SULFUR TOLERANT DIRECT METHANATION PROCESS

Allan Skov
Haldor Topsoe, Inc.
P. O. Box 58767
Houston, Texas 77258

Karsten Pedersen
Haldor Topsoe A/S
P. O. Box 213, Nymollevej 55
DK-2800 Lyngby, Denmark

Chiang-liu Chen and Ralph L. Coates
Questar Development Corporation
141 East First South
Salt Lake City, Utah 84147

ABSTRACT

A new sulfur tolerant catalyst for methane formation from carbon monoxide and hydrogen has been tested at Haldor Topsoe's laboratory and at Mountain Fuel Resources' entrained coal gasification Process Development Unit. The catalyst also effectively catalyzes the shift reaction, which permits direct methanation of raw coal gas. In contrast to nickel-based methanation catalyst, it is not necessary to add steam for prevention of carbon formation. Physical and chemical properties of the catalyst have been characterized and reliable reaction rate expressions have been derived for optimization of the reactor design. Results of 1080 hours of testing time with raw gases produced from five different type coals showed no poisoning of the catalyst by impurities contained in the raw gas and no carbon formation on the catalyst surface. Near 100 percent conversion was achieved with respect to CO or H_2. Besides methane, the product gas also contained ethane and a small amount of propane.

INTRODUCTION

Conventional methanation is normally carried out by reacting one molecule carbon monoxide with three molecules hydrogen to produce methane and steam:

$$CO + 3H_2 = CH_4 + H_2O \qquad -\Delta H^{o}298 = 49 \text{ kcal/mol} \qquad 1)$$

or one molecule carbon dioxide with four molecules of hydrogen to produce one molecule of methane and two molecules of steam:

$$CO_2 + 4H_2 = CH_4 + 2H_2O \qquad -\Delta H^{o}298 = 39 \text{ kcal/mol} \qquad 2)$$

The reactions are catalyzed by various metals of which supported nickel is commonly employed (1).

The raw product gas from coal gasification typically contains higher concentrations of carbon monoxide than hydrogen, and the CO/H_2 ratio ranges from 1 to 2 depending on the process. Therefore, in order to produce methane via reaction (1) above, the gas compositions have to be adjusted by the shift reaction:

$$CO + H_2O = CO_2 + H_2 \qquad -\Delta H^{o}298 = 10 \text{ kcal/mol} \qquad 3)$$

and the excess CO_2 has to be removed. Steam addition before methanation is required to prevent carbon formation on nickel catalysts and catalyst deactivation (2). Furthermore, since conventional catalysts are susceptible to sulfur poisoning, the hydrogen sulfide contained in the raw gas must be removed prior to methanation.

An alternate reaction for methane synthesis, which is known as direct methanation, is represented by the following reaction:

$$2CO + 2H_2 = CH_4 + CO_2 \qquad -\Delta H^o 298 = 59 \text{ kcal/mol} \qquad 4)$$

Haldor Topsoe, Inc., has recently developed a sulfur resistant catalyst for direct methanation as well as for the general reaction:

$$2nCO + (n+1)H_2 = C_nH_{2n+2} + nCO_2 + \text{Heat} \qquad 5)$$

The main product of this reaction is methane. The hydrocarbons formed in addition to methane are saturated. Since the catalyst is activated by sulfur, the hydrogen sulfide contained in the raw feed gas has a positive effect on the reaction rate. The catalyst was first tested at Haldor Topsoe's laboratory in Denmark with synthetic gas simulating raw coal gas composition.

Besides being tolerant to sulfur, it is an effective catalyst for the shift reaction. Thus it offers the potential of greatly simplifying the coal to SNG process by eliminating the need for a shift reactor and sulfur removal upstream of the methanation reactor. Figure 1 presents a simplified block flow diagram to produce SNG from coal using sulfur tolerant direct methanation catalyst.

DESCRIPTION OF THE TEST UNIT

The methanation test unit was fabricated and partially assembled at the Haldor Topsoe Research Laboratory in Denmark and shipped to Mountain Fuel Resources (MFR) entrained coal gasification process development unit (PDU) in Utah. The unit was assembled and connected to the plant facility.

Figure 2 presents a simplified piping and instrument diagram of the unit. The unit consists of rotameters for hydrogen, hydrogen sulfide, nitrogen, and air, the methanation reactor, a fluidized sand bed for temperature control, heating elements, product gas condenser, product gas meter, temperature controller, temperature recorder, and other ancillary instruments.

The raw product gas slip stream from the gasifier was piped from the recycle gas surge tank to the reactor. The pressure was controlled by a pressure regulator upstream of the reactor and the flow rate was controlled by a needle valve downstream of the reactor. The temperature in the catalyst bed was measured with thermocouples placed inside thermowells centrally located along the length of the bed. The sand bath temperature was monitored with thermocouples embedded in the bath at several locations.

The catalyst has been tested previously in the Haldor Topsoe laboratory with synthetic raw gas in several experiments including a long-duration test of 1100 hours. This particular batch of catalyst installed at the PDU site, designated SMC 324, had been tested 440 hours at Haldor Topsoe's laboratory before it was shipped to the PDU.

EXPERIMENTAL

During the test, raw feed gas samples and product gas samples were taken periodically, approximately three to six times daily, and sent to Mountain Fuel Supply Company's gas laboratory for analysis. The samples were analyzed with a gas chromatograph for H_2, CO, CO_2, H_2S, CH_4, C_2H_6, C_3H_8, and N_2. The water vapor content of the product gas was measured by periodically weighing the condensate collected in the condenser.

The needle valve at the reactor exit was adjusted to obtain a desired gas flow rate. The space velocity was calculated based on the inlet gas flow. The conversion of carbon monoxide and hydrogen was calculated by:

$$X_{CO+H_2} = 1 - \frac{Flow_{exit} * (CO + H_2)_{exit}}{Flow_{in} * (CO + H_2)_{in}} \qquad 6)$$

Direct sulfur resistant methanation testing was conducted at the MFR PDU for a cumulative total of 1080 hours between October 4 and November 21, 1984. Raw feed gases were produced from five different coals, Pittsburgh No. 8 eastern bituminous, North Dakota lignite, petroleum coke, Price River Utah bituminous and SUFCO Utah bituminous.

During the tests conversion was kept at 90 percent in order to evaluate the catalyst activity. Occasionally, the CO/H_2 ratio was adjusted with the addition of pure hydrogen into the feed. Hydrogen sulfide, in addition to that present in the feed gas from the coal, was added from time to time to study the effect of sulfur on the activity of the catalyst. Most of the tests were conducted at 300 psia pressure. When the pressure was varied to study the effect of pressure on the activity the feed flow to the reactor was reduced to attain the desired conversion.

RESULTS

Table 2 presents the range of test conditions and test results and Figure 3 presents a plot of catalyst activity versus time. The activity was calculated as the space velocity for 90 percent conversion based on the rate limiting component; i.e., the minor component which is H_2 for CO/H_2 ratio of greater than 1.1 and CO for CO/H_2 ratio of less than 1.1. Since the tests were conducted at different pressures and feed gas compositions, the space velocity to attain 90 percent conversion in pure H_2 + CO at 300 psia total pressure was calculated to obtain a standard value of the catalyst activity.

Figure 3 also includes the activity of the catalyst during the tests at Haldor Topsoe with synthetic raw gas. The figure shows that the activity remained constant for the first 500 hours tested at the PDU. At this time a plant air compressor failure occurred which resulted in a temperature runaway of the methanator for more than 10 hours. Temperatures exceeded 600°C. After that the activity stabilized at a level of 0.87 times the initial value. The activity remained at this value throughout the rest of the test period despite two more temperature runaways at about 720 hours of operation.

The type of coal appeared to have no effect on the activity of the catalyst. The effect of variations in hydrogen sulfide concentration were also small. There appeared to be no effect of hydrogen sulfide on activity below 0.07 volume percent concentration. The catalyst activity remained constant during a 100 hour test with hydrogen sulfide partial pressure as low as 1 ppm.

CONCLUSIONS

The direct, sulfur resistant methanation catalyst developed was successfully tested for 1080 hours at the MFR PDU with gases produced from five different type coals.

The catalyst was tested in several experiments with synthetic raw gas at the Haldor Topsoe laboratory in Denmark, including an 1100-hour continuous test. The particular batch sent to the PDU site had been tested for 440 hours in the laboratory.

Tests were conducted at 90 percent conversion level to evaluate catalyst activity at various test conditions. Near 100 percent conversion was achieved with respect to CO or H_2. The main hydrocarbon product was methane, which was produced in concentrations near 25 percent in the product gas. The product gas also contained ethane (about 2.5 percent) and propane (about 0.5 percent).

The activity was stable after more than 1500 hours of total operation. A slight drop in catalyst activity was observed after a temperature runaway above 600°C. This caused the activity to drop to 87 percent of the initial value. Two more temperature runaways thereafter had no effect on the activity.

The activity was not affected by the type of feedstocks to the gasifier. No poisoning of the catalyst by impurities contained in the raw feed gas was observed. The catalyst was examined after the tests and no carbon formation on the catalyst surface was observed.

The catalyst appears to be preferable to conventional methanation catalysts, especially in processing gas from coal gasification which contains high carbon monoxide.

The ethane and propane produced in addition to the methane provide a significant boost to the heating value of the product gas.

REFERENCES

(1) "Catalytic Aspects of High Temperature Methanation," Pedersen, K., Skov, A., and Rostrup-Nielsen, J.R., Amer. Chem. Soc. Preprints Fuel Chemistry Division 25(2), March 1980, Houston, Texas

(2) "Deactivation Phenomena of a Ni-based Catalyst for High Temperature Methanation," Gierlich, H. H., Fremery, M., Skov, A., Rostrup-Nielsen, J. R., pp. 459-469, Catalyst Deactivation, Elsevier, Amsterdam, 1980.

TABLE 1

PHYSICAL CHARACTERISTICS OF THE CATALYST

Name	SMC 324
Size, L x D	4.5 mm x 4.5 mm (0.18" x 0.18")
Density	1.75 gm/cm^3 (109 lb/cf)
Bulk Density	1.275 Kg/l (80 lb/cf)
Surface Area	100 m^2/gr
Crushing Strength	600 Kg/cm^2 (8700 lb/in^2)

TABLE 2

SUMMARY OF DIRECT METHANATION TEST CONDITIONS AND RESULTS

	Range of Test Conditions	Typical Test Data
Pressure, psia	90 - 300	300
Volumetric Flowrate, SCFH	1 - 8	3
Inlet Conditions (Adjusted with H_2), %		
CO/H_2 Ratio	0.7 - 1.5	1.0
H_2	30 - 45	35
CO	30 - 45	40
CO_2	10 - 40	15
H_2S	1 ppm - 3.5	0.1
CH_4	0 - 13	1
N_2	2 - 11	5
Outlet Conditions, %		
H_2	0 - 15	8
CO	2 - 15	8
CO_2	40 - 55	50
H_2S	2 ppm - 4.5	0.1
CH_4	16 - 39	25
C_2H_6	1 - 4	2.5
C_3H_8	0.2 - 0.7	0.5
N_2	Balance	Balance
Fractional Conversions		
CO	70 - 100	90
H_2	70 - 100	90

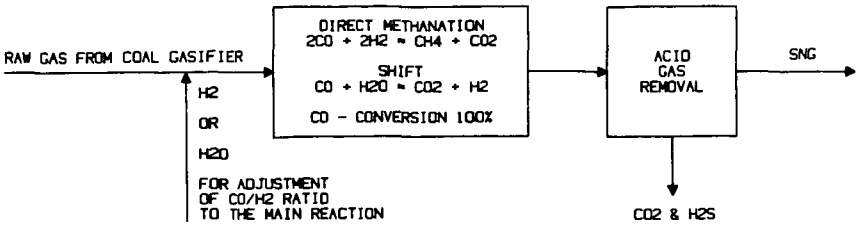

FIGURE 1. Block Flow Diagram, SNG from Coal by Direct Methanation Process

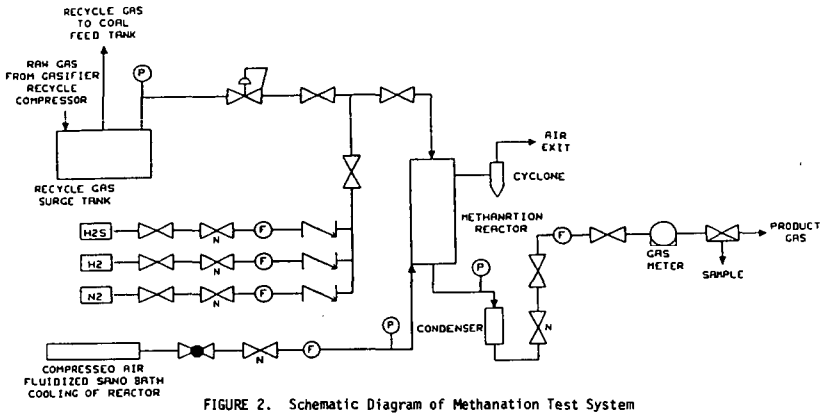

FIGURE 2. Schematic Diagram of Methanation Test System

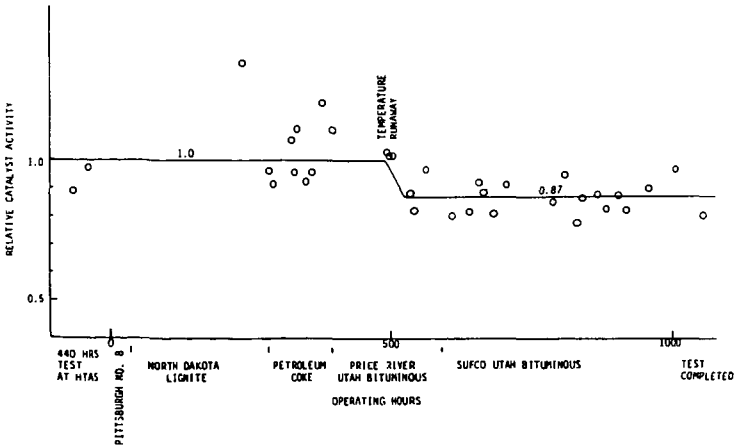

FIGURE 3. Relative Catalyst Activity Versus Time

Catalyst Transformation During Alkali-Catalyzed Carbon Gasification

F. Shadman, W.A. Punjak and D.A. Sams

Department of Chemical Engineering, University of Arizona
Tucson, Arizona 85721

The kinetics and mechanism of carbon gasification reaction catalyzed by alkali metals have been the subject of numerous studies and comprehensive reviews are available (1-4). Although the mechanism of catalyst action is not completely understood, there is a general agreement that the reaction follows a redox mechanism (5-6). In this mechanism, the alkali catalyst cycles between an oxidized and a reduced form. During this cycle the catalyst transfers oxygen from the gaseous reactant to the carbon surface; the net effect is production of CO. Presently, the disagreement is on the nature and the stoichiometry of the catalytic intermediate compounds. The purpose of this study is to characterize the mechanism and the kinetics of the processes in which sodium and potassium carbonates are reduced from their initial forms to the catalytic intermediate forms.

EXPERIMENTAL METHOD

Carbopack B (by Supelco) was used as the high purity carbon substrate. Catalyst in the initial form of sodium or potassium carbonate was applied by the incipient wetting technique. The catalyst/carbon ratio was controlled by varying the alkali concentration in the impregnation solution. Atomic emission spectroscopy was used to analyze the samples for alkali content. The catalyst type and concentration of the samples used in this study are given in Table 1.

Two reactor systems were used in the course of this study. The first utilized a small differential reactor for quick response times while the second used an electronic microbalance for direct measurement of sample weight. Both systems included a movable furnace which allowed rapid heating and cooling or programmed temperature change in the reactor. The details of experimental set-up are given elsewhere (7,10).

For each run, 25-30 mg of the impregnated carbon was loaded into the reactor. The reactor was then purged with Ultra high purity nitrogen to remove the oxygen before heating the sample. The experiments were conducted under Temperature and Concentration Programmed Reaction (TCPR) conditions. Three schedules of programmed conditions were used. In Schedule 1 (Fig. 1), the samples were rapidly heated to 800°C under nitrogen. After complete evolution of H_2O, CO_2 and CO, the samples were cooled rapidly and removed for analysis. Schedule 2 (Fig. 2) was similar except the samples were

quenched before complete catalyst reduction to determine the relationship between CO evolution and catalyst loss. In Schedule 3, (Fig. 3) the partial reduction under nitrogen was followed by gasification under a mixture of 15% CO_2 in nitrogen. After a short gasification stage to measure the gasification rate, the samples were quenched and removed for analysis.

RESULTS AND DISCUSSION

In an earlier study (11), a mechanism was suggested for the interaction between carbon and potassium carbonate under inert conditions above 700°C. This mechanism, which is expected to hold for both sodium and potassium carbonates, can be written in the following general form:

$$M_2CO_3 \xrightarrow{C} (\text{-COM}) + (\text{-}CO_2M) \quad (1)$$

$$(CO_2M) + C \longrightarrow (\text{-COM}) + CO \quad (2)$$

$$(\text{-COM}) + C \longrightarrow (\text{-CM}) + CO \quad (3)$$

$$(\text{-CM}) \longrightarrow M(g) \quad (4)$$

This mechanism allows for the sequential reduction of the catalyst followed by catalyst vaporization and loss.

In the early stage of the sample heat up, a small CO_2 peak is observed. This peak is due to the decomposition of bicarbonate to carbonate (10,11). During the rest of the reduction stage, carbon monoxide is the only significant gaseous product. Therefore, the time profile of CO is a direct measure of the overall reduction kinetics. The CO profile shown in Figure 1 is a typical profile for initial catalyst loadings above saturation. The CO concentration exhibits a plateau with almost constant CO gasification rate. As the initial loading is decreased, the width of the CO plateau decreases while the rate of CO production does not change significantly. For very low concentrations the profile does not exhibit a plateau. These results indicate that at catalyst loadings greater than what is required for surface saturation, catalyst is the excess reactant and carbon surface is the limiting reactant. Under these conditions, the reduction rate is determined by the carbon substrate area which is independent of catalyst loading. The very small increase in CO across the plateau is due to the increase in carbon surface area caused by conversion. At initial concentrations lower than saturation (initial metal to carbon atomic ratio of about 0.01 for potassium and 0.04 for sodium) the rate of reduction varies with both loading and time and no plateau is observed.

The rise and fall of the CO peak are primarily due to the effect of reaction kinetics and not simply an artifact of the reactor residence time response. Without these effects the rise and fall would have been much sharper. This is because dispersion in the reactor is relatively negligible. The rise is due to the increase in

the concentrations of ($-CO_2M$) and ($-COM$) supplied by reaction 1. The fall is due to the depletion of the carbonate.

The dependence of the average catalyst reduction rate on loading is shown in Figure 4. Total reduction time is a linear function of the initial catalyst loading. This indicates that the average rate is independent of loading as long as the carbon substrate is saturated. The rate will vary with loading for unsaturated samples as indicated by the curvature of the lines at low catalyst loadings. As expected, the shape of the curve indicates that the turnover number (measure of rate per catalyst atom) for an unsaturated surface is higher than that for a saturated surface.

The reduction mechanism suggests that the catalyst is reduced prior to loss by vaporization. To measure the relative rates of catalyst reduction and vaporization, a series of runs were conducted where the samples were removed after various levels of catalyst reduction and analyzed for catalyst content (Schedule 2). The results are shown in Figure 5 and indicate that the catalyst vaporizes rapidly upon complete reduction. This can occur only if reaction 4 is substantially faster than reaction 3.

An important observation is that the rate of catalyst loss is dramatically decreased after all the catalyst is reduced. In other words, the residual catalyst left on the surface at the end of the reduction process is relatively stable. This means that reaction 4 is somehow enhanced by the presence of carbonate. A possible explanation is that the strong attraction of carbonate to carbon sites causes the decomposition of ($-CM$) and the release of carbon sites which interact with carbonate.

CONCLUSION

The reduction of potassium and sodium carbonates is a prerequisite for the formation of surface catalytic sites, and further reduction of these surface sites is an integral part of the mechanism suggested for catalytic gasification. In addition, the alkali catalyst is lost from a site only after it has been completely reduced.

For a sufficiently high loading, a sodium or potassium impregnated carbon sample subjected to heat under an inert atmosphere will generate a CO concentration/time profile with a distinct plateau region. In this region, catalyst is the excess reactant and carbon surface area is the limiting reactant. For low loading samples, catalyst is the limiting reactant and no plateau is observed. The reduction rate is independent of loading for high loading samples while for low loading samples the rate is a function of both loading and time.

There is a saturation limit for the alkali catalyst on carbon substrates. This limit appears to be the same for both sodium and potassium on molar basis. In general, the surface saturation limit is independent of the initial loading but depends on the total surface area of the substrate.

REFERENCES

1. Wen, W.Y., Catal. Rev.-Sci. Eng., 22(1), 1 (1980).
2. McKee, D.W., Chem. Phys. Carbon, 16, 1 (1981).
3. Wood, B.J. and K.M. Sancier, Catal. Rev.-Sci. Eng., 26(2), 233 (1984).
4. Pullen, J.R., IEA Coal Research, No. ITCIS/TR26 (1984).
5. McKee, D.W., Fuel, 62(2), 170 (1982).
6. Moulijn, J.A., M.B. Cerfontain and F. Kapteijn, Fuel, 63(8), 1043 (1984).
7. Sams, D.A. and F. Shadman, accepted for publication in AIChE J.
8. Sams, D.A., T. Talverdian and F. Shadman, In Press, Fuel (1985).
9. Talverdian, T., "Catalyst Loss During Potassium-Catalyzed CO_2 Gasification of Coal Char and Carbon," M.S. Thesis, University of Arizona (1984).
10. Sams, D.A. "The Kinetics and Mechanism of the Potassium Catalyzed Carbon/Carbon Dioxide Gasification Reaction", Ph.D. Dissertation, University of Arizona (1985).
11. Shadman, F. and Sams, D.A., Proceedings of the 17th Biennial Conference of the American Carbon Society, Lexington, Ky., 182 (1985).

Table 1. Catalyst Specifications in the Studied Samples

Sample	Catalyst	$(M/C)_o$ atomic ratio
A	K	0.00089
B	K	0.0027
C	K	0.0054
D	K	0.013
E	K	0.021
F	K	0.025
G	K	0.027
H	Na	0.011
I	Na	0.029
J	Na	0.049
K	Na	0.067
L	Na	0.091
M	Na	0.131

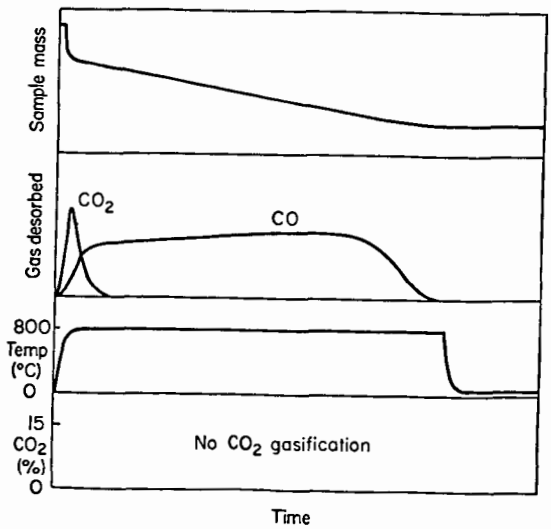

Figure 1. Temperature-programmed reaction; Schedule 1

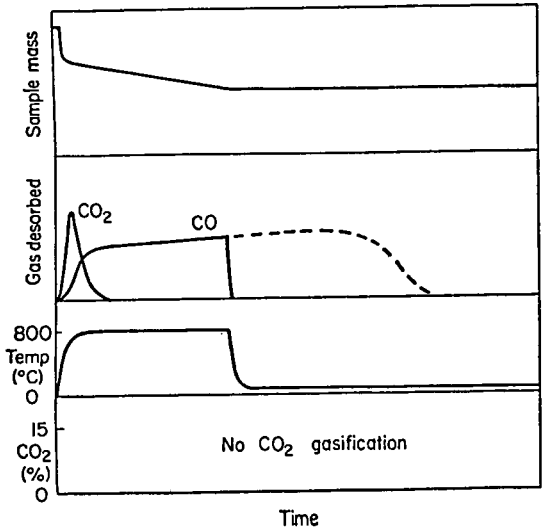

Figure 2. Temperature-programmed reaction; Schedule 2

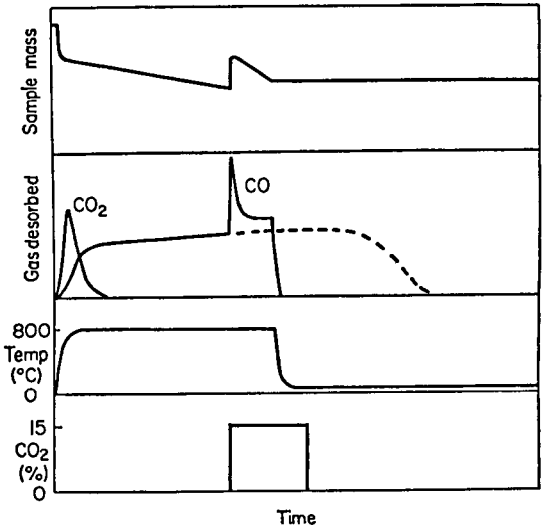

Figure 3. Temperature-and concentration-programmed reaction; Schedule 3

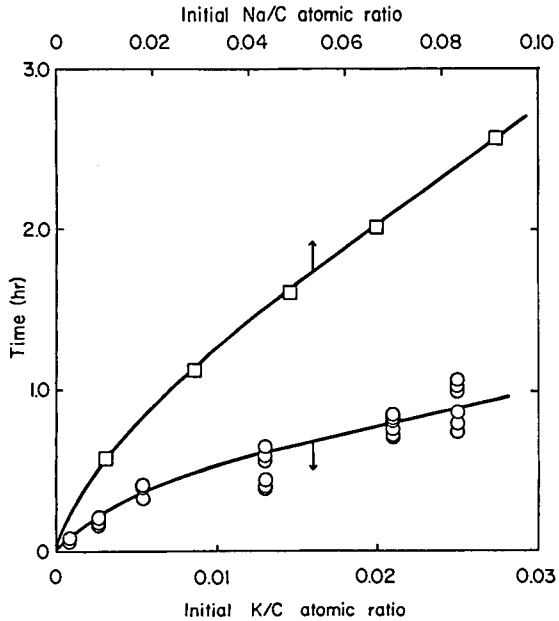

Figure 4. Dependence of total reduction time on the initial catalyst loading

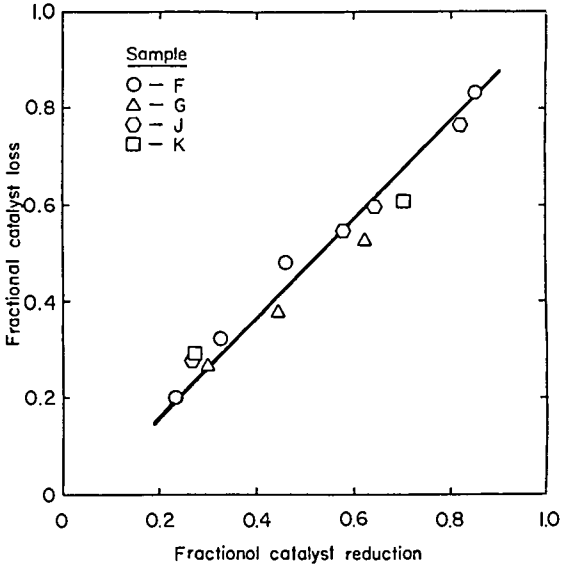

Figure 5. Catalyst loss during reduction

ROLE OF OXYGEN IN ALKALI-CATALYZED HYDROGEN GASIFICATION OF CARBON BLACK

Michael H. Treptau, Hossein Zoheidi, and Dennis J. Miller

Department of Chemical Engineering
Michigan State University
East Lansing, MI 48824-1226

INTRODUCTION

The hydrogen gasification of carbon in the presence of alkali metal salts has been reported in only a few studies [1-3], and little information about reaction kinetics or catalytic enhancement is available. The uncatalyzed reaction, in contrast, has received considerable attention [4,5]. Of particular interest are the results of Cao and Back [6] and Blackwood [7], who reported the effects of oxygen on the methane production rate.

Hydrogen gasification is under investigation in our laboratory because it is a direct route to methane production and because it offers a unique environment in which to study gasification catalyst behavior. Hydrogen gasification involves an elemental feed gas (H_2) and a single product (CH_4), thus facilitating accounting of carbon and oxygen from both reactant and catalyst during gasification. The work presented in this paper focuses on the importance of oxygen in hydrogen gasification, and discusses results of experiments involving both alkali-metal catalyzed and uncatalyzed reactions. This study is a continuation of earlier work [8].

EXPERIMENTS

The carbon used in this study is a graphitic carbon lampblack (Fisher Scientific) with an initial BET surface area of 20 square meters per gram and an impurity content of less than 0.1 per cent. The catalysts (K_2CO_3, Na_2CO_3, KCl) were deposited on the carbon by wet impregnation in metal to carbon molar ratios of approximately 0.01 and 0.02. Uncatalyzed carbon samples were also put through the same impregnation procedure but without addition of catalyst. Actual M/C ratios, measured by neutron activation analysis, are K/C = 0.0093 and 0.0192 for K_2CO_3, Na/C = 0.0111 and 0.0221 for Na_2CO_3, and K/C = 0.019 for KCl. Typical sample sizes gasified were 60-70 milligrams.

The gasification apparatus consists of a fixed bed differential reactor equipped with a gas collection system and gas chromatograph for rate measurement and product gas analysis. The pressure vessel is a Haynes Alloy tube (0.875" ID and 2.0" OD) designed for simultaneous operation at 1000°C and 1000 psi. Rate is measured as rate of methane evolution via timed collection of product gas; evolution rates as low as 0.005 ml/min can be accurately measured. Further details are given elsewhere [8].

All gasification experiments were carried out in pure hydrogen (Airco, 99.999%) at 500 psi pressure and a flow rate of 3-5 liters(STP)/minute/gram initial carbon. In all reactions the apparatus was evacuated three times and then purged in helium during initial heating. Hydrogen was then added to the reactor at 500°C in most experiments. In some experiments uncatalyzed samples were degassed by heating to 1000°C in vacuum for twelve hours before gasification, and in others hydrogen was added at room temperature.

RESULTS

All gasification experiments were conducted in a large excess of hydrogen, so that the methane formation reaction was far from equilibrium. In addition, repeated experiments in which sample size and flow rate were changed and in which sample temperature was measured allow us to conclude that the results represent intrinsic and reproducible kinetic rate measurements for the hydrogen gasification.

Catalyzed Gasification: The experimental data are represented as rate of methane evolution versus time during gasification. The start of reaction (t=0) is taken as the time where hydrogen is added to the reaction vessel (500°C); steady state temperature is reached after about 55 minutes. In the Figures, the symbols represent individual collection points; the curve represents the best fit of the rate data. Methane evolution rate is normalized to initial carbon weight; integration of the rate curve gives a carbon conversion close to that obtained by weighing the sample residue.

Methane evolution rate for gasification in the presence of Na_2CO_3 and K_2CO_3 catalysts at 865°C are given in Figure 1 for M/C = 0.02 and in Figure 2 for M/C = 0.01. The rate curve for sodium is scaled to the same M/C ratio as potassium. The results show that both catalysts enhance the rate of hydrogen gasification, but show different catalytic effects as carbon is consumed. For Na_2CO_3, rate is a maximum near the time where steady state temperature is first reached, whereas for K_2CO_3 the rate increases as gasification proceeds. The results for gasification in the presence of KCl are also given in Figure 1, and show that KCl has little catalytic effect in hydrogen gasification.

Activation energy of the hydrogen gasification reaction was measured over the temperature range of 780-900°C for the uncatalyzed reaction and in the presence of the carbonate catalysts. The Arrhenius plots are given in Figure 3 at 20% carbon conversion for all three samples; also shown (by dotted line) is the plot at 30% conversion for the Na_2CO_3 sample. The calculated activation energy at 20% conversion is 220 kJ/mole for K_2CO_3, 251 kJ/mole for Na_2CO_3, and 264 kJ/mole for the uncatalyzed reaction. The lower value for the potassium catalyst results from scatter in the data, as potassium catalyst gave the highest reaction rate and thus the fewest number of collection points. Therefore, the activation energy is the same within experimental uncertainty for both catalyzed and uncatalyzed reactions and approximately equal to 250 kJ/mole.

The different gasification rate curves for sodium and potassium catalyzed reactions led to investigation of the interaction between catalyst and carbon and evolution of oxygen species during heatup. In these experiments, the reactor was purged as usual, but the sample was heated in hydrogen and gas evolution was monitored during heatup. The results of these experiments are given in Table 1. The primary gas evolved from K_2CO_3 is CO_2, which appears in the temperature range of 300-500°C, while Na_2CO_3 releases primarily CO at 400-700°C. The uncatalyzed reaction releases very small quantities of each gas at similar temperatures, probably from weakly bound oxygen species on the carbon surface.

TABLE 1

Gas Evolution during Sample Heatup

(M/C = 0.02)

Catalyst	CO (mg)	CO_2 (mg)	Total Oxygen (mg)	Fraction of Oxygen in Catalyst Evolved as CO	as CO_2
K_2CO_3	0.50	1.05	1.04	0.12	0.31
Na_2CO_3	1.05	0.29	0.81	0.22	0.05
none	0.031	0.102	0.093	-	-

Uncatalyzed Gasification: The effects of indigenous oxygen, present on the surface or in the bulk of the unimpregnated carbon, was investigated by conducting several experiments in which the carbon was either degassed or partially reacted in oxygen. Carbon was degassed by heating to 1000°C in vacuum to remove adsorbed oxygen. Oxygen was replenished on the carbon surface by partial combustion in air at 400°C. The partial combustion was controlled by admitting a finite amount of oxygen into the pressure vessel and then allowing the reaction to go to completion.

Results of the experiments are given in Figure 4 as methane formation rate versus carbon conversion. The solid circles represent rate for an untreated sample. The open squares represent a sample initially degassed, gasified in hydrogen (to 20% conversion), partially combusted in oxygen (to 35% conversion), and then further gasified in hydrogen. The open triangles represent a sample initially gasified in hydrogen (to 25% conversion), partially combusted in oxygen (to 35% conversion), and then further gasified in hydrogen. The results show that degassing reduces gasification rate, and that partial combustion in oxygen recovers some reactivity toward hydrogen. It was necessary to partially combust the carbon to recover reactivity; an experiment in which the carbon was exposed to oxygen at room temperature showed no subsequent increase in reactivity toward hydrogen, thus indicating little reaction between oxygen and carbon.

DISCUSSION

Figures 1 and 2 illustrate that both sodium and potassium carbonate are effective hydrogen gasification catalysts. The curves also show that the gasification rate changes significantly as carbon is consumed, and in a different manner for each catalyst.

Two quantities pertaining to gasification of this carbon, measured in an earlier work [8], must be mentioned. First, specific BET surface area of the carbon black increases dramatically during gasification [8], increasing approximately linearly with conversion from 20 m^2/g initially to 400 m^2/g at sixty per cent conversion for both catalyzed and uncatalyzed reactions. Absolute carbon surface area therefore increases about six-fold up to 60% conversion. Specific reaction rate based on this area is nearly constant for the K_2CO_3-catalyzed samples over the course of gasification, but decreases strongly for other samples. This indicates that, at least for the uncatalyzed case, rate is not related to total surface area. Secondly, significant catalyst is lost from the sample during gasification [8]; the amount of catalyst after gasification, determined by neutron activation analysis, decreases linearly with conversion to approximately one-third of

the initial value at 80% for both Na_2CO_3 and K_2CO_3. Total surface area development and catalyst loss do not explain the increase in rate with conversion, however, and other factors must therefore account for the observed behavior.

The Arrhenius plot in Figure 3 shows that apparent activation energy is nearly the same both for catalyzed and uncatalyzed reactions and at different conversions. This is in accordance with results of other investigators [9-10] for steam and carbon dioxide gasification, and suggests that the role of the catalyst is to increase the number of active sites without changing the reaction mechanism. This indicates that the active sites in both catalyzed and uncatalyzed gasification must perform a similar function, and that different shapes of the rate curves in Figures 1 and 2 for sodium and potassium catalysts must be attributed not to different reaction mechanisms but to differences in active site population as gasification progresses. The value of apparent activation energy (250 kJ/mole) is somewhat higher than values reported (150-210 kJ/mole) [4,5,11] for uncatalyzed methane formation. The only study for which a higher activation energy (300 kJ/mole) was found was for the reaction with graphite at 1200-1600°C [12]. This is further evidence that the rate measurements represents intrinsic reaction kinetics, and suggests that values of activation energy measured for porous carbons and chars may include effects of diffusion resistances and mineral matter.

Results from degassing and partial combustion of uncatalyzed carbon, given in Figure 4, show that the presence of oxygen on the carbon surface strongly enhances gasification rate. This is in agreement with the results of Cao and Back [6], who report an order of magnitude increase in methane formation rate when 0.1% oxygen is added to the hydrogen feed stream, and with the results of Blackwood [7], who observed that methane formation rate was proportional to oxygen content of coconut char. If oxygen is the key entity which enhances gasification rate, then the observed decrease in rate with time for uncatalyzed and untreated carbon (solid circles in Figure 4) is consistent with the concept that surface oxygen is slowly stripped from the carbon during reaction at 865°C. This concept is supported by the slower or nearly nonexistent decrease in rate with time for the uncatalyzed reaction at lower temperatures, in which oxygen is not removed from the surface.

Degassing the carbon (open squares in Figure 4) decreases the rate to a low level (0.8 ml CH_4/min/gram C) which is essentially invariant with time. The finite rate after degassing results either from the intrinsic carbon-hydrogen reactivity or from the presence of low levels of oxygen impurities in the carbon or reactant gas. When the degassed sample is combusted in oxygen at 400°C, gasification rate increases by approximately 2.0 ml CH_4/min/gram C. Similarly, when a sample not initially degassed (triangles in Figure 4) is combusted in oxygen at 400°C the rate also increases by approximately 2.0 ml CH_4/min/gram C, suggesting that partial combustion results in formation of a similar number of new active sites in both cases. Further, these results indicate that new active sites are formed in addition to those already existing on the surface. The total methane evolution rate is therefore the sum of the rates from the original oxygen-bearing sites which are still active and from the sites created by partial combustion.

The different rate curves for sodium and potassium carbonate catalysts and the evolution of different gases during heatup shows that the catalyst-carbon interactions are substantially different for the two cases. For K_2CO_3 (M/C=0.02), the evolution of one-third of the oxygen in the catalyst as CO_2 is consistent with results reported by Mims and Pabst [13] and Wood and Sancier [14] for formation of a surface oxide. It is not known at this time

if a K-O-C type complex is formed in the presence of hydrogen; however, based on the fact that absolute rate increases and specific rate is maintained, it can be concluded that the potassium catalyst disperses in a stable state on the carbon surface and forms new active sites as gasification progresses. These observations are consistent with those reported for a surface oxide complex; however no conclusions can be made.

The low initial catalytic activity for K/C=0.01 samples and the observed pyrophoric nature of potassium-containing sample residues from low temperature gasification make it impossible to rule out intercalation of potassium as an intermediate step in gasification. This phenomena has been dismissed for carbon oxidation reactions but has not been investigated for the reducing hydrogen gasification environment, and it is possible that both intercalation and surface oxide formation take place. Intercalation is reported to be a sink for potassium [15], thus explaining the low initial activity for K/C=0.01 samples. Sodium does not intercalate; this may provide an explanation of observed gasification behavior.

For the Na_2CO_3 catalyst, evolution of primarily CO at higher temperatures during heatup suggests that the carbothermic reaction is taking place. It has been reported that sodium metal interacts with surface oxygen [16] to form an oxide complex similar to that for potassium; it is possible that such a complex is responsible for the catalytic activity.

Two observations suggest that the interaction of the sodium catalyst with carbon is not as strong as that of potassium. First, after gasification in hydrogen the carbon residues contained visible particles of sodium carbonate, indicating that significant agglomeration of catalyst occured. Also, the total amount of oxygen evolved during heatup for the M/C=0.02 samples (Table 1) was less for sodium than for potassium. These observations indicate that the overall interaction of sodium carbonate with carbon is not as strong as the interaction of potassium carbonate with carbon, and it is likely that sodium forms few new active sites as gasification proceeds. The observed rate is therefore seen to decrease with conversion.

The mechanism by which the oxygen-bearing species (whether oxygen in the uncatalyzed sample or an M-O- complex for the catalyzed reactions) promote hydrogen gasification has not been studied. However, there is some evidence which allows the role of these species to be postulated. Yang and Duan [17] have recently reported using etch pit analysis that the arm-chair {1121} face of graphite is more reactive than the zig-zag {1011} face, and that hydrogen inhibits gasification in CO_2 and H_2O by preferentially adsorbing on and thus stabilizing the zig-zag face. The presence of hydrogen results in the formation of hexagonal (zig-zag) etch pits of low reactivity. Along with this, chemisorbed hydrogen is known to strongly bind to carbon and reduce oxygen adsorption capacity [18]. In contrast, gasification in CO_2 alone results in round pits with arm-chair edges. For hydrogen gasification, Zielke and Gorin [11] postulated that reaction is sterically more suited to the arm-chair face. Thus it is likely that the function of the oxygen-bearing surface species is to maintain and propagate arm-chair reaction sites on the carbon during gasification. Removal of oxygen species, either by desorption or reduction, results in consumption of arm-chair sites, leaving only residual and unreactive zig-zag faces to which hydrogen strongly binds. Combustion in oxygen results in formation of new arm-chair faces, resulting in enhancement of hydrogen gasification rate. Similarly, the addition of catalyst results in the presence of a larger quantity and possibly more stable oxygen-containing species which propogate the arm-chair faces, thus catalyzing the reaction.

This idea is also consistent with results reported by Baker et al. [19] and Tomita and Tamai [20] for barium and transition metal catalyzed hydrogen gasification, in which reaction occurs via channeling of catalyst particles in the <1120> crystallographic direction. The residual zig-zag faces left by the channel show no reactivity. These catalysts therefore propagate the arm chair face at the head of the channel, resulting in continued gasification.

CONCLUSIONS

The similar apparent activation energy and surface area development for uncatalyzed and catalzyed hydrogen gasification reactions suggests that catalysts increase the number of available reaction sites without changing the reaction mechanism. Surface oxygen enhances the rate of gasification; this along with evolution of CO_2 from potassium carbonate during heatup makes possible the idea that a surface oxygen complex is the catalytic agent. Based on evidence in the literature, the role of surface oxygen is postulated to be propogation of the arm-chair configuration of edge sites during gasification. These arm-chair sites are believed to be the sites at which hydrogen gasification occurs.

ACKNOWLEDGMENT

This material is based upon work supported by the National Science Foundation under Grant No. CPE-83-07963.

REFERENCES

1. Gardner, N., E. Samuels, and K. Wilks, Coal Gasification, ACS Advances in Chemistry Series. 131, 209 (1974).
2. Walker, P.L. Jr., S. Matsumoto, T. Hanzawa, T. Muira, and I.M.K. Ismail, Proc. Int. Symp. on Catalyzed Carbon and Coal Gasification, Amsterdam, 11 (1982).
3. Wigmans, T., M. Elfrins, A. Hoogland, and J.A. Moulijn, Proc. Int. Conf. on Coal Science, Dusseldorf, 301 (1980).
4. Cao, J.R., and M.H. Back, Carbon 20, 505 (1982).
5. Tomita, A., O.P. Mahajan, and P.L. Walker Jr., Fuel 56, 137 (1980).
6. Cao, J.R., and M.H. Back, Carbon 23, 141 (1985).
7. Blackwood, J.D., Australian J. Chem. 12, 14 (1959).
8. Zoheidi, H., and D.J. Miller, Carbon (in review) (1986).
9. Adjorlolo, A.A., and Y.K. Rao, Carbon 22, 173 (1984).
10. Otto, K., and M. Shelef, Chem. Eng. Commun. 5, 223 (1980).
11. Zielke, C.W., and E. Gorin, Ind. and Eng. Chem. 47, 820 (1955).
12. Gulbransen, E.A., K.F. Andrew, and F.A. Brassart, J. Electrochem. Soc. 112, 49 (1965).
13. Mims, C.A., and J.K. Pabst, Fuel 62, 176 (1983).
14. Wood, B.J., and K.M. Sancier, Catal. Rev.-Sci. Eng. 26(2), 233 (1984).
15. Wigmans, T., R. Elfring, and J.A. Moulijn, Carbon 21, 1 (1983).
16. Yuh, S.J., and E.E. Wolf, Fuel 63, 1604 (1984).
17. Yang, R.T., and R.Z. Duan, Carbon 23, 325 (1985).
18. Bansal, R.C., F.J. Vastola, and P.L. Walker, Jr., Carbon 12, 355 (1974).
19. Baker, R.T.K., C.R.F. Lund, and J.J. Chludzinski, Jr., J. Catal. 87, 255 (1984).
20. Tomita, A., and Y. Tamai, J. Phys. Chem. 78, 2254 (1974).

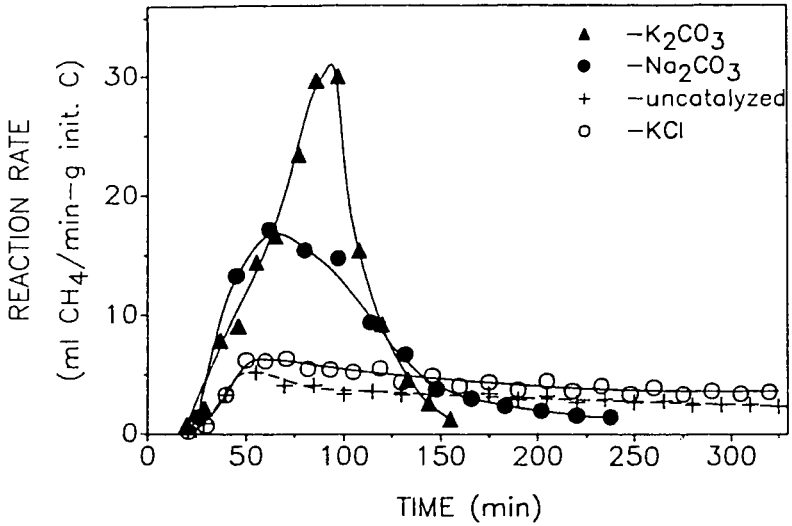

FIGURE 1. Methane evolution rate at 865°C for M/C=0.02

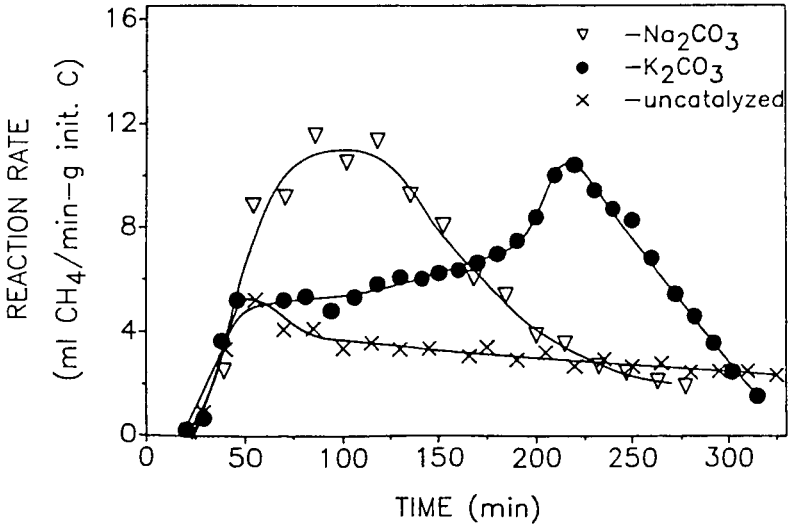

FIGURE 2. Methane evolution rate at 865°C FOR M/C=0.01

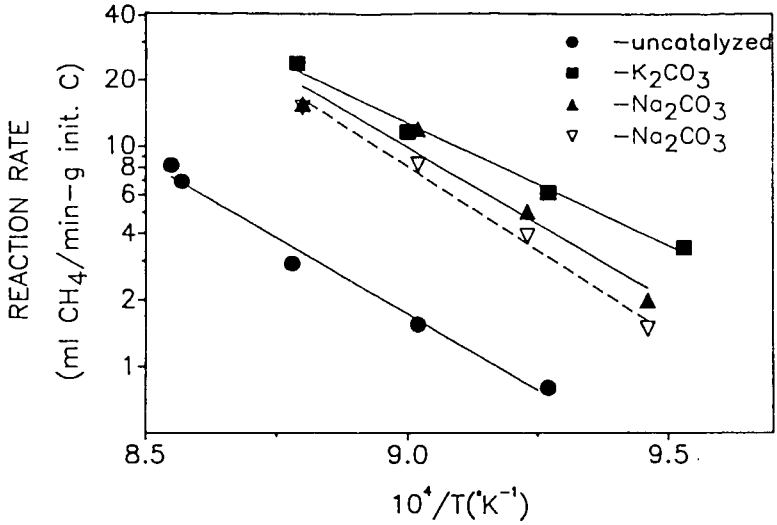

FIGURE 3. Arrhenius plot for M/C=0.02

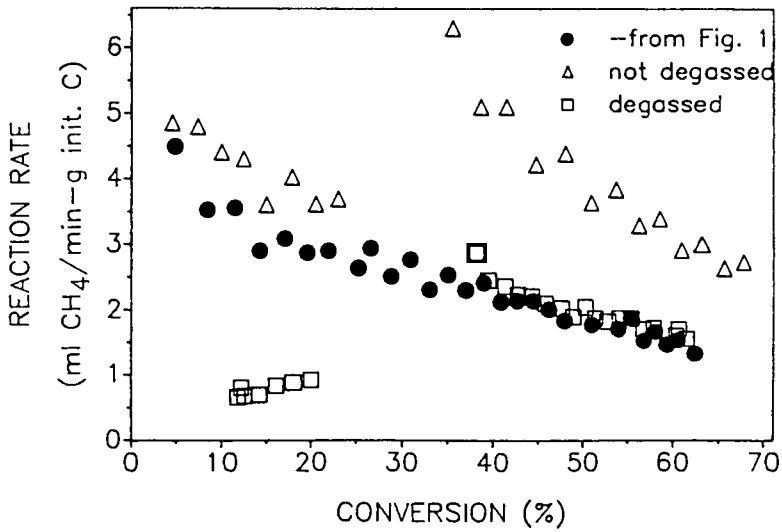

FIGURE 4. Oxygen effects on uncatalyzed rates.

STEAM GASIFICATION OF CARBONACEOUS SOLIDS CATALYZED BY A MIXTURE OF POTASSIUM AND NICKEL OXIDES BELOW 1000 K

J. Carrazza, G. A. Somorjai and H. Heinemann

Materials and Molecular Research Division
Lawrence Berkeley Laboratory
University of California
Berkeley, CA 94720

Introduction

The gasification of carbon with water vapor is an important reaction in the industrial production of H_2, CH_4, CO and CO_2. The use of catalysts is necessary if the process is carried out at temperatures below 1400 K. Two recent reviews discuss the properties of the various catalysts used for this purpose.(1,2) Alkaline and akaline-earth hydroxides and carbonates are the catalysts most commonly studied. These compounds only show catalytic activity at temperatures above 1000 K. Previous work in our laboratory shows that below this temperature KOH reacts stochiometrically with graphite and water vapor to produce H_2 and a stable surface compound.(3) Transition metals, in particular nickel and iron, are able to catalyse this process at temperatures as low as 750 K, but they deactivate much faster than the alkaline and alkaline-earth salts. Several authors have reported that nickel and iron are only active as catalysts for this process if the reaction conditions favors their presence in the metallic state.(4,5)

We have recently reported that several mixtures of a transition metal oxide with potassium hydroxide are excellent catalysts for the gasification of graphite with steam.(6) These catalysts are active at temperatures much lower than the alkaline and alkaline-earth salts and they deactivate more slowly than nickel and iron. In this previous publication it was shown that there is a synergistic effect between the transition metal and potassium.

This communication summarizes recent results in the study of this type of catalyst. We have focused on the use of mixtures of potassium hydroxide and nickel oxide, since they showed the highest activity of all the systems previously studied.(6) A kinetic study of the gasification of several chars and the dependence of the ratio of potassium to nickel on the rate of graphite gasification are presented. Also the interaction between nickel and potassium is studied using X-ray Photoelectron Spectroscopy (XPS).

Experimental

The gasification rates of graphite and five different chars have been obtained. The chars pretreatment, elemental composition and ASTM rank are summarized in Table 1. Nickel and potassium were loaded on the carbon substrate by incipient wetness using solutions of $Ni(NO_3)_2$ and KOH. A detailed explanation of the sample treatment after catalyst loading is given in a previous publication.(6)

A detailed explanation of the equipment used in these studies is given elsewhere.(6,7) The kinetic studies were done in a fixed bed flow reactor with an online gas chromatograph used for product analysis. The total gas production as a function of time was determined using a gas burette after the steam was condensed. The XPS study was done in an Ultra High Vacuum (UHV) chamber coupled to a high pressure cell. This apparatus allowed us to treat the sample under reaction conditions and to further transfer it to UHV for surface characterization without exposure to air.

All the kinetic results were obtained in isothermal experiments. The steam flow through the sample was equivalent to 1 ml of liquid water per minute. The reactor diameter was 0.6 cm. The reaction temperature was measured using a chromel-alumel thermocouple in contact with the external wall of the reactor. At the beginning of each experiment, a stabilization period of 15 min was allowed before data was collected. The principal reaction products were H_2 and CO_2. The gasification rates were determined measuring the H_2 production because its solubility in water is much smaller than that of CO_2. The carbon conversions were determined by dividing the number of H_2 moles produced by two times the initial number of carbon moles.

The XPS experiments were carried out using a Mg-anode source (hv = 1253.6 eV). The data was collected using a detector pass energy equal to 40 eV. The position of the peaks was calibrated with respect to the position of the C_{1s} peak of graphite (binding energy = 284.6 eV).

Results

The rate of graphite gasification as a function of time has been studied at 893 K for several mixtures of nickel and potassium oxides and for the components deposited alone. Some of the results are shown in Figure 1. The activity corresponding to nickel deposited alone is given by Curve A. A very fast initial activity is observed, but the sample deactivates almost completely after two hours, giving a total carbon conversion of 20%. When potassium is deposited alone from a KOH solution, no steady state gasification rate is observed after 15 min of initiating the experiment. Curve B shows the rate when nickel and potassium oxides are codeposited on graphite with a Ni/C molar ratio equal to 1.0×10^{-2} and a Ni/K molar ratio equal to 0.1. Initially, the steady state rate is two orders of magnitude lower than that of nickel deposited alone (Curve A), but after 6.0 hours the Ni-K mixture has kept its initial activity while Ni alone has deactivated completely. The carbon conversion for this catalyst after 6.0 hours is 2.5%, ten times lower than that of nickel alone. But when the experiment represented by Curve B was followed 400 hours, a total carbon conversion of 20% was obtained and the catalyst was still active. When a mixture of nickel and potassium oxides is deposited on graphite with a Ni/K molar ratio equal to 10.0 and a Ni/C molar ratio equal to 1.0×10^{-2}, an initial rate similar to that of nickel deposited alone is obtained (Curve C), but instead of deactivating completely after two hours, the rate levels out at the same rate obtained with the 1:10 Ni:K mixture (Curve B). These results indicate that for the 10:1 Ni:K mixture only a fraction of the total nickel loading interacts with potassium. The remaining fraction behaves like Ni metal and it is completely inactive after one hour. The reaction rate decreases faster than in Curve A because there is less free nickel on the surface.

The rate of gasification of several chars with steam was studied as a function of time in the presence of a 1:1 mixture of nickel and potassium oxides. A description of the five chars studied is given in Table 1. For all of them, the steady state rate after 1.0 hour is at least one order of magnitude higher than that of graphite (see Figure 2a). This is reflected in a much higher carbon conversion after 6.0 hours (see Figure 2b), even though by then the char steam gasification rates have decreased to values similar to those of graphite.

A comparison of the gasification rates for a 1:1 mixture of potassium and nickel oxides with that of the components deposited alone is given in Figures 3a and 3b for two of the chars studied (Illinois No. 6 High Temp. Treat. and

Montana). In the case of Illinois No. 6 char, it is clear that the mixture is more active than the sum of the rates of the components deposited alone. (Compare Curves A and D in Figure 3a.) In contrast to the results obtained with graphite, the mixture in this case is more than two times as active as nickel deposited alone. For Montana subituminous char the rate of gasification of the mixture is similar to that of nickel alone and higher than that of potassium (see Figure 3b).

A surface science study of the interaction of potassium, nickel and carbon in the presence of water is currently being done and some preliminary results are included in this communication. XPS of the $Ni_{2p3/2}$ signal of two systems, a 1:1 Ni:K mixture codeposited on graphite and nickel deposited alone have been obtained after exposing them to 24 torrs of water vapor at 950 K. The kinetic results show that at this temperature both systems are catalytically active. Figure 4 Curve A shows the spectrum corresponding to nickel deposited alone. There is a peak at 854.2 eV with a small satellite peak at 862.7 eV. This is characteristic of nickel in the metallic state and agrees with results obtained by us for nickel foil. The shoulder at 857.5 eV is due to small amounts of NiO in the sample. When nickel and potassium are codeposited on graphite (Curve B in Figure 4) the binding energy of the $Ni_{2p3/2}$ XPS peak is at 856.4 eV. This indicates that nickel is present in its +2 oxidation state. The much larger satellite peak at 864.6 eV also shows that nickel forms an oxide at this temperature in the presence of potassium. The lower binding energy of the $Ni_{2p3/2}$ peak in the nickel-potassium mixture compared to NiO shows that there is an electronic interaction between nickel and potassium.

Discussion

The kinetic results presented in this paper indicate that mixtures of potassium and nickel oxides are good catalysts for the gasification of carbonaceous solids with steam. The high reaction rates and carbon conversions obtained with the several chars studied (Figures 2 and 3) and the graphite gasification activity after 400 hours support this conclusion.

In a previous publication we concluded that there is a cooperative effect between potassium and nickel in this catalyst.(6) The results in this paper present the clearest evidence obtained so far for this effect. In Figure 3a the gasification rate of Illinois N-6 char in the presence of the mixed catalyst is higher than that of the mathematical sum of the rates of the components deposited alone. The XPS results in Figure 4 show that nickel deposited alone is active as a gasification catalyst when it is present in the metallic state, while in the nickel-potassium mixture, the nickel is catalytically active being in the +2 oxidation state. Also, the shift to lower binding energies for the $Ni_{2p3/2}$ peak in the potassium-nickel catalyst when compared to the position of the NiO peak is evidence for chemical interaction between nickel and potassium. We propose that this synergistic effect is due to the formation of a mixed oxide (K_xNi_yO) that is not readily reduced by carbon under our reaction conditions (< 1000K). There is evidence in the literature for the presence of several nickel-potassium mixed oxides,(8) but we do not have enough information to decide which one of them is present in our system.

The results presented in Figure 1 show that there is no interaction between the nickel metal catalyst and this potassium-nickel mixed oxide. When the ratio of nickel to potassium is high enough to allow the coexistence of these two catalysts on the graphite surface, the catalytic behavior observed can be explained by just adding the rates of the two catalysts; i.e. a very

high initial rate due to nickel metal that decays to a lower value and then remains constant for a long period of time due to the catalytic activity of the nickel-potassium mixed oxide.

Mixtures of transition metals and alkaline metals as catalysts for steam gasification of various carbon sources have been reported previously. Wigmams and Moulijn(9) reported that there was no interaction between nickel and K_2CO_3 for the steam gasification of chars at 1023 K. Similar results were obtained in our laboratory when the gasification of graphite was studied above 1000 K. Also, XPS data obtained in our laboratory show that at 1000 K the nickel is present in the metallic state, even in the presence of potassium. We suggest that these results are due to the decomposition to this mixed oxide and reduction of the nickel by carbon. In contrast with the results reported by Muolijn and Wigmams, a cooperative effect between a transition metal and an alkaline metal has been reported by other authors. Adler and Hüttinger(10) found that mixtures of $FeSO_4$ and K_2SO_4 deposited on PVC coke were better catalysts than the salts deposited alone. Also, Suzuky et. al.(11) reported that $Na(HFe(CO)_4)$ is a good catalyst for the gasification of various coals with steam. They suggest that this high activity is due to the interaction between iron and sodium.

Further work is currently being done to obtain more direct evidence of the existence of these mixed oxides and to characterize and understand their catalytic behavior toward carbon gasification.

Acknowledgment

The authors want to thank Dr. B. J. Wood of SRI International for providing the char samples used in this work and their elemental analysis.

This work was supported by the Assistant Secretary for Fossil Energy, Office of Management Planning and Technical Coordination, Technical Coordination Division of the U.S. Department of Energy under Contract Number DE-AC03-76SF00098, through the Morgantown Energy Technology Center, Morgantown, W.VA. 26505.

J. Carrazza acknowledges CEPET of Venezuela for a research fellowship.

References

1. B.J. Wood and K.M. Sancier, Catal. Rev.-Sci. Eng. 26, 233 (1984).
2. W.Y. Wen, Catal. Rev.-Sci. Eng. 22, 1 (1980).
3. F. Delannay, W.T. Tysoe, H. Heinemann and G.A. Somorjai, Carbon 22, 401 (1984).
4. D.W. McKee, Carbon 12, 453 (1974).
5. P.L. Walker, Jr., S. Mataumoto, T. Hanzana, T. Muira and I.M.K. Ismail, Fuel 62, 140 (1983).
6. J. Carrazza, W.T. Tysoe, H. Heinemann and G.A. Somorjai, J. Catal. 96, 234 (1985).
7. A.L. Cabrera, H. Heinemann and G.A. Somorjai, J. Catal. 75, 7 (1982).
8. M.G. Baker and A.P. Dawson, J. Less. Commona Met. 45, 323 (1976).
9. T. Wigmams and J.A. Moulijn, Stud. Surf. Sci. Catal. 7, 501 (1981).
10. J. Adler and K.J. Hüttinger, Fuel 63, 1393 (19B4).
11. T. Suzuki, M. Mishima and Y. Watanabe, Fuel 64, 661 (1985).
12. O.P. Mahajan, R. Yarzab and P.L. Walker, Jr., Fuel 57, 643 (1978).

TABLE 1

Characteristics of Coal Char and Graphite Samples Used in this Study

Name	ASTM Rank[a]	Pretreatment	Analysis (wt%)[b] C	H	N	O	S[c]	Ash[d]
Western Kentucky Washed (WK)	HV.B.Bit.	Unspecified	72.3	3.2	1.4	7.9	3.2	12
North Dakota Husky (NDHL)	Lignite	Partial Steam Gasification T = 1200K	71.2	1.1	0.37	13-17	2.0	8-12[e]
Montana (MS)	Subbituminous	Partial Steam gasification: T = 1200K	66.0	1.1	0.20	-	0.92	-
Illinois N-6 High Temp. (I 6 HT)	HV.C. Bit.	Heated Under He T = 1300K	-	-	-	-	-	-
Illinois N-6 Low Temp. (I 6 LT)	HV.C. Bit.	Pregasifier Heater T 670K	72.0	3.3	1.5	10.9	2.6	9.1
Graphite UCP-2		None	100	0	0	0	0	0

[a] HV. = High volatility B and C indicate bituminous classes.
[b] Dry mineral matter containing basis. Oxygen by difference.
[c] Total sulfur.
[d] By low temperature technique (oxygen plasma).
[e] Not measured. Range of values reported in reference 12.

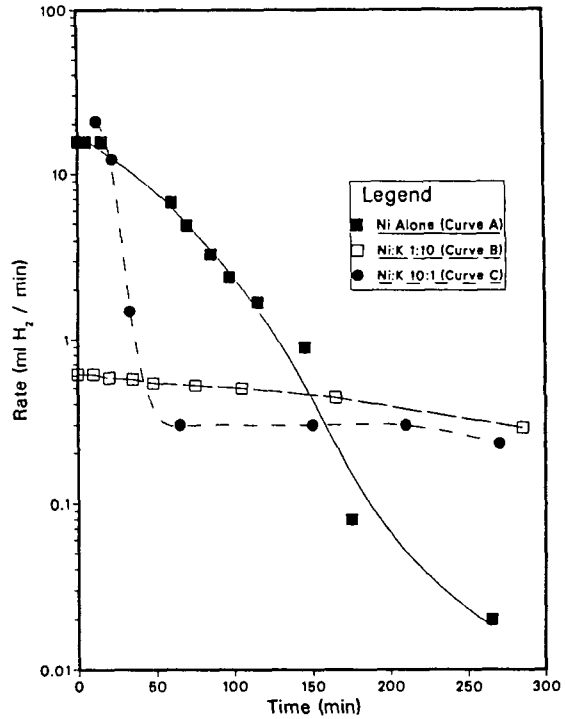

Figure 1: Steam gasification rates of graphite at 893 K catalyzed by three different compounds: nickel metal (Curve A) and two mixtures of nickel and potassium oxides, Ni:K 1:10 (Curve B) and Ni:K 10:1 (curve C). In all cases the Ni/C molar ratio is equal to 1.0 $\times 10^{-2}$.

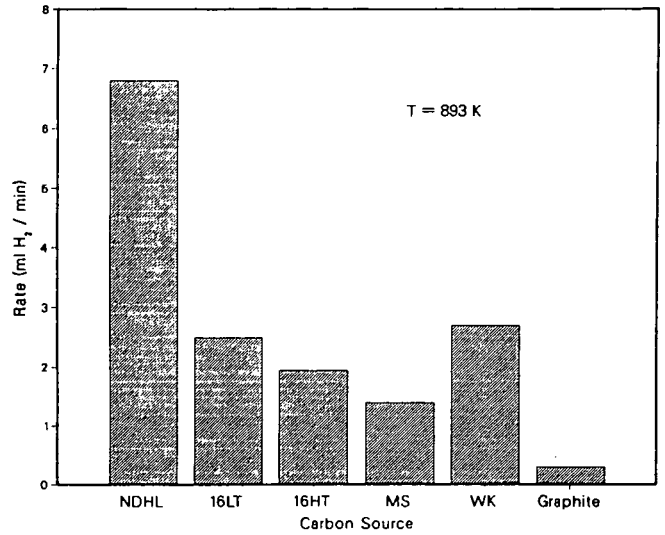

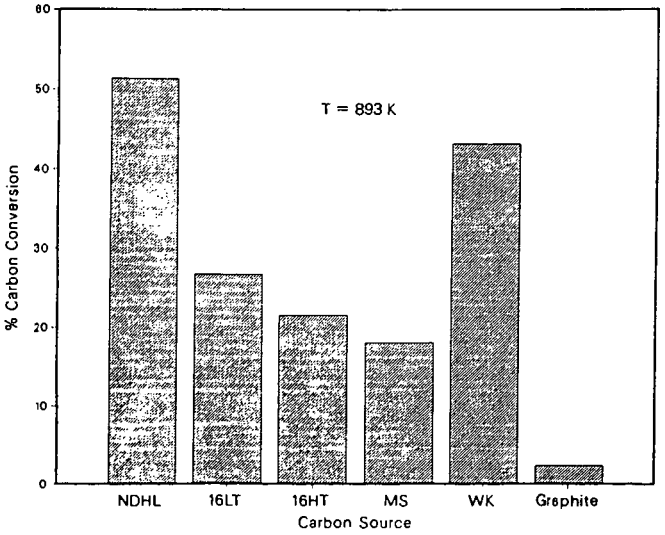

Figure 2a (Top). Steady state steam gasification rates of several carbonaceous solids after 1.0 hours when a mixture of nickel and potassium oxides is used as a catalyst.
Figure 2b (Bottom). Percentage of carbon conversion obtained after 6.0 hours when the same catalyst is used.

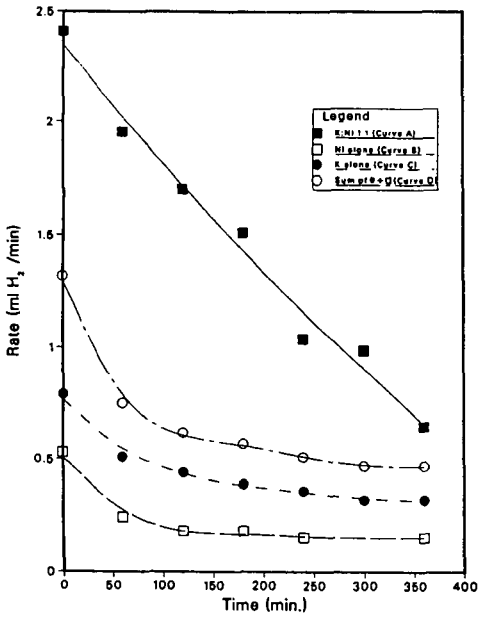

Figure 3a

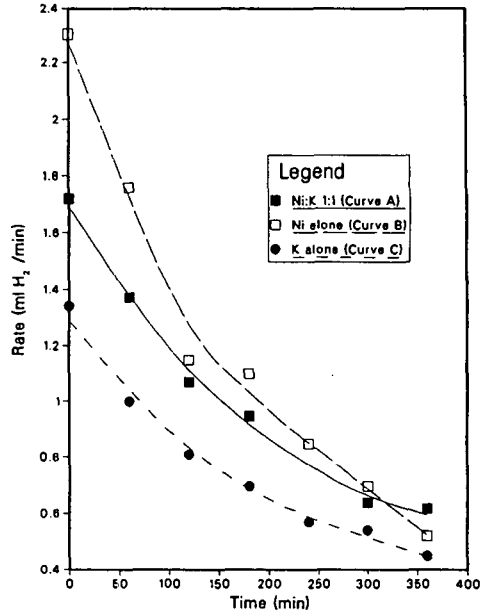

Figure 3b

Figure 3: Steam gasification rates at 893 K for two chars, Illinois M' 6 High Temp. (left) and Montana (right), catalyzed by three different compounds, a 1:1 mixture of nickel and potassium (Curve A), nickel alone (Curve B) and potassium alone (Curve C). In figure 3a, Curve D is the mathematical sum of curves B and C.

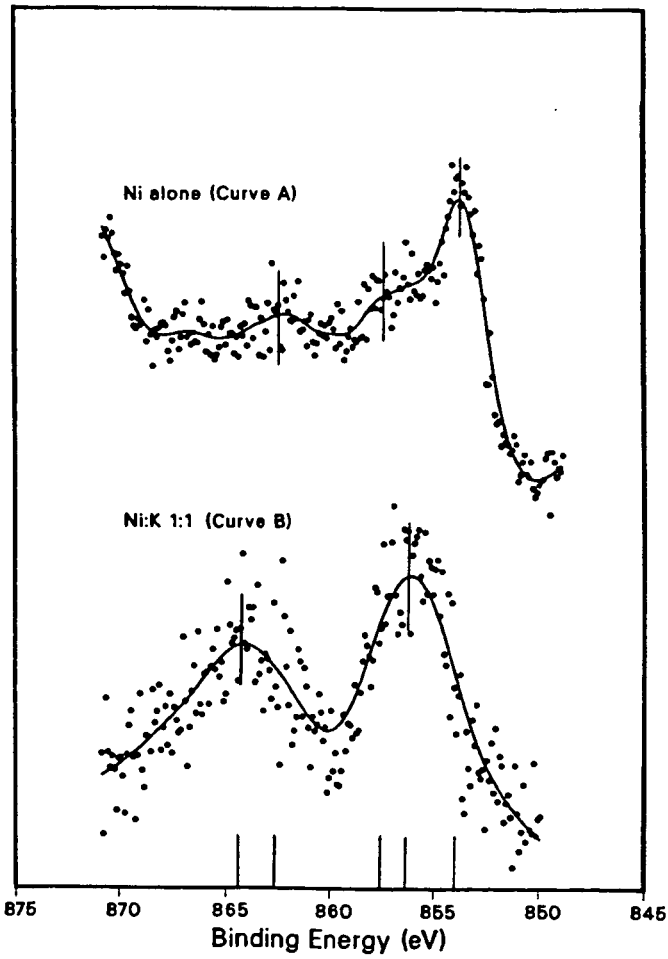

Figure 4. $Ni_{2p3/2}$ XPS of nickel (Curve A) and a 1;1 Ni:K mixture (Curve B) deposited on graphite. The spectra was taken after exposing the samples to 24 torr of water at 923 K for 15 min.

CATALYZED STEAM GASIFICATION OF LOW-RANK COALS TO PRODUCE HYDROGEN

R.E. Sears, R.C. Timpe, S.J. Galegher, and W.G. Willson

University of North Dakota Energy Research Center
Box 8213, University Station
Grand Forks, North Dakota 58202

Abstract

Advance coal gasification technologies using low-rank coal is a promising alternative for meeting future demand for hydrogen. Steam gasification tests conducted at temperatures between 700° and 800°C and atmospheric pressure resulted in product gas compositions matching those predicted by thermodynamic equilibrium calculations, 63-65 mol% hydrogen and less than 1 mol% methane. Steam gasification tests with four low-rank coals and a single bituminous coal were performed in a laboratory-scale thermogravimetric analyzer (TGA) at temperatures of 700°, 750°, and 800°C to evaluate process kinetics with and without catalyst addition. Catalysts screened included K_2CO_3, Na_2CO_3, trona, nahcolite, sunflower hull ash, and recycled lignite ash. North Dakota and Texas lignite chars were slightly more reactive than a Wyoming subbituminous coal char and eight to ten times more reactive than an Illinois bituminous coal char. Pure and mineral (trona and nahcolite) alkali carbonates and recycled ash from K_2CO_3-catalyzed steam gasification tests substantially improved low-rank coal steam gasification rates. The reactivities obtained using trona and nahcolite to catalyze the steam gasification were the highest, at nearly 3.5 times those without catalysts.

Introduction

Hydrogen is a key component in petroleum refining, petrochemical processing, the production of coal-derived synfuels, and can also be used directly as a fuel. Over the next 45 years, the demand for hydrogen has been projected to increase by a factor of 15 to 20 (1). Most of the hydrogen currently used in chemical applications is produced through steam reforming of natural gas; and in refining applications partial oxidation of petroleum is also used. Advanced coal gasification technologies appear to be the most probable alternative for meeting the future demand for large quantities of hydrogen. Low-rank coals (lignites and subbituminous coals) are candidate feedstocks for such applications because of their low mining cost and higher reactivity relative to higher rank coals.

The two most important considerations in the design of a process for producing hydrogen from coal are to maintain operating conditions that thermodynamically favor the production of hydrogen and carbon dioxide over carbon monoxide and methane, and to obtain reaction rates that result in reasonable gasifier throughput. Optimization of the hydrogen content of the product gas requires steam gasification at relatively mild temperatures in the range of 700° to 800°C and at atmospheric pressure. In tests at the University of North Dakota Energy Research Center (UNDERC), a dry synthesis gas containing 63 mol% hydrogen was produced by steam gasification of low-rank coal (2), which is predicted by equilibrium thermodynamics. These mild conditions do not, however, promote high reaction rates. As a result, achieving the maximum coal reactivity by the use of catalysts is perhaps the most critical factor in producing hydrogen from coal.

The physical and chemical nature of low-rank coals (LRCs) offer several advantages for a gasification process producing hydrogen. One of these is their enhanced reactivity compared to coals of higher rank. This increase in reactivity is caused by higher concentrations of active sites, higher porosity, and a more uniform dispersion of alkali impurities that act as inherent catalysts (3,4,5).

The high volatile matter content of lignites could also support their use in steam gasification to produce hydrogen. If introduced into the hot zone of a gasifier, devolatilization products may be cracked to form additional hydrogen (6). Under suitable reaction conditions raw product gas from such a system would then contain essentially only hydrogen, carbon dioxide, carbon monoxide, and only small quantities of methane and sulfur gases. In addition to producing hydrogen and simplifying downstream gas clean-up, cracking of tars and oils in the gasifier would also reduce contaminant concentrations in the process condensate.

Even with the higher reactivities of LRCs, it will be necessary to enhance reaction kinetics through the use of catalysts to obtain economic reactor throughput. There is a wealth of data relating to the use of a variety of catalysts to enhance the steam gasification kinetics (7 - 16). Alkali metals are generally accepted as the premier steam gasification catalyst (12,13,16) and thus their interactions with ash constituents and subsequent recovery are important factors in the process economics. Catalyst recovery problems associated with the formation of insoluble potassium aluminosilicates were identified during recovery of the K_2CO_3 catalyst in the Exxon Catalytic Coal Gasification (CCG) process (6). For some high sodium LRCs, a problem of sodium dilution of the recovered potassium catalyst could be significant. However, if sodium carbonates are also effective catalysts, the problem of alkali recovery will be mitigated, especially with high sodium LRCs.

The overall objective of the program at UNDERC is to establish the feasibility of using low-rank coal gasification to produce hydrogen. This paper summarizes the findings of a thermogravimetric analysis (TGA) study of steam-char gasification kinetics. This work focused on low-rank coals, with limited testing using a bituminous coal for comparison purposes, and the addition of various catalysts to enhance low-rank coal reactivity.

Experimental

The reaction between low-rank coal chars and steam was studied using a DuPont 951 Thermogavimetric Analyzer (TGA) interfaced with a DuPont 1090 Thermal Analyzer. The TGA reaction chamber was an open quartz tube, secured to the balance by means of a threaded nut as shown at point (A) in Figure 1. The opposite end of the quartz tube (point (B) in Figure 1) was connected by rubber tubing to a ventilation hood. The commercially available TGA system was modified for char/steam experiments by adding the steam sidearm shown as point (C) in Figure 1. This port was sealed with a high-temperature gas chromatography septum. The steam inlet line (1/8-inch stainless steel) was passed through this septum and into the reaction chamber (point (D) in Figure 1). Steam was prepared using a "Hot Shot" MB-3L electric steam boiler. The length of steam line from the exit of the boiler to the reaction chamber sidearm was heated continuously at 200°C using electrical heat tape. The reaction chamber was heated in a program-controlled tube furnace.

Approximately 20 mg, weighed to the nearest 0.01 mg, of as-received coal ground to particle sizes of -100 x +140 mesh, was evenly distributed on a tared 11-mm diameter platinum pan supported at the end of the TGA's quartz balance beam. Coal samples were devolatilized in argon prior to the introduction of steam into the reaction chamber. Argon flow was maintained at approximately 160 cc/min while the coal sample was heated from room temperature to the target reaction temperature (700° to 800°C) at a rate of 100°C/min. The average time for devolatilization of these samples was about 15 minutes.

Char samples produced by the devolatilization procedure were weighed in the TGA reaction chamber without cooling. Argon flow was reduced from 160 to 60 cc/min, and steam to the reactor was then started at rates of 1-5 mg/min. Steam flow rates were determined prior to experiments by collecting steam from the gas outlet (point (B) in Figure 1) in a cold, tared vessel for approximately 15 minutes.

Weight, time, and temperature were recorded by the DuPont 1090 Thermal Analyzer as the char-steam reaction proceeded. Experiments were terminated when the sample's weight loss approached zero, or in the case of very slowly reacting materials after 150 minutes of reaction time. The 1090 Thermal Analyzer was then used to plot sample weight loss versus time and to print sample weight, temperature, and reaction time data. Product gases from the system were not analyzed.

Both aqueous impregnation and dry catalyst mixing were evaluated in the TGA steam gasification test. Preliminary TGA tests showed that reactivity was not dependent on catalyst addition technique; therefore, only dry-mix systems were used in the remainder of the TGA test program.

Results

The matrix of char-steam gasification tests conducted by laboratory TGA included experiments for evaluation of coals, catalysts, temperature, and catalyst loading. Indian Head and Velva lignites from North Dakota, Martin Lake lignite from Texas, Wyodak subbituminous coal from Wyoming and River King bituminous coal from Illinois were evaluated. Proximate and ultimate analyses of these coals are given in Table 1. The coal analyses in Table 1 show an uncharacteristically low moisture content for Indian Head lignite. The low moisture content of this sample, 12.6 wt%, resulted from storage in a large nitrogen purged bunker in which a definite moisture gradient was observed from top to bottom, but did not effect the reactivity of the char.

Table 1. Coal Proximate and Ultimate Analysis

	Indian Head A[a]	Indian Head B[b]	Velva	Martin Lake	Wyodak	River King
Test Coal Analyses:						
Moisture, %	12.6	29.5	33.7	25.1	27.5	11.5
Ash, wt%, mf	17.7	9.0	10.4	22.1	9.6	12.1
Volatile Matter, wt%, mf	38.4	41.2	42.8	39.5	42.3	42.5
Fixed Carbon, wt%, mf	43.9	49.8	46.8	38.4	48.1	45.3
Heating Value, Btu/lb, as-rec'd	8,383	7,721	6,755	7,258	8,043	11,000
Ultimate Analysis of Raw Coals, wt%, mf:						
Ash	17.7	9.0	10.4	22.1	9.6	12.2
Carbon	58.9	65.0	62.4	56.7	65.7	68.3
Hydrogen	3.3	4.2	3.8	3.8	4.3	5.1
Nitrogen	1.6	1.9	1.4	1.2	1.2	1.3
Sulfur	1.0	0.8	0.5	1.9	0.5	4.0
Oxygen (by diff)	17.5	19.1	21.5	14.3	18.7	9.1

[a]Low-moisture Indian Head coal used for majority of TGA work.
[b]Indian Head sample used to verify initial TGA results.

Various alkali sources were tested as catalysts to promote the steam-carbon reaction. These were K_2CO_3, Na_2CO_3, trona, nahcolite, sunflower hull ash (a naturally high potassium containing ash), and recycled lignite gasification ash. These substances were selected as prospective catalysts based on their high alkali content. Catalysis with inexpensive or "disposable" catalysts would substantially improve the economics of a hydrogen-from-coal process. Likewise, trona and nahcolite, naturally occurring alkali carbonate materials, are inexpensive relative to pure carbonates (0.04/lb for trona compared to 0.34/lb for K_2CO_3 and 0.20/lb for Na_2CO_3). This cost differential suggests their use as disposable catalysts.

Reactivity of Coals for Steam Gasification

Tests were performed to establish the uncatalyzed reactivities of the five test coal chars and plotted in Figure 2. It shows the higher reactivity of low-rank coals compared to that of River King bituminous coal. The higher reactivity of low-rank coal chars, documented by many research groups (3,4,5), is believed to be a result of the higher mineral content, higher concentrations of active sites and increased porosity of the low-rank coals. Figure 2 also illustrates the linearity of conversion over the 0 to 50 % carbon conversion range.

Over the initial linear portion of the curves in Figure 2, the carbon conversion rates for the three lignites were nearly identical, with Indian Head being only slightly less reactive than the Velva and Martin Lake lignites. However, a definite hierarchy of reactivity developed as the available carbon supply was depleted. During reaction of the final 40% of the carbon, Martin Lake lignite showed the most rapid conversion, followed by Velva and Indian Head.

Steam gasification kinetic data was collected over the range of 700° to 800°C for assessing temperature effects. The increase in reactivity of each LRC with increasing temperature is shown in Figure 3. Increasing the gasification temperature from 700° to 800°C was found to increase reactivities from 2.5 times for Martin Lake lignite to 3.8 times for Wyodak subbituminous coal. Equilibrium gas composition modeling and actual product gases from a 1-lb fixed-bed system showed that the hydrogen content of the gas is virtually unaffected by this temperature increase (17). Apparent energies of activation were also calculated from this data and have been reported previously (18).

Steam Gasification of Catalyzed Coals

Figure 4 shows the rates of carbon conversion at 750°C for each test coal with a 10 wt% K_2CO_3 loading. Comparison of the data in Figure 2 to that in Figure 4 shows that K_2CO_3 addition significantly enhanced the reactivity of each coal. As was the case for the uncatalyzed coals, the reactivity of the catalyzed low-rank coals was far superior to that of the K_2CO_3-catalyzed bituminous coal. However, the reactivity ranking of the four low-rank coals was not the same as that observed without catalyst addition. In Figure 2 Martin Lake lignite was shown to have the most rapid uncatalyzed conversion rate; however, in Figure 4, Martin Lake was shown to have the poorest reactivity of the four similarly catalyzed low-rank coals. Conversely, Wyodak subbituminous coal was the least reactive uncatalyzed low-rank coal, but showed excellent carbon conversion rates in tests using K_2CO_3.

The effect of temperature on the reactivity of each of the four K_2CO_3-catalyzed low-rank coals is illustrated in the bar graph of Figure 5. The trend in reactivity of the K_2CO_3-catalyzed coals with a temperature increase from 700° to 800°C was very similar to that shown for the uncatalyzed coals in Figure 3, with reactivity increasing by a factor of two over the temperature range. For the uncatalyzed coals, the average reactivity increased by a factor of three over this temperature range. It has previously been reported that the addition of K_2CO_3 decreased the apparent energies of activation by as much as 60% compared to the uncatalyzed coals (18).

Several TGA steam gasification tests were performed to evaluate the effect of K_2CO_3 concentration on lignite reactivity. Velva lignite was used for these tests as it resulted in the highest reactivity of the four LRCs tested. Tests were conducted at 750°C using catalyst loadings from 2 to 20 wt%. Data collected from these experiments were used both to evaluate the effect of catalyst loading for each of the two carbonates, and to compare the two carbonates catalytic effect over a range of loadings. Table 2 presents the average reactivities at 50% carbon conversion for the range of loadings evaluated with both K_2CO_3 and Na_2CO_3, which indicates a lesser dependence of reaction kinetics on catalyst loading using Na_2CO_3. Neither catalyst produced a significant rate increase at loadings over 10 wt%; however, the reactivity increase with increasing catalyst loading upto 10 wt% was more pronounced for K_2CO_3 catalysis. Over the 2 to 10 wt% loading range, reactivity values for K_2CO_3-catalyzed Velva lignite increased from 3.3 to 5.5 (g/hr)/g, while the corresponding increase for the Na_2CO_3-catalyzed lignite was from 4.8 to 5.5 (g/hr)/g.

Table 2. Effect of Variable Catalyst Loadings on Velva Lignite Char Reactivity in Steam at 750°C

Catalyst Loading wt% of As-received Coal	$\bar{K}_{0.5}$, (g/hr)/g	
	K_2CO_3	Na_2CO_3
0	2.0	2.0
2	3.3	4.8
5	4.1	4.9
10	5.5	5.5
15	5.7	5.9
20	5.7	6.1

Comparison of Catalyst Effectiveness

Data plotted in Figure 6, compares carbon conversion rates for uncatalyzed Velva lignite and for Velva catalyzed with each of the six additives found to give positive catalytic effects. The nearly identical reactivities observed for K_2CO_3 and Na_2CO_3 catalysis are illustrated, as the two conversion curves are superimposable throughout the gasification phase. Figure 6 also illustrates the catalytic effects of sunflower hull ash and the mineral additives. Twenty percent sunflower hull ash (23 wt% potassium) was less effective than 10% loadings of the carbonates; however, reactivity was much improved over the uncatalyzed coal, with complete conversion occurring in less than 20 minutes. The reactivity for the 20% sunflower hull ash/Velva lignite system at 750°C was 4.3 (g/hr)/g as compared to only 2.0 (g/hr)/g without additives.

Perhaps the most significant results illustrated in Figure 6 were the rapid carbon conversions obtained using trona and nahcolite as gasification catalysts. Both trona and nahcolite produced more rapid conversion of Velva lignite than did addition of the pure carbonates. Approximately 90% carbon conversion was achieved in 8 minutes using either 10 wt% trona (29% sodium) or nahcolite (15% sodium), whereas when using the same wt% pure K_2CO_3 (47% potassium) or Na_2CO_3 (37% sodium) about 10 minutes was required to achieve 90% conversion. For trona catalysis a reactivity of 6.9 (g/hr)/g was obtained compared to 5.5 (g/hr)/g using an identical loading of either K_2CO_3 or Na_2CO_3 at the same gasification conditions. At these conditions, nahcolite catalysis resulted in a reactivity slightly lower than that obtained using trona (6.2 (g/hr)/g).

The effectiveness of these naturally occurring mineral catalysts is important to the development of a commercial hydrogen-producing steam coal gasification process. Based on the relative costs of the feedstock, use of these materials would be more favorable to process economics than would pure alkali carbonates. An additional consideration is that cost and availability of these materials may be such that catalyst recovery would be unnecessary.

Conclusions

Uncatalyzed lignites and a subbituminous coal were found to be eight to ten times more reactive with steam at 700°-800°C than an Illinois bituminous coal. This relationship, within this narrow temperature range, is important as this is the range that thermodynamically favors the production of hydrogen from steam gasification at atmospheric pressure. The reactivity of the uncatalyzed coals increased 3 to 4 times with an increase in steam gasification temperature from 700° to 800°C.

For the catalyzed coals during steam gasification:

- Reactivity increased approximately 2 times over the 700° - 800°C temperature range for low-rank coals catalyzed with potassium carbonate.
- Sodium carbonate was found to be as effective a catalyst as potassium carbonate for the steam gasification of low-rank coal chars on a mass loading basis.
- Alkali carbonate loadings equal to 10 wt% of the as-received coal mass resulted in low-rank coal reactivities 2.5 to 3.5 times higher than those measured for the uncatalyzed low-rank coals.
- Naturally occurring mineral sources of sodium carbonates/bicarbonates, trona and nahcolite, are as effective in catalyzing low-rank coal steam gasification as the pure carbonates.
- Use of these naturally-occurring carbonates sources should be a primary focus of continued research. The low cost of trona or nahcolite relative to the pure carbonates suggests that a potential for their use as disposable catalysts exists which would enhance operability and process economics in a hydrogen-from-coal gasification process.

Acknowledgments

The authors would like to acknowledge Robert C. Ellman and John G. Hendrikson who were instrumental in development and initial supervision of the research. This research was sponsored through the Grand Forks Project Office (GFPO) of the United States Department of Energy. A special thanks for their enthusiastic support is extended to Leland E. Paulson, Technical Project Officer, Fred Bauer of the GFPO, and to Madhav Ghate, Manager AR & TD Gasification - Morgantown for funding.

References

1. Pohani, B.P. J. Japan Petrol. Inst., 27, 1, 1984.

2. Low-Rank Coal Research, University of North Dakota Energy Research Center, Quarterly Technical Progress Report, July-September, 1984, DOE/FE/60181-1682.

3. Johnson, J.L. "Kinetics of Coal Gasification." Wiley and Sons, New York, 1979, 324 pp.

4. Linares-Solano, O.P.Mahajan, and P.L. Walker. Fuel, 58, 327, 1979.

5. Walker, P.L., S. Matsumoto, T. Hanzawa, T. Muira, and I.M.K. Ismail. Fuel, 62, 140, 1983.

6. Euker, C.A. and R.D. Wesselhoft. Energy Progress, 1, 12, 1981.

7. Taylor, H.S. and H.J. Neville, J. Am. Chem. Soc., 43, 2055, 1921.

8. Dent, F.J. et al., Trans. Instn. Gas Engrs., 88, 150, 1938.

9. Weller, S. and Pelipetz, M.C., Ind. Energy Chem., 43, 243, 1951.

10. Walker, P.L. et al., Chem. and Phy. of Carbon, 4, 287, 1968.

11. Haynes, W.P. et al., ACS Div. Fuel Chem. Proc., 18, No.2, 1, 1973.

12. Willson, W.G. et al., Adv. in Chem.-Coal Gasif., 154, 203, 1974.

13. Veraa, M.J. and A.T. Bell, Fuel, 57,194, 1978.

14. Serageldin, M.A. and W.P. Pan, Thermochimica Acta, 76,145, 1984.

15. Radovic, L.R. et al., Fuel, 63, 1028, 1984.

16. Tomita, A. et al., Fuel, 62, 150, 1983.

17. Low-Rank Coal Research. University of North Dakota Energy Research Center, Quarterly Technical Progress Report, April-June 1984, DOE/FE/60181-1642.

18. Timpe, R.C. et al., ACS Div. Fuel Chem., 30, No.4, 481, 1985.

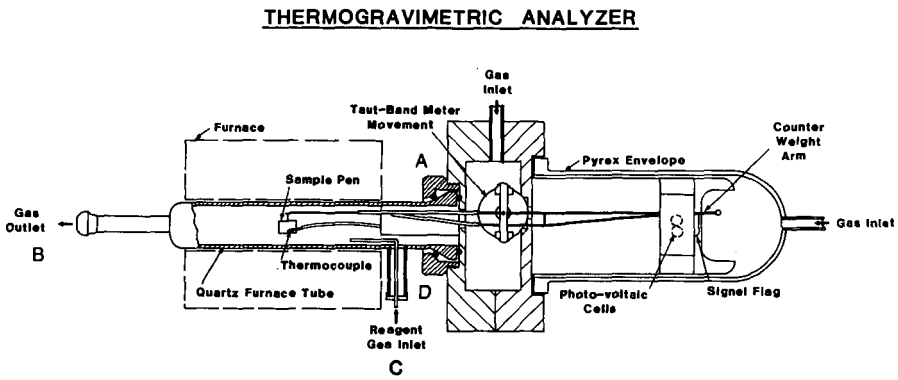

Figure 1. Thermogravimetric analyzer.

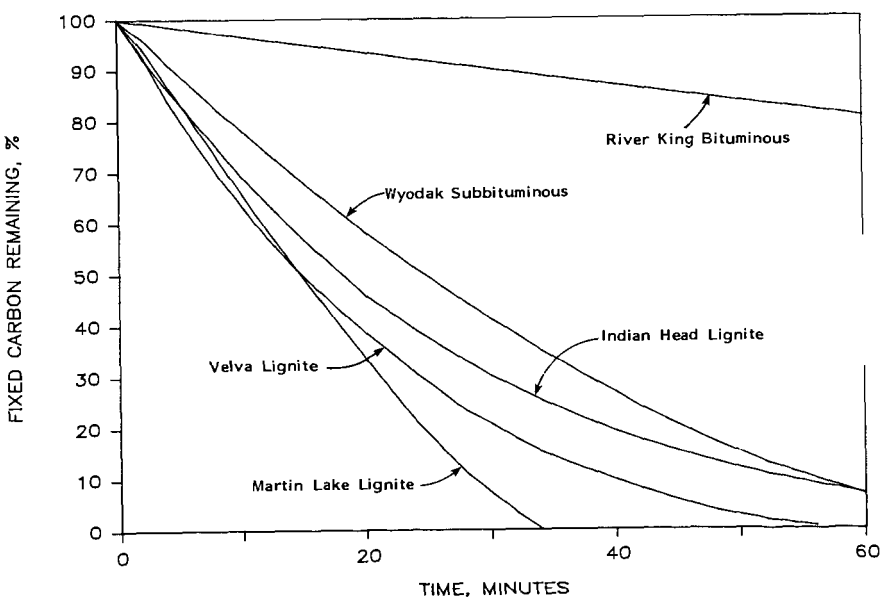

Figure 2. Rate of carbon conversion at 750°C - variation with coal rank.

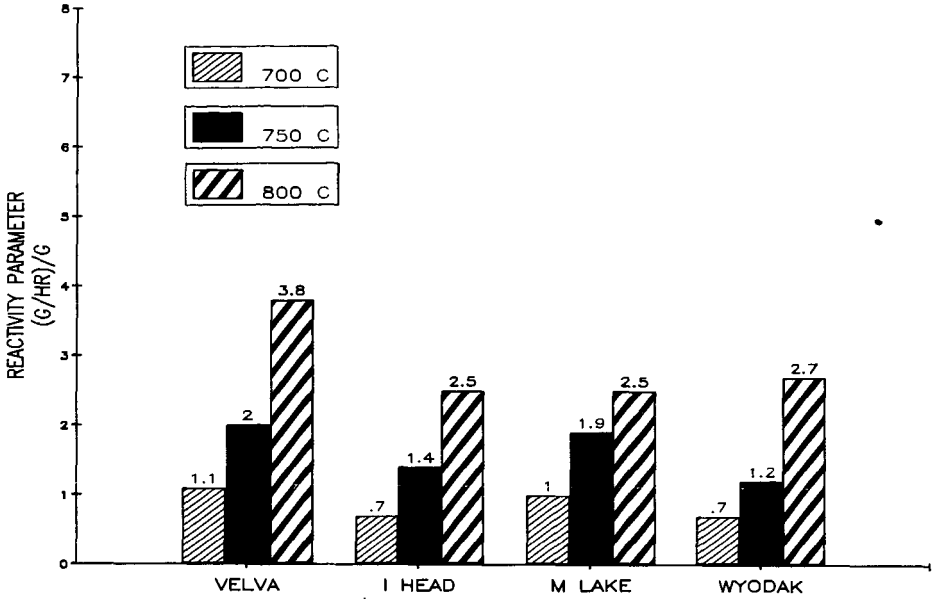

Figure 3. Reactivity of uncatalyzed low-rank coal chars as a function of steam gasification temperature.

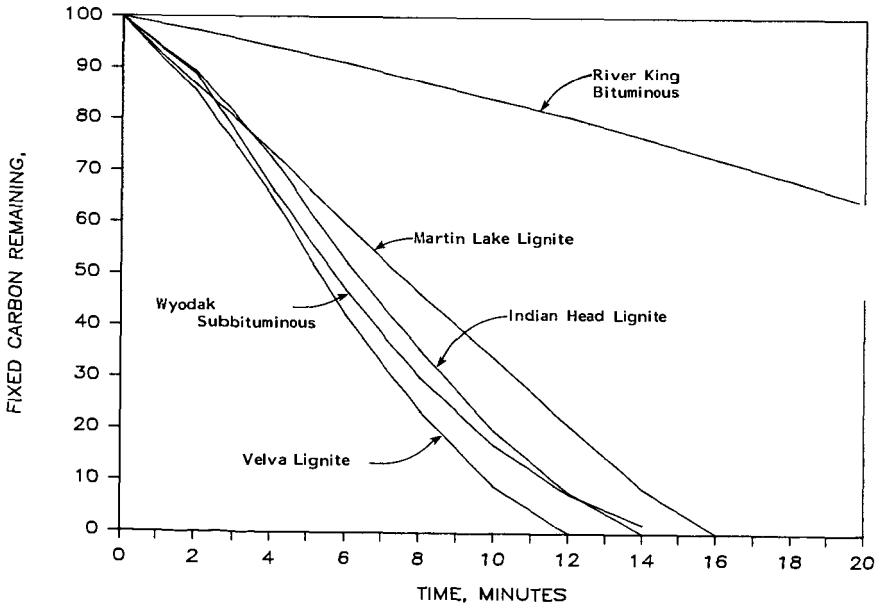

Figure 4. Carbon conversion of K_2CO_3-catalyzed coal chars at 750°C.

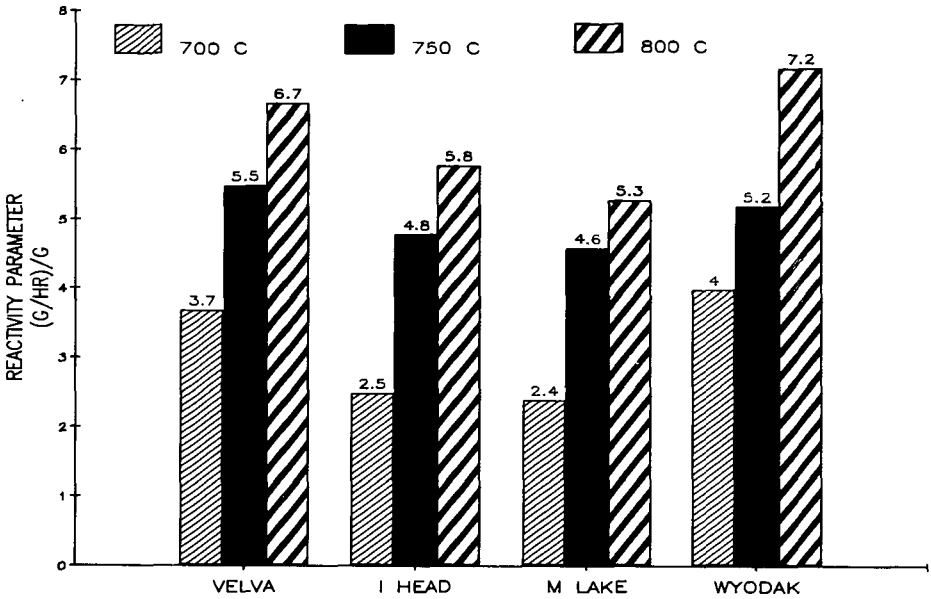

Figure 5. Effect of steam gasification temperature on the reactivity of K_2CO_3-catalyzed low-rank coal chars.

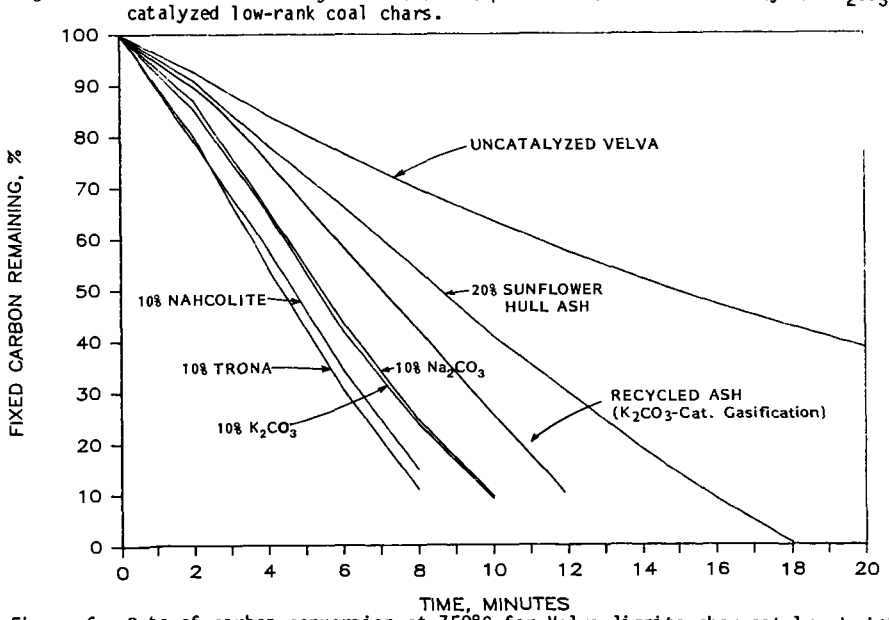

Figure 6. Rate of carbon conversion at 750°C for Velva lignite char catalyzed with various alkali sources.

COAL GASIFICATION WITH INTERNAL RECIRCULATION CATALYSTS

by

A H. Hill, G. L. Anderson
Institute of Gas Technology
3424 S. State Street
Chicago, IL 60616

and

M. R. Ghate, W. Liou
U.S. Department of Energy
Morgantown Energy Technology Center
P.O. Box 880
Morgantown, WV 26507

One of the primary economic penalties of many catalytic coal gasification processes is recovery of the added catalysts from the spent char. For example, the EXXON catalytic coal gasification process as presently conceived, requires several stages of digestion with calcium hydroxide to recover potassium from the converted char and then the digestion only recovers between 65 and 85% of the potassium.[1]

Recently, IGT has been exploring a process concept that might avoid this complex and costly situation. In the IGT process concept, a coal gasification process with an inherent thermal gradient (e.g., Lurgi, staged fluidized-bed processes, etc.) and a catalyst that is semivolatile under gasification conditions are used. The semivolatile catalyst is sufficiently volatile at the highest temperature encountered in the lower section of the gasifier, that it is completely vaporized from the char before the char is discharged. The catalyst, however, is nonvolatile at the lowest temperature encountered in the upper section of the gasifier so that it precipitates on the cold, feed coal. The catalyst, therefore, is automatically recycled from the product char to the fresh coal and the need for catalyst recovery is eliminated.

Three different materials have been undergoing testing by IGT as semivolatile catalysts. These materials were selected based on an examination of their vapor pressures and the following process assumptions. It was assumed that a catalyst loading of approximately 5 wt % is sufficient for catalyzing the gasification reactions, that the temperatures in the gasifier vary from 600° to 1600°F, that the gasifier operates at 1000 psig with a product gas/coal feed ratio of 15 SCF/lb, and that a rate of loss of catalyst in the product gas of less than 1% of the circulation rate of the catalyst in the gasifier is acceptable. With these assumptions, the requisite vapor pressure of the "semivolatile" catalyst in the hottest section and the coldest section of the gasifier was calculated to be greater than 1.0 atmosphere at 1600°F (870°C) but less than 10 mm Hg at 600°F (315°C).

The materials identified to have the proper physical properties are shown in Table 1. Arsenic in its elemental form is relatively stable under reducing conditions. Some arsine, AsH_3, formation is expected; but at high total arsenic partial pressures and moderate temperatures, more than 99% of the gas phase arsenic is expected to be present as As_2 and As_4. Although less is known about the behavior of cadmium, studies have shown that fines generated in coal gasification are highly enriched in cadmium, indicating "semivolatile"

Table 1. MATERIALS WITH VAPOR PRESSURES IN THE DESIRED RANGE FOR A "SEMIVOLATILE" CATALYTIC COAL GASIFICATION PROCESS

Element	Temperature (°F) for a Vapor Pressure of: 10 mm HG	1 atm
Arsenic	819	1130
Cadmium	903	1403
Cesium Hydroxide	1160	1790

behavior in the gasifier. Cesium hydroxide, on the other hand, is known to enhance the reactivity of carbon towards steam.[2] Studies have also presented evidence for the volatility of cesium hydroxide under gasification conditions.[3]

This paper summarizes the results of 1) laboratory-scale batch reactor screening tests conducted to evaluate the performance of arsenic, cadmium and cesium hydroxide as catalysts for coal gasification and 2) continuous bench-scale tests with cesium hydroxide, the most effective catalyst tested in the initial screening tests, to determine the volatility of cesium hydroxide, i.e., its release from the char before discharge, under continuous gasification conditions.

EXPERIMENTAL

Laboratory-Scale Screening Tests. During the catalyst screening portion of the project, 49 char gasification tests were conducted in the laboratory-scale batch reactor catalyst testing unit pictured in Figure 1. The reactor is constructed of Rene 41 steel and is 12-inches high with a 0.05-inch I.D., a 2-inch O.D., and a 28-cm^3 capacity. The high temperature valve (Figure 1) has an extended stuffing box which allows the body of the valve to be located in the furnace with the reactor. This is necessary to avoid condensation of both the steam and semivolatile catalyst during the test. Tests were conducted with devolatilized North Dakota lignite and Illinois No. 6 bituminous coal chars. The chars were prepared in a separate 1-inch-diameter fluidized-bed reactor with nitrogen as the fluidizing gas. Analyses of the chars used in the study are presented in Table 2.

The batch reactor char gasification tests were conducted under the following conditions:

Temperature:	1200°, 1300°, 1400°F
Initial Pressure:	~160 psig
Gasifying Medium:	Steam, Hydrogen
Char Particle Size:	~200 Mesh
Char Residence Time:	3, 6 h
Catalyst Loading:	10 Wt %
Char Sample Weight:	~200 mg

The experimental procedure was as follows. With arsenic or cadmium, the char and the appropriate amount of powdered metal were thoroughly mixed in a high-speed pulverizing shaker. About 220 milligrams of the mixture was then weighed out and placed in a small quartz test tube. A sufficient amount of water (~240μl) was then added to the mixture with a volumetric syringe such that the resultant water-to-carbon molar ratio was 1. In tests with cesium hydroxide, a 50 wt % solution of cesium hydroxide in water was added to the char in the test tube. Additional water was then added to give the required water/carbon molar ratio of 1.

Table 2. ANALYSIS OF THE CHARS USED IN THE LABORATORY-SCALE BATCH REACTOR GASIFICATION TESTS

Elemental Analysis*	North Dakota Lignite	Illinois No. 6 Bituminous
	wt % dry	
Carbon	75.88	80.90
Hydrogen	0.65	0.58
Nitrogen	0.86	1.21
Ash	20.86	14.16
Total	98.25	96.85

* Carbon, hydrogen and nitrogen determined by ERBA analyzer (Automated Elemental Analyzer) which was used to analyze residues of all batch reactor tests.

The test tube containing the char/catalyst/water mixture was placed into the reactor, the reactor was reconnected to the system, and the system and reactor were then evacuated. To prevent losing the added water during evacuation, the reactor was placed in a dry-ice bath to freeze the water in the test tube. After evacuating the reactor, the dry-ice bath was removed, and the reactor was allowed to come to ambient temperature. The reactor was then placed into the furnace and was charged with sufficient hydrogen (~160 psig) such that the resultant hydrogen-to-carbon molar ratio is 1. After the reactor was charged with hydrogen, the high-temperature valve was closed, the remainder of the system was evacuated, and the furnace was allowed to heat up to the desired operating temperature. When the desired time had elapsed, the furnace was turned off and opened, allowing the reactor to cool to ambient temperature.

The reactor valve was then opened and the total system pressure was measured. This allowed the total moles of non-condensible gas in the system at the end of the test to be calculated. A sample of the product gas was then taken for analysis, and reactor was depressurized and opened. The test tube containing the mixture was removed from the reactor, and the residue was submitted for chemical analysis.

Bench-Scale Tests. Cesium hydroxide catalyzed and uncatalyzed char gasification tests were conducted in a 2-inch I.D. bench-scale unit (BSU). Nine tests were conducted in the BSU with North Dakota lignite and Illinois No. 6 bituminous chars. The chars used in the BSU gasification tests were prepared in an IGT 4-inch I.D. fluidized-bed reactor. Analyses of the chars used in the gasification tests are given in Table 3. The cesium hydroxide catalyst (Alfa Products®) was obtained as a hydrated solid containing about 85 wt % cesium hydroxide. It was deposited on the char by evaporation from solution under vacuum at 105°C.

The BSU is shown in Figure 2. It consists of a reactor (2-inch I.D., 39.125-inches long) and associated equipment for feeding and measuring the flow rates of char, steam, reference/purge gas (argon); for collecting and/or measuring the flow rates of residue char, liquid product, and product gas; and for collecting representative samples of the product gas.

In this unit char is fed to the top of the reactor by a calibrated screw feeder from a pressurized feed hopper, while the residue char is discharged from the bottom of the reactor into a pressurized residue receiver by a discharge screw. A piston-type metering pump is used to pump water from a reservoir into a steam generator that provides steam for the reactor.

Table 3. ANALYSES OF CHARS USED IN THE BSU GASIFICATION TESTS

Char Type	North Dakota Lignite	Illinois No. 6 Bituminous
Proximate Analysis, wt %		
Moisture	6.06	0.00
Volatile Matter	14.38	2.34
Fixed Carbon	64.69	81.59
Ash	14.87	16.07
	100.00	100.00
Ultimate Analysis, wt %		
Ash	15.83	16.07
Carbon	71.25	77.63
Hydrogen	1.87	0.91
Sulfur	1.54	2.58
Nitrogen	0.79	1.11
Oxygen	8.72	1.70
	100.00	100.00

The reactor steam enters the bottom of the reactor above the discharge screw through a dip tube. Metered and preheated argon is added as an internal reference and carrier gas and enters the bottom of the reactor between discharge screw and the exit of the steam dip tube.

Effluent gases from the top of the reactor pass through two water-cooled condensers in series. The condensed liquids are drained into separate vessels and weighed. An "aliquot" sample of the product gas is taken for componential analysis by feeding a portion of it into a water-sealed gas holder during selected periods of each test. "Spot" gas samples are also taken throughout the test period for componential analysis.

In a typical run, the reactor was initially filled with char and/or a char/catalyst mixture. After charging the reactor the system was flushed with argon. The temperatures of the reactor, steam pre-heater, super-heater and line heaters were then brought to operating temperatures in 1 to 2 hours and (except for Test 9) were maintained at these values for the duration of the test.

Gasification data were collected beginning immediately after the reactor furnace heaters were turned on and continued to be collected for 3 hours after the introduction of the steam to the reactor (fixed-bed operating period). Steam was fed after the lower zones of the reactor reached 1400°F.

Gasification data were also collected for an additional 5 hours after the 3-hour fixed-bed operating period under moving-bed conditions. Steady-state conditions were attained during the last two hours of the moving-bed operating period of Tests 2 and 3. "Steady-state" is defined as a condition wherein the reactor pressure is stable, the temperature profile in the bed, char feed rate and bed height are essentially constant.

In this study product gas compositions were determined by gas chromatography. Feed and residue char compositions and the carbon content of the condensate samples were determined by standard ASTM methods. The cesium content of the catalyzed feed and residue chars, steam condensate and the water used to rinse the reactor and product gas exit lines were determined by atomic absorption spectroscopy.

After each test was completed, the weight of the char fed was determined by weighing the char initially charged to the feed hopper and the char remaining in the feed hopper at the end of the test. The residue char was

also weighed after the test. Feed and residue char rates were calculated by dividing these weights by the measured char feeding time.

Results and Discussion. Figures 3 and 4 compare the measured effects of arsenic, cadmium and cesium hydroxide on the rate of gasification of lignite and bituminous char in the laboratory-scale batch reactor char gasification tests. The relative rate of gasification of the uncatalyzed and catalyzed chars are expressed in Figures 3 and 4 as reactivity ratios, i.e., the ratio of carbon conversions (X_c) obtained in the catalyzed tests and the average of all the carbon conversions (X_c) in the uncatalyzed tests at each temperature. A reactivity ratio value of one (shown by the horizontal line in each figure) indicates no effect of the catalyst on the char reactivity by the catalyst.

Although a great deal of scatter remains in the data shown in Figures 3 and 4, it is apparent that cesium hydroxide is more effective than arsenic or cadmium for char gasification. Increasing the reaction temperature strongly increases the catalytic effect of cesium hydroxide on the bituminous char reactivity, but has little effect on the lignite char reactivity.

A summary of the BSU gasification tests is given in Table 4. A number of operational problems prevented all but Tests 2 and 3 from being conducted under continuous moving-bed conditions. In Tests 4 and 5 (in which the catalyst was placed in reactor Zones 2 and 3 only), the formation of a clinker-like mass blocked the downward movement of the bed and, therefore, prevented residue discharge. In Tests 6, 7 and 9, moving-bed conditions could not be attained because the catalyzed char adhered to the reactor walls and prevented residue discharge.

The dry gas production rates for the tests with uncatalyzed and catalyzed bituminous char during the reactor heat-up and the fixed-bed operating periods are shown in Figure 5. The addition of catalyst to the bituminous char increased the gas production rate by as much as 72%.

The tests with catalyzed lignite char also showed consistently higher gas production rates than the tests without catalyst. In Tests 4 and 5, the catalyst was placed in the hottest zone of the reactor. The gasification rate with this distribution of catalyst quickly increased to very high values but then decreased rapidly as gasification proceeded, to the rates obtained with the uncatalyzed char. Distributing the catalyst evenly throughout the reactor, as was done in Tests 6 and 7, resulted in gasification rates that were initially slightly higher than in the tests with the uncatalyzed chars but the rate of gasification tended to decrease less rapidly with time. Although the lignite char showed higher overall gasification reactivity, the catalyst is 33% more effective in catalyzing the gasification of the less reactive bituminous as compared to the lignite char.

The dry gas constituent production rates during the reactor heat-up and fixed-bed operating periods for the uncatalyzed and catalyzed bituminous char are shown in Figure 6. Hydrogen and carbon dioxide account for most of the increases in the catalyzed dry gas production rates in both the bituminous and lignite char gasification tests. In the two lignite gasification tests, where the catalyst was concentrated in the two hottest zones of the reactor (Tests 4 and 5), a small increase in the production rate of carbon monoxide and methane relative to the hydrogen was observed.

Figures 7 and 8 compare the cumulative carbon gasified as a function of time for both char types during the fixed-bed operating period. A significant increase in the total amount of carbon gasified is shown in the catalyzed char tests. The extent of the increase is highly dependent on where the catalyzed char was initially placed in the reactor before heating.

The disposition of the cesium catalyst in the various solid and liquid product streams from the bench-scale reactor has been investigated. The results have thus far indicated minimal movement of the cesium from its initial position under the applied test conditions. This suggests that either higher temperatures or lower pressures might be required to effect cesium volatilization from the char.

Plans are to conduct larger-scale BSU tests, wherein the operating problems encountered in the 2-inch BSU might be avoided, to answer this question.

ACKNOWLEDGEMENT

This work has been supported by the U.S. Department of Energy (Morgantown Energy Technology Center) under Contract Number DE-AC21-84MC21203

REFERENCES

1. Gallagher, J. E., Jr. and Euker, C. A., Jr., "Catalytic Coal Gasification for SNG Manufacture," International Journal of Energy Research 4, 137-147 (1980).

2. Cabera, A. L., Heinemann, H. and Somorjai, G. A., "Methane Production From the Catalyzed Reaction of Graphite and Water Vapor at Low Temperatures (500-600 K)," J. of Catalysis 75, 7-22 (1982).

3. Kosky, P. G. et al., "Coal Gasification Catalysis Mechanisms," Final Report to DOE for the period September 29, 1980-November 29, 1982. DOE/MC/14591-1397 (DE83011051), by General Electric Company, September 1982.

PAP/acsah/40

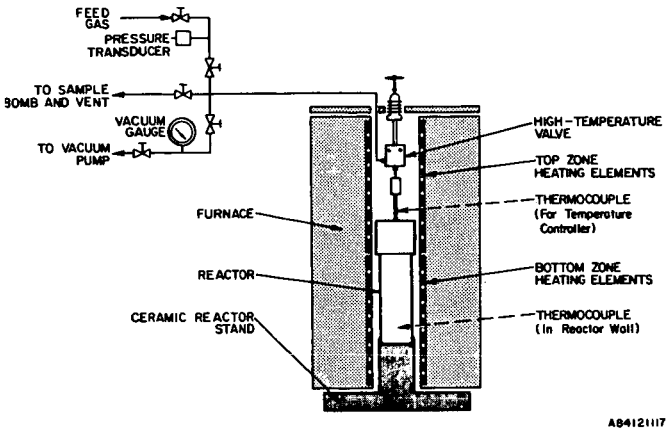

Figure 1. LABORATORY-SCALE BATCH REACTOR CATALYST TESTING UNIT

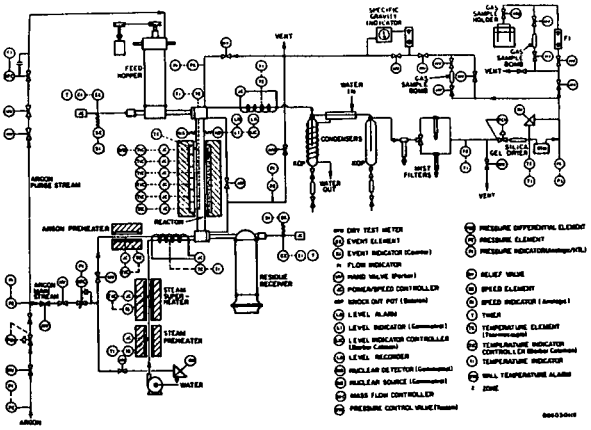

Figure 2. BENCH-SCALE REACTOR UNIT

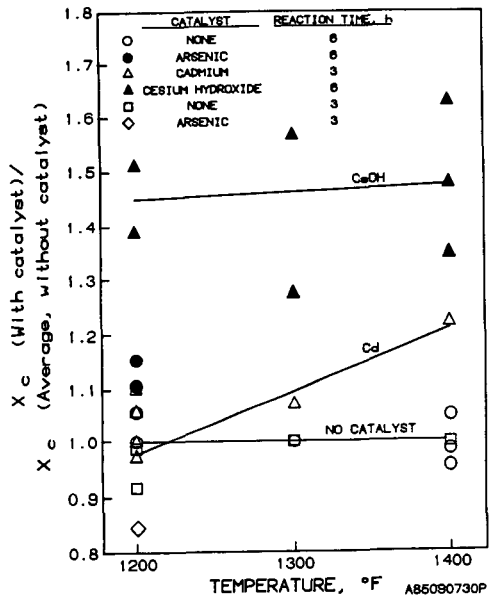

Figure 3. COMPARISON OF THE EFFECT OF ARSENIC, CADMIUM AND CESIUM HYDROXIDE ON THE REACTIVITY OF LIGNITE CHAR

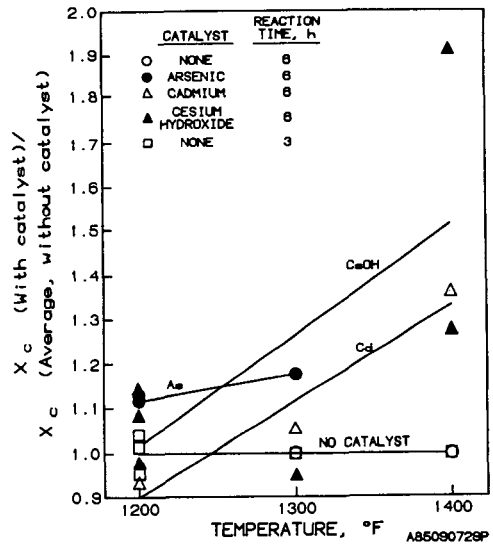

Figure 4. COMPARISON OF THE EFFECT OF ARSENIC, CADMIUM AND CESIUM HYDROXIDE ON THE REACTIVITY OF BITUMINOUS CHAR

Table 4. SUMMARY OF THE NORTH DAKOTA LIGNITE AND ILLINOIS NO. 6 BITUMINOUS CHAR BSU GASIFICATION TESTS

Test No.	1	2	2	2	3	3	3	4	5	6	7	8	9
Char	Lignite											Bituminous	
Char Particle Size (U.S. Sieve)	-6+12												
Catalyst	None							CsOH				None	CsOH
Operating Period, min													
Fixed-Bed Operation[a]	292	210	0	0	225	0	0	222	234	225	235	291	322[i]
Moving-Bed Operation	0	0	300	0	0	300	0	0	0	0	0	0	0
Steady-State Operation	0	0	0	120	0	0	120	0	0	0	0	0	0
Operating Data													
Reactor Pressure, psia	152	152	152	152	152	152	152	152	152	152	153	149	149
Average Reactor Temperature, °F													
Zone 7 (top)	825	777	892	892	675	518	518	741	761	665	676	578	709
6	1000	--	--	--	--	--	--	--	1049	893	911	1037	1019
5	--	--	--	--	--	--	--	--	1146	1001	1024	1128	1106
4	1299	1330	1375	1375	1191	1161	1161	1237	1243	1128	1136	1225	1193
3	1432	1396	1406	1406	1321	1297	1297	1345	1330	1265	1267	1337	1303
2	1450	1428	1301	1391	1435	1406	1406	1430	1446	1473	1433	1479	1476
1 (bottom)	1372	1117	1174	1174	1338	1390	1390	1343	1369	1384	1410	1381	1372
Initial Reactor Char Charge, g[b]													
Below Steam Injection Point, uncatalyzed	1244	8	8	8	1277	1277	1277	487	532	535	535	875	260
Above Steam Injection Point, uncatalyzed		888	888	888				487	605	0	175		0
Above Steam Injection Point, catalyzed	0	0	0	0	0	0	0	191	255	775	508	0	610
Cesium Hydroxide, g	0	0	0	0	0	0	0	85	87	88	170	0	88
Char Fed from Hopper, g[b]	201	204	2473	908	0	2351	908	161	194	152	169	112	177
Char Feed Rate, g/min[b]	0	0	8.24	7.57	0	7.84	7.57	0	0	0	0	0	0
Char Residue, g[c]	907	0	1703[d]	383	0	2216[d]	593	939	938	904	1055[c]	844[c]	933[c,i]
Char Residue Discharge Rate, g/min[c]	0	0	5.68[d]	3.19	0	7.39[d]	4.94	0	0	0	0	0	0
Carbon in Condensate, g	4.4	0	12.6[e]	0	1.9	10.3[e]	3.4	3.0	3.6	3.5	3.4	1.3	1.1(1.1)[h]
Steam Feed Rate, g/min	6.70	6.38	6.91	6.91	6.60	6.85	6.85	6.63	5.88	6.84	5.92	8.34	8.41
Argon Reference Gas Rate, SLPM	4.96	4.96	4.96	4.96	4.96	4.96	4.96	4.96	4.96	4.96	4.96	4.96	4.96
Argon Feed Hopper Purge Rate, SLPM	0.25	0.25	0.25	0.25	0.25	0.25	0.25	0.25	0.25	0.25	0.25	0.25	0.25
Average Gas Composition, %[f]													
H_2	63.3	64.2	53.5	52.2	66.1	57.0	56.2	63.6	63.6	65.2	59.1	60.6	62.0
CO_2	27.6	26.6	23.9	22.5	27.3	25.7	25.0	23.9	23.9	26.8	26.2	30.4	33.0
CO	5.7	4.5	14.3	16.5	4.3	9.7	10.7	8.3	8.6	4.6	9.0	5.7	2.5
CH_4	3.2	4.5	8.1	8.6	2.3	7.6	8.1	4.0	3.8	3.3	5.6	3.3	2.5
C_2H_6	0.2	0.2	0.2	0.2	<0.001	<0.001	<0.001	0.2	0.1	0.1	0.1	<0.001	<0.001
C_3H_8	0.02	0.02	0.02	0.03	<0.001	<0.001	<0.001	0.004	0.007	0.003	0.004	<0.001	<0.001
C_6^+	<0.001	<0.001	<0.001	<0.001	<0.001	<0.001	<0.001	<0.001	<0.001	<0.001	0.002	<0.001	0.03
Total	100.0	100.0	100.0	100.0	100.0	100.0	100.0	100.0	100.0	100.0	100.0	100.0	100.0

[a] Time from when steam was first fed to reactor until beginning of moving-bed operating period or end of test.

[b] Data on an as-received basis.

[c] Data on a moisture-free basis.

[d] Also includes fixed-bed operating period.

[e] Also includes reactor heat-up and fixed bed operating periods.

[f] Includes gas produced during reactor heat-up for fixed-bed operating periods only.

[g] Reactor volume filled with gravel

[h] Produced after fixed-bed operating period, when the temperatures of all reactor zones were raised to 1400°F.

[i] Includes 44 minutes when all reactor zones were at 1400°F.

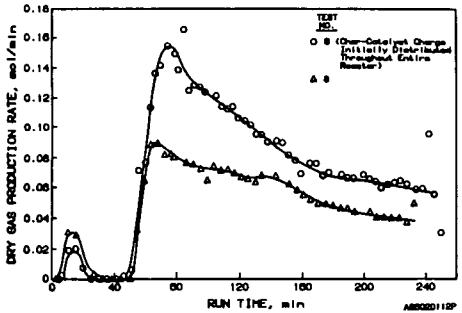

Figure 5. GASIFICATION RATES FOR UNCATALYZED AND CATALYZED BITUMINOUS CHAR

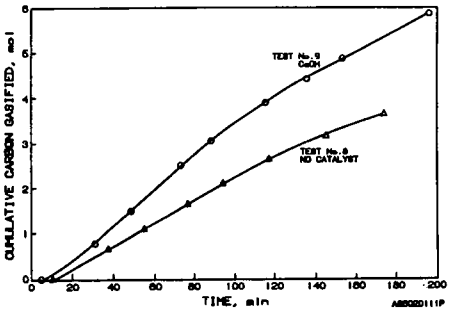

Figure 7. EFFECT OF CATALYST ON THE CUMULATIVE CARBON GASIFIED FOR THE BITUMINOUS CHAR

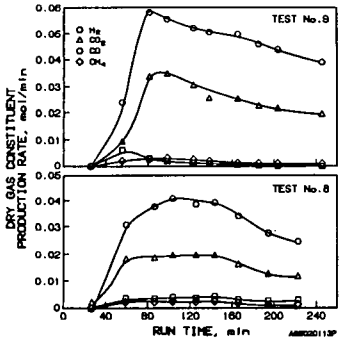

Figure 6. DRY GAS PRODUCTION RATES OF H_2, Co_2, CO AND CH_4 FOR THE UNCATALYZED AND CATALYZED BITUMINOUS CHAR

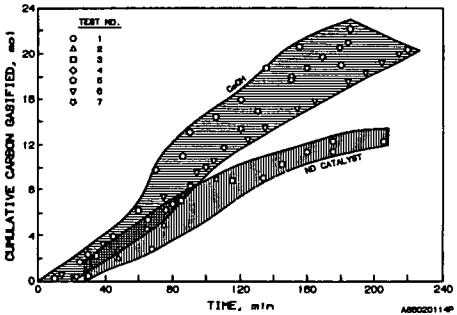

Figure 8. EFFECT OF CATALYST ON THE CUMULATIVE CARBON GASIFIED FOR THE LIGNITE CHAR

OXYGEN CHEMISORPTION AS A TOOL FOR CHARACTERIZING "YOUNG" CHARS

E. M. Suuberg, J. M. Calo, and M. Wojtowicz
Division of Engineering
Brown University
Providence, Rhode Island 02912

The introduction of the concept of active surface area (ASA) as measured by oxygen adsorption [N. R. Laine, F. J. Vastola, and P. L. Walker, Jr., J. Phys. Chem., 67, 2030 (1963)] has led in recent years to various attempts to correlate char reactivity towards oxygen-containing gasification agents (e.g., CO_2). As may be seen from the literature, this approach has met with some, although not universal, success. Theories have been advanced which suggest that only a portion of active sites may participate in actual gasification reactions.

Hampering a fundamental understanding of what the role of active sites might be is lack of information on their nature. A wide variety of conditions has been suggested for measurement of ASA, generally involving temperatures in the range from 100°C to 350°C and oxygen pressures from fractions of a torr to atmospheric. Only in a few cases have these conditions been critically evaluated. In this paper, a series of experiments is reported upon, which seek to establish the importance of these conditions on determining the ASA of "young" chars (i.e., not heat treated for extended times).

1.0 Introduction

Gasification of carbonaceous solids has historically been and remains an area of significant scientific and technological interest (1-7). It has been well established that the reactivity of char to gasification generally depends upon three principal factors: (a) the concentration of "active sites" in the char; (b) mass transfer within the char; and (c) the type and concentration of catalytic impurities in the char. This paper is concerned with the nature of the active sites, and attempts to elucidate further what is normally being measured as active sites. It has been shown, or at least implied, by the results of various workers that active surface area (ASA) is a better predictor of char reactivity than is total surface area (TSA) (8-10). The most frequently employed technique for determining active sites in chars is oxygen chemisorption (8-16).

The gradual pyrolytic evolution of hydrocarbons (possibly including heteroatoms) to highly carbonaceous solids is accompanied by dramatic changes in the gasification reactivity of such materials. Here we are concerned with the gasification behavior of chars that have already undergone active pyrolysis in which most hydrocarbon gases and tars are evolved. The issues involved in transient high rate hydrogasification or steam reactivity during pyrolysis (e.g., 1, 17, 18) are not addressed here.

Active sites in relatively pure carbons are normally thought to be associated with various types of imperfections in the carbon structure. Work with graphite has suggested the important role of carbon crystallite edges or dislocations. The majority

of mechanistic theories of carbon gasification are based on the "pure-carbon-surface-imperfections" model. This is appropriate for chars that have been heat-treated at high temperatures for extended periods of time and thus have relatively low residual oxygen and hydrogen contents (i.e., "old" chars). Some caution must be exercised in applying results obtained from pure carbons to "young" chars. This point will be considered further below.

Carbon gasification theories are based largely upon chemisorption-desorption mechanisms (some also allow for surface diffusion of intermediates). There is some evidence to suggest that the same type of oxygen-carbon complexes are involved in oxygen, steam, and carbon dioxide gasification (2,19). A correlation has also been demonstrated between active sites involved in hydrogen gasification and those involved in carbon dioxide gasification, although there is no direct proof that the sites involved are indeed the same in both cases (1). There is, however, a legitimate concern that the concept of "active sites" may be too broad, and that active sites may in fact be quite different in "young" chars than in "old" chars. It is the issue of what exactly is being measured by oxygen chemisorption which will be addressed in this paper.

There exists a distinction between "active" sites that are reactive and those that are nonreactive at a given temperature. The reactive "active" sites are responsible for the release of surface carbon oxides, while the nonreactive "active" sites will chemisorb oxygen but will not release surface oxides at the temperature under consideration. Raising the temperature of the carbon converts some nonreactive to reactive "active" sites (5,8). This mechanism, combined with the expected Arrhenius-type enhancement of chemical reaction rates, results in increasing gasification rate with temperature.

The preceding effect, however, is not always observed, and thus other factors must also play a role. For example, it has been observed that the rate of carbon combustion normally increases with increasing temperature, up to about 1500K. In the 1500-2000K temperature range, however, it has often been noted that the rate of combustion actually decreases with increasing temperature (5, 20-23). One explanation for this behavior is known as "thermal annealing" (3,5, 24-26). This same effect has also been postulated as being responsible for a decrease in reactivity towards other gases as well (1, 27, 28). There is a trend towards lower reactivity with increased time and temperature of char heat treatment (1, 29-35). This behavior reflects a progressive and continuous ordering of the remaining carbon and is actually an extension of the pyrolysis process.

It would, therefore, seem logical to associate the temperature dependence of the annealing process in chars with the activation energies of the latter phases of pyrolysis; i.e., 100 to 200 kcal/mol typical for high temperature H_2 release (36) and graphitization (37), respectively. In fact, this range is consistent with the results of a few studies on pure, relatively graphitic carbons (21, 26). The values of annealing reaction activation energies derived from experiments with younger chars have been generally lower, however.

In the present study, we examine the chemisorption behavior of relatively young chars only, so in comparing this study to those on graphites or chars produced by prolonged heating at high temperature, caution must be exercised. In this study, the effects of temperature and oxygen pressure on chemisorption behavior are considered.

Experimental

Two different kinds of chars were examined in the course of this study. One was prepared from pyrolysis of a previously demineralized North Dakota lignite, the composition of which is shown in Table 1. Demineralization was accomplished by washing the sample with HCl, followed by HF and again followed by HCl, according to the technique of Bishop and Ward (38). The residual mineral matter content of the lignite was determined to be approximately 0.8%. The other char which was examined was derived from a phenol-formaldehyde resin, carefully synthesized so as to avoid any cation contamination.

Table 1

	C	H	N	S	Ash	O
North Dakota Lignite+	65.6	3.6	1.1	0.8	11.0	17.9
Phenolic Resin	73.9	5.5	0	0	0	20.6
Phenolic Resin Char*	87.2	1.6	0	0	0	11.2

All analyses on a weight percent, dry basis. Oxygen by difference.
+The analysis is for the as-received lignite, prior to demineralization.
*Pyrolysis as indicated in the text.

Both samples were pyrolyzed at similar conditions. Pyrolysis was performed under inert gas (helium). The resin samples were heated at a rate of 4 to 5°C/min to a maximum temperature of 950°C, held for about 2 hours at temperature, and then cooled to room temperature at a rate of 2 to 25°C/min. Samples were never permitted to contact oxygen while at high temperatures, except during the actual chemisorption experiments. The weight loss during pyrolysis was approximately 40%. The total surface area of chars produced this way was roughly 300m^2/g. The lignite sample was heated at a rate of about 3°C/min to 1000°C, held at this temperature for 2 hours, and then cooled to room temperature at a rate comparable to the heating rate. The weight loss of the lignite during pyrolysis was 42.3%.

Prior to chemisorption, samples were always outgassed for about 2 hours at 950°C, under helium.

Generally, chemisorption was performed in a TGA type device. About 50-100 mg of powdered sample was placed in a quartz bucket, the system tared, and mass change followed as a function of time, at the desired oxygen partial pressure and temperature. Experiments were performed to assess the effects of oxygen pressure and temperature on oxygen chemisorption behavior.

Effect of Temperature on Oxygen Chemisorption Behavior

There exists a voluminous literature on low temperature oxidation of coals and a significant number of studies on low temperature oxidation of chars. Generally, the analysis of oxygen uptake in these systems has been analyzed in terms of the Elovich equation, expressed as

$$dq/dt = a \exp(-bq)$$

where q is the amount of oxygen chemisorbed per gram of char, and a and b are constants. Recent work on 550°C cellulose char has shown the data on oxygen uptake at temperatures between 74 and 207°C to be reasonably fit by this equation, and implies a linear increase in chemisorption activation energy from 13 to 25 kcal/mol with increasing extent of uptake (39). These data were interpreted, together with ESR data, to suggest that far more oxygen is chemisorbed than there are free radical sites initially available. A chain reaction via peroxy radicals was ruled out on the basis of the high activation energies. A Diels Alder reaction was postulated, but not vigorously supported. This is representative of the uncertainty concerning oxygen uptake mechanisms on chars. The mere fact that the Elovich equation fits data does little to establish mechanism; as has been pointed out, the Elovich equation may be consistent with several different types of sorption isotherms (5). Its validity in interpreting results from porous samples has been questioned as well (40).

It is against this background of uncertainty in mechanism that the data on the effect of temperature on chemisorption are analyzed. Generally, a fresh young char surface, when first exposed to oxygen, rapidly picks up oxygen and then continues to pick up oxygen at an ever decreasing rate for many hours subsequently (consistent with the form of the Elovich equation).

The effect of temperature on the amount of oxygen chemisorbed by a char has been studied to a limited extent previously. An Australian brown coal char pyrolyzed for more than 10 hours at 1000°C showed a trend of increasing oxygen capacity with increasing temperature of chemisorption between 25 and 200°C (41). Experiments with a higher rank coal char prepared at similar temperatures showed that oxygen capacity increased with temperature only up to about 100°C (16), while a 550°C cellulose char showed increasing oxygen uptake with increasing temperature up to at least 207°C (39). An activated graphon (highly graphitized carbon black) showed increasing chemisorption capacity with increasing temperature up to at least 550°C (13). The actual temperature dependence of saturation amounts of uptake was seen to be quite complex (12).

As a result of the uncertainty concerning the effect of temperature on chemisorption behavior, several tests were performed with the chars of interest in this study. In both series of experiments, chars with initially clean surfaces were subjected to "staircase" temperature profiles under an atmosphere of dry air. Figure 1 shows the results of these tests. In the case of the resin char, there is evidence for increased capacity with increasing temperature up to 300°C, at which temperature the mass begins to decrease due to decomposition of the surface oxides. In the case of the lignite char, the effect of temperature is much less pronounced and mass loss becomes evident at 250°C.

Thus, it must be concluded that the effect of temperature on chemisorption may vary widely from char to char, and there is a legitimate question as to what exactly is being measured at any arbitrary condition. Depending upon the situation, the maximum uptake may be an artifact due to competing processes of continued chemisorption and desorption of complexes. In the case of the resin char, the apparent activation energy for the high temperature decomposition process is 29 kcal/mol.

Effect of Oxygen Pressure on Chemisorption Behavior

The effect of oxygen pressure on chemisorption behavior has also been

studied to only a limited extent previously. It was found for 1000°C Australian brown coal char that both reversibly sorbed and chemisorbed oxygen increased in amount with increasing pressure of oxygen (from 161 torr to 760 torr) (41). On the other hand, a sample of higher rank coal char which had been pyrolyzed at 1000°C showed no variation in oxygen chemisorption capacity for pressures ranging from about 7.6 torr to 760 torr (16). In another study, a graphon sample displayed oxygen chemisorption capacity which was markedly pressure dependent in the pressure range 0.5 torr to 700 torr (13). The increase in oxygen chemisorption with oxygen pressure was also observed at high temperatures (615°C, 42).

In seeking to better characterize oxygen chemisorption as a diagnostic technique, a series of experiments was conducted in the present study at various partial pressures of oxygen. The results of these tests are shown in Figure 2. It is apparent that the partial pressure of oxygen has a marked influence on the rate of uptake of oxygen, and apparently, on the ultimate oxygen capacity of the sample.

Conclusions

The obvious conclusion that can be drawn from this work is that oxygen chemisorption can hardly be termed a site-specific analytical technique, at least when applied to typical young chars. The fact that apparent oxygen capacities are sensitive to temperature and pressure does not necessarily imply that oxygen chemisorption is not useful as a correlative tool; it has been shown that active site concentrations, as measured by chemisorption of oxygen, do correlate reasonably well with char reactivity in several cases (e.g., 8,9). Still, the solid evidence for the relationship between chemisorbed oxygen complexes and gasification have come mainly from a series of very careful studies on very "old" chars, oxidized at moderate temperatures (8,11-15).

This raises the question as to what value oxygen chemisorption techniques are in characterizing young chars. Clearly, as a characterization technique, chemisorption is difficult enough so as to make actual gasification reactivity tests look more attractive, if this is the information which is actually desired. At present, when applied to young chars, the oxygen chemisorption technique must derive its value from being a tool for studying the actual mechanism of gasification of these materials.

Acknowledgment

We gratefully acknowledge the support of the U. S. Department of Energy through grant DE-FG22-83PC60800.

References

(1) Johnson, J. L., Kinetics of Coal Gasification, Chapter I, Wiley, 1979.
(2) Laurendeau, N. M., Prog. Energy Combust. Sci., 4, 221 (1978).
(3) Von Fredersdorff, C. G., and Elliott, M. A., in Chemistry of Coal Utilization, Supplementary Volume, (H. H. Lowry, Ed.), Chapter 20, Wiley, 1963.
(4) Walker, P. L., Jr., Rusinko, F., Jr., and Austin, L. G., in Advances in Catalysis, XI, 133 (1959).
(5) Essenhigh, R. H., in Chemistry of Coal Utilization Second Supplementary Volume, (M. Elliott, Ed.), Chapter 19, Wiley, 1981.

(6) Field, M. A., Gill, D. W., Morgan, B. B., and Hawksley, P. G. W., Combustion of Pulverized Coal, BCURA, Leatherhead, England (1967).
(7) Mulcahy, M. F. R., and Smith, I. W., Rev. Pure Appl. Chem., 19, 81 (1969).
(8) Laine, N. R., Vastola, F. J., and Walker, P. L., Jr., J. Phys. Chem., 67, 2030 (1963).
(9) Radovic, L. R., Walker, P. L., Jr., and Jenkins, R. G., Fuel, 62, 849 (1983).
(10) Tong, S. B., Pareja, P., and Back, M. H., Carbon, 20, 191 (1982).
(11) Vastola, F. J., Hart, P. J., and Walker, P. L., Jr., Carbon, 2, 65 (1964).
(12) Hart, P. J., Vastola, F. J., and Walker, P. L., Jr., Carbon, 5, 363 (1967).
(13) Lussow, R. O., Vastola, F. J., and Walker, P. L., Jr., Carbon, 5, 591 (1967).
(14) Bansal, P. C., Vastola, F. J., and Walker, P. L., Jr., J. Coll. and Int. Sci., 32, 187 (1970).
(15) Phillips, R., Vastola, F. J., and Walker, P. L., Jr., Carbon, 8, 197 (1970).
(16) Canston, P.l, and McEnaney, B., Fuel, 64, 1447 (1985).
(17) Suuberg, E. M., Peters, W. A., and Howard, J. B., Fuel, 59, 405 (1980).
(18) Graff, R., and LaCava, A., U.S.D.O.E. Report FE-2340-9, 1978.
(19) Ergun, S., and Mentser, M., in Chemistry and Physics of Carbon, 1, (P. L. Walker, Jr., Ed.), Chap. 4, Dekker, 1965.
(20) Eucken, A., Z. Angew. Chem., 43, 986 (1930).
(21) Strickland-Constable, R. T., Trans. Faraday Soc., 40, 333 (1944), also Nagle, J., and Strickland-Constable, R. T., Proc. 5th Conf. on Carbon, Vol. p. 154, Pergamon (1962).
(22) Meyer, L., Z. Phys. Chem., 17(B), 385 (1932).
(23) Duval, X., J. Chim. Phys., 47, 339 (1950) and 58, 3 (1961).
(24) Duval, X., Ann. Chim. (Paris), 10, 903 (1955).
(25) Spokes, G. N., and Benson, S. W., Fundamentals of Gas-Surface Reactions, p. 318, Academic Press, (1969).
(26) Blyholder, G., Binford, J. S., Jr., and Eyring, H., J. Phys. Chem., 62, 263 (1958).
(27) Moseley, F., and Patterson, D., J. Inst. of Fuel, 38, 378 (1965), also 40, 523 (1967).
(28) Zahradnik, R. L., and Glenn, R. A., Fuel, 50, 77 (1971).
(29) Walker, P. L., Jr., in Scientific Problems of Coal Utilization, (B. R. Cooper, Ed.), p. 237, U.S.D.O.E., 1978.
(30) Jenkins, R. G., Nandi, S. P., and Walker, P. L., Jr., Fuel, 52, 288 (1973).
(31) Hippo, E., and Walker, P. L., Jr., Fuel, 54, 245 (1975).
(32) Blackwood, J. D., and McTaggart, F. K., Aust. J. Chem., 12, 533 (1959).
(33) Blackwood, J. D., Cullis, B. D., and McCarthy, D. J., Aust. J. Chem., 20, 1561 (1967).
(34) Gray, J. A., Donatelli, D. J., and Yavorsky, P. M., ACS Div. Fuel Chem. Prep., 20 (4), 103 (1975).
(35) Blake, J. H., Bopp, G. R., Jones, J. F., Miller, M. G., and Tanbo, W., Fuel, 46, 115 (1967).
(36) Chermin, H. A. G., and Van Krevelen, D. W., Fuel, 36, 85 (1957).
(37) Fischbach, D. B., in Chemistry and Physics of Carbon, 7, (P. L. Walker, Jr., Ed.), p. 1, 1971.
(38) Bishop, M., and Ward, D. L., Fuel, 37, 191 (1958).
(39) Bradbury, A., and Shafizadeh, F., Carbon, 18, 109 (1980).
(40) Harris, J., and Evans, D., Fuel, 54, 276 (1975).
(41) Allardice, D., Carbon, 4, 255 (1966).
(42) Phillips, R., Vastola, F., and Walker, P., Carbon, 7, 479 (1969).

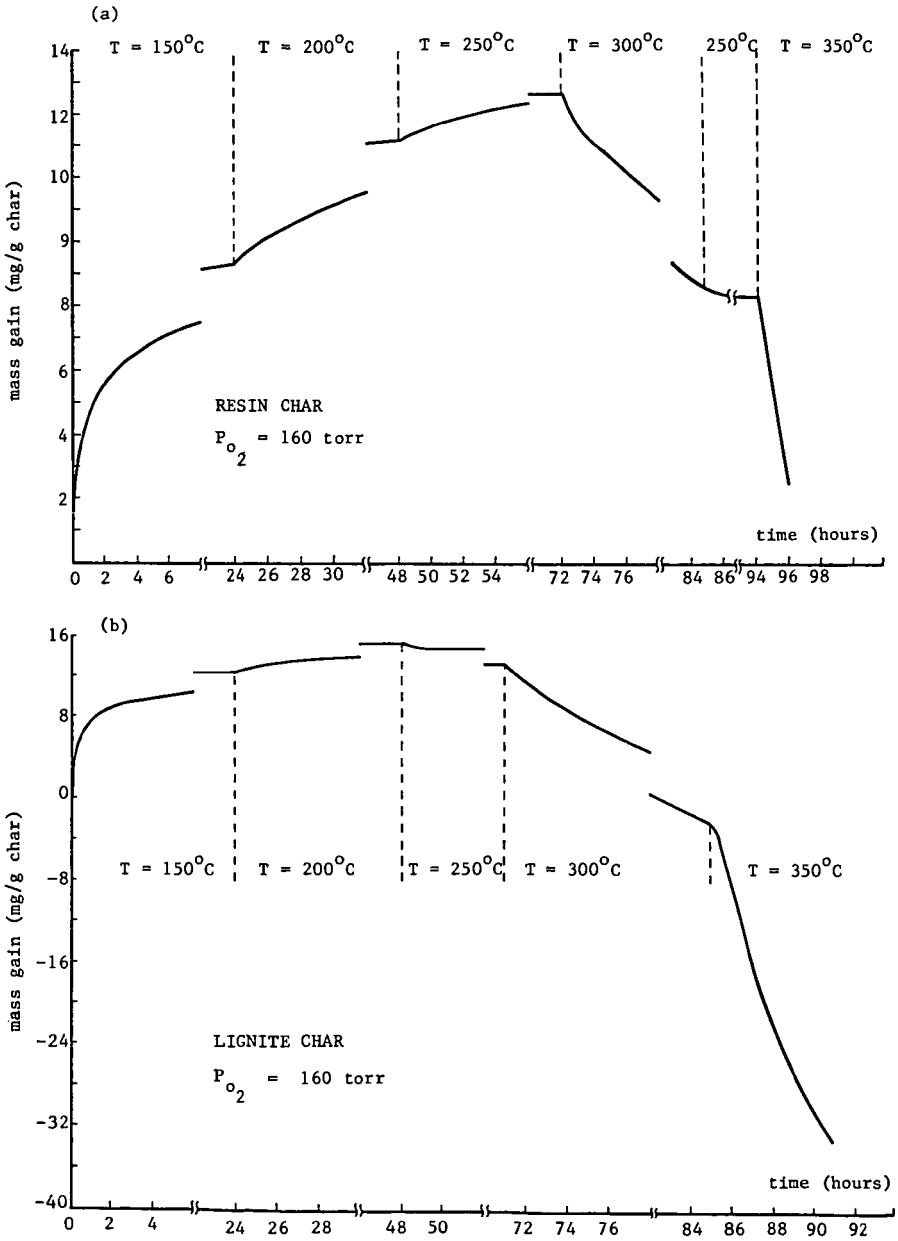

Figure 1. Effect of Temperature Changes on Oxygen Chemisorption Behavior
(a) Resin Char (b) Lignite Char

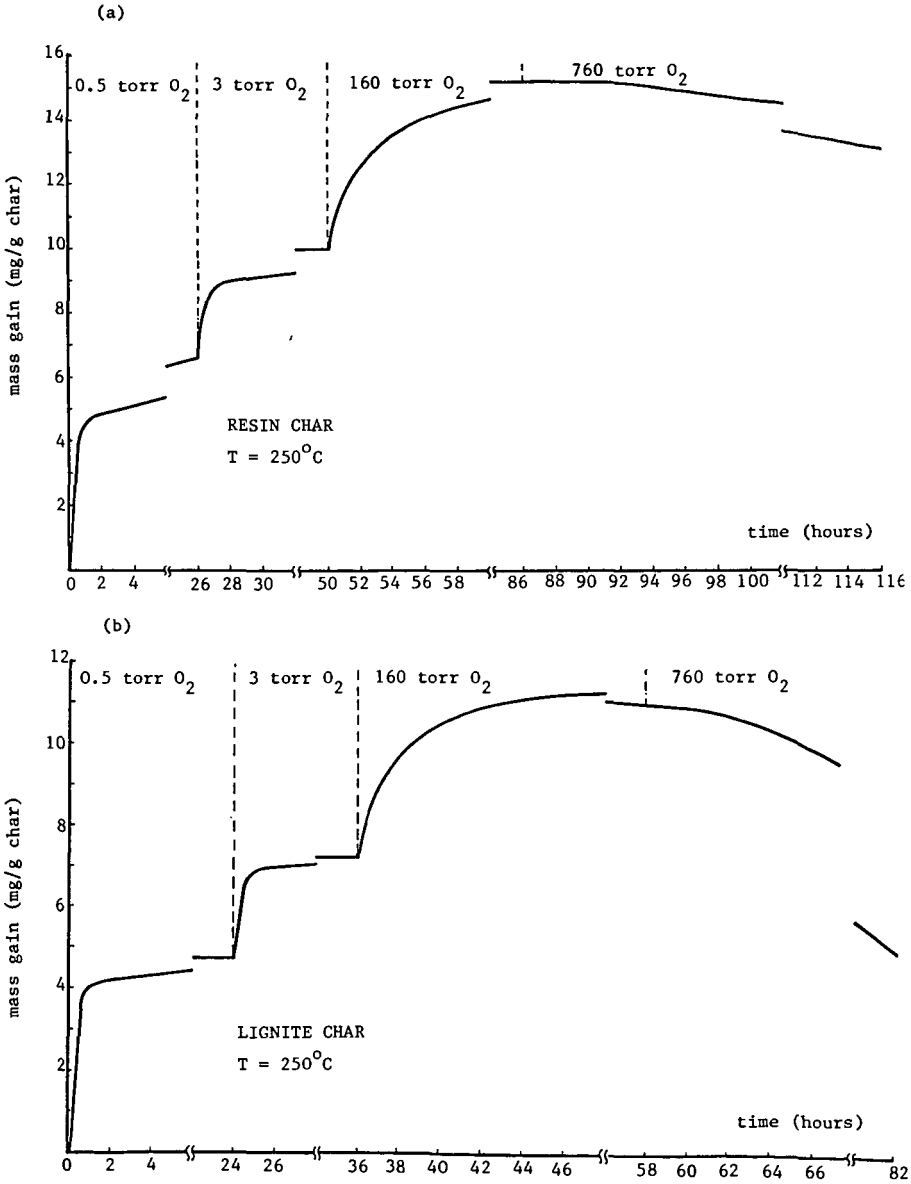

Figure 2. Effect of Oxygen Partial Pressure Changes on Oxygen Chemisorption Behavior

(a) Resin Char (b) Lignite Char

IN-MINE VARIATION AND ITS EFFECTS ON COAL GASIFICATION

Scott F. Ross and David R. Kleesattel

University of North Dakota Energy Research Center
Box 8213, University Station
Grand Forks, North Dakota 58202

Abstract

As reported earlier (1), four different lithologic layers have been identified in the Freedom Mine (Mercer County, North Dakota) which supplies the lignite for the Great Plains Gasification Associates plant in Beulah, North Dakota. The layers were identified on the basis of readily observable megascopic characteristics including luster, fracture characteristics and the presence of clay and silt zones. Lignite sampled from each of the four layers has been pyrolyzed in a bench scale reactor system designed to simulate the production of gas liquor condensate from the pyrolysis zone of an actual gasifier. The yields of water-soluble organic effluents from each of the layers were found to differ significantly, particularly the yields of phenol, cresol and catechol.

Introduction

The treatment and removal of water-soluble organic effluents from wastewater is an important issue facing coal gasification technology. The extent of treatment is governed by the reuse or environmentally acceptable disposal of the wastewater. Downstream effluent treatment is also dependent on the nature and quantity of tars pyrolysis and devolatilization reactions in the upper portion of the gasifier. It is desirable to develop a laboratory test to simulate the production of water-soluble organic effluents from a gasifier, thereby eliminating expensive pilot-plant tests. Such a test could eventually be a method of assessing the gasification potential of various coals, and the resulting data base would be helpful in designing effluent treatment systems for gasification plants.

In working towards the development of such a test, the technique was found to be sensitive to changes in coal quality which occur withing the same mine. With the discovery of distinct lithologic layering within a mine which supplies coal to an actual commercial gasifier, an investigation into the effects of in-mine variation on coal gasification was initiated.

Experimental

A laboratory scale tubular reactor was constructed which allows for the pyrolysis of up to five grams of coal in a variety of gas atmospheres. A Lindbergh split-type furnace with a maximum temperature of 1100 C and a programmable heating rate of 5°C/min. to 45°C/min. allowed for reproducible heating of the samples. A liquid nitrogen cooled trap was used for the collection of water-soluble organic effluents. After completion of the experiment the trap was allowed to warm to above 0°C and the water-soluble organics analyzed by gas chromatography (2).

The coal samples used in this study were collected at the Freedom Mine (Mercer County, North Dakota). The samples were ground to -60 mesh and pyrolyzed in a nitrogen atmosphere using a heating rate of 45°C/min. and a final temperature of 850°C.

TOSCO Material Balance Assays were provided by J & A Associates, Inc., Golden, Colorado. The procedure has been described elsewhere (3).

Standard quantitative maceral analyses (4) were performed on representative samples from each of the four lithologic layers. Lignite samples were prepared for micropetrographic analysis as described in ASTM procedures (5).

Results and Discussion

During a mine study in May 1984, major lithologic units occurring as layers in the Beulah-Zap bed of the Sentinel Butte Formation (Paleocene) were observed. The seam was subdivided into four lithologic units on the basis of overall megascopic characteristics (Figure 1). The criteria for these subdivisions were:

1. appearance of the broken surfaces of the units on a large scale as they appear in the high wall;

2. luster of the coal;

3. fracture characteristics, hardness and surface appearance of the coal on a small scale (1-10 cm);

4. presence of lithologically distinct units including thin layers of fragmental coal, clay, and silt layers and concretionary zones.

There is evidence to suggest that the units are not entirely local in extent but persist widely in the Beulah-Zap bed (6).

Lignite was sampled from each of the four layers in a vertical sequence with th samples being collected within a few meters of each other. The samples wer pyrolyzed as described above and the water-soluble organic effluents wer analyzed. The yields of the water-soluble organics from each of these four samples and their corresponding proximate and ultimate analyses are given in Table 1. Based on the pyrolysis yield data, the top three layers appear to be quite similiar. However, layer four shows considerable differences in the yields of methanol, phenol, cresols and catechol. In fact, layer four appears to be an entirely different coal. Layer four is separated from the other three layers by a locally thin, inorganic-rich zone or clay layer, suggesting that a marked difference in the depositional environment could have occurred. The proximate and ultimate analyses for the four layers are quite similiar, however, and provide no explanation as to why the fourth layer should behave so differently upon pyrolysis than the other three layers. In particular, a comparison of maf ultimate data for layers 2 and 4 shows great similarity, yet pyrolysis yields of water-soluble organics are radically different. This suggests that a plant operator could not rely on routine coal analysis as the predictor of wastewater characteristics.

The data from the TOSCO Material Balance Assays are given in Table 2. The most obvious difference is the tar yields for the four layers. There is a 44% decrease in tar yield between layer 1 and layer 2. The yields of water, CO and C_1 also differ significantly between the four layers. However, unlike with the water-soluble organic effluent data, the fourth layer doesn't stand out as being different from the other three layers.

Petrographic analyses for the four layers are presented in Table 3. Unlike the proximate and ultimate analyses, which suggest little difference between the four layers, the petrographic analyses indicate that there might be considerable organic structural differences between the layers. There exists a good correlation between catechol yields upon pyrolysis and the amount of corpohumimite found in each layer. A linear estimation of the data results in a correlation coefficient of 0.92.

Table 1. Pyrolysis Yields for Four Lithologic Layers in the Freedom Mine[a]

Coal	(Top) Layer 1	Layer 2	Layer 3	(Bottom) Layer 4
Compound:				
Methanol	990	1010	940	1590
Acetone	1350	1320	1490	1420
Acetonitrile	240	250	260	190
2-Butanone	360	340	420	350
Propionitrile	70	130	280	190
Phenol	2110	1720	1800	3820
o-Cresol	610	520	580	980
p-Cresol	680	570	600	1190
m-Cresol	710	630	720	1420
Catechol	990	1010	1200	3150
Proximate Analysis (as rec'd; % by wt):				
Moisture	23.51	23.11	27.93	30.62
Volatile matter	29.32	33.93	34.22	36.74
Fixed carbon	31.61	36.56	32.91	27.93
Ash 15.55	6.40	4.94	4.72	
Ultimate Analysis (maf; % by wt):				
Hydrogen	4.66	5.09	4.75	5.13
Carbon	68.20	69.14	70.37	69.32
Nitrogen	1.08	1.11	1.12	1.07
Sulfur	2.75	0.66	0.68	0.84
Oxygen	23.30	23.99	23.09	23.65

[a]Compound yields are reported in micrograms/g maf coal.

Table 2. TOSCO Material Balance Assay

Fischer Assay Yields	Normalized Values (Moisture Free) Layer 1	Layer 2	Layer 3	Layer 4
Tar (lb/ton)	119.3	67.1	103.7	89.1
(gal/ton)	14.6	8.2	12.7	10.9
Gas (lb/ton)	311.9	333.5	329.0	306.6
(scf/ton)	3311.0	3597.7	3627.6	3402.9
Water (lb/ton)	129.9	192.3	158.7	191.2
(gal/ton)	15.6	23.1	19.0	22.9
Char (lb/ton)	1438.9	1407.1	1408.5	1413.1
H_2 (lb/ton)	1.22	1.11	1.33	1.14
CO (lb/ton)	30.76	37.51	36.85	40.89
CO_2 (lb/ton)	243.23	256.50	251.62	224.00
Cl (lb/ton)	17.44	19.78	22.32	20.63

Table 3. Petrographic Analyses of Freedom Mine, Four Lithologic Layers

Maceral Analysis (% Volume)	Layer 1	Layer 2	Layer 3	Layer 4
Humanite Group				
Ulminite	35.5	38.9	38.2	42.8
Humodetrinite	25.2	23.1	21.9	18.0
Gelinite	0.5	0.4	1.4	1.3
Corpohuminite	1.0	2.6	2.0	6.2
Liptinite Group				
Sporinite	0.9	2.4	1.4	3.3
Cutinite	0.7	0.5	0.5	0.5
Resinite	2.7	1.9	0.9	1.7
Suberinite	0.0	0.5	0.4	1.5
Alginite	1.2	0.4	0.9	1.2
Liptodetrinite	5.0	5.9	3.8	5.3
Fluorinite	0.0	0.4	0.0	0.0
Bituminite	0.0	0.0	0.0	2.0
Inertinite Group				
Fusinite	4.5	4.6	8.5	2.7
Semifusinite	6.8	8.1	7.2	5.3
Macrinite	0.7	0.5	0.2	0.0
Sclerotinite	0.3	0.5	0.4	0.3
Inertodetrinite	8.9	7.6	8.5	4.2
Micrinite	1.3	0.7	1.8	1.3

Conclusions

The composition of gas liquor condensate can vary greatly due to variations within an individual seam. The samples used in this study were collected within a few meters of each other but indicate significant vertical variation exists in a particular mine. The ultimate analyses of these layers are virtually identical, but the actual chemistry, as evidenced by the pyrolysis results and the TOSCO Material Balance Assays, is very different from layer to layer. These differences could result in substantial changes in wastewater composition and operability of a tar/water separator in an actual gasification plant when coal from different layers is gasified.

Petrographic analysis reflects, to an extent, the structural chemistry of the coal because the macerals generally derive from different kinds of plant constituents, and these original plant constituents in turn have different structures. Therefore, petrography should be a useful predictor of some pyrolyzate yields.

Reasonably steady operation of wastewater treatment plants and tar/water separators depend on having reasonably steady wastewater composition and tar production, or at least the ability to predict these in advance. In order to achieve this it is important to characterize the pyrolysis behavior of the coal layers to provide for blending or preferential mining and selective utilization.

Acknowledgment

This work was supported by the U.S. Department of Energy, Contract No. DE-FC21-83FE60181.

The authors would like to acknowledge John W. Diehl for doing the gas chromatographic analyses and Harold H. Schobert for his helpful comments.

Literature Cited

1. UNDERC Quarterly Technical Progress Report for the Period July-September 1984, Section 15, DOE/FE/60181-1682, November 1984.

2. Olson, E.S. and J.W. Diehl, 186th ACS National Meeting, Washington, D.C., Abstract of Papers, Anyl 63, (1983).

3. Goodfellow, Lawrence and M. T. Atwood, presented at the 7th Oil Shale Symposium, April 18-19, 1974.

4. Stach, E., Taylor, G.H., Mackowsky, M.T., Chandra, D., Teichmuller, M., and Teichmuller, R., 1982, 3rd edition, Coal Petrology, Gerbruder-Borntraegger, Berlin-Stuttgart, 535 p.

5. Annual Book of ASTM Standards, 1980, Gaseous Fuels: Coal and Coke, Part 26, D 2797-72 (1980), Preparing Coal Samples for Microscopical Analysis by Reflected Light, pp. 363-371.

6. Kleesattel, D.R., M.A. Thesis, University of North Dakota, 1985.

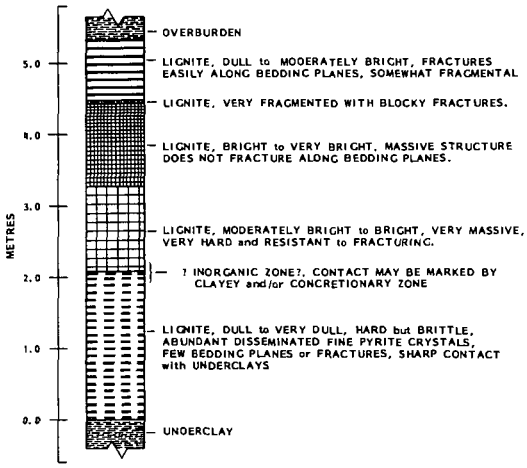

Figure 1. Lithologic units of the Beulah-Zap lignite bed as described at the Freedom Mine.

ACS/CA 1986-178

VARIATIONS IN CHAR REACTIVITY WITH COAL TYPE AND PYROLYSIS CONDITIONS

Peter R. Solomon, Michael A. Serio and Steven G. Heninger

Advanced Fuel Research, Inc. 87 Church Street, East Hartford, CT 06108

Understanding char reactivity is important since the consumption of char is the slowest and, therefore, the controlling process in combustion or gasification. Reviews of char reactivity (1,2) demonstrate that there is a wide variation in observed reactivities. Work described by Smoot (3) highlights the very large variations (one and half orders of magnitude) in char reactivity with method of formation. Similarly, Ashu et al. (4) found an enhanced reactivity of char caused by rapid heating of the precursor coal. More recently, in a vertical tunnel furnace, Essenhigh and Farzar (5) measured very rapid burnout times for small coal particles. They ascribed this to the firing condition which gave rates of heating in the 10^6 K/s regime, compared with the more usual value of 10^4 K/s in slower burning flames. Nsakala has reported a wide variation in reactivity associated with rank (6).

The gasification or combustion reactions of char are generally described as falling into three rate controlling regimes where the reaction rate is limited by: 1) intrinsic reactivity of the char itself, 2) diffusion of reactants within the char pores, and 3) diffusion of reactants between the char's surface and the ambient atmosphere. In this work the focus is on the intrinsic reactivity where the controlling factors are the surface area, active site density, and catalytic effect of minerals. The objective or the study described here was to determined how these factors vary with coal rank, char formation conditions and mineral matter content.

This paper reports on an empirical study of the reactivity of a set of chars from a variety of different coals prepared by pyrolysis at heating rates between 0.5 and 20,000°C/sec to temperatures between 400 and 1600°C. Reactivities were measured with a TGA, using the widely used method of monitoring the weight loss at constant temperature in the presence of O_2 or CO_2. A new technique was developed in which the weight loss was measured while the sample was heated at a constant heating rate in the presence of the reactive gas. This method has the advantage that the same conditions can be used for chars of widely varying reactivity. Reactivities measured by the two methods correlated well with each other. The paper will present correlations of the reactivities with the char formation conditions and the char properties (including surface area, hydrogen concentration and mineral concentration).

EXPERIMENTAL

Char Preparation - Chars for this study were prepared from the 200 x 325 mesh sieved fractions of coals and lignites listed in Table I. The chars were prepared by pyrolysis in an inert atmosphere in one of four reactors: 1) an atmospheric pressure entrained flow reactor (EFR) (7,8) with coal particle temperatures between 650 and 1600°C at heating rates of ~10,000°C/sec; 2) a heated tube reactor (9) with coal particle temperatures between 650°C and 950°C at heating rates of ~ 20,000°C/sec; 3) a thermogravimetric analyzer (TGA) with coal particle temperatures of 450°C to 900°C at heating rates of 0.5°C/sec; and 4) a heated grid reactor (HGR) with coal temperatures of 400°C to 900°C at heating rates of ~1000°C/sec. (10).

Reactivity Measurements - Initial char reactivity measurements were made using the isothermal measurement developed st Pennsylvania State University (11). In this method, the char is heated in a TGA in nitrogen to the desired temperature, usually 400-500°C. The temperature level is chosen to make sure no oxygen diffusion limitations are present, i.e., by varying the flow rate, bed depth and particle size. After the weight of the sample has stabilized at the selected temperature level, the nitrogen flow is switched to air and the weight loss is monitored. The time for 50%

burnoff, $\tau_{0.5}$, is used as the reactivity index. Another group at Penn State has used the maximum rate of weight loss as a reactivity index, which is determined in a similar isothermal experiment (12).

In our char characterization work, we had difficulty applying the isothermal techniques to chars formed over a wide range of conditions. A temperature level selected for one char was inappropriate for another. The temperature was either too high for the rate to be chemically controlled or too low for the $\tau_{0.5}$ to be reached in a reasonable time period.

In order to overcome this difficulty, a non-isothermal technique was developed. A Perkin-Elmer TGA 2 was used for this method. The sample size is about 1.5 mg. The sample is heated in air at a rate of 30 K/min until a temperature of 900°C is reached. The TGA records the sample weight continuously and, at the end of the experiment, the weight and derivative are plotted. Some representative curves for the North Dakota (Zap) lignite, the Montana Rosebud subbituminous coal and the Pittsburgh Seam bituminous coal are shown in Fig. 1. The Zap and Pittsburgh were chars prepared in the (EFR), in which it was calculated that the particles were heated at about 7000 K/s to 700°C before being quenched. The Montana Rosebud char was prepared in the heated tube reactor (HTR) under similar conditions. The samples were oxidized with an air flow of 40 cc/min and a nitrogen purge flow of 40 cc/min. The Zap lignite indicates burnout of several components of the char of different reactivity, while the Rosebud and Pittsburgh coals show more homogeneous burnout at higher temperatures.

The characteristics of the weight loss curve can be understood as follows: 1) At low temperature, there is an initial weight loss as moisture is removed. 2) As the temperature is raised, the reactivity of the char increases until the fractional weight loss rate is sufficiently large to be observed. The sample size and oxygen flows are chosen so that the initial 10% of weight loss occurs under intrinsic reactivity control. 3) As the temperature continues to increase, the reactivity increases until eventually all the oxygen reaching the sample bed is consumed and the weight loss is controlled by the oxygen supply to the sample bed alone. Then the fractional weight loss rate becomes constant for all samples. 4) When the char has components of different reactivity, the weight loss can switch between being oxygen supply limited and being intrinsic reactivity limited as each component is consumed.

Figure 2 compared the weight loss curves for the same char sample but with different sample sizes. The curves are identical for the initial weight loss which is controlled by the intrinsic reactivity. As expected, the fractional rate of weight loss $(1/m_o)(dm/dt)$ decreases with increasing sample size in the oxygen supply limited regime.

RESULTS

Comparison of Isothermal and Constant Heating Rate Reactivity Tests - The temperature (T_{cr}) at which the derivative of the fractional weight loss with respect to time reaches a value of 0.11 wt. fraction/min was chosen as an index of reactivity to be compared with the $\tau_{0.5}$ values measured by the isothermal technique. The actual critical slope used is arbitrary. A value is chosen which is large enough to be unambiguously determined, but small enough so that reaction occurs in the chemically controlled regime. Values of $\ln\tau_{0.5}$ were plotted against $1/T_{cr}$ and a good correlation was observed.

It was subsequently decided that a comparison to $\tau_{0.1}$ (time for 10% burnoff) would be more relevant since the initial reactivity indicated by T_{cr} would be measured, rather than an integral reactivity over a large extent of conversion which is affected by reactivity variations due to changes in the pore structure or sample

inhomogeniety. A plot of ln $\tau_{0.1}$ vs $1/T_{cr}$ is shown in Fig. 3. This plot includes data for chars from all three coals in all four reactors. The experimental conditions covered the following ranges: heating rate = 0.5 to 20,000 K/sec; temperature = 400 to 1600°C; residence time = .020 s to 30 min; pressure = 0 to 200 psig.

It can be shown that a plot of ln $\tau_{0.1}$ vs $1/T_{cr}$ will be linear with a slope equal to E/R, where E is the global activation energy for the intrinsic oxidation rate and R is the gas constant. For the reaction

$$C\ (\text{solid}) + O_2\ (\text{gas}) = CO_2\ (\text{gas}) \qquad (1)$$

the global rate of disappearance of carbon can be represented as follows:

$$dm/dt = -k_s\ C_s^n\ W\beta S \qquad (2)$$

where dm/dt is the mass loss of carbon per particle in unit time (g/min), k_s is the intrinsic reaction rate constant based on unit surface (cm/min), C_s^n is the concentration of oxygen at the surface in moles/cm^3 raised to some power n, W is the molecular weight of carbon in g/mole, β is the ratio of active area per unit accessible surface area (cm^2/cm^2) and S is the accessible surface area in cm^2 per particle. Since the reaction occurs under chemical reaction control, the concentration of oxygen at the surface will be equal to the bulk concentration, which allows one to drop the subscript.

In the isothermal experiment, the burn-off rate is nearly constant up to 10% weight loss:

$$dm/dt \cong \Delta m/\Delta t \cong -\ 0.1\ m/\tau_{0.1} \qquad (3)$$

Substituting Eq. 2 for dm/dt:

$$-k_s\ C^n\ W\beta S = 0.1\ m/\tau_{0.1} \qquad (4)$$

$$\tau_{0.1} = \left[0.1\ m/k_s(T_o)C^n\ W\right] \cdot \left[1/\beta S\right] \qquad (5)$$

$$= K_1\ \left[1/\beta S\right] \qquad (6)$$

The quantities in the first set of brackets in Eq. 5 are nearly constant for a given isothermal (temperature = T_o) experiment at low conversions and independent of coal type, while the second set of brackets contain quantities which vary with coal type and char formation conditions.

For the non-isothermal experiment, the relative rate of mass loss is constant at some critical temperature, T_{cr}:

$$\left[1/m\right] \cdot \left[dm/dt\right] = -\ 0.11 = \left[1/m\right] \cdot \left[-k_s(T_{cr})C^n\ W\beta S\right] \qquad (7)$$

$$k_s(T_{cr}) = \left[0.11\ \ m/C^nW\right] \cdot \left[1/\beta S\right] \qquad (8)$$

$$= K_2\ \left[1/\beta S\right] \qquad (9)$$

The result obtained is that k_s is proportional to an experimental constant and inversely proportional to char properties.

For data collected on the same char sample, (βS) can be eliminated between Eqs. 6 and 9:

$$\tau_{0.1} = \left[K_1/K_2\right]\ k_s(T_{cr}) = \left[0.9/k_s(T_o)\right]\ k_s(T_{cr}) \qquad (10)$$

or

$$\tau_{0.1} = 0.9 \exp\left[-E/R \left[1/T_{cr} - 1/T_o\right]\right] \qquad (11)$$

assuming that k_s can be expressed as an Arrhenius expression $k_s(T) = k_o \exp(-E/RT)$.

Consequently, a plot of $\ln \tau_{0.1}$ vs $1/T_{cr}$ will have a slope equal to $-E/R$ of the intrinsic global oxidation rate. In the absence of catalytic effects, the value of E should be the same for chars from all coals and chars from the same coal prepared under a wide variety of conditions. The nearly linear data in Fig. 3 appears to support this conclusion. A problem may arise if T_{cr} and T_o are significantly different. The mechanism of the oxidation reaction probably changes with temperature, as indicated by the wide range of activation energies and reaction orders reported for the char oxidation reaction in the literature (13). The best fit value of about 35 kcal/mole determined from Fig. 3 is intermediate in reported values and close to the value of 31 kcal/mole determined by Radovic and Walker for a wide range of chars in TGA experiments (14).

In our case, the Zap lignite chars appear to fall on a line of lower slope. This is probably due to catalytic effects. When a lignite char was acid-washed, it was less reactive in the non-isothermal test. The companion isothermal test has not yet been done, so we have not yet determined where the acid-washed char falls on the plot of Fig. 3.

Variations in Reactivity - The reactivities were determined for a number of chsrs which had been prepared under carefully controlled conditions to study their pyrolysis behavior (7-11,15). Examples to illustrate the observed trends are presented in Fig. 4. Figure 4a illustrates the results for the Zap lignite. The three curves are for: 1) 150 msec with maximum temperature of 700°C (with reactivity measured in air); 2) 460 msec with maximum temperature of 1600°C (in air); 3) same as 2 but reactivity in CO_2. The curves illustrate the observation that the reactivity goes down with increased exposure to high temperature (or "extent of pyrolysis") and that for the same chars, CO_2 reactivity is lower than oxygen reactivity. Measurements of surface area S showed that char for conditions 1 and 2 were similar, suggesting that the differecne in reactivity is causes by a change in the density of active sites, β . Figure 4b shows results for Pittsburgh Seam coal. The three curves are for; 4) 150 msec with a maximum temperature of 700°C (in air); 5) 660 msec with a maximum temperature of 1100°C (in air) and 6) same as 5 but reactivity in CO_2. For equivalent cases (1 and 4), the reactivity for the Pittsburgh Seam coal is lower than for the Zap lignite prepared under equivalent conditions. Surface area measurements show the Pittsburgh Seam coal (which melts during pyrolysis) to have about 1/4 the surface area of the Zap lignite. This difference in surface area is not sufficient to account for the differences in reactivity, however. The extra reactivity appears to result from the lignite's mineral content, but could also be due to a difference in active site densities. Figure 4c compares curve 7 for the Zap lignite with curve 8 for the demineralized coal and curve 9 for a Montana Rosebud pyrolyzed under similar conditions and having a similar surface area. Curves 8 and 9 are similar, but lower in reactivity than the raw lignite. Figure 4 illustrates the variation in reactivity with surface areas, with active site density, β and with mineral content.

Figure 5 summarizes the results for a number of samples. The critical temperature T_{cr} is plotted as a function of the hydrogen content which is used as a measure of the extent of pyrolysis. For each char type, there is a trend for increasing T_{cr} with decreasing hydrogen. Most of the change occurs below 2 1/2% hydrogen, after the evolution of aliphatic hydrogen is complete. That is, the T_{cr} varies primarily with the concentration of aromatic hydrogen. It should be noted that there is also ring oxygen in the char which is removed at about the same rate as the hydrogen and which may be related to the reactivity changes. This variation is due to a variation in β possibly correlated with the ring condensation accompanying the elimination of aromatic hydrogen.

The vertical displacement of the curves is due to the variations in char surface area and catalytic activity of the minerals. The most reactive chars are for the Zap lignite. The chars have surface areas in the neighborhood of 200 m^2/g. As pyrolysis proceeds the critical temperature T_{cr} first decreases and then increases with temperature as hydrogen is lost. There does not appear to be any drastic effects due to heating rate, as chars for a wide range of conditions all fell along the same curve. The low values of T_{cr} are believed to be due to the char's mineral content (high Na and Ca). When the coal was demineralized (symbol ▼), T_{cr} increased substantially. A Montana Rosebud char with a similar surface area shows a somewhat higher T_{cr} than the raw Zap.

The highest T_{cr} values are for the Pittsburgh and Kentucky coals. These swell upon pyrolysis. Initial surface area measurements of the Pittsburgh coal show approximately 50 m^2/g, suggesting that the lower surface areas are responsible for the lower reactivity. Note that the reactivity of slowly heated Pittsburgh Seam coal is higher than that of a rapidly heated char.

CONCLUSION

A new reactivity test has been developed which allows relative rates of reactivity to be determined for chars of widely varying reactivity. The method was applied to study the dependence of reactivity on coal properties and pyrolysis conditions. Reactivities are seen to decrease with decreasing aromatic hydrogen concentration. Reactivities were insensitive to heating rate for a lignite but were quite sensitive to heating rate for a bituminous coal. Mineral catalytic effects were also observed.

ACKNOWLEDGEMENT

The authors are grateful for the support of the United States Army under contract DACA88-85-C-0020 in the development of the constant heating rate reactivity test and the support of the Morgantown Energy Technology Center of the United States Department of Energy under contract DE-AC21-85MC22050, for support of the study of char reactivity.

TABLE I

SAMPLE PROPERTIES

WT% DAF

	Zap, North Dakota Lignite	Montana Rosebud Subbituminous	Pittsburgh Seam Bituminous	Kentucky #9 Bituminous
Carbon	66.5	72.1	82.1	81.7
Hydrogen	4.8	4.9	5.6	5.6
Nitrogen	1.1	1.2	1.7	1.9
Sulfur	1.1	1.2	2.4	
Oxygen (Diff.)	26.5	20.3	8.2	
Ash (Dry Wt%)	7.1	10.0	9.2	14.1

REFERENCES

1. Essenhigh, R.H., "Chemistry of Coal Utilization", 2nd Supplementary Vol., M.A. Elliott, Editor, John Wiley & Sons, NY, pg. 1162.
2. Smith, I.W., 19th Symposium (Int) on Combustion, The Combustion Institute, Pittsburgh, PA, pp 1045-1065, (1982).
3. Wells, W.F., Kramer, S.K., Smoot, L.D., and Blackham, A.U., 19th Symposium (Int) on Combustion, The Combustion Institute, Pittsburgh, PA, pp 1539-1546, (1982).
4. Ashu, J.T., Nsakala, N.Y., Mahajan, O.P., and Walker, P.L., Jr., Fuel, **57**, 251, (1978).
5. Essenhigh, R.H. and Farzar, H., 19th Symposium (Int) on Combustion, The Combustion Institute, Pittsburgh, PA, pp 1105-111, (1982).
6. Nsakala, N.Y., Patel, R.L., and Lao, T.C., "Combustion and Gasification Characteristics of Chars from Four Commercially Significant Coals of Different Rank", Final Report, Electric Power Research Institute, Report No. 1654-6, (1982).
7. Solomon, P.R., Hamblen, D.G., Carangelo, R.M., and Krause, J.L., 19th Symposium (Int) on Combustion, The Combustion Institute, Pittsburgh, PA, pp 1139-1149, (1982).
8. Solomon, P.R. and David G. Hamblen, D.G., in Chemistry of Coal Conversion, R.H. Schlosberg, Editor, Plenum Press, NY, Chapter 5, pg. 121, (1985).
9. Solomon, P.R., Serio, M.A., Carangelo, R.M., and Markham, J.R., Fuel, **65**, 182, (1986).
10. Solomon, P.R., Hamblen, D.G., and Carangelo, R.M., in Analytical Pyrolysis, K.J. Voorhees, (Editor), Butterworths, London, Chapter 5, pg. 121 (1984).
11. Mahajan, O.P., Yarzab, R., and Walker, P.L., Jr., Fuel, **57**, 643, (1978).
12. Jenkins, R.G., Nandi, S.P., and Walker, P.L., Jr., Fuel, **52**, 288, (1973).
13. Larendeau, N.M., Prog. Eng. Combust. Sci, **4**, pp. 221-270, (1978).
14. Radovic, L.R. and Walker, P.L., Jr., Fuel, **62**, 849, (1983).
15. Solomon, P.R., Serio, M.A., Hamblen, D.G., Best, P.E., Squire, K.R., Carangelo, R.M., Markham, J.R., and Heninger, S.G., "Coal Gasification Reactions with On-line In-situ FT-IR Analysis" DOE/METC Final Report Contract No. DE-AC21-81FE05122, (1986).

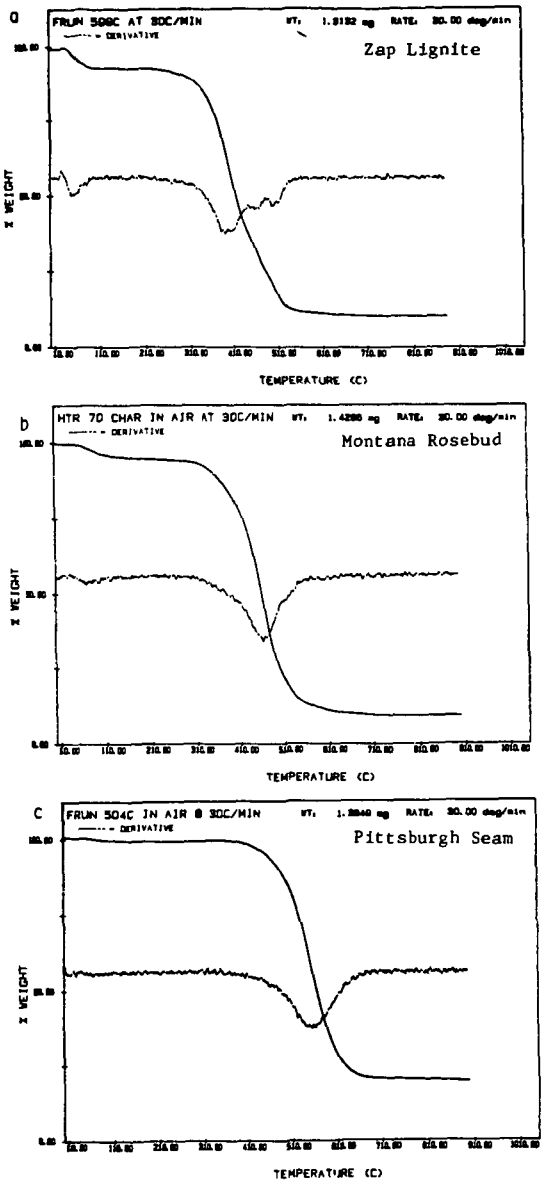

Figure 1. Non-isothermal TGA Reactivity Tests at 40 cc/min Air Flow. a) Zap Lignite, b) Montana Rosebud, and c) Pittsburgh Seam.

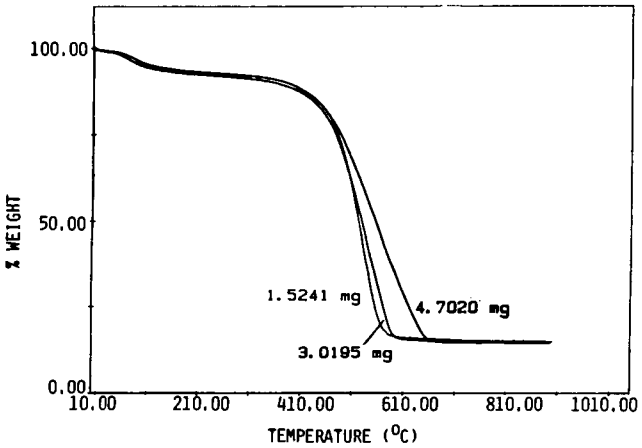

Figure 2. Comparison of Weight Loss Curves for Zap Lignite at 3 Sample Weights.

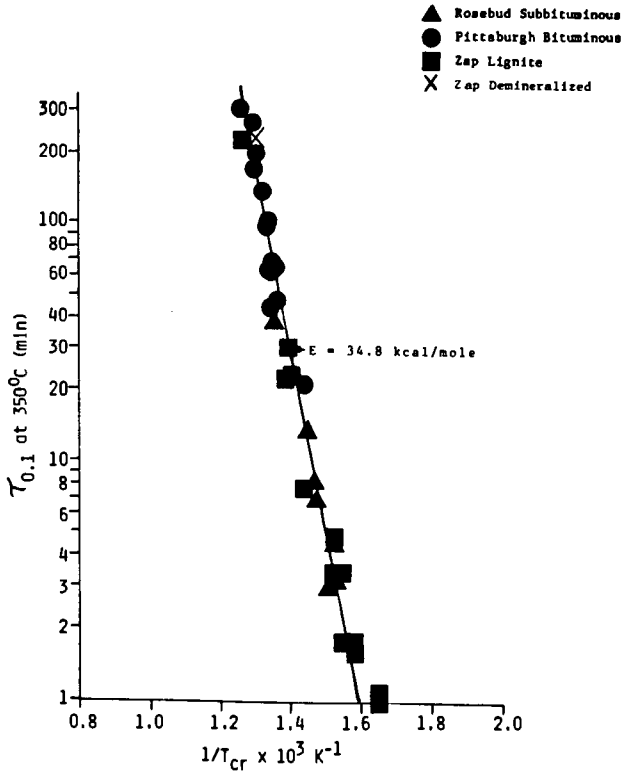

Figure 3. $\tau_{0.1}$ (time for 10% burnoff) vs $1/T_{cr}$. T_{cr} is the Temperature at which the Weight Loss Rate Equals -.11 wt. Fraction/min.

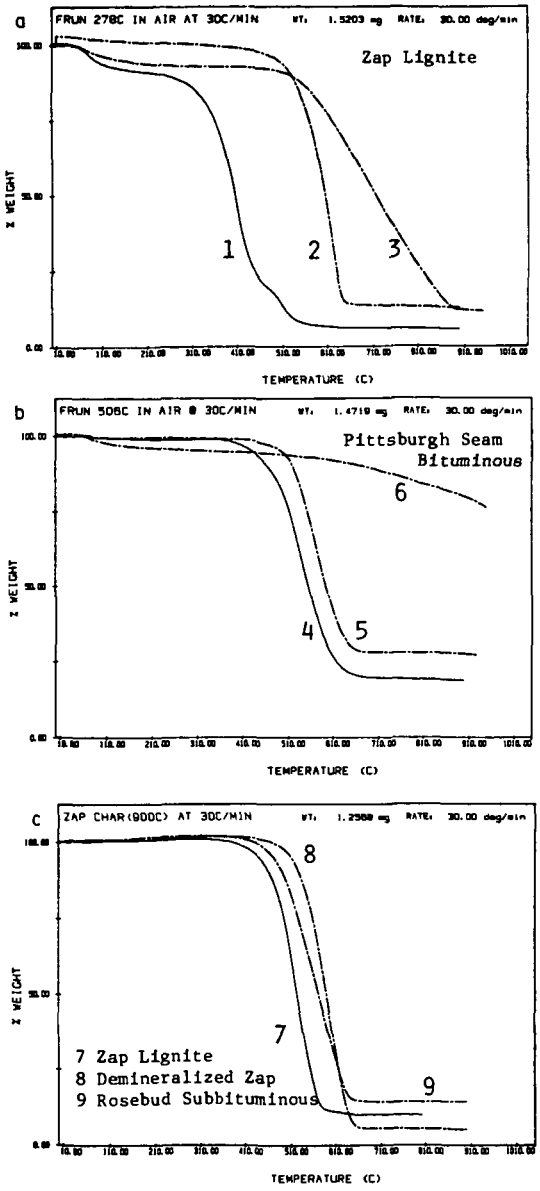

Figure 4. Comparison of Char Reactivity Curves Prepared for Three Coals Under a Variety of Conditions. Curves 3 and 6 are for Reactivity in CO_2. All the Rest are for Reactivity in Air.

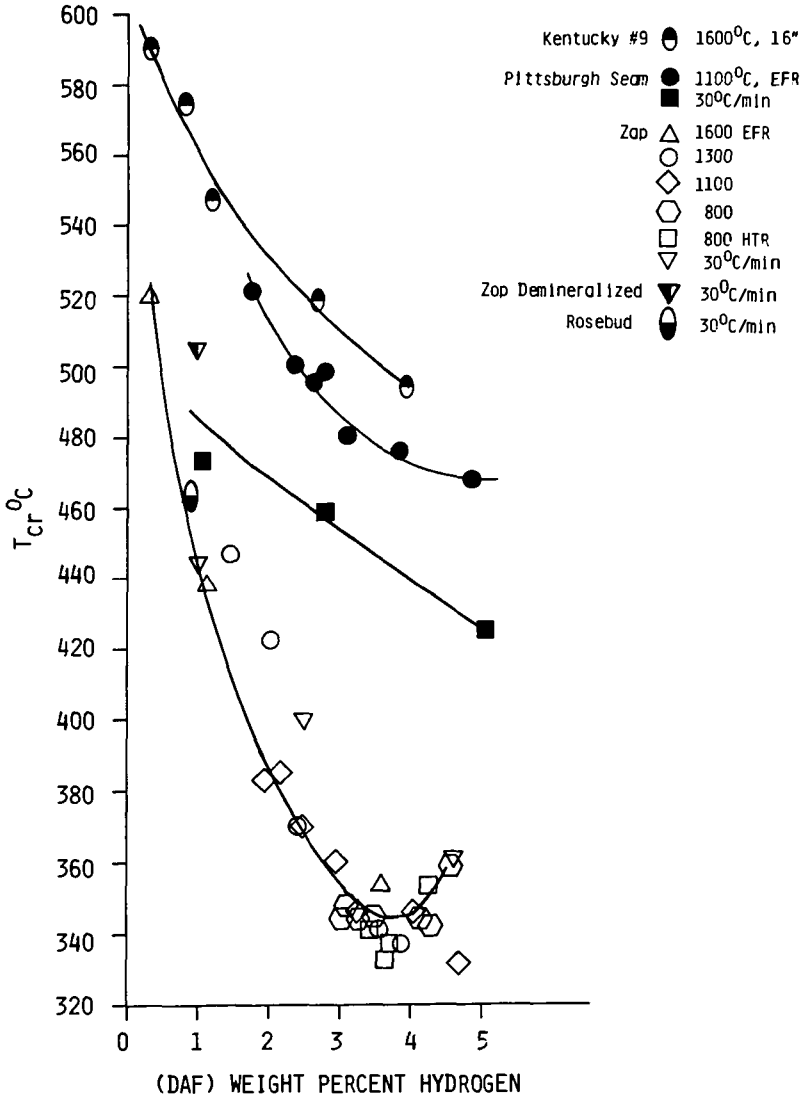

Figure 5. Variations in Reactivity with the Hydrogen Concentration in the Char (the extent of pyrolysis) and with Coal Type.

COAL PYROLYSIS IN A HIGH PRESSURE ENTRAINED FLOW REACTOR

Michael A. Serio, Peter R. Solomon and Steven G. Heninger

Advanced Fuel Research, Inc. 87 Church Street, East Hartford, CT 06108

INTRODUCTION

Many of the proposed coal gasification processes operate at elevated pressure. Since these processes also operate at elevated temperature, pyrolysis processes are important. However, there is relatively little data on pyrolysis yields at elevated pressure, particularly for continuous flow systems or on how pressure affects the reactivity of the char to subsequent gasification.

Most of the existing studies were done in batch, captive sample systems (1-3). For example, the work of Suuberg et al. (2) showed a significant effect of pressure on a bituminous coal and a modest effect for a lignite coal. The most important effect of pressure was a reduction in tar and increase in char yield at high pressure. However, one difficulty with interpreting the results from batch, captive sample systems is the pressure and residence time of the volatiles are not varied independently. As pressure is increased, the residence time of volatiles increases inside the particle as well as near the hot zone of the reactor.

In batch, semi-flow carbonization experiments, the effects of external pressure and external residence time can be varied independently. A review of the literature on semi-flow experiments by Dryden and Sparham (4) indicated that increases in inert gas pressure at constant volatile residence time did not have a significant effect on product yields. However, it should be noted that these experiments were done with very long volatile residence times (20 to 100 s). Recent work by Schobert et al. (5) examined the effect of pressure on tar yield in a semi-flow system (at constant residence times of about 1 s) and a pressure dependence of the tar yield was observed.

Entrained flow reactors are well suited to studies of pressure effects on pyrolysis and closely resemble real coal gasification systems. However, one must consider the effect of pressure on heat transfer as well. For example, Sundaram et al. (6) examined the effect of the pressure of various inert gases (He, CO, N_2 A_r) on carbon conversion and found that yields went through a maximum before declining. It is likely that, at the short residence times of their experiments (0.6 to 1.9 s at 900°C), the enhanced heat transfer due to gas pressure was more beneficial than the detrimental effects on mass transfer.

This paper will present pyrolysis data for product yields for four coals from an entrained flow reactor operated at pressures up to 300 psig. In addition, the effect of pressure on char reactivity will be discussed.

EXPERIMENTAL

A schematic of the high pressure reactor (HPR) system is given in Fig. 1. The furnace consists of a high pressure shell (capable of containing pressures up to 600 psig), a thick layer of insulation and a high temperature region heated by Kanthal Super 33 electrical heating elements. The high temperature section (capable of temperatures up to 1650°C) contains an alumina bed heat exchanger and a test section. The ambient gas enters the furnace through the heat exchanger to bring it up to furnace temperature and then turns downward into the test section. Coal is injected at a fixed point at the top of the test section using a water cooled injector. It mixes with the ambient gas and, after a fixed distance, enters a water-cooled collector. The reactor design is similar to a previously described atmosphere pressure entrained flow reactor (EFR) (7). The major differences are the smaller diameter test section in the HPR (1.27 cm vs 5.08 cm) and the absence of an optical port.

After the collector, the reaction products enter a cyclone to separate char, followed by a Balston filter to remove tar and soot. An electrostatic precipitator was tested for use after the cyclone but did not work as well as the filter. The gas stream is reduced in pressure and collected in a holding tank. The sample tank is a steel tank with glass-lined walls which is used to collect the total gaseous effluent from the reactor system during a typical run. It is initially evacuated and, during a run, the pressure gradually increases as it fills. After an experiment, a sample is taken from the tank and analyzed in an FT-IR cell and a GC. This allows the concentration of each species to be determined and the total yield of each product is calculated from a knowledge of the tank volume and pressure. The FT-IR can quantitatively determine many gas species observed in coal pyrolysis including CO, CO_2, H_2O, CH_4, C_2H_2, C_2H_4, C_2H_6, C_3H_6, HCN, NH_3, COS, CS_2, SO_2, and heavy paraffins and olefins. Additional characterization is performed by gas chromatograph to determine hydrogen, H_2S, O_2, N_2, C_3H_8, C_4's, and C_5's. The overall material balance is generally better than 90 to 95%.

Routine monitoring of three temperatures (top of heating elements, bottom of heating elements, and top of preheated bed) is done with permanently mounted thermocouples. Platinum alloy thermocouples are used to meet the high temperature requirements and to allow the use of oxidizing atmospheres. Power is supplied to the heating elements by using welding power supplies with continuously variable voltage adjustment. The voltage is adjusted to maintain the reference temperatures (above) constant during a run. These reference temperatures are calibrated against the furnace wall and gas temperatures by a set of profiling experiments. The furnace wall temperature and the injector-collector separation are inputs into the particle-temperature model which allows description of the coal particle time-temperature history.

The coal feeder consists of a tube which passes up through a bed of coal, with feeder gas supplied above the bed. To feed coal, the gas is turned on and the feed tube is slowly lowered from a position where the entrance is above the bed. When the entrance of the tube reaches the bed level, the coal is entrained in the gas entering the feed tube. The rate of feed is controlled by the rate at which the tube is lowered. The total weight of coal fed during a run is determined by weighing the feeder system before and after the run.

At the end of a run, the water-cooled collector is removed and any tar or char which sticks to the collector is rinsed out with solvent and weighed. Most of the char is collected in the cyclone. Fine solids (e.g., soot and coal fines) and condensed tar vapor which pass through the cyclone are collected in a filter. The filter and other parts of the collection system are extracted with solvent (methylene chloride), which is subsequently evaporated to determine the tar yield.

RESULTS AND DISCUSSION

The high pressure reactor (HPR) described above was used to determine the effects of pressure on pyrolysis behavior for four coals. The reactor was designed to provide similar temperatures and residence times as are employed in our atmospheric pressure reactor (EFR). To keep the gas requirements reasonable, a 1.27 cm I.D. tube was employed for the test section. It was found that swelling coals tended to plug the test section, so the coals tested were limited to subbituminous coals or lignites. The four coals tested were Montana Rosebud subbituminous, Gillette subbituminous, Jacob's Ranch subbituminous, and Zap (North Dakota) lignite. The coal analyses are presented in Table I. The pyrolysis yields for experiments at 800°C, 0.47 s residence time and 300 psig are given in Figs. 2-5 for these coals, respectively.

The most extensive amount of data was taken with the Montana Rosebud subbituminous due to a complementary program at AFR and Morgantown Energy Technology Center (METC) using this coal. The effects of pressure on product yields are observed to be modest in all cases. In general, with increasing pressure (at constant residence time and

temperature) there is a slight reduction in tar, olefin, and ethylene yields and increase in benzene, ethane and CH_4 yields. The trend for paraffin yield varies with the coal, as does the benzene yield trend. The subbituminous coals show a minimum benzene yield at intermediate pressures.

Data was obtained for the Zap, Jacob's Ranch, and Gillette coals at 685°C for the same residence time and range of pressures (not shown). The trends for tar, olefins, C_2H_4, and C_2H_6 were similar, but the CH_4 and benzene yields declined with pressure. The complex variations of volatile yields with temperature and pressure would be expected since both in the internal secondary chemistry of the coal and the external gas phase chemistry there are temperature and pressure-dependent sources and sinks for the various species. For example, Suuberg et al. (2) have shown that methane yields increase with increasing external gas pressure in batch, capture sample experiments. This was attributed to evolution of CH_4 during secondary repolymerization of tar to form char. Arendt and van Heek (8) observed similar results for CH_4 yields in both batch and semi-flow reactors. Higher yields of methane under increased external gas pressure have also been attributed to the auto-hydrogenation phenomenon, where hydrogen evolved from the coal back reacts to form CH_4 (9). A recent paper has suggested that this reaction is more affected by residence time than external gas pressure for high and low rank coals (10).

There is also experimental evidence which suggests a decline in CH_4 yield would occur with increasing pressure. Methane decomposition is catalyzed in the presence of coal char (11,12). This has been attributed both to surface area and catalysis effects. At high pressure, the enhanced residence time of CH_4 in the pores would increase decomposition. In addition, the gas phase decomposition of CH_4 is believed to involve the following pressure dependent initiation reaction:

$$CH_4 + M = CH_3 + M + H \qquad (1)$$

where M is any other molecule (13). This reaction would also be favored at high pressures. Consequently, numerous processes can operate on even such simple and relatively unreactive molecules as CH_4, making apriori prediction of pressure trends for volatile yields over a wide range of temperature difficult.

In entrained flow systems, one must also contend with the effects of gas pressure on heat transfer. In our system, increasing the pressure also affects the shape of the temperature profile and, consequently, the length of the isothermal zone. In order to achieve the same nominal residence time it was necessary to reduce the gas flow rate at higher pressures. For this reason, an assessment of pressure effects for data from the reactor requires consideration of the effect of pressure on the particle time-temperature history due to: 1) changes in the experimental conditions, 2) changes in the physical properties of the entraining gas with pressure. To do this, an entrained flow reactor model was developed which is a modification of one developed recently for our atmospheric pressure reactor (EFR) (14,15). The latter model was validated by comparison to actual temperature measurements. For the HPR, direct validation is not possible because of the lack of an optical port in the reactor. Instead the model was validated by fitting CH_4 yields from low pressure HPR data (26 psig) where it was assumed that the validated kinetics from the EFR would still hold.

After the modified particle temperature model was developed and validated, the results of the HPR experiments were simulated. These simulations are shown as solid lines in Figs. 2-5. These trends, which account only for the effects of pressure on particle time-temperature history (and not on the pyrolysis chemistry) indicate that there are real pressure effects superimposed on a slight variation in the time-temperature history. The trends of the model predictions should be compared to the data trends in Figs. 2-5 to discern a pressure effect rather than the absolute values. This is because the pyrolysis model does not match all of the atmospheric pressure data (e.g., C_2H_4 yields) due to an incomplete description of gas phase cracking.

High Pressure Experiments in a Heated Tube Reactor - A set of experiments was done at 800°C with Montana Rosebud coal in an electrically heated tube reactor at 1 atm and 5 atm pressure. The results for char, tar, and gas yields are shown in Fig. 6 for the two sets of experiments, which were done at the same volumetric flow rate. The total particle residence time at 200 cm distance is about 200 ms.

Initially, product yields are reduced when compared to the one atmosphere case. This is a result of the fact that the higher gas density causes a greater heat load on the tube and hence increases the distance required to heat the gas plus coal mixture to the equilibrium temperature. It is interesting that the maximum tar yield is lower in the 60 psig case. However, it is possible that an experiment in between 50 and 100 cm would reveal a higher tar yield. The asymptotic yield of about 10% is similar for both sets of experiments. It also agrees with the 26 psig data from the HPR. The advantage of the HTR relative to the HPR is that the good time resolution allows the maximum tar yields to be better defined.

Comparison of Tar Yield Data from Three Reactors - In Table II, tar yield data are listed for all three entrained flow reactors used at AFR. In each case, the final particle temperature was about 800°C. The residence times were lower for the HTR experiments but, due to the higher heating rate, the time at final temperature was nearly the same in each case ($\sim$0.2 s) according to our calculations. The lower pressure ($<$5 atm) results agree well between reactors. It is also apparent from the lower temperature HPR data in Table II, and the shorter residence time HTR data in Fig. 6, that some tar cracking occurred even under these relatively mild conditions. The reductions in tar yield due to cracking of about 35% agree well with previous data on Pittsburgh Seam bituminous coal tars cracked separately (16). The approximately 25% reduction in tar yield over a pressure range of 3 to 13 atm is in good agreement with the generalized plot developed by Suuberg (17).

Char Reactivity Measurements - Some reactivity measurements of the chars produced from the HPR experiments were made using a newly developed non-isothermal technique (18). The chars are heated at a constant rate (30°K/min) in a TGA in air. A reactivity index is defined based on a critical temperature to achieve a measurable weight loss rate, which is inversely related to reactivity. These data are given for the HPR chars in Table III. There does appear to be a slight decrease in char reactivity with increasing pressure. However, a portion of this could be attributed to the slightly increased severity of the higher pressure experiments. Additional data will be required on the kinetics of thermal deactivation in order to be more conclusive.

CONCLUSIONS

1. Pyrolysis experiments in a high pressure entrained flow reactor with three subbituminous and one lignite coal revealed an effect of pressure on product yields, even after allowing for changes in heat transfer. The tar and light hydrocarbon yields were most affected.

2. The relative reduction in tar yield as the pressure was increased from 3 to 13 atm was about 25%, in agreement with literature data.

3. The maximum tar yield was not observed in the 817°C, 0.5 s experiments, even at low pressure, due to tar cracking.

4. There was a small but consistent reduction of char reactivity with increased pressure. Some of this effect may be due to the slightly increased severity of the high pressure experiments.

ACKNOWLEDGEMENT

The authors gratefully acknowledge financial support of this work by the United States Department of Energy, Morgantown Energy Technology Center, under Contract No's. DE-AC21-81FE05122, DE-AC21-84MC21004, and DE-AC21-85MC22050.

REFERENCES

1. Anthony, D.B., Howard, J.B., Hottel, H.C., and Meissner, H.P., 15th Symposium (Int) on Combustion, The Combustion Institute, Pittsburgh, PA, p. 1303, (1975).
2. Suuberg, E.M., Peters, W.A., and Howard, J.B., "A Comparison of the Rapid Pyrolysis of a Lignite and a Bituminous Coal", in Thermal Hydrocarbon Chemistry, A.G., Oblad, H,H. Davis, and R.T. Eddinger, (Eda.), Adv. in Chem. Series, No. 183, pp 239-257, Am. Chem. Soc., Washington, DC (1979).
3. Niksa, S., Russel, W.B., and Saville, D.A., 19th Symposium (Int) on Combustion, The Combustion Institute, Pittsburgh, PA, p. 1151, (1982).
4. Dryden, I.G.C. and Sparham, G.A., B.C.U.R.A. Monthly Bulletin, **27**, 1, (1963).
5. Schobert, H.H., Johnson, B.S., and Fegley, M.M., ACS Fuel Chem. Preprints, **23**, #3, 136, (1978).
6. Sundaram, M.S., Steinberg, M., and Fallon, P.T., ACS Div. of Fuel Chem. Preprints, **28**, #5, 106, (1983).
7. Solomon, P.R., Hamblen, D.G., Carangelo, R.M., and Krause J.L., 19th Symposium (Int) on Combustion, The Combustion Institute, Pittsburgh, PA, 1139, (1982).
8. Arendt, P. and van Heek, K.H., Fuel, **60**, 779, (1980).
9. Rennhack, R., Brennstoff-Chemie, **45**, 300, (1964).
10. Makino, M. and Toda, Y., Fuel, **58**, 573, (1979).
11. Kamishita, M., Mahajan, O.P., and Walker, P.L., Jr., Fuel, **56**, 444, (1977).
12. Stephens, D.R. and Clements, W., (Ed.) LLNL Underground Coal Gasification Project Quarterly Report, April to June 1983, Lawrence Livermore National Lab.
13. Back, M.H. and Back, R.A., Chapter 12 in Pyrolysis: Theory and Industrial Practice, Albright, L.F. Crynes, B.L., and Corcoran, W.H., (Eds.), Academic Press, NY, (1983).
14. Serio, M.A., Solomon, P.R., Hamblen, D.G., Markham, J.R., and Carangelo, R.M., "Coal Pyrolysis Kinetics and Heat Transfer in Three Reactors", paper submitted to 21st Symposium (Int) on Combustion, (Jan. 1986).
15. Solomon, P.R., Serio, M.A., Hamblen, D.G., Best, P.E., Squire, K.R., Carangelo, R.M., Markham, J.R., and Heninger, S.G., a) Final Report for METC Contract No. DE-AC21-81FE05122, (1985)., b) First Quarterly Report for METC Conctract No. DE-AC21-85MC22050, (1986).
16. Serio, M.A., Peters, W.A., Sawada, K., and Howard, J.B., "Secondary Reactions of Nascent Coal Pyrolysis Tars", paper in Proceedings, International Conference on Coal Science, Pittsburgh, PA, Aug. 15-19, 1983, pp 533-536.
17. Suuberg, E.M., Chapter 4, in Chemistry of Coal Conversion, R.H. Schlosberg, (Ed.), Plenum Press, New York, (1985).
18. Solomon, P.R., Serio, M.A., and Heninger, S.G., "Variations in Char Reactivity with Coal Type and Pyrolysis Conditions" ACS Div. of Fuel Chem., Anaheim Meeting, (1986).

TABLE I

SAMPLE PROPERTIES

WT% DAF

	Zap, North Dakota Lignite	Gillette Subbituminous	Montana Rosebud Subbituminous	Jacob's Ranch Subbituminous
Carbon	66.5	72.0	72.1	74.3
Hydrogen	4.8	4.7	4.9	5.2
Nitrogen	1.1	1.2	1.2	1.1
Sulfur (Organic)	1.1	0.5	1.2	0.6
Oxygen (Diff.)	26.5	21.6	20.3	18.8
Ash (Dry Wt%)	7.1	5.0	10.0	7.8

TABLE II

OBSERVED TAR YIELDS (DAF) FROM VARIOUS REACTORS AT 800°C, 0.1–0.5 S RESIDENCE TIME

Coal:			Zap Lignite	Gillette	Montana Rosebud	Jacob's Ranch
Reactor	Pressure (atm)	Time (s)				
HTR	1.0	0.2	10.3		10.0	
HTR	5.0	0.2			10.0	
EFR	1.0	0.4	10.0*			
HPR	2.6	0.5	6.0 (8.0)	9.4 (13.6)	9.2	7.6 (11.0)
HPR	13.0	0.5	4.5 (7.5)	7.8 (11.5)	6.0	6.5 (9.5)

NOTES: Values in parentheses are for 658°C experiments at the same residence time and pressure.

* Tar plus missing.

HTR = Heated Tube Reactor
EFR = Entrained Flow Reactor
HPR = High Pressure Reactor

TABLE III

CRITICAL TEMPERATURE FOR OXIDATION OF CHARS FORMED AT VARIOUS PRESSURES

Coal:	Zap Lignite	Gillette	Montana Rosebud	Jacob's Ranch
Pressure (atm)				
2.6	365	368	403	370
7.8	366	378	415	370
13.1	378	381	419	376
21.4	---	---	429	---

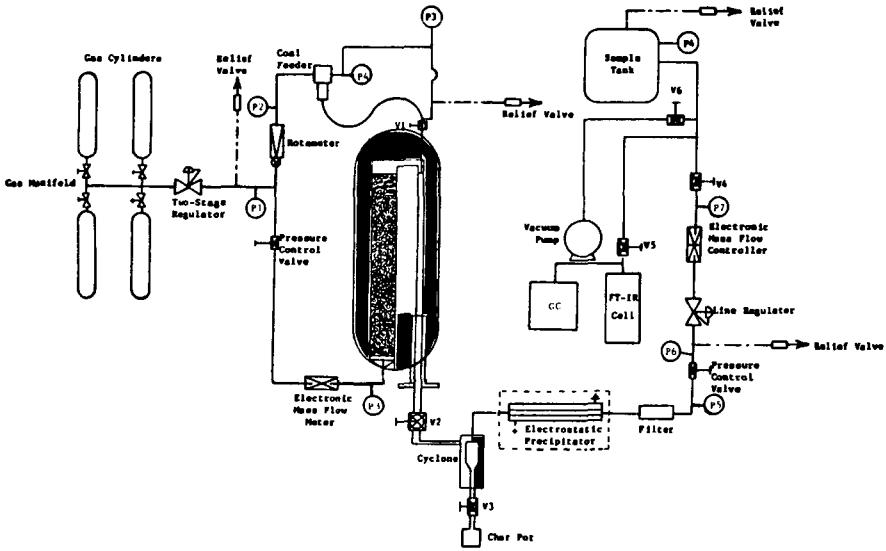

Figure 1. Schematic of High Pressure Entrained Flow Reactor System.

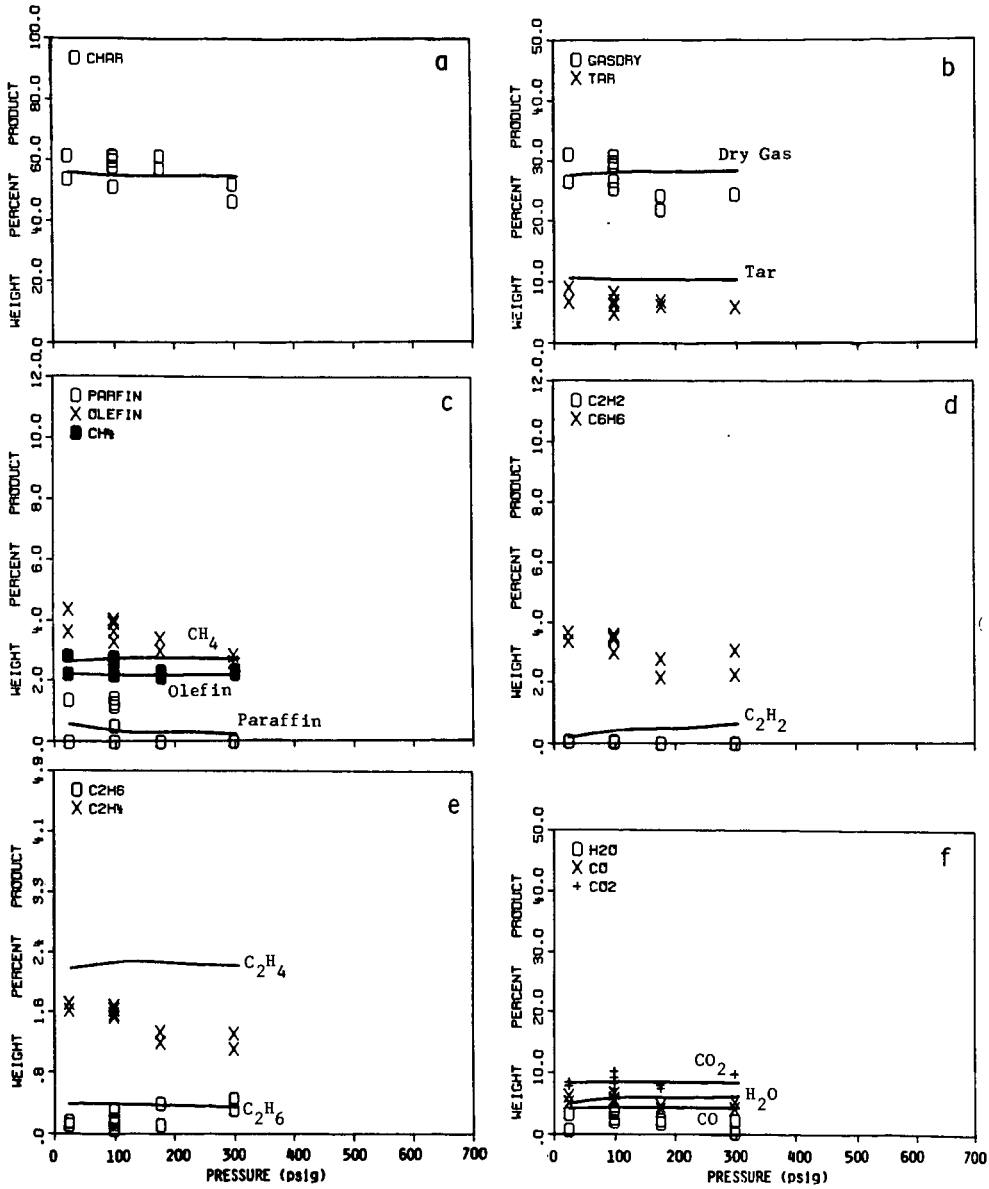

Figure 2. Pyrolysis Product Distribution for Montana Rosebud Subbituminous Coal as a Function of Pressure. Temperature = 817°C, Residence Time = 0.47 sec.

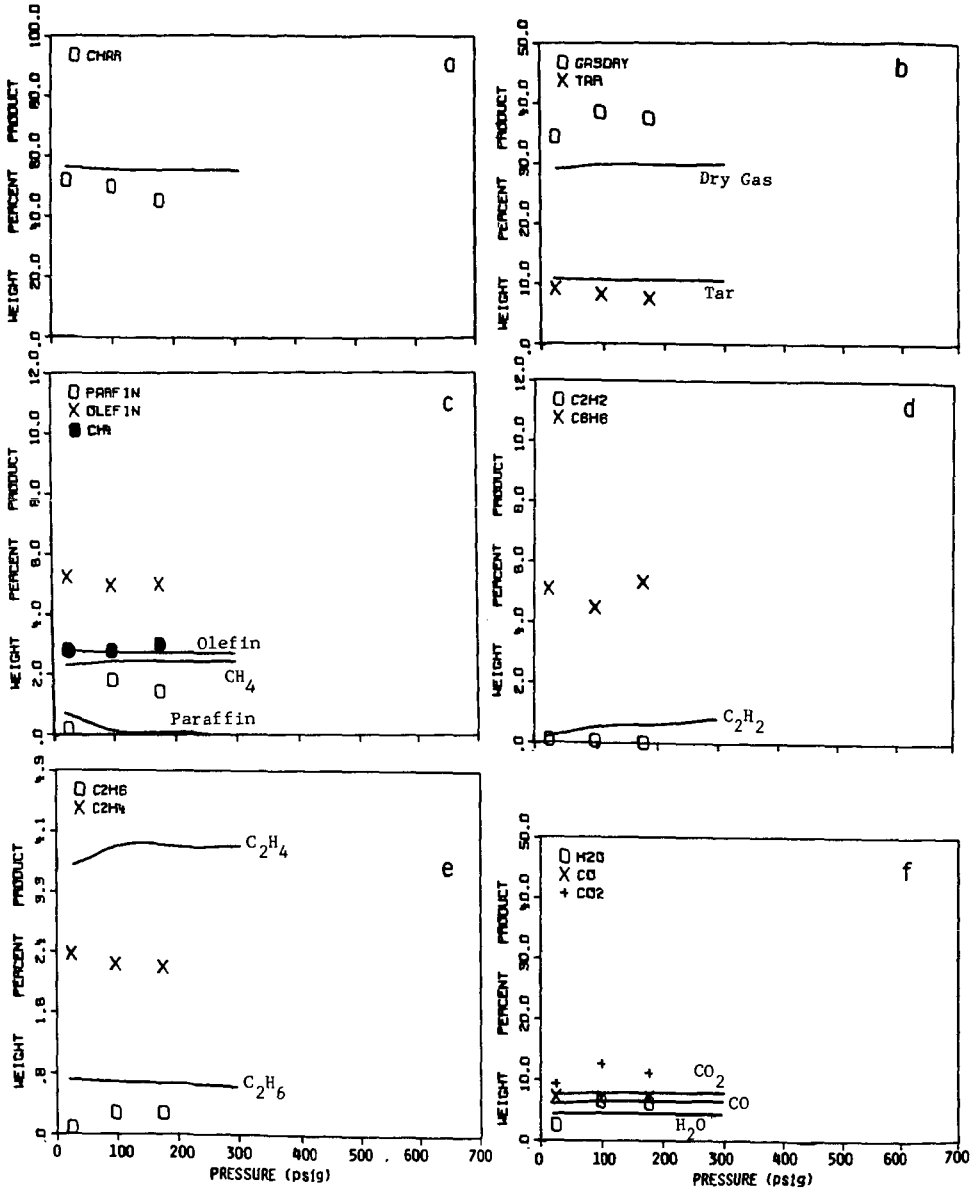

Figure 3. Pyrolysis Product Distribution for Gillette Subbituminous Coal as a Function of Pressure. Temperature = 817°C, Residence Time = 0.47 sec.

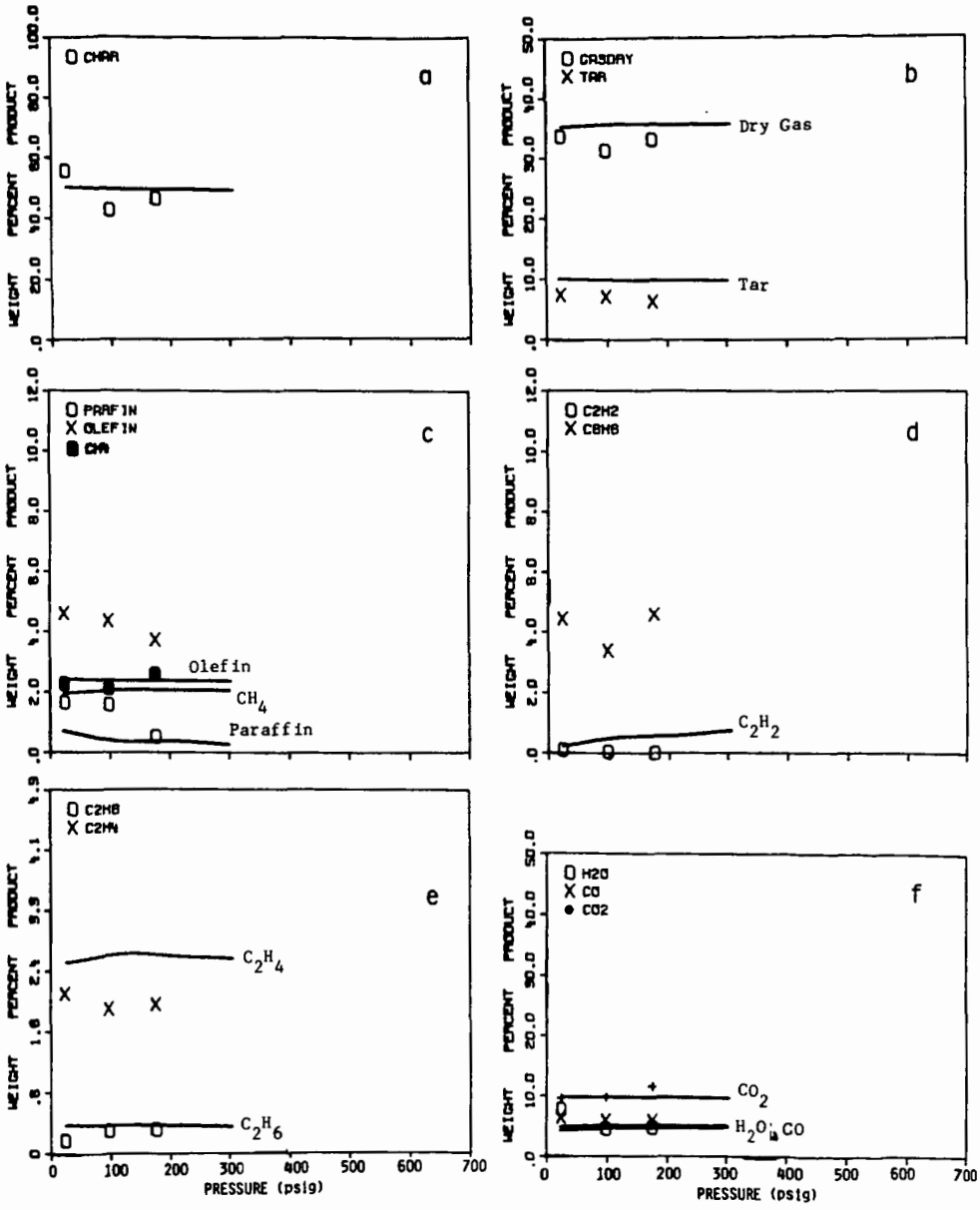

Figure 4. Pyrolysis Product Distribution for Jacob's Ranch Subbituminous Coal as a Function of Pressure. Temperature = 817°C, Residence Time = 0.47 sec.

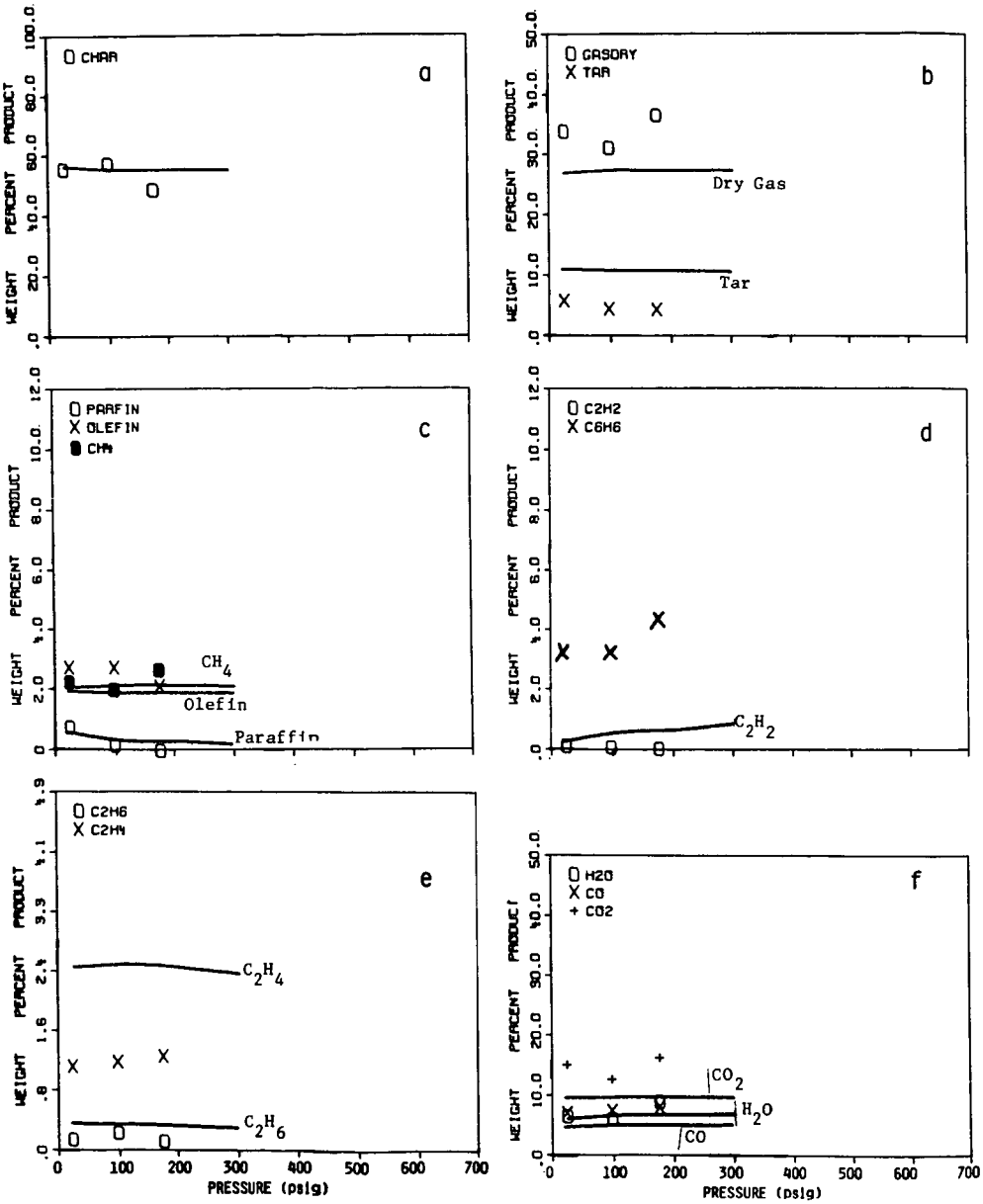

Figure 5. Pyrolysis Product Distribution for Zap, North Dakota Lignite as a Function of Pressure. Temperature = 817°C, Residence Time = 0.47 sec.

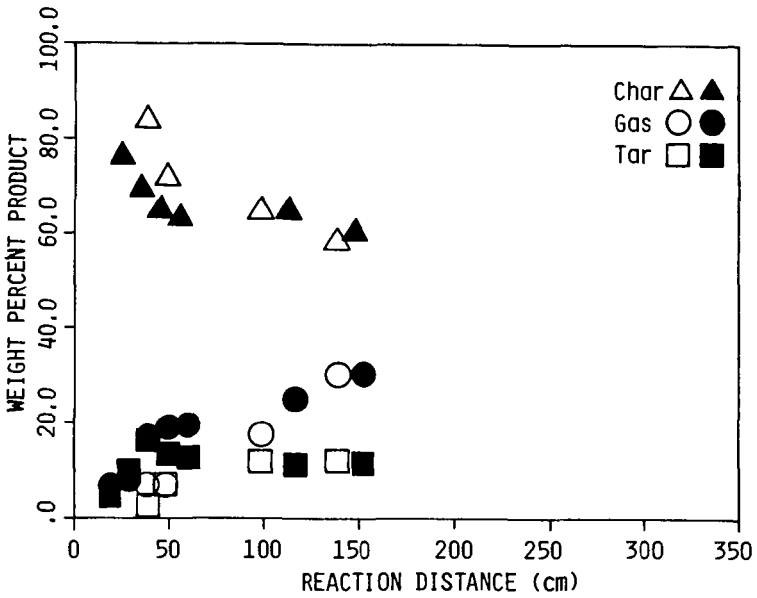

Figure 6. Comparison of Pyrolysis Data from One Atmosphere Pressure (*solid symbols*) and 5 atm pressure (open symbols) Experiments in the Heated Tube Reactor with Montana Rosebud Coal (200 x 270 mesh). The Equilibrium Tube Temperature was 800°C.

RESPONSE SURFACE MODEL PREDICTIONS FOR THE FLASH PYROLYSIS OF MONTANA ROSEBUD COAL

Larry A. Bissett

Morgantown Energy Technology Center
P.O. Box 880
Morgantown, WV 26507-0880

Abstract

Experiments covering a broad range of reaction conditions are being conducted to determine and model the effects of coal gasification environment on product yields. The research uses a 3-inch I.D., down-flow entrained reactor that turbulently mixes preheated gases with coal to achieve high particle heating rates. As part of the test program, a pyrolysis series reacting Montana Rosebud coal in a nitrogen-argon atmosphere was completed. A 3-variable, composite factorial experimental design was used in which reaction conditions ranged from 1,500° to 2,500°F temperature, 100 to 900 psig pressure, and 2.19 to 10.00 seconds gas residence time. Quadratic response surface models were used to analyze the product yield and composition data as a function of the reaction conditions. Trends predicted by some of the statistically significant regression models are presented and discussed.

Introduction

For advancement to continue towards tailored, economic, and environmentally sound coal conversion technologies, further understanding of reaction mechanisms and product formations in relation to processing conditions and the physical and chemical structure of coal is needed. Devolatilization and associated phenomena are especially important in entrained gasification and pulverized coal combustion due to the small particle sizes, high temperatures, and short residence times involved. Although numerous studies have been conducted, recent reviews have concluded that there is little experimental verification at high-temperature, high-pressure conditions that exist in some current and advanced processes (1,2). Therefore, this project was initiated to determine the effects of gasification environment on product yields over a broad range of mild to severe conditions. A broad-range study was chosen to aid in the detection of reaction mechanism changes and to help integrate results from other related investigations.

Experimental

A down-flow entrained reactor designed to be able to preheat reactant gases to 3,000°F along the horizontal axis and maintain the reaction mixture at 2,500°F along the vertical axis at pressures up to 1,000 psig is used for the research. Details of the reactor and experimental system have been previously presented (3,4). The reactor is uniquely characterized by a mixing configuration that turbulently combines argon-conveyed coal with highly preheated reactant gases and subsequently transitions the flow to laminar-like before it enters a 3-inch I.D., 4-foot long alumina reaction tube. The turbulent, nearly adiabatic mixing between reactant gases and coal results in high particle heating rates approaching 10^5°F per second. In addition to being essential for properly studying the phenomena of interest, this enables reaction temperatures to be reached near the exit of the nozzle and provides the potential for achieving axial isothermal temperature profiles in the reaction tube.

A comprehensive test program with Montana Rosebud subbituminous coal is being conducted. The program is organized into three major test classes to study inert, steam, and carbon dioxide environments, and an additional class to investigate char gasification reactions. The classes are further subdivided into test series to

investigate other variables. The Class 3A pyrolysis tests reported here were conducted in an inert environment of 75 mole percent nitrogen and 25 mole percent argon and consisted of a composite factorially designed series to investigate the effects of reaction temperature, pressure, and gas residence time. The composite factorial experimental design enabled a wide range of conditions to be studied with 15 different tests and permitted the use of response surface and statistical techniques for data analyses. To help ensure that each test point carried about the same weight, uniform variable spacing was used for testing and analyzing. The variable levels and respective codes are given in Table 1. To facilitate the ability of the quadratic response surface models to adequately represent the true response surfaces, the temperature levels were equally spaced reciprocally as absolute temperature, and the pressure and gas residence time levels were equally spaced logarithmically as absolute pressure and seconds, respectively.

TABLE 1. Composite Factorial Variable Levels

Variable	Levels				
METC Test Code	1	2	3	4	5
Factorial Code	-2	-1	0	1	2
Temperature, °F	1,500	1,681	1,898	2,165	2,500
Pressure, psig	100	178	309	530	900
Gas Residence Time, sec	2.19	3.20	4.68	6.84	10.00

Experimentally, the gas environment, gas-coal ratio (400 scf/lb), and total material fed to the reactor during steady-state conditions were held essentially constant throughout the test series. A 200 x 270 mesh fraction of Montana Rosebud coal with an average particle diameter of 57 microns was used. Expressed as weight percent, the average ultimate analysis of the coal was 64.1 carbon, 4.4 hydrogen, 17.9 oxygen, 1.1 nitrogen, 1.0 sulfur, 10.4 ash, and 1.0 moisture; and the average volatile matter content was 40.6.

Results and Discussion

The overall material balance accountability of coal to product gases, liquids, and chars was greater than 98 weight percent. Quadratic response surface models which considered linear, quadratic, and interaction effects were used to analyze 50 variables. The Statistical Analysis System (SAS) computer program was used to perform the least squares regressions (5). Thirty-six variables had potentially adequate regression model fits at the 0.05 significance level or higher. Some regression model predictions of product yields and compositions from this test series have been previously reported (6). Only the regression models for elemental retentions in char will be discussed here.

Table 2 lists the experimental elemental char retentions, defined as the weight percentage of each major coal element that remained in the char, for this test series. The test numbers are derived from the METC test codes for the variable levels given in Table 1. The "3A" identifies the test class and is followed by three numbers which sequentially identify the temperature, pressure, and gas residence time levels. A fourth number is used when a test condition is repeated and represents the repetition number. Thus, Table 2 also illustrates the 15 different variable combinations involved with the composite factorial design and shows

that the center point condition (i.e., 3A333) was repeated 4 times to determine experimental variation. Test No. 3A333-1 failed and therefore does not appear in the table.

Nitrogen was the only elemental retention that could not be adequately represented by a quadratic response model at the 0.06 significance, or alpha, level or higher. Of the four that could be adequately represented, all had statistically significant predicted temperature effects to at least the 0.07 alpha level, only hydrogen and sulfur retentions had significant predicted pressure effects to at least the 0.04 alpha level, and all but oxygen retention had significant predicted gas residence time effects to at least the 0.08 alpha level. The significance levels provided the criteria for selecting which regression models and what variable ranges were used for predictive purposes. In general, full experimental ranges were used when significance values were 0.05 or higher, and only small variations around the center point of the experimental design were used when significance values were between 0.05 and 0.10.

Figure 1 shows how the predicted carbon, hydrogen, oxygen, and sulfur retentions in char vary with reaction temperature at the experimental center point pressure and gas residence time conditions. Oxygen is the least retained (i.e., most converted) element, and is predicted to be essentially absent in the char at temperatures above 2,000°F. Hydrogen retention decreases steadily with temperature and begins to approach zero at the highest temperature. This behavior most likely reflects thermally induced dehydrogenation and condensation of the larger aromatic structures in the char. Carbon and sulfur retentions both initially decrease, but then increase at higher temperatures. This behavior mostly accounts for a similar trend in char yield, which was also shown to pass through a minimum (6). The tendency for carbon retention to increase at higher temperatures is probably due to the increased cracking of volatile species, either in the hotter, outer regions of the particles as they devolatilize or in the extraparticle environment. The possibility of decreased yields at higher temperatures due to secondary reactions was recognized prior to this experimental confirmation (7). The tendency for sulfur retention to increase may be due to the high-temperature reaction of hydrogen sulfide with char to form thiophenic structures, as has been reported (8), or capture of the sulfur by ash components.

Figure 2 indicates an interaction between temperature and pressure effects on hydrogen retention. The nature of the predicted pressure effect changes with reaction temperature and decreases in magnitude as temperature increases. The pressure effect is relatively unimportant at higher temperatures. At lower temperatures, however, hydrogen retention increases faster with pressure than hydrogen yield decreases which, if there is no pressure effect on carbon retention as indicated by a poor significance level, implies that the overall hydrogen-carbon ratio of the nonchar products decreases. Thus, in very general and relative terms, pressure may tend to shift the aromatic hydrocarbon spectrum to heavier components at lower temperatures, but has little or no effect at higher temperatures due to extremely low organic yields. This behavior may be due to equilibrium considerations or reflect pressure effects on the sequence of secondary cracking reactions.

Figure 3 shows that near the experimental center point temperature and at the center point gas residence time, sulfur retention is predicted to maximize in roughly the 200 to 300 psig pressure range. At lower pressures, sulfur retention decreases slightly with temperature and, conversely, increases slightly with temperature at the higher pressures. The occurrence of maxima and the inverted temperature dependencies suggest the presence of multiple phenomena. Candidate explanations could include some of the possible effects of pressure on the following: (1) reaction rates of sulfur species with char and ash, (2) initial distribution of devolatilized sulfur species, (3) sequence and rates of secondary reactions, (4) coal and char physical changes during devolatilization that affect reactant accessibility,

and (5) various sulfur absorption equilibriums. Planned analyses of the chars to obtain the proportion of organic and inorganic sulfur forms may clarify these trends.

Figure 4 shows how the predicted hydrogen and carbon retentions vary with gas residence time near the experimental center point temperature and at the center point pressure. Hydrogen retention decreases just slightly with residence time and has a comparatively much greater sensitivity to temperature. The decrease is probably due to an annealing-like phenomena which results in the slow dehydrogenation and condensation of aromatic structures in the char. The predicted trends show that the dehydrogenation rate increases with temperature. Carbon retention is predicted to increase with time at the lower temperatures, but decrease with time at the highest temperature. Furthermore, carbon retention increases with temperature at gas residence times less than approximately 3.5 seconds, but decreases with temperature at longer residence times. The explanation for this behavior is not clear, but may possibly involve the relative kinetics of some of the cracking and gasification reactions and the initial cracking sequence. Initially, more intraparticle cracking of volatile species may be occurring during devolatilization as temperature increases, and, hence, carbon retention increases with temperature at the shortest residence times. The volatile species that escaped intraparticle cracking at the lower temperatures may then, with time, continue cracking in the extraparticle environment and lead to a gradual increase in carbon retention. Because significant cracking may have already occurred at the highest temperature, there would be little material left for long-term extraparticle cracking and, hence, no tendency for carbon retention to increase. However, gasification reactions of the char with carbon dioxide and water formed during pyrolysis would have the opportunity to proceed and may account for the gradual conversion of carbon at the highest temperature. At the lower temperatures, the gasification reactions may not be fast enough to counter deposition resulting from cracking reactions, and thus, carbon retention continues to increase. To validate these explanations, more data are needed for yields at residence times under 2 seconds and for cracking rates of various light hydrocarbons in the presence of char at the experimental conditions.

Figure 5 shows that sulfur retention in char is very sensitive to gas residence time and relatively insensitive to temperature. The trends indicate that a low-sulfur char is initially produced, but increases in sulfur content as time proceeds. This implies that a large percentage of the sulfur in the coal is initially released to the extraparticle environment and that various mechanisms then return some of the sulfur to the char. Various organic sulfur compounds crack into hydrogen sulfide and carbon disulfide, and these as well as the hydrogen sulfide initially formed from pyrite probably back react with the char and ash components. Depending on the initial forms of the devolatilized sulfur and relative reaction rates, these trends could predominantly reflect the kinetics of either hydrogen sulfide absorption reactions or organic sulfur compound cracking reactions. The suggested asymptote at approximately 75 percent sulfur retention possibly reflects approach to equilibrium or an absorption limit of the ash. Further analyses of sulfur forms in the chars may indicate the dominant effects.

Conclusions

A composite factorial experimental design and response surface methods were successfully applied to study the flash pyrolysis of Montana Rosebud coal over wide ranges of temperature, pressure, and gas residence time. Statistically significant regression models were used to predict product yield and composition trends. The regression model predictions reported here for elemental retentions in char lead to the following conclusions: (1) char yields increased at the higher temperatures investigated due to carbon deposition from the cracking of volatiles and sulfur absorption by char and ash components, (2) carbon, hydrogen, and oxygen retentions

were most sensitive to temperature and sulfur retention was most sensitive to residence time, (3) pressure may tend to shift the aromatic hydrocarbon spectrum to heavier components at the lower temperatures investigated, (4) sulfur retention was likely affected by multiple phenomena, (5) char annealing effects and continued cracking of light hydrocarbons were present in the residence time range studied, and (6) a low-sulfur char was initially produced, but increased in sulfur content with time to an apparent asymptotic value due to back reactions of sulfur species with the char and ash.

References

1. Howard, J. B., W. A. Peters, and M. A. Serio. 1981. EPRI Report No. AP-1803.

2. Talwalkar, A. T. 1983. DOE/MC/19316-1408 (DE83006592).

3. Bissett, L. A. 1983. DOE/METC/84-8 (DE84000217):116-128.

4. Bissett, L. A. 1984. DOE/METC/85-2 (DE85001955):65-72.

5. Statistical Analysis System Institute. 1982. SAS User's Guide: Statistics.

6. Bissett, L. A. 1985. DOE/METC-85/6024 (DE85008618):80-89.

7. Howard, J. B. 1981. Chapter 12. Chemistry of Coal Utilization, Second Supple. Vol., Ed. M. A. Elliott, New York: John Wiley and Sons, Inc.

8. Calkins, W. H. 1985. ACS Div. of Fuel Chem. Preprints. 30(4):450-465.

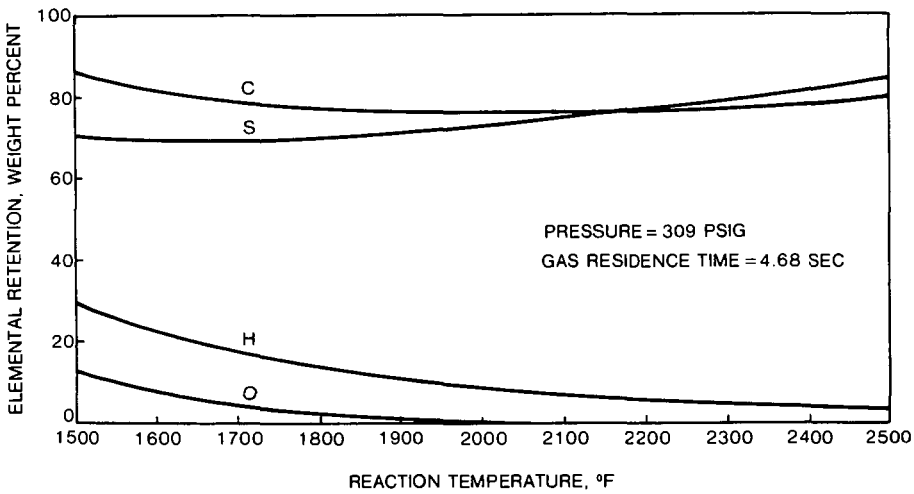

Figure 1. Regression Model Prediction for Elemental Retention in Char vs. Reaction Temperature, Class 3A Nitrogen-Montana Rosebud Coal Tests, METC Advanced Gasification Facility Entrained Reactor

TABLE 2. Elemental Char Retention, Weight Percent, Class 3A
Nitrogen -- Montana Rosebud Coal Tests, METC
Advanced Gasification Facility Entrained Reactor

Test No.	Temperature, F°	Pressure, psig	Gas Residence Time, sec.	Carbon	Hydrogen	Oxygen	Nitrogen	Sulfur
3A133	1,500	309	4.68	85.9	31.7	11.0	89.6	67.9
3A222	1,681	178	3.20	75.1	16.3	7.3	69.3	66.2
3A224	1,681	178	6.84	82.9	15.8	13.3	36.2	70.9
3A242	1,681	530	3.20	78.1	19.6	11.1	69.8	47.1
3A244	1,681	530	6.84	85.6	19.7	5.8	76.6	70.1
3A313	1,898	100	4.68	78.1	6.7	1.5	80.4	62.3
3A331	1,898	309	2.19	77.0	12.7	5.5	73.5	41.1
3A333	1,898	309	4.68	77.5	11.0	0.1	89.5	67.6
3A333-2	1,898	309	4.68	76.6	10.0	2.4	58.9	71.4
3A333-3	1,898	309	4.68	76.3	11.5	0.2	70.5	76.5
3A333-4	1,898	309	4.68	75.5	11.9	0.5	68.2	70.6
3A335	1,898	309	10.00	76.4	8.0	1.6	76.9	74.5
3A353	1,898	900	4.68	76.3	12.5	11.2	67.6	51.1
3A422	2,165	178	3.20	76.2	8.0	1.1	80.2	59.0
3A424	2,165	178	6.84	71.3	2.6	0	41.4	66.4
3A442-1	2,165	530	3.20	78.0	5.2	0.7	62.4	68.6
3A444	2,165	530	6.84	78.0	6.5	3.9	56.4	71.4
3A533	2,500	309	4.68	80.5	3.0	0	49.4	89.0

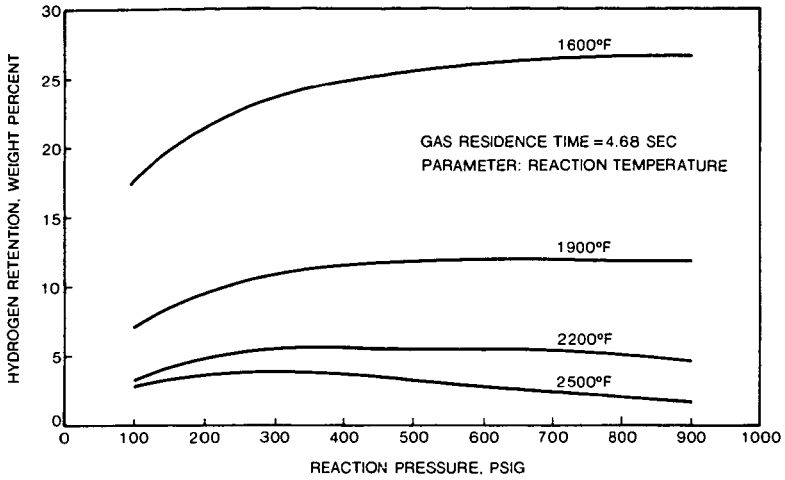

Figure 2. Regression Model Prediction for Hydrogen Retention in Char vs. Reaction Pressure, Class 3A Nitrogen-Montana Rosebud Coal Tests, METC Advanced Gasification Facility Entrained Reactor

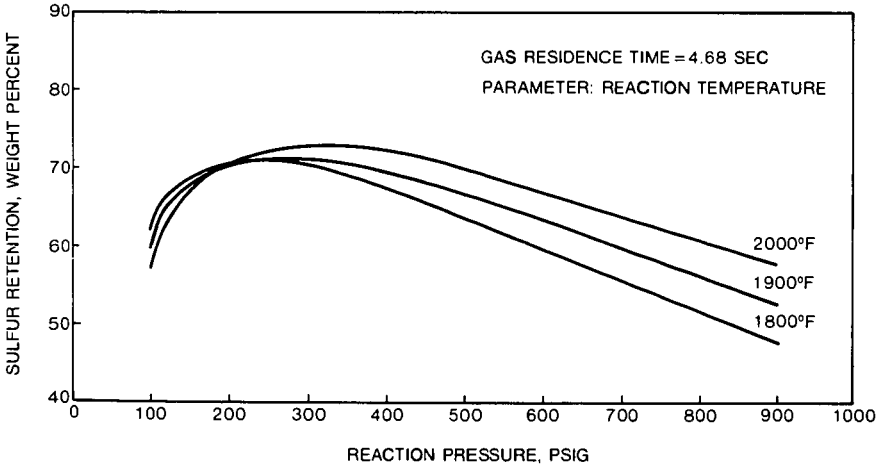

Figure 3. Regression Model Prediction for Sulfur Retention in Char vs. Reaction Pressure, Class 3A Nitrogen-Montana Rosebud Coal Tests, METC Advanced Gasification Facility Entrained Reactor

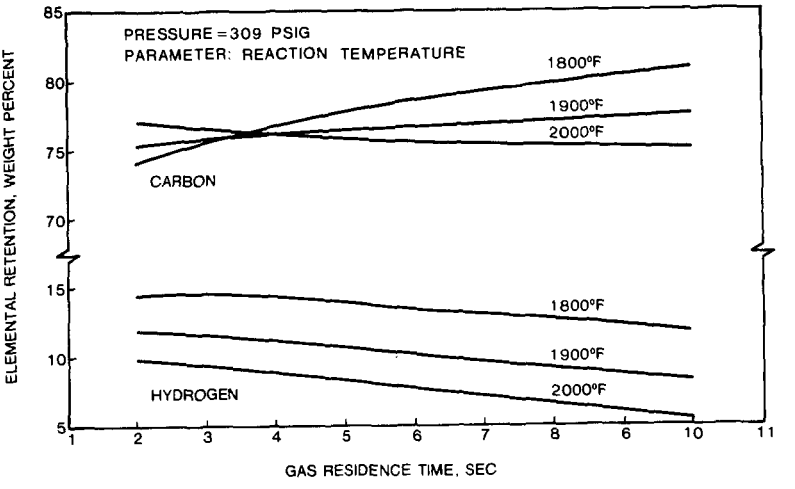

Figure 4. Regression Model Prediction for Carbon and Hydrogen Retention in Char vs. Gas Residence Time, Class 3A Nitrogen-Montana Rosebud Coal Tests, METC Advanced Gasification Facility Entrained Reactor

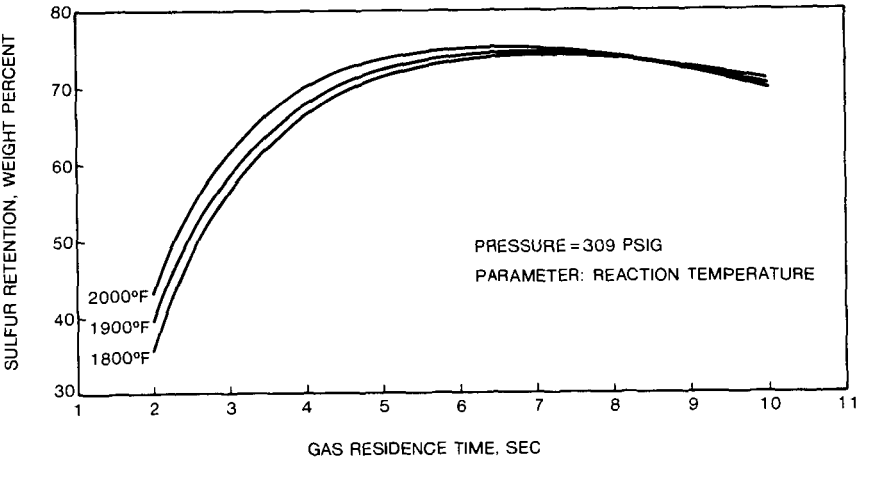

Figure 5. Regression Model Prediction for Sulfur Retention in Char vs. Gas Residence Time, Class 3A Nitrogen-Montana Rosebud Coal Tests, METC Advanced Gasification Facility Entrained Reactor

Flash Pyrolysis of New Mexico Sub-Bituminous Coal in Helium-Methane Gas Mixtures

Muthu S. Sundaram, Peter T. Fallon and Meyer Steinberg
Process Sciences Division
Brookhaven National Laboratory
Upton, New York 11973

ABSTRACT

A New Mexico sub-bituminous coal was flash pyrolyzed in gas mixtures of helium and methane at 1000°C and 50 psi in an 1-in. I.D. entrained down-flow tubular reactor. The mixture contained 0 to 40% helium in methane. Under tested experimental conditions, pyrolysis in gas mixtures resulted in higher yields of ethylene and BTX than in pure methane. For example, under a coal flow rate of 1.0 lb/hr and methane flow rate of 4.0 lb/hr, pyrolysis in pure methane produced 7.7% C_2H_4 and 9.0% BTX on the basis of carbon contained in coal; under similar coal and methane flow rates, as high as 14.8% C_2H_4 and 15.3% BTX were obtained on pyrolysis in 25% He + 75% CH_4 gas mixture. The data show that the coal flow rate and methane flow rate both independently affect the yields of C_2H_4 and BTX. At constant methane flow rate, increase in coal flow rate decreases the yields of C_2H_4 and BTX; at constant coal flow rate, increase in methane flow rate increases the yields of C_2H_4 and BTX.

Keywords: coal; natural gas; pyrolysis; gasification.

INTRODUCTION

The aim of the flash pyrolysis of coal is the production of smaller molecules from it in a shortest possible particle residence time. Therefore, the objective of studying the process chemistry of coal pyrolysis is to investigate the experimental parameters that permit this aim to be achieved and to establish the optimum conditions that produce a favorable product slate. The basic process parameters that influence the product yields during flash pyrolysis of coal are: (1) reaction temperature, (2) gas pressure and (3) residence times of coal particles and ensuing tar vapors. In addition to these major process parameters, product yields can be influenced by other factors such as the nature of the pyrolysis gas and its partial pressure and the gas-to-coal ratio.

Previous work on flash pyrolysis of coal at Brookhaven National Laboratory was performed with inert pyrolysis gases, He, N_2 and Ar, and reactive gas, H_2.[1] Because of its process potential, our recent work has concentrated on the flash pyrolysis of coal with reactive methane gas.

Methane, in the form of natural gas, has become a readily available, low-cost raw material. Utilization and conversion of coal in conjunction with natural gas to produce higher valued fuel and feedstocks, becomes an attractive process proposition.

In general, pyrolysis experiments have been carried out in pure gases, either inert or reactive. In a few instances, mixtures of inert gases e.g. N_2-Ar[2] or reactive gases e.g. H_2-H_2O were used as pyrolysis atmospheres.[3] The potential and usefulness of mixtures of inert and reactive gases towards the selectivity of pyrolysis products, heretofore, has not been investigated.

In order to determine if a relative increase in the heat transfer coefficient of the pyrolyzing gas could be used to increase the yields of ethylene and BTX from coal, a detailed examination of the pyrolysis of a New Mexico sub-bituminous coal was conducted in gas mixtures of helium and methane. The effects of gas mixture composition, coal feed rate and gas feed rate on the yields of ethylene and BTX are reported in this paper.

EXPERIMENTAL

The flash pyrolysis experiments were carried out in a 1-in. diameter-by-8-ft-long downflow entrained tubular reactor, details of which have been reported.[4] The gas mixture consisted of 0-40% helium by volume and the balance methane. Preheated methane or helium-methane gas mixture was fed into the reactor to desired total pressure. The partial pressure of methane was maintained constant at 50 psi in the experiments reported here. A New Mexico sub-bituminous coal, with analysis shown in Table 1, was used in the study. The coal, 150μm or less in size, premixed with 10% by weight of Cab-O-Sil (a fumed silica powder) to prevent agglomeration, was dried in a vacuum oven overnight. The high temperature gas feed is mixed with coal at the top of the reactor causing the pyrolysis reactions to take place. Routine gas analyses were performed with an on-line gas chromatograph. The product yields were determined on the basis of conversion of carbon contained in the coal feed.

Table 1

Analysis of New Mexico Sub-bituminous coal (wt%)

Moisture (As Received)	7.8			
Proximate Analysis:		Ultimate Analysis:		(daf)
Dry Ash	22.8	Carbon	-	72.4
Dry V.M.	34.9	Hydrogen	-	5.6
Dry V.M.	34.9	Nitrogen	-	1.4
Dry P.C.	42.4	Oxygen (by diff)	-	20.6

RESULTS AND DISCUSSION

Ethylene is an important raw material for the polymer market. Less attention has been focused in the past on the production of ethylene using coal as the raw material.We have shown earlier that there are definite advantages in the use of methane as an atmosphere in the flash pyrolysis of coal. At temperatures higher than 800°C, 2-5 times greter yields of ethylene are obtainable in methane atmosphere when compared to flash pyrolysis in an inert helium atmosphere.[5] The enhancement in the ethylene yield was determined to be due to an interaction between coal and methane at the pyrolysis conditions.[6] Though greater selectivity towards ethylene and BTX production can be achieved by pyrolysis of coal in a methane atmosphere, its relatively low thermal conductivity can limit the total volatiles yield obtainable from coal. Hydrogen is highly reactive and it also has the highest thermal conductivity of all gases; however, it is unsuitable if the aim is to maximize ethylene and BTX yields as they become hydrocracked in the presence of hydrogen. This, then, leads to the possibility of pyrolyzing coal in a mixture of helium with high thermal conductivity and methane with high reactivity.

One of the important process parameters that influenced the ethylene and BTX yields was found to be the methane-to-coal feed ratio. When the gas flow rate was held constant, the yields of C_2H_4 and BTX tend to increase with lower mass loadings of coal. The results of flash pyrolysis of New Mexico sub-bituminous coal in pure methane at 1000°C and a constant methane flow rate of 3.8 lb/hr are shown in Figure 1. The curves for both C_2H_4 and BTX follow the same pattern. The top curves show the total yield of C_2H_4, C_2H_6 and BTX. At the lowest coal flow rate, the ethane yield was 1.0% and no ethane was produced at higher coal flow rates. The decrease in the yields of BTX, C_2H_4 and C_2H_6 at higher coal flow rates can be explained on the basis of accelerated decomposition of the above products on the surface of the hot char particles, the area of which also increases with higher mass loadings of coal. Furthermore, higher mass loadings of coal can also affect the heat transfer between the pyrolyzing gas and the coal particles which, in turn, can reduce the yield of the volatiles from coal. Thus, it becomes necessary to optimize the flow rates of coal and methane in order to maximize the desired product yields.

Table 2 shows the yields of the products obtained when the coal was pyrolyzed in gas mixtures of helium and methane. Three different compositions of gas mixtures were used which contained 6 to 40% He in methane. As shown in Table 2, the partial pressure of methane was constant at 50 psi in all experiments. The coal flow rate ranged from 0.8 to 1.3 lb/hr and the methane flow rate from 2.1 to 4.6 lb/hr. The flow rates shown here were obtained by averaging the flow rates throughout the run which lasted for about an hour. Though instantaneous flow rate of coal is not known, it is not expected to vary because successive gas analyses using on-line GC were consistent for a steady state reaction conditions. The instantaneous flow rate of the pyrolyzing gas which was recorded throughout the run, did not reveal any significant differences.

Table 2

Flash Pyrolysis of New Mexico Sub-bituminous Coal at 1000°C
in Helium-Methane Gas Mixtures
(Partial Pressure of Methane: 50 psi)

Run No.	684	871	868	779	795	766	848	812	849	854	817	837	860	844	841	827
Helium (Vol %)	0	6	6	6	6	6	12	12	12	12	25	25	25	25	40	40
Methane (Vol %)	100	94	94	94	94	94	88	88	88	88	75	75	75	75	60	60
Total Pressure, psi	50	53	53	53	53	53	57	57	57	57	67	67	67	67	83	83
Coal Feed Rate (lb/hr)	1.00	1.22	1.22	0.75	0.81	0.87	1.00	1.18	1.22	1.28	0.97	0.93	0.95	1.01	1.09	1.24
Methane Feed Rate (lb/hr)	4.05	4.13	2.85	4.55	4.92	4.33	3.18	4.60	3.25	1.96	3.98	3.44	2.1	2.69	3.19	3.31
Coal Res. Time (sec)	1.5	1.4	1.9	1.3	1.2	1.3	1.7	1.2	1.7	2.2	1.2	1.3	2.3	1.9	1.6	1.2
Methane/Coal Ratio	4.1	3.4	2.3	6.1	6.1	5.0	3.2	3.9	2.7	1.5	4.1	3.7	2.2	2.7	2.9	2.7
Product Yields, (wt% Coal Carbon Basis)																
C_2H_4	7.7	7.9	4.7	14.1	10.5	6.7	7.6	8.6	6.1	3.3	14.8	10.7	6.1	6.1	7.3	9.3
C_2H_6	0.1	1.5	0.7	1.9	2.2	1.7	1.3	1.6	1.0	0.8	3.0	1.8	1.4	1.4	1.2	1.0
BTX	9.0	10.7	8.8	18.2	14.4	N.D.	11.1	10.2	10.2	7.5	15.3	13.7	10.3	10.5	11.3	10.6
CO	8.0	9.6	6.4	5.3	6.6	5.6	6.3	5.8	5.6	6.8	7.6	7.4	6.2	6.6	6.7	4.6
CO_2	1.7	1.6	1.0	1.8	1.9	1.5	1.5	1.8	1.3	1.6	2.3	1.5	1.5	1.4	1.4	1.3
Total																

N.D. - Not Determined.

Figure 2 shows the yields of ethylene and BTX as a function of volume percent helium in the pyrolyzing helium-methane gas mixture at methane-to-coal ratio of 3.9 to 4.1 and coal particle residence time of 1.2-1.5 sec. Both curves show that, under the conditions investigated, the yields of C_2H_4 and BTX increase with the amount of helium in the gas mixture. It also appears that the yields of C_2H_4 and BTX will be going through a maximum, since the yields with pure helium are much lower than with the mixtures of CH_4 and He. The data in Table 2 indicate that the effect of the helium concentration in the gas mixture on C_2H_4 and BTX yields is more pronounced at high methane-to-coal ratios than at low methane-to-coal ratios.

Figure 3 shows the effect of the methane flow rate on the yield of ethylene at a constant coal flow rate of 1.0-1.2 lb/hr. The curves for the three different gas mixtures used in our experiments, which contained 6, 12 and 25% helium by volume, all follow similar trends. For all gas mixtures, C_2H_4 yield increased with the flow rate of methane. It is seen from Figure 3 that for a given methane flow rate, the yield of C_2H_4 increased with the helium content of the gas mixture. If the increased ethylene yield came from the pyrolysis of methane alone, i.e., if the ethylene yields were additive, an effect opposite to this would have been noticed. A similar trend is noted in Table 3 with respect to BTX yield. Thus, there is greater selectivity in the production of ethylene and BTX in the presence of He/CH_4 than in the presence of either pure He or pure CH_4. This indicates an attractive process application for the production of ethylene and BTX from coal via Flash Methanolysis.

ACKNOWLEDGEMENT

We gratefully acknowledge the support provided by the Advanced Research and Technology Development Program of the U.S. Department of Energy, Morgantown Energy Technology Center, Morgantown, W. Virginia.

REFERENCES

1. Steinberg, M., Fallon, P. T., and Sundaram, M. S., "Falsh Pyrolysis of Coal with Reactive and Non-Reactive Gases." Report to DOE, No. DOE/CH/00016-1402 (DE 833011264). Available from NTIS, Springfield, Va., 22161.

2. Sundaram, M. S., Steinberg, M., and Fallon, P. T., "Flash Pyrolysis of Coal in Non-Reactive Gases." BNL 35947, ACS Div. Fuel Chem., Prepr. 30(1), 231 (1985).

REFERENCES (cont.)

3. Falk, A. Y. and Schuman, M. D., "Advancement of Flash Hydrogasification." Proc. 5th Ann. Gasification Projects Contractors' Meeting, p. 338, June 1985.

4. Sundaram, M. S., Steinberg, M., and Fallon, P. T., "Flash Hydropyrolysis of Coal for Conversion to Liquid and Gaseous Fuels: Summary Report," DOE/METC/82-48 (1982).

5. Sundaram, M. S., Steinberg, M., and Fallon, P. T., "Enhanced Ethylene Production Via Flash Methanolysis of Coal," ACS Div. Fuel Chem., Prepr. 29(2), 124 (1984).

6. Sundaram, M. S. and Steinberg, M., "Flash Methanolysis of Coal: A Mechanistic Study." Submitted to Fuel, BNL 37302 (July 1985).

Figure 1

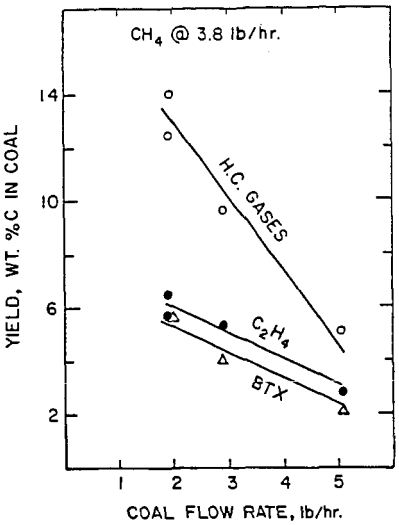

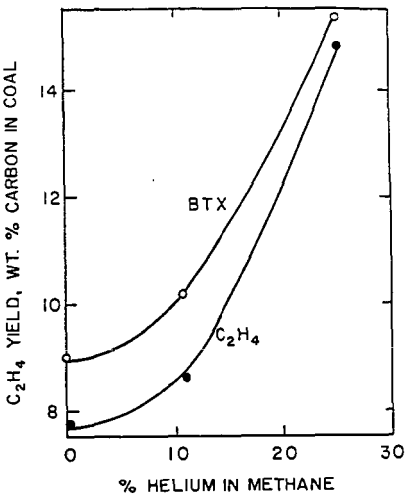

Figure 2

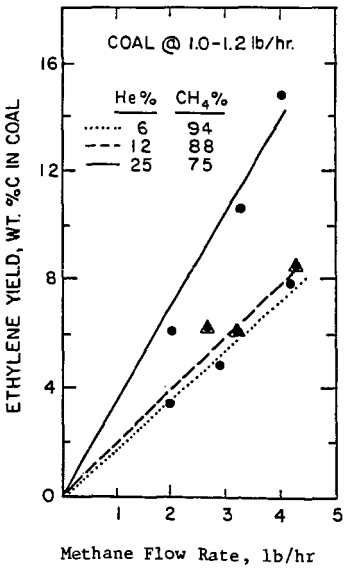

Figure 3

Figure 1. Effect of Coal Flow Rate on C_2H_4 and BTX yield

Figure 2. Effect of Helium Concentration in Methane on C_2H_4 yield

Figure 3. Effect of Gas Composition and Methane Flow Rate on C_2H_4 yield

PREDICTING DEVOLATILIZATION AT TYPICAL COAL COMBUSTION CONDITIONS WITH THE DISTRIBUTED-ENERGY CHAIN MODEL

By

Stephen Niksa
Mechanical Engineering Department
Stanford University
Stanford, CA 94305

and

Alan R. Kerstein and Thomas H. Fletcher
Combustion Research Facility
Sandia National Laboratories
Livermore, CA 94550

INTRODUCTION

Hypothetical ultimate yields for rapid coal devolatilization arose from the historical notions that a well-defined amount of volatile precursors are present in coal, and that their rate of release is directly proportional to a decaying reactant concentration. However, as reviewed elsewhere(1,2), wet chemical and spectroscopic analyses of coal structure from the past decade suggest a far less direct relationship between the reactive species in coal and the pyrolysis products. According to the aromatic/hydroaromatic model, bituminous coals are composed of aromatic "nuclei" interconnected by various bridges and substituted with smaller functional groups on their periphery. Although there is no well-defined repeating unit, bituminous coal is an extensively crosslinked macromolecular network which swells on solvation and exhibits viscoelasticity(3).

The aromatic/hydroaromatic model suggests three broad classes of chemical reactions: dissociation of bridges, recombination of nuclei, and elimination of peripheral groups. When peripheral groups present initially are converted to light gas, there is a direct correspondence between their initial concentrations and ultimate gas yields. But in contrast, when a bridge breaks, tars do not form at a rate governed by stoichiometric proportions, and furthermore, there is no predetermined concentration of tar precursors, per se, present initially in the coal. In depolymerizations, stoichiometric proportionalities are replaced by probabilities assigned from molecular conformation; i.e., the spatial arrangement of the atoms in s molecule(4). The probabilities relate the fragment size distribution to the concentration of unbroken bridges in the network, independent of the chemical reaction rates. During devolatilization, nuclei disconnect and recombine concurrently, and many fragments never become small enough to vaporize. Tar and char yields are determined by competitive kinetics which depend on complex conformational probabilities as well as chemical reaction rates. Each nucleus can become either tar or char, depending on the transient conditions for the competition. The fate of nuclei is not predetermined, as implied in formulations which include hypothetical ultimate yields for tar and char. Moreover, the disintegrating macromolecular skeleton of coal and the reintegration of intermediates into char are not taken into account in the historical notions mentioned above, nor in any of the available devolatilization rate models.

We formulated the Distributed-Energy Chain Model (DISCHAIN) to account for the conformational aspects of coal depolymerization and char formation in a phenomenological way. The derivation of the model and the qualitative mechanisms for product formation have been described(5). Rate parameters have been specified by correlating transient weight loss from a bituminous coal over a broad range of thermal histories for heating rates to 10^3K/s and temperatures to 1300K(6). In the present study, predictions from DISCHAIN are compared with volatiles yields from very similar bituminous coals for heating rates between 10^3 and 10^5K/s and temperatures between

800 and 2100K. No further adjustments of any of the parameters in the model have been made. Nevertheless, predicted yields and reaction times differ significantly among the comparisons, reflecting the influence of the different transient histories in the cases considered.

PRODUCT FORMATION FOR VARIOUS HEATING RATES

Chain statistics introduce several novel qualitative features into the formation mechanism for devolatilization products. In DISCHAIN, the monomer formation rate is not directly proportional to either the bridge dissociation or the char formation rate. Limiting cases establish that (1) the conversion of bound aromatic units into monomers accelerates with progressive bridge dissociations, regardless of the chemical reaction rate for bridge dissociation, and (2) the number of char links needed to eliminate all monomers is less than the original number of monomers. Most important, the formation of stable char links is concurrent with the disintegration of bridges during slow heating. This inhibits the subsequent formation of monomers, thereby accounting for reduced yields for lower heating rates.

The mechanistic basis for yield enhancement at faster heating rates in DISCHAIN is not solely the disparity of the activation energies for tar and char formation. Rather, the heating rate dependence is the joint result of the competition between the processes of char and tar formation in conjunction with suppression of monomer generation due to char formation. The activation energy disparity determines the selectivity to tar and char from the common intermediate; i.e., monomer. Independently, chain statistics determine the conversion of the bound aromatic units into the intermediate. Obviously, bound aromatic units which never become monomers are excluded from the competition between char and tar formation.

To further illustrate the role of monomer selectivity, predicted tar yields at four heating rates are shown in Figure 1. In these simulations, the thermal histories are linear temperature ramps at the indicated heating rates to 1900K. The onset of devolatilization moves to higher temperatures for greater heating rates, due to kinetic restraints(7). The devolatilization rate increases in rough proportion to increases in the heating rate. Reaction time constants range from 3 s at 10^2K/s to 5 ms at 10^5K/s. Each transient yield reaches an asymptote while the temperature ramp is being traversed, even at 10^5K/s.

Faster heating tends to preclude char formation, which increases the monomer selectivity, and higher temperatures shifts the selectivity to tar formation. Consequently, ultimate tar yields increase by 70 % over this range of heating rates. Since the mass of aromatic units distributed between char and tar is fixed, char yields are decreasing throughout this range of conditions. Gas yields, which are not shown, are fixed at 8%, although at 10^5K/s, peripheral groups are transported away with tar before they can be eliminated as gases. Product distributions consisting of tars but no light gases have actually been observed during laser pyrolysis at very high heating rates(8).

COMPARISONS WITH TRANSIENT CONVERSION MEASUREMENTS

Predictions from DISCHAIN are compared with three sets of data for single-particle, transient devolatilization of high volatile bituminous coals for a broad range of thermal histories. In Bautista's wire grid study of vacuum pyrolysis, thermal histories consist of uniform heating at 10^3K/s to temperatures between 750 and 1200K, followed by sufficiently-long reaction times to observe ultimate yields at each temperature(9). In Kobayashi's entrained-flow study of pyrolysis at atmospheric pressure, the operating conditions encompass heating rates between 10^4 and 10^5K/s and temperatures between 1000 and 2100K(1). Time-temperature histories are based on calculations which account for mixing between the dilute coal jet and the preheated coaxial gas stream. In Midkiff et al.'s study of an excessively fuel-rich stabilized coal flame, the nominal heating rate is 10^5K/s and the ultimate temperature is 2000K(11).

The different pressures in these studies may seem objectionable in light of significant reductions in yield for pressures between vacuum and a few atmospheres. Many models invoke competing mass transport and redeposition of tar from the gas phase within and around the particles to rationalize this effect, but this basis is inconsistent with measured tar deposition rates and time scales for volatiles escape. Only a summary explanation is given here, as additional detail is given elsewhere(6).

Vaporization mechanisms determine which heavy compounds leave the condensed phase, depending on the molecular weight, temperature, and pressure. DISCHAIN presumes instantaneous vaporization and escape of all tars formed when monomers dissociate, which is a limiting form for low pressures if volatiles escape by viscous flow. Therefore, the model applies to vacuum pyrolysis regardless of temperature, and to pyrolysis at atmospheric pressure, provided that temperatures are high enough to compensate for the influence of pressure on tar vaporization. Regarding the assumed instantaneous vaporization of tar, the equilibrium vapor pressure of heavy compounds increases rapidly with increasing temperature, so that this assumption is well satisfied throughout the combustion temperatures in both of the selected studies at 1 atm. Based on an equilibrium vapor pressure law for coal liquids(12), the ratio of the vapor pressure and the internal pressure are identical at 1000K and an internal pressure of 1 atm, and at 1250K and an internal pressure of 10 atm.

Predicted product distributions for gas, tar, char, and unreacted coal are compared with measured yields of gas and total weight loss for vacuum pyrolysis in Figure 2. The simulations are based on uniform heating at 10^3K/s to the stated reaction temperature, followed by an isothermal reaction period between 6 and 30 s, depending on reaction temperature. In all cases, ultimate yields were reached before the end of the experimental reaction time. Model predictions were converted to the daf-basis with a reported ash content of 9.2 %.

The relative yielda of tar and gas are reliably predicted only beyond 900K, while predicted and measured weight loss differ by several percent at temperatures below 1000K. The predicted temperature dependence is more consistent for tar yields than for gas yields. Predicted yields for unreacted coal and char seem reasonable, but cannot be assessed quantitatively. Unreacted coal persists through 1000K as a result of the broad range of dissociation energies for bridges. The amount of char increases monotonically throughout this temperature range, but exhibits a maximum for higher temperatures and heating rates.

In succeeding comparisons, only weight loss is shown because gas phase chemistry alters the product distribution at high temperatures. The product distributions from DISCHAIN constitute flux conditions for detailed modeling of the rate phenomena in the vicinity of the particles, rather than conditions in the free stream.

The comparison for the atmospheric entrained flow study appears in Figure 3. The simulations are based on thermal histories calculated by Kobayashi which account for mixing effects near the injector(10). These thermal transients are significantly longer than for an individual particle injected into a quiescent gas at the reactor temperature, as expected. Also shown in Figure 3 are correlations from the competing two-step model(10). Kobayashi assigned rate parameters in order to fit these data; in contrast, rate parameters from DISCHAIN were not readjusted from the values assigned from data at much slower heating rates and lower temperatures.

Predicted weight loss is within the experimental error at both the extremes in temperature, but several percent too high at 1510K and 1260K (not shown). Predicted reaction time scales are as reliable as those from the correlation assigned from this data. Also, the predicted ultimate yield of 62 % at 2100K is substantially greater (15 % daf) than the greatest value in the data set used to assign the parameters in DISCHAIN (47 % 10^3K/s and 1300K). Moreover, it is 22 % daf greater than the measured yield at 10^2K/s and 1300K (12). Since the parameters have not been adjusted, these yield enhancements can be attributed to the influence of heating rate. as described in the previous section.

The final comparison involves a stabilized one-dimensional coal flame(11). Factors beyond devolatilization arise in coal flames, but most complications are absent under excessively fuel-rich conditions. The coal density was 470 mg/l, corresponding to fuel equivalences of 3.30 with respect to the whole coal and 1.34 with respect to the ASTM proximate volatile matter. All oxygen was consumed before one-third of the ultimate volatiles yield was observed, and heterogeneous oxidation was negligible.

Complete transient thermal histories, from the point of injection to the onset of devolatilization, have not yet been measured for any coal flame, including this one. Midkiff, et al. report transient weight loss, gas temperatures, and optically-determined particle temperatures on a time coordinate referenced to the first measurement point, rather than the point of injection. The first reported temperature, 1750K, exceeds the threshold for devolatilization at heating rates as fast as 10^7K/s (DISCHAIN predicts that devolatilization begins at 1250K for a heating rate of $2x10^5$K/s; c.f. comparison with Kobayashi's data at 1940K in Figure 3). Therefore, a simulated thermal history, instead of the measured particle temperatures, has been used to obtain the predictions discussed below.

Predicted weight loss is compared to the sum of the measured losses of volatile matter and fixed carbon in Figure 4. The thermal history in the simulations consists of uniform heatup at 10^5K/s to 2000K, the ultimate temperature observed in the experiment. The time coordinate for the predictions and measurements is referenced to the onset of devolatilization. The reaction time scale is adequately described, but the predicted ultimate yield exceeds the measurements by 5 %. However, soot was observed but not separated from the collected char samples, so the measured yields are less than the true values. An upper bound for this influence far exceeds the discrepancy in this comparison, as Nenninger et al. observed soot yields of 22 % from the high temperature pyrolysis of a high volatile bituminous coal(13).

CONCLUSIONS

The accuracy of the predicted reaction time scales and yields from DISCHAIN is significant because hypothetical ultimate yields are absent, model parameters were not adjusted, and a wide range of thermal histories was spanned in the comparisons with data. Experimental errors necessarily increase as coal combustor conditions are approached. Nevertheless, this evaluation is more stringent than previous comparisons between devolatilization models and measurements, and provides the basis for the following conclusions:

1. Bridge dissociation concurrent with char formation diminishes the conversion of bound aromatic nuclei in coal into unattached tar precursors, which constitutes a mechanistic basis for enhanced yields for faster heating rates.

2. Predicted yields based on the same parameters ranged from 40 % at 10^2K/s and 1300K to 62 % at 10^5K/s and 2100K, in agreement with measured yields at the respective conditions within the experimental error.

3. Predicted reaction times and yields from DISCHAIN agree quantitatively with transient measurements from high volatile bituminous coals for heating rates between 10^3 and 10^5K/s and reaction temperatures between 800 and 2100K.

REFERENCES

1 Gavalas, G.R., "Coal Pyrolysis," Elsevier, New York (1982).

2 Davidson, R.M., "Molecular Structure of Coal," IEA (Rep. No. ICTIS/TR 08), London, 1980.

3 Larsen, J.W., in "Coal Science," R.A. Meyers, Ed., Academic Press, NY (1982).

4 Tanford, C., "Physical Chemistry of Macromolecules," John Wiley and Sons, New York (1961).

5 Niksa, S. and Kerstein, A.R., Combust. Flame, to appear (1986).

6 Niksa, S., Combust. Flame, to appear (1986).

7 Niksa, S., Heyd, L.E., Russel, W.G., and Saville, D.A., Twentieth Symp. (Int.) on Comb., The Combustion Institute, Pittsburgh (1984), p. 1445.

8 Ballantyne, A., et al., Final Report prepared for the U. S. Dept. of Energy, Pittsburgh Energy Technology Center, Contract No. DE- AC22-84PC30291, October, 1983.

9 Bautista, J.R., "Time-Resolved Product Distributions of Softening Coals," Ph.D. Thesis, Department of Chemical Engineering, Princeton University, Princeton, NJ (1984).

10 Kobayashi, H., "Devolatilization of Pulverized Coal at High Temperatures," Ph.D. thesis, Department of Chemical Engineering, MIT, Cambridge, MA (1976).

11 Mickiff, K.C., Altenkirch, R.A., and Peck, R.E., Paper No. 1- 2A, CSS/WSS Joint Technical Mtg., Combustion Institute, San Antonio, TX (1985).

12 Unger, P.E. and Suuberg, E.M., Fuel 63:606 (1984).

13 Nenninger, R. D., Howard, J. B., and Sarofim, A. F., Proc. Int'l. Conf. on Coal Science, p. 521, IEA, Pittsburgh, PA (1983).

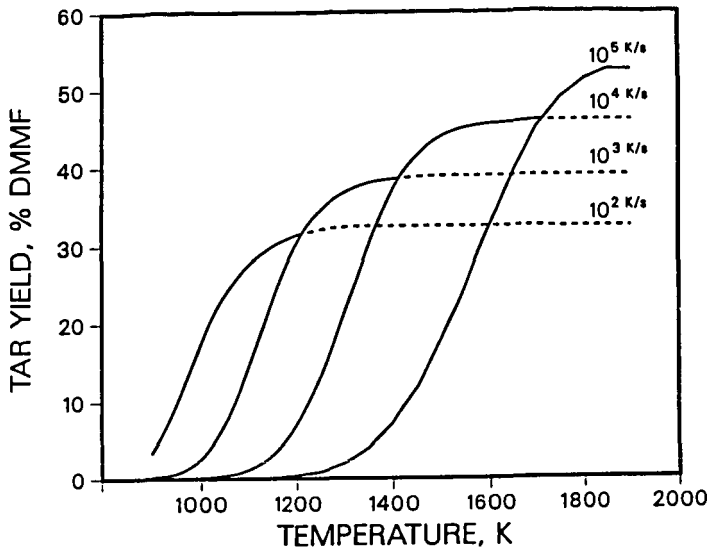

Figure 1. Predicted transient yields for tar during heatup at 10^2, 10^3, 10^4, and 10^5K/s along a linear temperature ramp to 1900K.

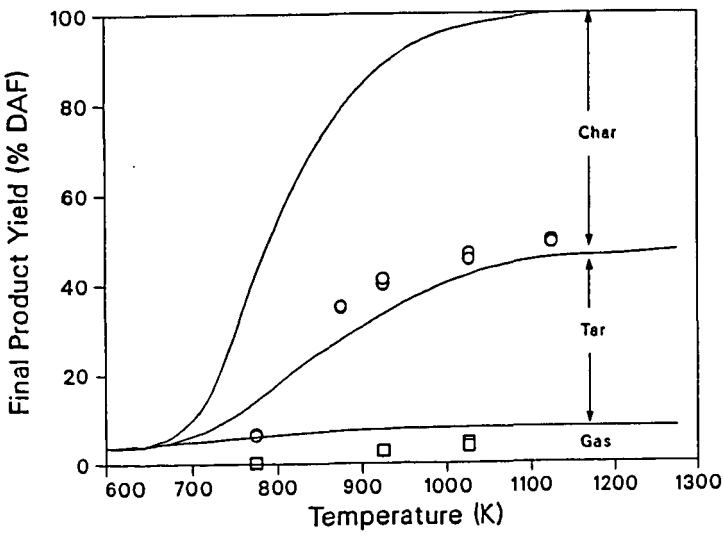

Figure 2. Comparisons between predicted and measured weight loss (○) and gas yields (□) from vacuum pyrolysis of Pittsburgh seam bituminous coal, from Bautista[16].

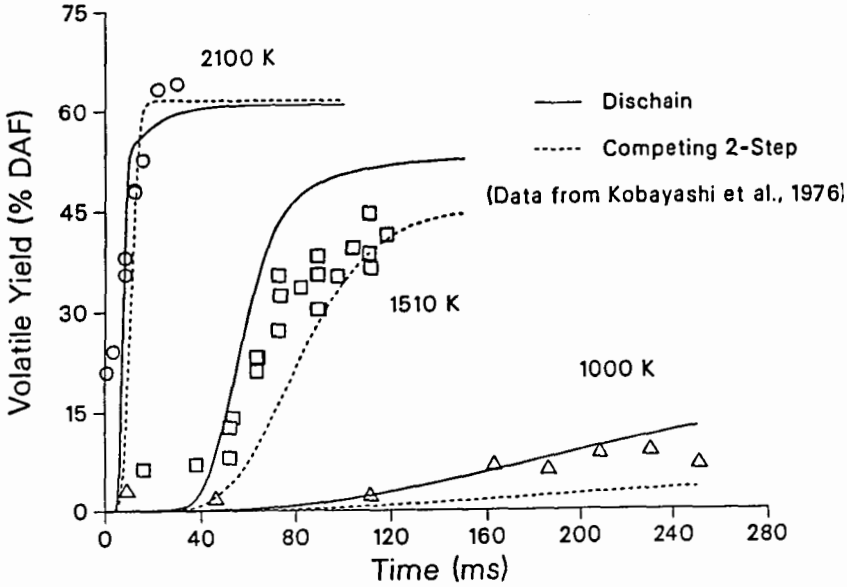

Figure 3. Weight loss observed in an atmospheric entrained flow reactor by Kobayashi[17] compared to predictions from DISCHAIN (solid curves) and from Kobayashi's[6] competing two-step model (dashed curves).

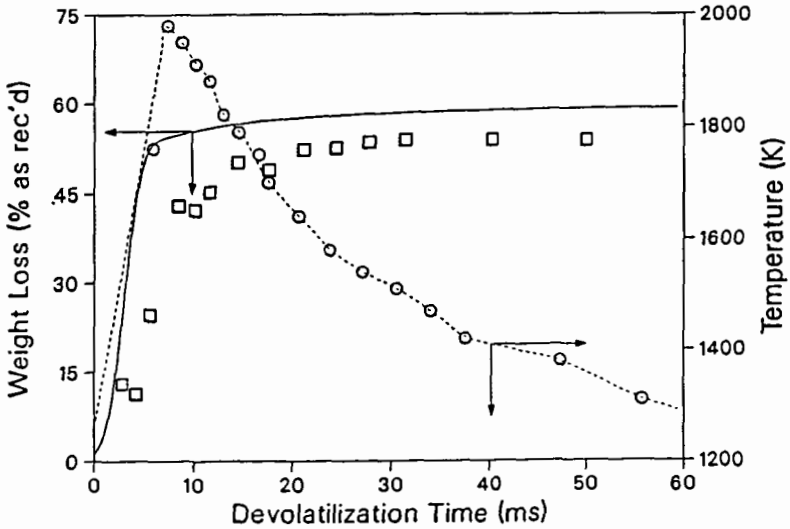

Figure 4. Predicted weight loss (solid line) for uniform heating at 10^5K/s to 2000K compared to the sum of losses of volatile matter and fixed carbon (□) reported by Midkiff, et al.[18]. The simulated temperature profile (dashed line) includes optically-measured particle temperatures (○) during the cooling phase.

ADVANCED COAL GASIFICATION AND DESULFURIZATION WITH CALCIUM BASED SORBENTS

J. Weldon, G. B. Haldipur, D. A. Lewandowski, K. J. Smith

KRW Energy Systems Inc.
Madison, PA 15663

1.0 ABSTRACT

In-bed desulfurization using calcium based sorbents has been evaluated in the KRW pressurized fluidized bed gasifier as part of a joint program with KRW Energy Systems Inc. and the U. S. Department of Energy. For combined cycle power generation or synthesis gas applications such a system has large potential economic advantages over second generation gasifiers which use conventional cold gas cleanup.

In addition to achieving over 90% desulfurization, the process has also demonstrated significant gains in cold gas efficiency and fines consumption. Pilot plant performance data are presented for the KRW gasifier-desulfurizer process and the preliminary results of an in-bed waste characterization study are also presented. Though untreated in-bed wastes contain potentially hazardous calcium sulfide, laboratory-scale tests have shown that roasting processes can be adapted for converting the waste to a non-hazardous form.

2.0 INTRODUCTION

The production of low-Btu (120-160) Btu/scf gas from coal for use in combined cycle power generation is attractive to the utility industry because the feedstock is an abundant domestic natural resource and because it offers economic advantages over conventional coal fired steam plants.(1)

Conventional stack gas clean-up technologies are proving to be capital expensive and have the added disadvantage of poor thermal efficiency. In-bed clean-up with calcium sorbents offers an effective and economical method of removing the sulfur species from the product gas without pre-cooling. The particulate free hot gas can then be used directly in a gas turbine providing improved overall process efficiency.

The market incentive for an economical coal gasification combined cycle electric power generating plant will be substantial in the 1990's. According to the U. S. Department of Energy (1), 18% of the current U. S. generating capacity is greater than 25 years old. The KRW coal gasification combined cycle hot gas cleanup process is ideally suited to the needs of the electric power industry in the 1990's on the basis of environmental, cost and plant size considerations.

3.0 BACKGROUND

3.1 KRW Coal Gasifier

The KRW gasifier is a pressurized fluidized bed process which can convert a variety of solid carbonaceous feedstocks into low-Btu (100-160 Btu/scf) or medium-Btu (200-300 Btu/scf) gas. The essential features of the gasifier are shown in Figure 1. Run-of-mine coal or lignite in the size range of 1/4-inch x 0 is surface dried, pressurized in lockhoppers, and injected concentrically into a high energy oxidizing jet located in the combustion zone. The coal is rapidly devolatilized and decaked, and the residual char is gasified by steam in the upper region of the fluidized bed. The jet induces a vigorous toroidal motion of solids between the lower heat producing combustion region and the upper heat consuming gasification region. The coal ash undergoes partial melting and sintering in the hotter combustion jet, and the resulting 'glue' action causes fine ash particles to agglomerate. These ash agglomerates are separated from the char in a fluidized bed

separator located in the bottom section of the gasifier, are cooled with recycle gas, and are extracted by means of a rotary feeder and depressurizing lockhoppers. Fines elutriated from the gasifier are captured in an external cyclone and recycled directly to the gasifier by means of a nonmechanical valve. Fines escaping the cyclone are captured in a full-flow sintered metal filter. This filter is capable of operation up to 1200°F and removing all fines one micron or greater in size. The gasifier may be operated either in the air-blown mode for low-Btu gas (100-160 Btu/scf) or in the oxygen-blown mode for medium-Btu fuel or synthesis gas (200-300 Btu/scf).

The process has been demonstrated for a wide range of feedstocks and conditions at the Waltz Mill 15-30 tons/day Process Development Unit (PDU) under funding by the DOE and its predessor agencies. In addition to its ability to process a variety of feedstocks, the process has also demonstrated effective utilization of coal fines, high overall carbon conversion efficiency, and virtual elimination of tar and oil in the product gas.

3.2 In-Bed Desulfurization

In-bed desulfurization has been identified as a potential hot gas cleanup concept for meeting environmental regulations on sulfur emissions from the KRW gasifier. Such a system would have economic advantages over cold gas clean-up in a coal gasification combined cycle power generation application. KRW has conducted four in-bed PDU tests in 1984 and 1985 to demonstrate the feasibility of this concept. In addition to achieving over 90% desulfurization to meet the New Source Performance Standards for sulfur emissions, the process cold gas efficiency improved by 20% over conventional PDU gasifier operation.

Hot gas clean-up via the in-bed concept involves the removal of sulfur bearing gases, H_2S and COS, by reacting them with dolomite ($CaCO_3.MgCO_3$) or limestone ($CaCO_3$) to form sulfided or spent sorbent (CaSMgO or CaS). Sorbent is fed into the gasifier freeboard to mix with the the bed char and remove H_2S and COS from the product gas. The spent sorbent is eventually withdrawn through the gasifier annulus along with ash agglomerates.

The overall reaction occurring in the gasifier bed is:

$$CaCO_3(MgCO_3) + H_2S \rightarrow CaS(MgO) + 2CO_2 + H_2O \qquad 1)$$

for the dolomite/hydrogen sulfide reaction, or similarly:

$$CaCO_3 + H_2S \rightarrow CaS + CO_2 + H_2O \qquad 2)$$

for the limestone/hydrogen sulfide reaction. Calcium sulfide (CaS) is a reactive waste which can recombine with acidic water to release toxic H_2S gas. Further treatment is necessary to convert the CaS to the environmentally acceptable sulfate:

$$CaS + 2\ O_2 \rightarrow CaSO_4 \qquad 3)$$

The primary goal of oxidation is to reduce the activity of the sulfide with the environment and render the waste non-hazardous. The waste could then be disposed of in conventional solid waste landfills.

4.0 DESULFURIZATION PERFORMANCE

The development program has comprised a series of PDU tests to first demonstrate gasifier operability and, thereafter, to optimize the desulfurization process. During tests TP-036-1 and TP-036-2, the gasifier was successfully operated with dolomite injection in a controlled and balanced manner. The subsequent tests, TP-036-3 and TP-036-4, demonstrated that high levels of desulfurization could be achieved with both dolomite and limestone sorbents. Table 1 summarizes the significant achievements of the in-bed desulfurization program.

TABLE 1. SUMMARY OF KRW IN-BED DESULFURIZATION RESULTS*

Coal Type	Coal Sulfur Content (%)	Sorbent Type	H_2S (ppm)	COS (ppm)	Ca/S Molar Feed Ratio	Steady State Desulfurization Achieved (%)
Pgh. #8	2.3	Glass Dolomite	550	263	1.67	86
Pgh. #8	4.5	Glass Dolomite	679	216	1.55	92
Pgh. #8	4.5	Greer Limestone	651	258	1.84	90
Wyoming	2.0	Glass Dolomite	484	167	2.0	91

*preliminary

The equivalent desulfurization for limestone injection into conventional furnaces and atmospheric fluidized bed combustors (AFBC) require Ca/S molar feed ratios of 3 to 6 (2, 3) compared to the ratios of 1.5 to 2.0 demonstrated by the KRW process. The advantages of desulfurization in the reducing gasifier environment are attributed to the faster rate of hydrogen sulfide/calcium oxide reaction compared to the sulfur dioxide/calcium reaction and the absence of sintering. Sintering is indicated by low BET surface areas (4). Sorbent surface area measurements of the bed material were relatively high at 10-40 m^2/g compared to typical calcine surface areas which range from 0.5 to 40. m^2/g for calcined carbonates (5). The reducing environment apparently does not increase sintering.

PDU results indicate desulfurization is a function of the sulfur input rate and output rate. The sulfur species concentrations in the product gas were characteristically in the range of 500-650 ppm for H_2S and 160-270 ppm for COS for large variations in feedstock sulfur content. Since the sulfur output rate is limited, the degree of desulfurization increases as the sulfur input rate (coal sulfur content) increases.

Desulfurization varies inversely with product gas steam concentration based on recent PDU tests. A negative correlation coefficient of 0.8 was found linking steam and hydrogen sulfide concentrations for the KRW Data Base. Equilibrium effects via the reaction

$$H_2S + CaO \leftrightarrow CaS + H_2O \quad 4)$$

are probably negligible because the value of the equilibrium constant is so large for gasifier temperatures in the range of 1600 to 1900°F (6). In fact, H_2S concentrations were generally on the order of 200-400 ppm higher than equilibrium levels, so it seems improbable that equilibrium limits desulfurization. (If, however, gas phase diffusion of H_2O from the reacting core is the limiting rate the equilibrium concentrations of H_2S in the particle core may limit desulfurization). KRW investigations of the mechanism by which H_2O limits desulfurization are currently underway.

Small incremental increases in desulfurization were also achieved with large increases in the calcium/sulfur feed ratio as shown in Table 2.

Table 2
Incremental Increase In Desulfurization as a
Function of Ca/S Ratio for Pgh. 4.5% Sulfur Coal

Ca/S Feed Ratio	Observed % Desulfurization	Observed H_2S ppm	Equilibrium H_2S ppm
1.84	91	651	180
3.41	94	424	242

These results differ significantly from fluidized bed combustor experience where desulfurization is directly proportional to and highly dependent on the Ca/S feed ratio.

5.0 WASTE CHARACTERIZATION

Because of the complexity of environmental regulations, an investigation of waste characterization testing and disposal laws' was conducted. Section 3001 of the RCRA directs the EPA to promulgate criteria for identifying and listing hazardous waste. In a large number of cases, it is possible to determine a wastes classification by its specific exclusion or identification as a hazardous waste. For other wastes, the EPA has prescribed tests to determine whether it possesses one of four hazardous characteristics - corrosivity, ignitability, reactivity, and extraction procedure (EP) toxicity. Since coal gasification wastes are not on any of the promulgated hazardous wastes lists by specific and nonspecific sources, it is the responsibility of the generator to determine if the released waste possesses any of the four hazardous characteristics.

Reactivity and EP toxicity are the most critical characteristic for in-bed waste disposal. Presently, the EPA has not yet promulgated a test procedure or a quantitative threshold for toxic gas generation reactivity. During the interim they have recommended a draft test method and interim reactivity thresholds

(7, 8). The quantitative threshold for the total available sulfide measured via the draft test method is 500 mg evolved H_2S/Kg waste when subjected to an acid leach (ph = 2.0) for 30 minutes. Wastes releasing more than that level may be regulated as hazardous.

Unsulfated in-bed solid waste samples from the fines loss, separator pit sludge and gasifier discharge were analyzed for reactive sulfide levels and EP toxicity. Table 3 contains typical EP toxicity test results.

TABLE 3. TYPICAL RCRA EP TOXICITY TEST RESULTS OF KRW IN-BED DESULFURIZATION SOLIDS WASTES (mg/ℓ)

Metal	Ag	As	Ba	Cd	Cr	Hg	Pb	Se
Maximum Allowable Concentration	5	5	100	1.0	5.0	0.2	5.0	1.0
Gasifier Discharge	0.03	0.048	<0.1	<0.005	0.03	<0.03	<0.002	<0.004
Fines Loss	0.01	0.068	0.4	<0.005	<0.01	<0.03	0.012	0.009
Separator Pit Sludge	0.01	0.002	0.6	<0.005	<0.01	<0.03	<0.002	<0.004

The level of EP toxic metals in samples taken during TP-036-3 and TP-036-4 were all significantly below the RCRA toxic levels.

Typical reactive sulfide levels for the in-bed process are shown in Table 4.

TABLE 4. REACTIVE SULFIDE TEST RESULTS FOR KRW IN-BED DESULFURIZATION SOLID WASTES FROM TP-036-3

Sample	Sulfide Wt %	Reactive Sulfide (mg/kg)
Untreated Gasifier Discharge	8.6	>1200
Fine Loss	1.3	<5
Separator Pit Sludge	0.9	<5

The fines loss samples from the process had extremely low reactive sulfide levels of less than 5 ppm. Separator pit sludge, which consists of wet fines carryover from the quench/cooling system, also had less than 5 ppm reactive sulfide. However, all untreated PDU withdrawal wastes generated during TP-036-3 sorbent injection may be potentially hazardous when subjected to the interim EPA reactivity test.

As part of an extensive study of the characteristics of in-bed wastes, the gasifier discharge material was sulfated in laboratory scale reactors under a variety of experimental conditions. Table 5 summarizes the reactor conditions, reactive sulfide levels, and sulfur analysis of several samples.

TABLE 5. EXPERIMENTAL CONDITIONS, SULFUR ANALYSIS AND REACTIVE SULFIDE LEVELS OF SULFATED GASIFIER DISCHARGE

Reactor Type	Furnace Temp. (°F)	Oxygen Concen. (Vol %)	Gas Flow Rate (liters/min)	Contact Time (hrs)	Reactive Sulfide (mg/kg)	Total Sulfur (Wt%)	Percent Sulfation (mole %)
Packed Bed	1500°F	21	5	1	5	5.00	80.7
Fluidized Bed	1500°F	5	>10	1	<5	NM	NM
Open Dish	1500°F	21	0	1	<5	7.48	63.4
Open Dish	1500°F	21	0	3	<5	8.02	74.0

NM - Not Measured

The configuration and experimental conditions tested were adequate for reducing the reactive sulfide levels of the withdrawal sample to less than 500 mg/kg. These results are encouraging for the in-bed program because sulfation is the simplest and most direct method of treating in-bed wastes. Further studies of reaction kinetics are necessary to determine the optimal conditions for sulfation of the in-bed wastes to meet RCRA requirements. Tests are underway at the PDU to evaluate the technical feasibility of a continuous waste treatment process.

6.0 GASIFIER PERFORMANCE

Gasifier performance was observed to improve during in-bed testing. The results of those set points in which gasifier performance was significantly enhanced due to sorbent injection are shown for tests TP-036-3 and TP-036-4 in Table 6.

TABLE 6. PILOT PLANT PERFORMANCE WITH IN-BED DESULFURIZATION

Coal	Sorbent	Air/ Coal (lb/lb)	Gasifier Bed Temp. (°F)	Carbon Conversion Efficiency (%)	Cold Gas Efficiency (%)
Pittsburgh	--	4.28	1846	90	50
Pittsburgh	Dolomite	3.39	1950	90	73
Pittsburgh	Dolomite	3.37	1970	91	72
Pittsburgh	Limestone	3.27	1830	92	70
Wyoming	Dolomite	3.03	1820	91	65

Results from set points without sorbent injection are also shown for comparison. The benefits of sorbent injection are an increase in the cold gas efficiency and a decrease in the apparent fines elutriation rate.

Cold gas efficiencies increased dramatically during in-bed desulfurization from 50 to 70%. The increase in cold gas efficiency and corresponding drop in air/coal ratio may indicate improved gasification.

The catalytic effect of calcium on gasification rates has been documented by Walker (9), Freund (10), and Van Heek and Muhlen (11). Freund (9) found calcium catalyzed carbon reacted at a rate 100 times the rate of uncatalyzed carbon for the gasification of CO_2. Catalytic effects are one of several potential contributing factors being investigated by KRW.

Fines loss rates and elutriation decreased dramatically with the bed weight of the gasifier/desulfurizer as shown in Figure 2. Increasing bed weight reflects the replacement of low density char (25 lb/ft^3) by high density sorbent (80 lb/ft^3) and the reduction of bed voidage. Reduced fines loss and elutriation rates are primarily the result of increased gasification rates and longer fines residence times. Improved gasification is attributed to the presence of the calcium based sorbents in the bed. Low bed voidage indicates low gas bypassing as bubbles. Fluidized bed filtering of fine material increases with decreased gas bypassing (12). The filter mechanism increases the fines residence time in the bed so that a larger portion is consumed before escaping the bed surface.

7.0 CONCLUSIONS

In-bed desulfurization integrated with hot particulate removal is potentially the most economical fossil energy process for converting all types of U.S. coals to electricity while complying with New Source Performance Standards (NSPS) for sulfur removal.

The in-bed program for direct injection of calcium-based sorbents into the KRW gasifier has demonstrated

- desulfurization exceeding 90% for a 4.5% sulfur coal
- cold gas efficiencies over 70%
- feasible waste treatment by sulfation

Future development work at KRW includes pilot-scale sulfation of the gasifier discharge and demonstration of through put improvements. Laboratory scale investigations of desulfurization and the effect of calcium-based sorbents on char gasification will be conducted in parallel with the pilot plant testing to determine the controlling mechanisms for the relevant reactions.

KRW is also developing an external bed desulfurization system using zinc ferrite sorbent which is capable of removing sulfur compounds in a hot (1100°F) coal gas stream to a level of 10ppm. Installation and testing of the external bed desulfurization system is currently underway at the KRW Process Development Unit.

REFERENCES

1. Pitrillo, (Director, U. S. DOE's Morgantown Energy Technology Center) "A view of the Future. Technical Choices of the Utility Industry -- Power and Fuel Mix Alternatives". Keystone Energy Future Project, February 4, 1986.

2. Green, O. P. "The Utility Perspective on Dry SO_2 Control Technologies". First Joint Symposium on Dry SO_2 and silmultaneous SO_2/NO_x Control Technologies. November 13-16, 1984, San Diego, CA.

3. Keairns, D. L., et. al. Chemically Active Fluid Bed for SO_x Control: Vol I. Process Evaluation Studies. EPA-600/7-79-158a, December 1979.

4. Borgwardt, R. H. "EPA Experimental Studies of the Mechanisms of Sulfur Capture by Limestone". First Joint Symposium Dry SO_2 and Simultaneous SO_2/NO_x Control Technologies. November 13-16 1984, San Diego, CA.

5. Borgwardt, R. H. "Properties of Carbonate Rocks Related to SO_2 Reactivity". Environmental Science and Technology, Vol. 6, No. 4, April 1972.

6. Spencer, J. Sulfidation of Half-Calcined Dolomite in Hydrogen-Sulfide/Deuterium/Water/Nitrogen-2 -- Kinetics, Structure and Mechanisms. Carnegie-Mellon University. PH.D., 1985.

7. "Interim Methods for Toxic Gas Generation Reactivity". Office of Solid Waste and Emergency Response. U.S. EPA, Washington, D.C., July, 1985.

8. "Test Method to Determine Hydrogen Sulfide Released from Wastes". Office of Solid Waste and Emergency Response. U.S. EPA, Washington, D.C., July 1985.

9. Walker, P.L. et. al. "Catalysis of Gasification of Coal Derived Cokes and Chars". Fuel, Vol. 62, February, 1983. pg. 140.

10. Freund, H. "Gasification of Carbon by CO_2: A Transient Kinetics Experiment". Fuel, Vol. 65, February 1986.

11. Van Heek, K. H. and H. J. Muhlen. "Coal Properties and Constitution". Fuel, Vol 64, October 1985, Pg. 1408.

12. Peters, M. H., Liang Shih Fan and T. L. Sweeney. "Simulation of Particulate Removal in Gas Solid Fluidized Beds." AICHe Journal, Vol. 28, No. 1, January 1982.

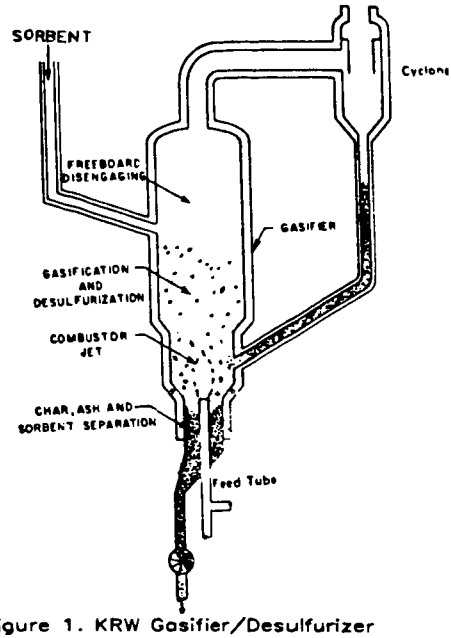

Figure 1. KRW Gasifier/Desulfurizer

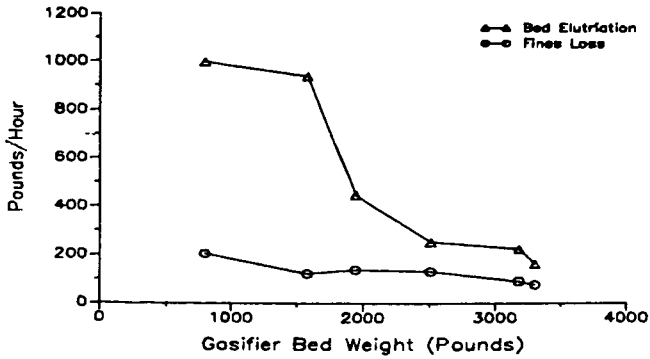

Figure 2. Variation of Fines Elutriation and Loss with Bed Weight in Gasifier/Desulfurizer

MOUNTAIN FUEL RESOURCES 30 TONS PER DAY ENTRAINED FLOW COAL GASIFICATION PROCESS DEVELOPMENT UNIT

Chiang-liu Chen and Ralph L. Coates

Questar Development Corporation
141 East First South Street
Salt Lake City, Utah 84147

INTRODUCTION

Pressurized gasification of coal in experimental entrained flow gasifiers was studied rather extensively during the period between 1953 and 1962 at the U.S. Bureau of Mines Morgantown Coal Research Center (1,2). A laboratory-scale gasifier with some similarity to the Bureau of Mines unit was operated by the Eyring Research Institute (MFI) between 1974 and 1978 (3,4). This work was followed by extensive process design studies carried out by Mountain Fuel Resources (5) which also led to the issuance of a U.S. patent (6). One of the important conclusions from this study was that feeding the dry coal to an entrained flow gasifier with recycle product gas was inherently more efficient than feeding the coal as a water slurry.

A 30 tons per day process development unit (PDU) was designed, constructed and operated between 1980 and 1984 to provide data for further scale-up of system components. Controlled continuous dry-feeding of pulverized coal into the gasifier at pressures between 100 and 260 psia (600 and 1700 kPa) was achieved. The unit was operated for more than 2000 hours on six different feedstocks. Most of the tests were conducted with Utah bituminous coal, achieving above 90 percent carbon conversion without char recycle.

DESCRIPTION OF PDU

Coal, 2" x 0" in size, was brought to the PDU site by trucks and piled on asphalt pads. The coal was reduced to less than 1/4" in size in a hammer mill, then pulverized to 70 percent minus 200 mesh in a roller mill. The pulverized coal was carried by hot gas into a cyclone where 90 to 95 percent of the coal was separated and dropped into a 20 ton storage bin. The remaining fine coal carried over from the cyclone was collected in a baghouse and also stored in the storage bin.

Coal was conveyed from the storage bin to a 3 ton lock hopper with nitrogen and, after being filled with coal, the lock hopper was pressurized with recycled product gas to the same pressure as the coal feed hopper below and the coal was discharged into the feed hopper. From the feed hopper the coal was fed into the coal feed line and carried to the gasifier by recycled product gas. Approximately 8 to 10 percent of the product gas was recycled to carry the pulverized coal. Twin augers located in the bottom of the coal feed tank were used to regulate the rate of coal flow into the feed line. Figure 1 presents a simplified process flow diagram of the PDU.

The gasification reactions were carried out at pressures up to 260 psia and at temperatures around 1565°C (2850°F) in a refractory-lined chamber approximately 2.3 cubic feet (0.065 cubic meters) in volume. Both heated oxygen and superheated steam were fed to the reactor. The reactor residence time was in the range of 0.5 to 1 second for most of the tests conducted. A radiant heat exchanger is located immediately below the gasifier in the same pressure vessel. The raw product gas leaves the vessel at a temperature about 670°C (1240°F). Approximately 50 to 60 percent of the ash in the form of slag droplets and char is collected at the base of the vessel. A water spray is used to cool the slag. Periodically, the slag and char are discharged into a slag lock hopper. Then the lock hopper is depressurized and the contents discharged into the slurry discharge tank where they are combined with fly ash, soot, and water discharged from the scrubber. This mixture is then pumped

to a hydroclone. The underflow from the hydroclone is discharged to the waste water pond and the overflow to the recycle water pond.

The hot product gas from the radiant heat exchanger vessel passes through a section of double-wall pipe heat exchanger and into a scrubber and packed tower. The gas is metered and sampled on-line for analysis downstream of the scrubber and then is flared.

GASIFIER

A schematic drawing of the pressure vessel containing the gasification chamber, the heat exchanger internals, and slag quench section is presented in Figure 2. This vessel is 48 inches in diameter and 20.5 feet in length. The diameter of the refractory-lined reaction chamber is 16 inches. The refractory is supported by a water-jacketed cylinder. Coal, oxygen and steam are injected into the gasifier at the top of the chamber. Coal is injected through a water-cooled 1-1/2 inch feed nozzle and oxygen and steam mixture is injected through an annular space around the coal feed injector. Figure 3 shows a schematic drawing of the injector nozzle and head assembly. The head is fabricated from beryllium copper alloy, which is cooled by passing water through a slot parallel to the surface facing the reactor.

The heat exchanger internals inside the pressure vessel consist of three separate sections. The first section, the radiant heat exchanger, is a cylindrical membrane wall manufactured from steam tubes with strips of metal welded between them. Saturated water from the steam drum enters the tubes from the bottom and flows up through the tubes producing steam. The tube wall is also equipped with four soot blowers. The second section is a coil that cools the lower portion of the pressure vessel and protects it from the hot product gas. A small amount of steam is generated in this coil through convective heat transfer. The third section is located in the bottom of the vessel and consists of the slag quench equipment. A spray ring is installed in the bottom of the exchanger. Cooling water from the recycle water pond is sprayed through nozzles on this ring to form a pool of water in the bottom of the vessel.

Corrosion tests were conducted by IIT Research Institute (7) by installing test coupons in the slag quench pool. Test results show that at the bottom of the radiant heat exchanger, where corrosion coupons were submerged in the slag quench pool most of the time and the temperature scarcely exceeded 220°F, materials like A515 carbon steel, aluminized carbon steel, 2 1/4Cr-1Mo, 1 1/4Cr-1Mo, 9CR-1Mo, and 410 SS suffered from heavy corrosion. Types 304 SS and 316 SS exhibited acceptable overall corrosion, but they have a tendency to pit in this environment. The Incoloy 800 specimens showed excellent resistance to general corrosion and pitting.

TEST RESULTS WITH UTAH BITUMINOUS COAL

Extensive tests were conducted with Utah bituminous coal from Southern Utah Fuel Company's (SUFCO) Mine No. 1 located near Salina, Utah. Table 1 presents typical proximate and ultimate analyses of the pulverized coal. The coal received at the plant usually contained about 8 to 10 percent moisture.

The range of the principal operational parameters and test results from July through September 1984 are presented in Table 2. Figure 4 presents product gas rate, and gas composition versus coal feed rate. The gas production rate averaged 29.3 SCF/lb of coal. For the range of coal feed tested, carbon monoxide was found to increase and carbon dioxide to decrease slightly with coal feed rate, while hydrogen seemed to reach a maximum at about 1400 pounds per hour coal rate. The ranges of the dry volume percent of the major gas components are 51 to 60 percent for CO, 30 to 36 percent for H_2, and 6 to 12 percent for CO_2. The cold gas efficiency and fraction carbon gasified increase with oxygen/coal ratio and coal feed rate for the range of conditions tested. It is obvious that the fraction of carbon gasified will increase toward a value of 1 with increasing oxygen to coal ratio;

however, the cold gas efficiency is expected to reach a maximum value then start to fall as hydrogen and carbon monoxide react with oxygen and reduce the heating value of the product gas.

COMPUTER MODEL PREDICTIONS

Several sets of computations were made with a theoretical gasifier model to assess the effect of systematic variations in reactor conditions on performance of the gasifier and product gas composition. Model parameters were empirically determined from fitting the experimental data. Table 2 also presents a range of predicted performance by computer model. The variations examined were: (1) oxygen/coal feed ratio, (2) steam/coal feed ratio, (3) recycle gas/coal ratio, and (4) reactor heat loss. Results from these computations are presented in Figures 5 through 8. The cases were run using the model parameters as optimized for the July-September SUFCO coal data. The predicted product gas volume and product gas composition are plotted versus the oxygen coal feed ratio, with other variables as parameters.

It was found that the heating value of the product gas is at a maximum for an oxygen/coal ratio of between 0.8 and 0.9. Variations in the recycle gas to coal ratio were calculated to have only a weak influence on the product gas composition and volume. The steam/coal ratio, Figure 6, demonstrates a strong influence on the product gas composition with little effect in the product gas volume. The carbon monoxide concentration is highest for a lower steam/coal ratio. For lower oxygen feed rates, the temperature is a strong factor in the product gas volume. However, at an oxygen/coal ratio between 0.8 and 0.9, the cold gas efficiency is unaffected by the steam feed rate.

Variations in the reactor heat loss were calculated to significantly affect the product gas volume and composition, mainly through lowering the reactor temperature. Figure 7 shows significantly lower product gas volume and quality with a higher reactor heat loss. Figure 8 again presents the effect of reactor heat loss; however, here the oxygen/coal feed ratio was adjusted to yield the desired reactor temperature. For a constant reactor temperature, a higher reactor heat loss deteriorates the product gas quality only slightly.

The oxygen/coal feed ratio is the controlling parameter on reactor temperature and performance. The effect of variations in steam, recycle gas ratio and the reactor heat loss on the cold gas efficiency are relatively small compared with the effects of varying the oxygen/coal ratio.

Table 3 presents a direct comparison of PDU data with the design assumptions for a scale-up unit utilizing SUFCO Utah bituminous coal.

CONCLUSIONS

The dry-feed, entrained coal gasification PDU was operated successfully for a total of about 2200 hours. Controlled continuous dry-feeding of pulverized coal into the gasifier at pressures up to 260 psia was achieved. Reactor throughputs of up to 754 lbs/hr/ft^2 or 317 lbs/hr/ft^3, gas yields of about 32 SCF/lb coal and gas heating values of 294 BTU/SCF were achieved. Carbon conversion efficiencies above 90 percent without char recycle were achieved with Utah bituminous, Wyoming subbituminous, and North Dakota lignite coals. Cold gas efficiencies as high as 80 percent were achieved with SUFCO coal. Sufficient reproducible data were obtained for scale-up design for applications utilizing Utah bituminous coal from SUFCO Mine No. 1.

ACKNOWLEDGEMENT

The authors gratefully acknowledge support of this work by the Department of Energy under Contract No. DE-AC21-81FE05121, Gary R. Friggens, Contractor Monitor.

REFERENCES

1. Holden, J.H., et al., "Operation of Pressure-Gasification Pilot Plant Utilizing Pulverized Coal and Oxygen: A Progress Report," Report of Investigations 5573, U.S. Dept. of the Interior, Bureau of Mines (1960).

2. Holden, J.H., Plants, K.D., et al., "Operating a Pressurized Gasification Pilot Plant Using Pulverized Coal and Oxygen: Effect of Heat Loss on Economy," Report of Investigations 5956, U.S. Dept. of the Interior, Bureau of Mines (1962).

3. Coates, R.L., "High Rate Coal Gasification," in Volume 3, "Coal Processing Technology," American Institute of Chemical Engineers, New York, N.Y., 1977, pp. 89-94.

4. McIntosh, M.J., and Coates, R.L., "Experimental and Process Design Study of a High Rate Entrained Coal Gasification Process," Final Report under Contract No. EX-76-C-01-1548, Eyring Research Institute, Provo, Utah, 1978.

5. Coates, R.L., and Mantyla, R.G., "Process Design Studies for High-Rate, Entrained-Flow Coal Gasification," Proceedings of the First International Gas Research Conference, June 1980, Chicago, Illinois, published by Government Institutes, Inc., Rockville, Md., October 1980, pp. 224-242.

6. U.S. Patent No. 4,272,255, "Apparatus for Gasification of Carbonaceous Solids."

7. Yurkewyez, R., "Corrosion and Degradation of the Test Materials in the Mountain Fuel Resources 30 Ton/Day Coal Gasification Process Development Unit," Report of Materials Evaluation conducted in 1983-1984 by IIT Research Institute for the Metal Properties Council, Inc., support by the U.S. Department of Energy, Morgantown Energy Technology Center, Report No. MPCI-22241-2, January 31, 1985.

TABLE 1

SUFCO UTAH BITUMINOUS COAL ANALYSIS

PROXIMATE ANALYSIS, Wt.%		ULTIMATE ANALYSIS, Wt.%	
Moisture	2.55	Moisture	2.55
Ash	9.23	Carbon	69.60
Volatile	39.37	Hydrogen	4.84
Fixed Carbon	48.85	Nitrogen	1.15
	100.00	Chlorine	0.02
		Sulfur	0.42
Btu/lb	12180	Ash	9.23
		Oxygen (diff.)	12.19
			100.00

TABLE 2

RANGE OF THE PRINCIPAL OPERATIONAL PARAMETERS AND SUMMARY OF THE RESULTS AND CORRELATIONS OF THE SUFCO COAL DATA, JULY - SEPTEMBER 1984

Range of Test Conditions		
Reactor pressures, psia	90.4 - 212	
Coal feed rates, lbs/hr	653 - 1812	
Oxygen/coal ratios	0.62 - 0.94	
Steam/coal ratios	0.11 - 0.22	
Recycle gas/coal ratios	0 - 0.33	
Range of Results	Actual	Predicted
Gas Yields, SCF/lb coal	23 - 36	24.5 - 35.4
Gas Composition, %		
Carbon monoxide	50.7 - 59.8	49.8 - 61.7
Hydrogen	27.5 - 36.8	29.9 - 40.7
Carbon dioxide	5.4 - 15.0	6.0 - 12.8
Methane	0.0 - 2.7	0.2 - 2.2
High Heating Values, BTU/SCF	266 - 307	282 - 313
Fraction Carbon Gasified	0.67 - 1.00	0.72 - 1.00
Cold Gas Efficiencies	0.53 - 0.85	0.60 - 0.85
Range of Calculated Balances		
Hydrogen Balance	0.626 - 1.176	
Mass Balance	0.980 - 1.039	

TABLE 3

COMPARISON OF SCALE-UP UNIT DESIGN ASSUMPTIONS WITH JULY-NOVEMBER 1984 PDU DATA

	Scale-Up Unit Design Asaumptions	PDU Data Averages for SUFCO Coal Runs
Coal Rate, lbs/hr	11,686	1,055
Feed Ratios		
Oxygen/coal	0.80	0.849
Steam/coal	0.17	0.274
Recycle gas/coal	0.12	0.215
Reactor Pressure, psia	200	157
Reactor Throughput Rate		
Lbs/hr/ft^2	1,000	754
Lbs/hr/ft^3	190	317
Reactor Heat Loss		
BTU/lb coal	100	325
Product Gas Yield (net, dry)		
MSCFH	371	33.4
SCF/lb coal	31.7	31.5
Product Gas Composition		
Hydrogen	31.6	33.6
Carbon monoxide	56.0	51.3
Carbon dioxide	9.0	12.1
Methane	1.2	0.9
Nitrogen, argon	2.0	2.1
Hydrogen sulfide	0.2	-
Total	100.0	100.0

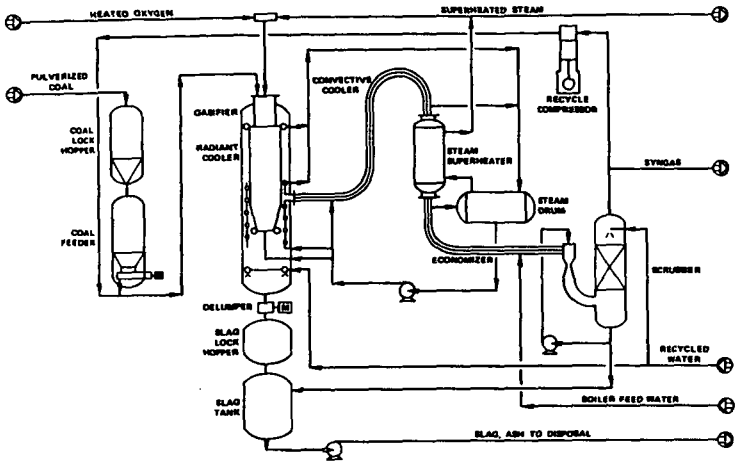

FIGURE 1. Simplified Process Flow Diagram

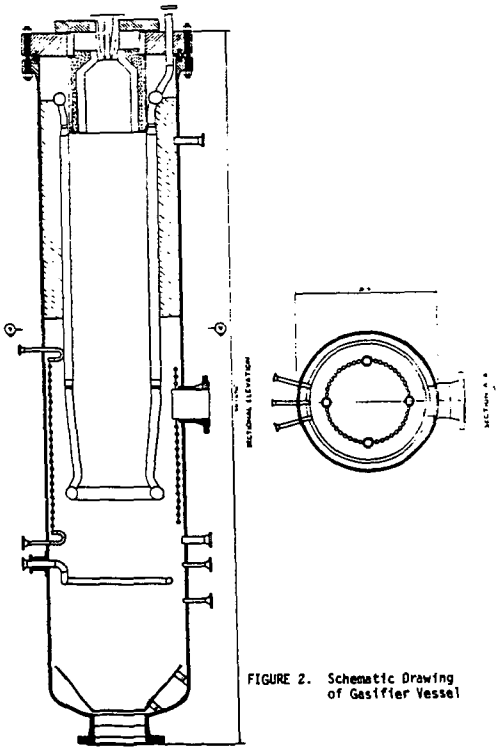

FIGURE 2. Schematic Drawing of Gasifier Vessel

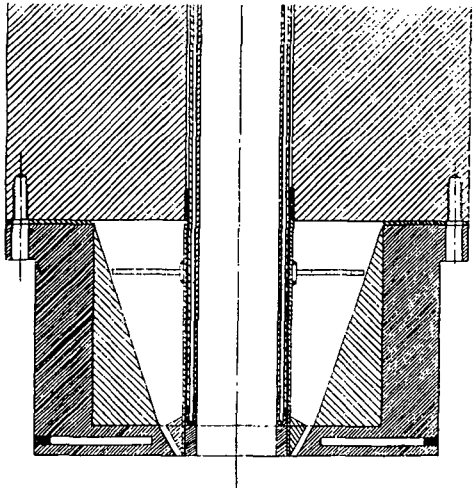

FIGURE 3. Schematic Drawing of Injector Nozzle and Head Assembly

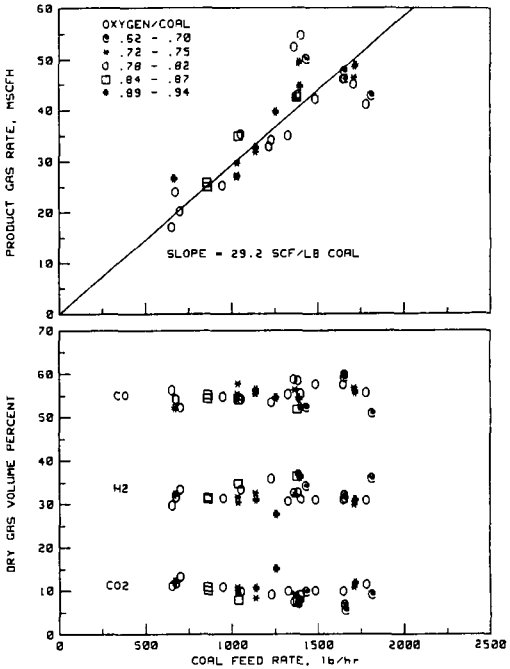

FIGURE 4. Gasifier Performance Data
Gas Composition and Product Gas Rate Versus Coal Feed Rate

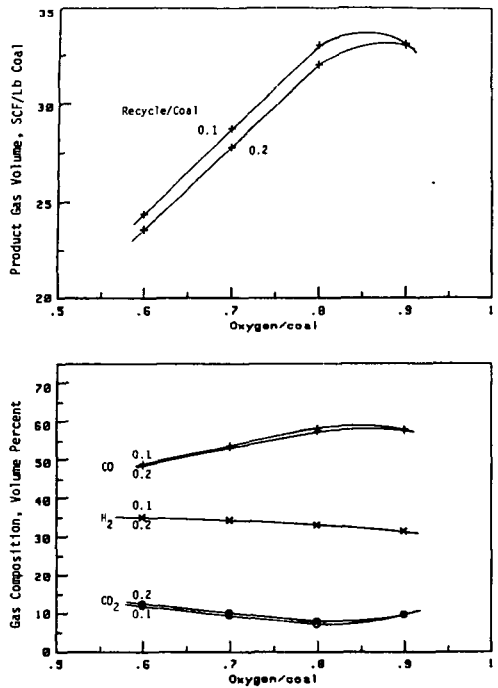

FIGURE 5. Predicted Performance of SUFCO Coal Using Best Fit Parameters from July - September 1984 Data Steam/Coal = 0.2, Reactor Heat Loss = 200 BTU/Lb Coal

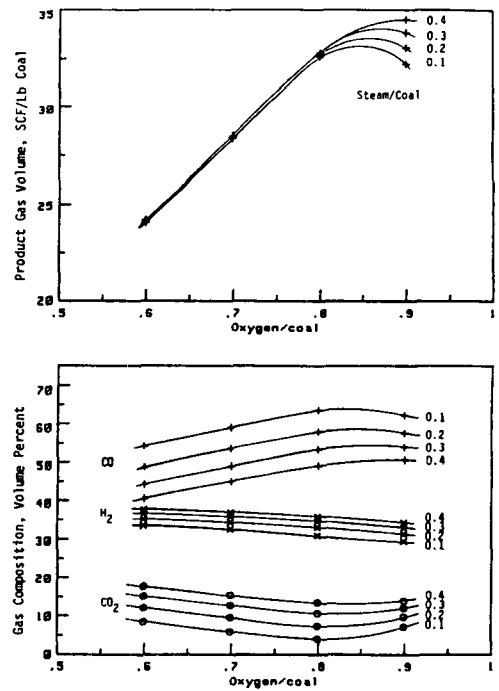

FIGURE 6. Predicted Performance of SUFCO Coal Using Best Fit Parameters from July - September 1984 Data Recycle/Coal = 0.12, Reactor Heat Loss = 200 BTU/Lb Coal

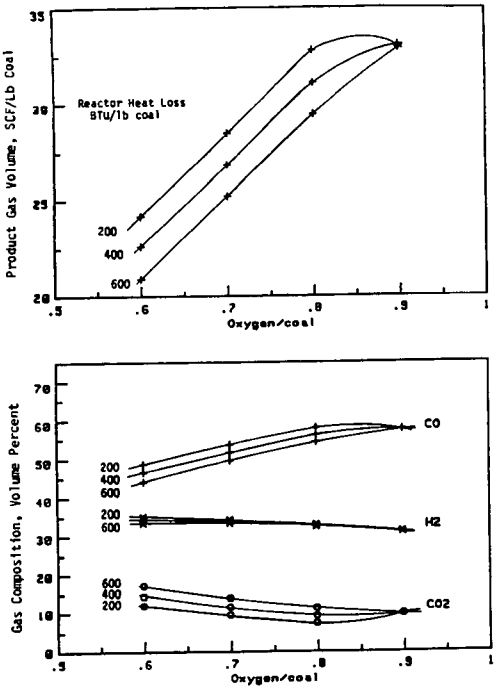

FIGURE 7. Predicted Performance of SUFCO Coal Using Best Fit Parameters from July - September 1984 Data Steam/Coal = 0.2, Recycle Coal = 0.12

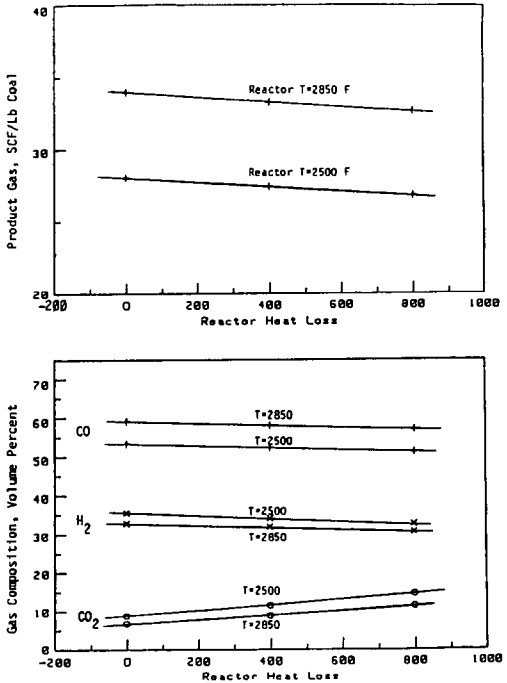

FIGURE 8. Predicted Effect of Heat Loss on Product Gas Steam/Coal = 0.2, Recycle Gas/Coal = 0.12

The competitive adsorption of fuel-type compounds on zeolite 13X

G. Jean, P. Chantal, S. Ahmed and H. Sawatzky

Energy Research Laboratories (CANMET)
555 Booth Street
Ottawa, Ontario, Canada
K1A 0G1

Introduction

The possibility of selectively removing the nitrogenous components of fuels by adsorption on zeolite 13X was recently reported (1-2). The purpose of this work is to develop an industrial process to remove heteroatom components from synthetic crude fractions in order to decrease the need for hydrotreating or reduce the required severity of hydroteating. The emphasis has been given to nitrogenous compounds since they dictate the severity of the process. Two of the most important criteria determining the success of an adsorption process are the adsorption capacity and the degree of selectivity. As found in the first two studies using a model solution there is a large degree of discrimination between nitrogenous compounds; the extent of adsorption is inversely proportional to the size and the acidity of the compound. The overall adsorption capacity obtained with the model solution is 10%. However, when using a real naphtha the capacity obtained is much smaller, being of the order of 1-3%. One of the potential reasons for this lower capacity could be the competitive adsorption of non-nitrogenous compounds contained in the naphthas.

The present study was undertaken to investigate the degree of competition between nitrogenous compounds and other compounds mainly olefins and oxygenated compounds. Very little competition from non-nitrogenous compounds was observed. Olefins were able to compete with nitrogenous compounds only at very high concentrations.

Experimental

All experiments were performed at room temperature in a continuous-flow fixed-bed adsorption apparatus. The zeolite is dry-packed in a stainless steel column 20 cm long and 0.4 cm ID. The first series of tests were done with a zeolite dried at 160 C . The feed is pumped at a constant flow of 0.5 mL/min and samples of the effluent are collected every 5 mL and subsequently analyzed by gas chromatography.

The adsorption capacity of individual compounds was obtained using a 1 wt% solution in toluene of the desired compound. For the competitive runs a solution of 1 wt% of each compound in toluene (2 wt% total) was used.

Results and discussion

Several factors affect the magnitude of adsorption; the adsorption capacity depends on the operating conditions such as inlet concentration, bed depth, flow rate and most importantly the affinity of the sorbate for the surface. For a given set of operating conditions the capacity measures the relative affinity of the sorbate for the solid and the solution. In the first part of this study the effect of the nature of the solution on the adsorption of aniline is investigated (Table 1). The maximum capacity is obtained for a toluene solution; the extent of aniline adsorption decreases following the addition of heptane, cyclohexene and indene. It should be noted that the degree of reproducibility between packings gives an error of 10-15%. Thus the results indicate that an olefinic solution might interfere with the adsorption of the nitrogenous compounds. This could explain the results recently reported showing a large difference in adsorption capacities for two naphthas; the lowest capacity was obtained for a naphtha abnormally high in olefins (Ref. 1, Table 2; adsorption capacity of 1 wt% for the naphtha containing 62% olefins).

Table 2 presents a summary of the adsorption capacities of various compounds. The extent of adsorption seems to be proportional to the polarity and the basicity of the compound. The indene-indoline-indole series illustrates this point; the capacities for these compounds are 3.99, 13.7 and 14.81 wt% respectively. At a concentration of 1 wt%, the olefins have very little affinity

for the zeolite as indicated by their low capacities; they do interfere with the adsorption of aniline as shown in Table 3. Oxygenated compounds have a strong affinity for the zeolite. The extent of adsorption of phenol compares to those of aniline and indole, two of the most retained nitrogenous compounds. Under competition, phenol is quite successful in displacing the nitrogenous compounds (Table 4). These results suggest that naphthas high in oxygenated compounds could be treated using the adsorption process. This could be advantageous for synthetic crude naphthas such as coal derived liquids.

The study on competition between nitrogenous compounds show that the adsorption capacity of individual compounds is a good predictor of the adsorption process for a complex mixture. Indeed the order of affinity indicated by the adsorption capacity of the individual compound is very similar to the order obtained for a solution containing eighteen compounds (1). Except for a few cases the individual capacities also predicted the relative capacities for the "two compound competitions" showed in Tables 3-7. The results indicate that the total capacity obtained is of the order of 15 wt% . The adsorption is not dominated by a single nitrogenous compound.

Conclusion

The data obtained in this study show that there should be little competition from non-heteroatom compounds except possibly from olefins. Both nitrogenous and oxygenated compounds have a strong affinity for the zeolite. The adsorption of oxygenated compounds presents a real advantage since these compounds are also problematic. Oxygenated compounds are present in significant amounts in a variety of synthetic crude fractions.

An adsorption process for the removal of heteroatom components, using a zeolite 13X , would not be efficient because of the low affinity of a number of nitrogenous compounds. For instance phenetylpiperidine and collidine are adsorbed at less than 8 wt% without any competition (Table 2) . This capacity will decrease in a multi-component solution because of site competition. Future work should concentrate of finding an adsorbent that can remove the less basic compounds.

1) G. Jean, S. Ahmed and H. Sawatzky, "The Selective Removal of Nitrogenous-Type Compounds from Fuels by using zeolites", Sep. Sci. Technol. 20(7 & 8), 555-564, 1985

2) G. Jean, E. Bonvie and H. Sawatzky, "Selective Removal of Nitrogenous Compounds Using Zeolites", ACS National Meeting Chicago Sep. 8-13: Preprint Fuel Division Vol. 30(4), 474-480, 1985

Table 1

Solvent effect on aniline adsorption capacity (wt% on zeolite)
1 wt% aniline in solvent

Solvent	Capacity %	Capacity relative to toluene
toluene	22.91	——
50:50 toluene/heptane	19.28	0.84
50:50 cyclohexene	15.13	0.66
50:50 1-indene	15.09	0.65

Table 2

Adsorption capacity for individual compounds (wt% on zeolite)
1 wt% in toluene

Compound	Capacity %	Compound	Capacity
Decene	1.21	Cycloheptanone	11.70
Indene	3.99	Octylamine	11.91
1-Phenethylpiperidine	5.73	Dibenzylamine	12.99
Aminoanthrancene	5.98	Indoline	13.70
2,4,6-Collidine	7.24	4-Ethylpyridine	14.01
1,2,5-Trimethylpyrrole	8.47	Quinoline	14.45
2-Phenylpyridine	8.69	Iso-Quinoline	14.72
Phenothiazine	9.04	Indole	14.81
2,2′-Dipyridyl	10.45	Phenol	16.08
Decylalcohol	11.18	Aniline	22.91

Table 3

Adsorption capacity for various compounds in the presence of Aniline (wt% on zeolite)
1 wt% compound and 1 wt% aniline in toluene

Compound	Capacity %	Relative Capacity	Aniline capacity %	Aniline Relative Capacity	Total Capacity
Decene	0.43	0.36	16.21	0.74	16.63
Indene	1.07	0.28	13.64	0.59	14.71
Dibenzylamine	3.66	0.28	15.38	0.67	19.04
Decylalcohol	5.43	0.49	15.16	0.66	20.59
Indole	7.39	0.50	12.66	0.55	20.05
2,2′-Dipyridyl	7.77	0.74	7.67	0.34	15.44
Quinoline	8.92	0.62	11.79	0.52	21.71
Indoline	9.86	0.72	16.82	0.74	26.68

Table 4

Adsorption capacities for various compounds in the presence of Phenol (wt% on zeolite)
1 wt% compound and 1 wt% phenol in toluene

Compound	Capacity %	Relative Capacity	Phenol capacity %	Phenol Relative Capacity	Total Capacity
Dibenzylamine	3.57	0.28	10.59	0.66	14.11
Quinoline	4.75	0.44	11.80	0.73	16.55
2,2′-Dipyridyl	5.71	0.55	9.06	0.56	14.77
Indole	7.61	0.51	13.27	0.83	20.88
Decylalcohol	7.68	0.69	11.41	0.71	19.09

Table 5

Adsorption capacities for various compounds in the presence of Octylamine (wt% on zeolite)
1 wt% compound and 1 wt% octylamine in toluene

Compound	Capacity %	Relative Capacity	Octylamine capacity %	Octylamine Relative Capacity	Total Capacity
2,2′-dipyridyl	8.21	0.79	6.62	0.56	14.83
4-Ethylpyridine	8.59	0.77	4.41	0.37	13.00
Dibenzylamine	8.91	0.69	6.98	0.59	15.89
Cylcloheptanone	9.40	0.80	5.68	0.48	15.08
Quinoline	9.70	0.90	6.89	0.56	16.59
Indole	10.06	0.68	6.76	0.62	16.82

Table 6

Adsorption capacities for various compounds in the presence of 4-Ethylpyridine (wt% on zeolite)
1 wt% compound and 1 wt% 4-ethylpyridine in toluene

Compound	Capacity %	Relative Capacity	4-Ethylpyridine capacity %	4-Ethylpyridine Relative Capacity	Total Capacity
Quinoline	5.65	0.52	5.59	0.50	11.24
Decylalcohol	5.74	0.51	9.45	0.85	15.19
Dibenzylamine	5.79	0.45	9.06	0.82	14.85
Indoline	6.19	0.45	7.29	0.66	13.48
Indole	7.13	0.48	6.82	0.61	13.95
Cylcloheptanone	7.90	0.68	9.53	0.86	17.43
2′,2′-Dipyridyl	8.34	0.80	5.89	0.53	14.23
Aniline	13.97	0.61	8.32	0.75	22.29

Table 7

Adsorption capacities for various compounds in the presence of Quinoline (wt% on zeolite)
1 wt% compound and 1 wt% quinoline in toluene

Compound	Capacity %	Relative Capacity	Quinoline capacity %	Quinoline Relative Capacity	Total Capacity
Decylalcohol	1.78	0.16	9.35	0.87	11.13
Dibenzylamine	4.23	0.33	9.46	0.88	13.69
2-Phenylpyridine	5.21	0.60	9.14	0.85	14.35
Indole	5.85	0.40	7.11	0.65	12.96
Indoline	7.23	0.53	8.63	0.80	15.86
2,2′-Dipyridyl	8.05	0.77	4.37	0.40	12.42
Aniline	11.19	0.52	8.92	0.62	20.11

BIOLOGICAL MARKER AND RELATED COMPOUNDS IN NATURAL AND SYNTHETIC LIQUID FUELS

M.G. Strachan, R. Alexander and R.I. Kagi
School of Applied Chemistry, Western Australian Institute of Technology, Bentley 6102, Western Australia

INTRODUCTION

Molecular level characterization of synthetic crudes using GC and GC/MS techniques has typically involved identifying the major components present, irrespective of chemical class (1-4). This approach differs considerably from the application of these methods for characterizing natural crude oils. These samples are only analyzed for particular compound types whose distributions and use in selected ratios can provide useful geochemical information. The compounds studied are what are generally termed "biological markers", aliphatic components directly related to a biological precursor. These compounds include; n-alkanes, acyclic isoprenoids, diterpanes, triterpanes and steranes (5,6). More recently, however, alkyl aromatics such as dimethylnaphthalenes (7), trimethylnaphthalenes (8,9) and methylphenanthrenes (10) hae also been employed in a similar manner.

The literature contains a paucity of reports of analyses of synthetic liquids specifically for biological marker compounds (11-14). These studies, which encompass both coal- and oil shale-derived liquids, suggest that the geochemical data obtained can provide useful information about the source material and different liquefaction processes. Interestingly, the coal derived liquids examined for biological marker compounds were almost exclusively produced from bituminous coals. This is surprising in view of the much reported liquefaction reactivity of the lower ranked, lignites and brown coals. Furthermore, as the use of alkyl aromatics as geochemical indicators is only a recent innovation, the extension of this application to synthetic liquids is as yet unreported.

Two Australian fossil fuel reserves whose liquefaction potential have been extensively investigated are the massive Latrobe Valley (Victoria, Australia) brown coal deposits, and the Rundle oil shale (Queensland, Australia) seams. In fact, a 50 ton-per-day pilot plant based on the SRC I & II processes, and using these brown coals as feedstock is currently nearing completion in the Labrobe Valley. This paper reports on a study of synthetic liquids, produced from these two sources, that have been characterized by GC and GC/MS in an anologous fashion to natural crudes. For comparative purposes, the data obtained from a terrestrial crude oil and a marine crude oil are also included. In addition, the effect of liquefaction process on the respective data is illustrated by the different coal derived liquids.

EXPERIMENTAL

Samples. The coal derived liquids were all produced from a medium-light lithotype Victoria brown coal from the Loy Yang Field (bore 1277, depth 67-68m). The liquefaction processes employed were: solvent extraction (CH_2Cl_2); slow pyrolysis (50°-1000°C at 3°C min^{-1}); hydrogenation (tetralin/H_2(10.3 mPa), 375°C, 2hrs) and CO/H_2O (bed moist coal/CO (6.8 MPa), 350°C, 2hrs). More detailed information on the liquefaction conditions and the product yields and analyses are given elsewhere (15,16).

The oil shale derived liquids were produced from the Rundle oil shale by solvent extraction (CH_2Cl_2) and by the Lurgi-Ruhrgas retorting process (17). In all cases, the synthetic liquids are operationally defined as the methylene dichloride soluble portion of the liquefaction product.

The two natural crude oils represent oils sourced from terrestrial organic matter and marine organic matter, respectively. The former is from the off-shore Gippsland Basin, Australia (the Latrobe Valley coals are part of the on-shore Gippsland Basin) and the latter, the North Sea, Denmark.

Separation Procedure. The sample (30mg) in methylene dichloride ($2cm^3$) was preadsorbed onto silicic acid using the method of Middleton (18). Upon removal of the solvent by rotary evaporation, the preadsorbed sample was placed on top of a column of silicic acid (3g). Successive elution with *n*-pentane; n-pentane/diethyl ether (95:5) and methylene dichloride/methanol (90:10) gave three fractions: (1) aliphatic hydrocarbons, (2) aromatic hydrocarbons and (3) heteronuclear compounds.

An aliquot of the aliphatic hydrocarbons fraction, in benzene, was subsequently treated with activated 5A molecular sieves to separate the *n*-alkanes from the branched and cyclic alkanes (19). Similarly, the aromatic hydrocarbons fraction was subjected to thin layer chromatography on alumina, with n-hexane as eluant, to yield a di- and trinuclear aromatic fraction (9). These fractions after appropriate reported workup procedures (19,9), and solvent removal were amenable for analysis by GC and GC/MS.

GC and GC/MS analysis. Gas chromatography was performed using a Hewlett-Packard (HP) 5880A chromatograph, fitted with a 50m x 0.2mm i.d. WCOT fused-silica column coated with 5% crosslinked phenylmethyl silicone (bp-5, SGE Australia). For all analyses, hydrogen was used as carrier gas at a linear velocity of 30 cm sec^{-1}, and detector (FID) and injector temperatures were 300°C and 280°C, respectively. In a typical analysis of a total aliphatic hydrocarbon fraction, the oven of the chromatograph was temperature programmed from 65°C to 280°C at 4°C min^{-1}, then held isothermal for 10 minutes. The oven temperature programme for analysis of the di- and trinuclear aromatics fractions was: 70°C for 1 minute; then 70°C to 190°C at 1°C min^{-1}; followed by 190°C to 300°C at 10°C min^{-1} and finally, held isothermal for 10 minutes. All GC analysis were integrated using the associated HP data terminal. Component identification was, in both cases, by comparison of the retention times with those of authentic isomers (8,10,19,20).

Only the branched/cyclic alkane fractions were analyzed by GC/MS. The analyses were performed using a HP 5895B capillary GC-quadrupole MS-computer data system, fitted with a 50m x 0.22mm i.d. WCOT fused-silica cross-linked methylsilicone column (Hewlett Packard). Samples for analyses were diluted to a 1% w/w solution in n-hexane and injected on-column at 50°C. The oven was then temperature programmed to 300°C at 4°C min^{-1}, and held isothermal for 20 minutes. Hydrogen was used as carrier gas at a linear velocity of 28 cm sec^{-1}. The samples were analyzed in the selected ion monitor (SIM) mode, using dwell times of 10 msec for each ion monitored. Typical MS operating conditions were: EM voltage 2200V; ionization energy 70eV; source temperature 250°C.

The ions monitored were typical of those used for crude oil biological marker studies. For example, m/z 217, 218, 259 (steranes and diasteranes); m/z 177,191,205 (triterpanes) and m/z 123, 193 (bicyclics and tetracyclics). Specific compounds were identified by comparison of their retention times with literature data. (21-23).

RESULTS AND DISCUSSION

Figure 1 shows gas chromatograms of the total aliphatic hydrocarbon fractions of the synthetic liquids and natural crude oils. The compound distributions evident in these chromatograms for the coal derived liquids differ markedly for the various liquefaction processes. The solvent extract is overwhelmingly dominated by triterpenoids (consistent with the higher plant input of the source material), while the hydrogenation product and pyrolysate have the *n*-alkanes in the highest relative abundance. It is interesting to note that this observation conflicts with that of Youtcheff and coworkers (12) who found no difference in the distributions of saturate hydrocarbons from several bituminous coal solvent extracts and their corresponding hydrogenation products. In addition, the pyrolysate also contains a homologous series of n-alkanes. The CO/H_2O product is quite distinctive in that it has a bimodal n-alkane distribution and appears to

contain a major group of components which have retention times between n-C_{22} and n-C_{23}. The oil shale derived liquids can also be differentiated from each other. The solvent extract is predominantly n-alkanes, having the C_{27} member as the most abundant component; while the retort oil is much more complex. Although it has the n-alkanes as the most abundant homologous series, it also contains a series of n-alkenes. However, it differs from the coal pyrolysate in having its n-alkane and n-alkene distributions maximising at lower carbon numbers. In fact, the general shapes of the n-alkanes distributions for the coal pyrolysate and oil shale retort are very similar to those for the terrestrial and marine crudes, respectively. This may suggest that the geochemical processes generating natural crudes are pyrolytic in nature.

Two geochemical indicators determined from chromatograms of the total aliphatic hydrocarbons are the Carbon Preference Index (CPI) and Pristane/Phytane ratio (Pr/Ph). The former is based on the n-alkanes, and the latter, the C_{18} and C_{19} acyclic isoprenoids. The CPI values for the oil shale derived liquids are much higher than those for both the coal derived liquids and natural crudes. Except for the solvent extract, the CPI values for the coal derived liquids are all less than unity, with that for the CO/H_2O product being appreciably so. Interestingly, the CPI values for the two natural crudes are almost identical. However, it is the Pr/Ph ratio values that clearly distinguish the coal derived-from the oil shale derived liquids, and the torrestrial from the marine crude. Both the coal derived liquids and the terrestrial crude have considerably higher values of this ratio than their corresponding counterparts. The similarities of values for the coal derived liquids and the terrestrial crude, and the shale derived liquids and the marine crude is not surprising, considering their respective source organic matter. The combined use of CPI and Pr/Ph does, hence, suggest that coal- and oil shale-derived liquids can be differentiated from each other and their respective natural counterparts.

Further confirmation of this possibility is afforded by GC/MS analyses of the respective branched/cyclic fractions. Table 1 presents the data for selected geochemical indicators based on several biological marker compounds. Typical mass fragmentograms of steranes (m/z 217) and triterpanes (m/z 191) are illustrated in Figure 2, for the coal pyrolysate and terrestrial crude oil. Component identification is given in Table 2. The mass fragmentograms show that the samples generally contain the same components, with differences being mainly in individual relative abundances. However, the m/z 191 mass fragmentograms do provide a ready means of distinguishing synthetic from natural crudes. The differences are most apparent in the high relative abundances of: 1) C_{29} to C_{30} $\alpha\beta$-hopanes (peaks F and D, respectively, in Fig. 2a) and 2) the C_{27} β-hopane (peak C in Fig. 2a) for the synthetic liquids compared with the natural crudes.

Kaurane is an unequivocal biological marker for higher plant material in fossilized organic matter (24). The epimer ratio (Table 1) is, therefore, useful for distinguishing the oil shale derived liquids and the marine crude from the coal derived liquids and the terrestrial crude. In fact, the respective values for the coal derived liquids and the terrestrial crude suggest, they too can be differentiated from each other.

The values for the drimane epimer ratios are similar for all the synthetic liquids, but are significantly lower than those for the natural crudes, whose respective values are almost identical. Conversely, the $\beta\beta/\alpha\beta$ hopane ratios and the moretane/hopane ratios are considerably higher for the synthetic liquids than for their natural counterparts. Again, it is difficult to distinguish, unambiguously, between the oil shale and coal derived liquids. However, these drimane and hopane (moretane) based parameters do permit unequivocal distinction between the natural and synthetic crudes. Similarly, the sterane epimer ratios are significantly different between the synthetic liquids and the natural crudes; the values

for the ratio being much higher in the latter. However, in natural crudes the above parameters have been shown to be maturity dependent; therefore, synthetic liquids produced under more severe thermal conditions may show values approaching those observed for their natural counterparts. This is in fact observed with the coal hydrogenation product and the marine crude. This suggests that this parameter should not be used in isolation, although generally most natural crude oils are generated from mature source rocks and have epimeric ratios of 1.1.

In contrast, the C_{29}/C_{27} sterane ratio can be used to differentiate the coal derived liquids and the terrestrial crude, from the oil shale derived liquids and the marine crude. The values are much higher for the former, than for the latter samples. Actually, this ratio could not be determined for the shale retort oil as the C_{27} sterane was immeasurable. Again the hydrogenation product appears anomalous, with the value for this parameter being much lower than for the other coal derived liquids.

Indeed, the values for the $\beta\beta/\alpha\beta$ hopane ratio and the sterane-based parameters, for the hydrogenation product are of geochemical interest. The low relative abundance of the C_{30} $\beta\beta$-hopane, and its similarity to those in natural crudes suggests that certain maturation processes can be replicated under laboratory conditions. This is further shown by the value of sterane epimer ratio, which unlike those for other synthetic liquids, indicates a significant degree of configuration isomerization. In addition, the low value for the C_{29}/C_{27} sterane value is consistent with dealkylation of the C_{29} sterane as a result of increased thermal stress. These observations thus suggest that hydrogen transfer processes may be important in the geosphere for crude oil formation.

Inspection of the alkyl aromatic-based parameters, which are presented in Table 3, shows that they too can be employed to distinguish synthetic from natural crudes, and coal derived from shale derived liquids. Figure 3 shows a typical gas chromatogram of a dinuclear and trinuclear aromatics fraction for the coal pyrolysate and terrestrial crude. The numbered peaks, which refer to those used in defining the parameters, are defined in Table 4. The parameters DNR-2, TNR-1 and MPI-1 allow differentiation of the synthetic from the natural crudes. The values for DNR-2 in the synthetic liquids are normally much lower than those observed in natural crudes. The value for the marine crudes, presented here (i.e. 72.6) is anomalously low for oils sourced from this type of organic matter, and is a direct result of the immaturity of this particular sample. For TNR-1 and MPI-1, the synthetic liquids generally have higher values than the natural crudes. However, both the coal pyrolysate and the oil shale retort have similar values to those observed for the terrestrial and marine crudes. This may be further evidence that pyrolytic processes play a role in oil generation.

The coal derived liquids and terrestrial crude have considerably higher values of DNR-6 and TDE-1 than the oil shale liquids and marine crude. Thus, these groups of samples may be distinguished from each other using these parameters. Hence, appropriate combinations of parameters permit the origin and source type of a liquid fuel to be ascertained. For example, high DNR-2 and TDE-1 values infer the oil is a natural terrestrial crude, whereas low values for these two parameters suggest it is an oil shale derived liquid.

In conclusion, the approach outlined here shows that: 1) natural and synthetic crudes can be fingerprinted using known geochemical parameters; 2) the choice of liquefaction process can considerably alter the distribution of total aliphatic hydrocarbons for a given source material; 3) natural and synthetic crudes can be distinguished from each other, as can be their source types, using appropriate combinations of biological marker and/or alkyl aromatic-based paramters; 4) geochemical processes such as the epimerization of steranes and the depletion of $\beta\beta$-hopanes can be replicated in the laboratory and 5) pyrolytic-, together with hydrogen

transfer processes may be important in the formation of natural crude oils.

ACKNOWLEDGEMENTS

The authors are grateful to Dr R.B. Johns, Dept. of Organic Chemistry, University of Melbourne, for supplying the coal derived liquids, and to Mr T.G. Harvey, CSIRO Materials Science Laboratory, Melbourne for the retorted oil shale sample. This work was carried out as part of the National Energy Research, Development and Demonstration Programme administered by the Dept. of Resources and Energy, Australia.

REFERENCES

1. Schultz, R.V., Jorgenson, J.W., Maskarine, M.P., Novotny, M. and Todd, L.J., Fuel, 1979, 58, 783.
2. Novotny, M., Strand, J.W., Smith, S.L., Wiesler, D. and Schwende, F.J., Fuel, 1981, 60, 213.
3. Parees, D.M. and Zamzelski, A.Z., J. Chromatog. Sci., 1982, 20, 441.
4. Paudler, W.W. and Cheplen, M., Fuel, 1979, 58, 775.
5. Mackenzie, A.S., In Advances in Petroleum Geochemistry, (Eds. Brooks J and Welte D.) Vo. 1, p.115, Academic Press, London, 1984.
6. Philp, R.P., Mass Spec. Reviews, 1985, 4, 1.
7. Alexander, R., Kagi, R.I., and Sheppard, P.N., Nature, 1984, 308, 442.
8. Rowland, S.J., Alexander, R. and Kagi, R.I., J. Chromatog., 1984, 294, 407.
9. Alexander, R., Kagi, R.I., Rowland, S.J., Sheppard, P.N. and Chirila, T.V., Geochim. Cosmochim. Acta, 1985, 49, 385.
10. Radke, M. and Welte, D.H., In Advances in Organic Geochemistry 1981 (Ed. Bjoroy M.) p504, John Wiley and Sons, 1983.
11. Jones, D.W., Pakdel, H. and Bartle, K.D., Fuel, 1982, 61, 44.
12. Youtcheff, J.S., Given, P.H., Baset, Z. and Sundaram, M.S., Org. Geochem., 1983, 5, 157.
13. White, C.M., Shultz, T.J. and Sharkey, A.G. Jr, Nature, 1977, 268, 620.
14. Ingram, L.L., Ellis, J., Crisp, P.T. and Cook, A.C., Chem. Geol., 1983, 38, 185.
15. Strachan, M.G., Ph.D. Thesis, University of Melbourne, 1985.
16. Johns, R.B., Verheyen, T.B., Yost, R.S. and Louey, M. "A Study of the Products of Brown Coal Converstion using Carbon Monoxide, Synthesis Gas and other Reductants", Victorian Brown Coal Council Progress Report No.1, Melbourne, August 1982.
17. Harvey, T.G., Matheson, T.W. and Pratt, K.C., Anal. Chem., 1984, 56, 1277.
18. Middleton, W.R., Anal. Chem., 1967, 39, 1839.
19. Volkman, J.K., Alexander, R., Kagi, R.I., Noble, R.A. and Woodhouse, G.W., Geochim. Cosmochim. Acta, 1983, 47, 2091.
20. Alexander, R., Kagi, R.I. and Sheppard, P.N., J. Chromatog., 1983, 267, 367.
21. Wardroper, A.M.K., Brooks, P.W., Humberston, M.J. and Maxwell, J.R. Geochim Cosmochim. Acta, 1977, 41, 499.
22. Mackenzie, A.S., Patience, R.L., Maxwell, J.R., Vandenbroucke, M. and Duranc, B., Geochim. Cosmochim. Acta, 1980, 44, 1709.
23. Seifert, W.K. and Moldowan, J.M., Geochim. Cosmochim. Acta, 1981, 45, 783.
24. Noble, R.A., Alexander, R., Kagi, R.I. and Knox, J., Geochim. Cosmochim. Acta, 1985, 49, 2141.

Table 1. Geochemical Parameters based on Biological Marker Compounds.

SAMPLE	Kaurane[a] $\frac{16\beta(H)}{16\alpha(H) + 16\beta(H)}$	Drimane[b] $\frac{8\beta(H)}{8\alpha(H) + 8\beta(H)}$	C_{30}[c] Hopanes $\beta\beta/\alpha\beta$	C_{30}[d] $\frac{\text{Moretanes}}{\text{Hopanes}}$ $(\beta\alpha/\alpha\beta)$	C_{29}[e] Steranes 20S/20R	C_{29}/C_{27}[f] Steranes
Coal						
Solvent Extract	0.07	0.56	2.00	1.50	N.D.	N.D.
Pyrolysate	0.24	0.58	0.55	1.53	0.20	10.8
Hydrogenation	0.65	0.55	<0.05	1.38	0.58	0.8
CO/H_2O	0.20	0.59	0.71	1.48	0.13	17.6
Oil Shale						
Solvent Extract	N.D.	0.78	4.70	0.77	0.10	0.89
Retort	N.D.	0.50	1.01	1.82	0.11	N.D.
Crude Oils						
Terrestrial	0.99	0.99	<0.05	0.10	0.84	5.11
Marine	N.D.	1.00	<0.05	0.13	0.57	0.64

a - 16β(H)-kaurane/16α(H)-kaurane + 16β(H)-kaurane

b - 8β(H)-drimane/8α(H)-drimane + 8β(H)-drimane

c - 17β(H), 21β(H)-hopane/17α(H), 21β(H)-hopane

d - 17β(H), 21α(H)-moretane/17α(H), 21β(H)-hopane

e - (20S)-5α(H), 14α(H), 17α(H)-ethylcholestane/(20R)-5α(H), 14α(H), 17α(H)-ethylcholestane

f - (20R)-5α(H), 14α(H), 17α(H)-ethylcholestane/(20R)-5α(H), 14α(H), 17α(H)-cholestane

N.D. Not determinable

Table 2. Identification of the Triterpanes (m/z 191) and Steranes (m/z 217) present in the Mass Fragmentograms shown in Figs. 2a and 2b.

Triterpanes (Fig. 2a) Peak	Compound	Steranes (Fig. 2b) Peak	Compound
A	17α(H), 22, 29, 30-trisnorhopane	A	20S-13β, 17α-diacholestane
B	18α(H), 22, 29, 30-trisnorneohopane	B	20R-13β, 17α-diacholestane
C	17β(H), 22, 29, 30-trisnorhopane	C	20S-24 ethyl-13β, 17α-diacholestane
D	17α(H), 21β(H)-30-norhopane	D	20R-5α, 14α, 17α-cholestane
E	17β(H), 21α(H)-30-normoretane	E	20R-24-ethyl-13β, 17α-diacholestane
F	17α(H), 21β(H)-hopane	F	20S-24-ethyl-5α, 14α, 17α-cholestane
G	17β(H), 21β(H)-30-horhopane	G	20R-24-ethyl-5α, 14β, 17β-cholestane
H	17β(H), 21α(H)-moretane	H	20S-24-ethyl-5α, 14β, 17β-cholestane
I	22S-17α(H), 21β(H)-homohopane	I	20R-24-ethyl-5α, 14α, 17α-cholestane
J	22R-17α(H), 21β(H)-homohopane		
K	17β(H), 21β(H)-hopane		
L	22S and R-17β(H), 21α(H)-homomoretane		
M	22S-17α(H), 21β(H)-bishomohopane		
N	22R-17α(H), 21β(H)-bishomohopane		
O	Unknown		
P	17β(H), 21β(H)-homohopane		
Q	22S-17α(H), 21β(H)-trishomohopane		
R	22R-17α(H), 21β(H)-trishomohopane		

Table 3. Geochemical Parameters based on Dimethylnaphthalenes, Trimethylnaphthalenes and Methylphenanthrenes.

SAMPLE	DNR-2[a]	DNR-6[b]	TMR-1[c]	TDE-1[d]	MPI-1[e]
Coal					
Solvent Extract	48.3	4.8	1.3	0.9	2.30
Pyrolysate	23.3	2.3	0.5	6.3	0.73
Hydrogenation	44.3	4.1	1.1	4.8	1.12
CO/H_2O	9.3	9.3	0.7	2.7	N.D.
Oil Shale					
Solvent Extract	23.1	1.9	1.3	1.6	1.08
Retort	26.1	1.2	0.8	0.3	0.80
Crude Oils					
Terrestrial	279.0	2.7	0.7	4.9	0.78
Marine	72.6	2.0	0.5	0.3	0.74

a - 2,7-dimethylnaphthalene/1,8-dimethylnaphthalene

b - 2,6- + 2,7-dimethylnaphthalenes/1,4- +2,3-dimethylnaphthalenes

c - 2,3,6-trimethylnaphthalene/1,4,6- + 1,3,5-trimethylnaphthalenes

d - 1,2,5-trimethylnaphthalene/1,2,4-trimethylnaphthalene

e - 1.5 x (2- + 3-methylphenanthrenes)/(phenanthrene)+ 1-methylphenanthrene + 9-methylphenanthrene

N.D. Not determinable

Table 4. Identification of the Aromatic Compounds used in the Parameters defined in Table 2 and shown in the Gas Chromatogram in Fig. 3.

Peak	Compound	Peak	Compound
1	2,6-dimethylnaphthalene	9	1,2,4-trimethylnaphthalene
2	2,7-dimethylnaphthalene	10	1,2,5-trimethylnaphthalene
3	1,4- and 2,3-dimethylnaphthalenes	11	phenanthrene
4	1,8-dimethylnaphthalene	12	3-methylphenanthrene
5	1,4,6- and 1,3,5-trimethylnaphthalenes	13	2-methylphenanthrene
6	2,3,6-trimethylnaphthalene	14	9-methylphenanthrene
7	1,2,7-trimethylnaphthalene	15	1-methylphenanthrene
8	1,2,6-trimethylnaphthalene		

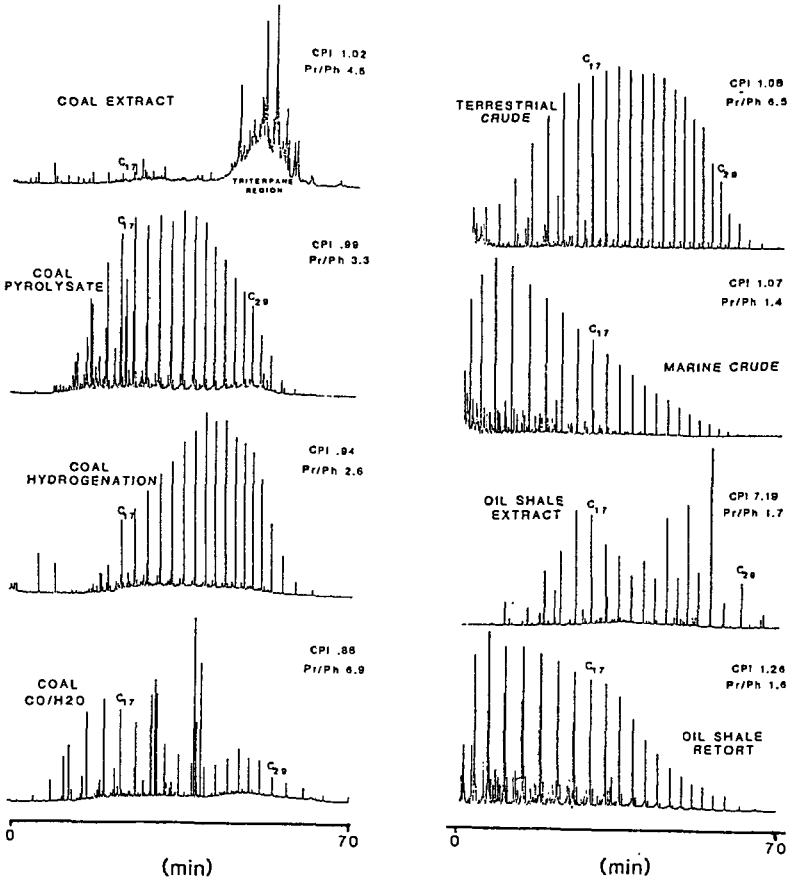

Figure 1. Gas chromatograms of the total aliphatic hydrocarbon fractions of the synthetic and natural crudes.

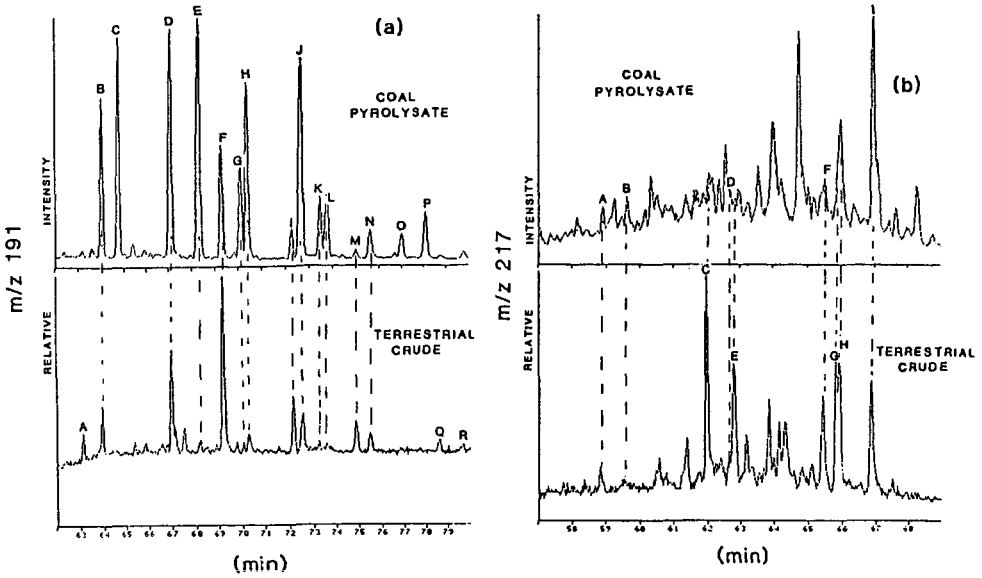

Figure 2. Mass fragmentograms for (a) triterpanes and (b) steranes from the coal pyrolysate and terrestrial crude.

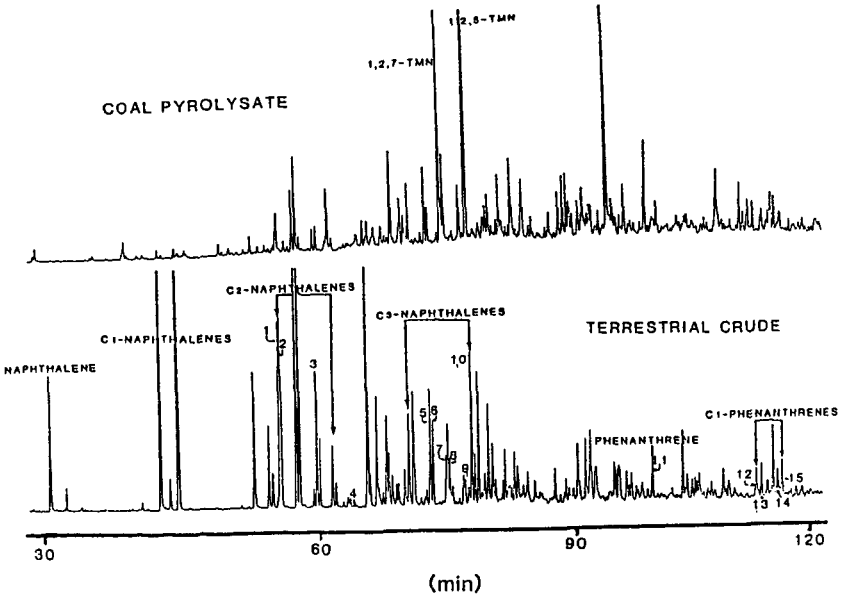

Figure 3. Gas chromatograms of the dinuclear and trinuclear aromatic fractions from the coal pyrolysate and terrestrial crude.

DETERMINATION OF FUEL AROMATIC CONTENT AND ITS EFFECT ON RESIDENTIAL OIL COMBUSTION

S.W. Lee, F. Preto and A.C.S. Hayden

Canadian Combustion Research Laboratory
Energy Research Laboratories
Energy, Mines and Resources Canada
Ottawa, Ontario, Canada
K1A 0G1

ABSTRACT

The increasing use of distillate fuel oils processed from synthetic crudes has caused concern for deteriorated performance due to increased levels of aromatic compounds and increased viscosity of these fuels. The performance characteristics of middle distillate fuels of varying physical and chemical properties, derived from both conventional and synthetic crudes, are being determined on residential combustion systems at the Canadian Combustion Research Laboratory.

The aromatic properties of the fuels are determined using a range of techniques: the fluorescent indicator absorption method (FIA) for total aromatics; the proton nuclear magnetic resonance method (PNMR) for aromaticity and hydrogen distribution; the gas chromatographic/mass spectrometric (GC/MS) method and column chromatographic method for aromatic compound types; the mass spectrometric (MS) method for paraffins, olefins, naphthenes and aromatics (PONA); theoretical calculations based on physical properties for total aromatics; and aniline point measurements.

In this study 22 fuels were examined, and observations correlating the fuel aromatic properties with transient particulate emissions are presented.

INTRODUCTION

An increased awareness of dependency on the oil exporting nations and the volatility of the world oil price market has changed the outlook of the oil industry. Ever since the energy crisis of the 1970's, industry and consumers have come to realize the potential savings of implementing energy conservation measures. The North American petroleum industry has reduced energy consumption significantly in recent years and according to a 1985 survey (1) an additional 14% reduction is technically feasible. One approach, taken by refiners, is to reduce the manufacturing cost by maximizing the use of lower cost components. At the present time, this approach

is highly attractive since good quality conventional resources are being depleted rapidly all over the world, while the global demand for middle distillates is expected to increase (2). The combined effects of energy conservation measures and the natural decline of good quality conventional feedstocks have created new concerns for refiners over fuel oil quality.

Due to cold climate and immense distances, Canada is one of the largest per capita users of oil in the world (3). As a result of these "hardships", Canadian industry and consumers face greater energy conservation challenges than almost anywhere else in the world. In addition to an overall reduction in energy consumption by the population, innovative solutions have to be considered to extend the life of the conventional resources. Such efforts include replacement of oil with alternate energy sources and development of alternate oil supplies such as those from frontier reserves, heavy oils and tar sands from western Canada. Middle distillates processed from synthetic crudes derived from the heavy oils and tar sands of Alberta and Saskatchewan are already on the Canadian market and their production is increasing. By 1990, Canadian tar sands development is expected to increase production capacity from the current 12% to 23% of Canadian crude oil demand with a future increase to 39% in the year 2005 (4). Regardless of fluctuating world oil prices, which depend on numerous unpredictable events and circumstances, it is in the industry's best interest to have at hand the technology which will best utilize the available indigenous resources.

Middle distillates processed from tar sand crudes contain higher proportions of aromatic and naphthenic compounds which can degrade combustion quality (5). The problems associated with the use of highly aromatic fuels are well known and widely documented (6 - 11). A better understanding of the relations between oil properties and their performance could help refiners to better handle such problems and allow more blending flexibility. In the case of heating oils, possible use of lower grade fractions will reduce manufacturing costs and allow diversion of more quality components into diesel fuel and gasoline. With these objectives in mind, an experimental program to study the effects of oil quality on residential oil combustion characteristics is being carried out at the Canadian Combustion Research Laboratory.

In the course of this study, it has become apparent that accurate and reliable analytical techniques for fuel property determinations are critical in order to achieve accurate correlation with performance characteristics. The suitability of the various techniques for use in petroleum refineries is also an important consideration. For example, in the determination of aromatics there are numerous methods available, but limitations associated with each technique restrict its use to certain areas. This paper describes the approaches taken to determine the aromatic content of middle distillate fuels, and presents the correlations observed between fuel aromatics and particulate emissions.

EXPERIMENTAL

Experimental facility.

Detailed descriptions of the experimental equipment and procedures developed for the fuel quality evaluation program have been reported elsewhere (12). Figure 1 is a schematic diagram of the equipment used in the combustion experiments. The experimental rig includes a commercial warm air furnace, a chilled air distribution system, fuel conditioning unit, continuous emission analyzers, and data acquisition and processing equipment. Special emphasis was given to the design of the test rig so that experimental conditions would simulate those of a "real life" residential environment.

Fuel variety.

The middle distillate oils selected for this study were obtained from six major Canadian oil companies and from the National Research Council of Canada. The oils include commercial No. 2 fuels, No. 2 fuels processed from synthetic crudes, light gas oils, light cycle oils, jet fuels, diesel fuels from conventional crudes, laboratory-blend synthetic diesels and oil blends prepared for specific properties.

Experimental procedure.

A typical experimental run required 40-60 minutes of preparation to set the control conditions in the test rig and to calibrate the analyzers. The actual test procedure started with an initial burner start-up (cold start), followed by a continuous one hour run, off for 10 minutes, followed by five 10 minute on/10 minute off cycles operations. A complete experimental run lasted a total of 170 minutes. The control conditions selected for evaluation of all the test fuels included the following: fuel temperature of 7°C and 15°C, oil pump pressure of 689 K pascal (100 psi), furnace exit draft of 0.1 cm (0.04 in) water column, cold air return temperature of 15°C and fuel firing rate of 2.6 litres per hour (0.65 U.S. GPH). The oil nozzle used was of the hollow type (NS) with 80° spray angle. The combustion air supply was set independently for each fuel to obtain a steady-state smoke number of 2 when tested with a Bacharach smoke test instrument prior to the run.

Gaseous emissions of O_2, CO_2, CO, NO_x, and hydrocarbons, along with selected temperatures were continuously monitored during the entire run. Data acquisition was carefully planned at selected intervals so that the critical start-up and shut-down transient emissions were recorded. Particulate emissions were measured during the start-up transient period using calibrated diesel exhaust smoke opacity meter (Celesco model 107, Berkeley Instruments) which had been previously modified for these tests.

Fuel characterization methods.

The analytical techniques used to characterize the fuels include ASTM standard methods for density, viscosity, distillation, flash point, pour point, analine point and aromatic components. Additional techniques used for the determination of aromatics are proton nuclear magnetic resonance (PNMR) for aromaticity and gas chromatography/mass spectrometry (GC/MS) for hydrocarbon compound types.

Proton nuclear magnetic resonance spectroscopy.

Two laboratories were utilized for this analysis. Laboratory 1 used a Varian CFT-20. Laboratory 2 applied a 90 MHz Varian EM-390 spectrometer. Sample to solvent concentration ratios of 50/50 were used to record the spectra. Chloroform $-d_1$ (99.9%) with ME_4Si was used as solvent.

Mass spectroscopy.

A Finnigan 4500 quadropole mass spectrometer was used for MS and GC/MS determinations of PONA and mono-, di-, and poly-aromatic fractions. The samples were separated using a 1.83 m column (3% Dexil 300 on acid washed Chromosorb W) heated from 60°C to 300°C at a programmed rate of 8°C/min. Chemical ionization (methane) mass spectra were acquired continuously during the gas chromatographic separation on a 3 second cycle. The series of peaks characteristic of each given class of compounds - paraffin, naphthenes, and aromatics - were summed continuously throughout the run in characterizing the compound type classes. The olefin content was determined using the PNMR method and any interfering peaks in the mass spectra were corrected. The detailed PONA method is available in the published literature(13).

RESULTS AND DISCUSSIONS

Determination of aromatic components in test fuels.

While it is well known that aromatic hydrocarbons increase particulate emissions and cause related problems in combustion, the method for determining aromatics is not straightforward. The FIA (fluorescent indicator absorption) method is the most widely used standard method (ASTM D 1319) in the oil industry, although it is known to have poor accuracy. Its application is also limited to light distillate oils. GC/MS and NMR methods provide better accuracy and precision but are labour and cost intensive. The industry has

not completely accepted these sophisticated instrumental techniques since they require specially trained operators and temperature controlled environments. High performance liquid chromatography (HPLC), with its efficient chromatographic column, is known to provide good separation of hydrocarbons but its detection technique is somewhat limited. The two most common detection systems, ultraviolet (UV) and refractive index (IR), are very compound specific to hydrocarbon compound types and require extensive calibration for all compounds present in oils. Therefore, this method is not practical for refinery applications although the instrumentation is less costly and less sophisticated than for GC/MS and NMR. Two detectors considered to be preferable to the UV and IR are the flame ionization detector (FID) and the dielectric constant (DC) detector. As part of the research program described herein, further work is being carried out to develop a nonconventional simple method for determining the aromatics in oils by HPLC with FID detection.

Due to the above discussed variations and limitations involved in aromatic analysis, it was decided to apply several different techniques to determine the aromatic components of the test fuels evaluated in this study. Table 1 shows the aromatic data of 22 test fuels as determined by different techniques. Since it is critical to have accurate fuel property data in establishing the fuel quality/performance characteristics, attempts were made to have duplicate analyses done by independent laboratories whenever possible. Aromatic content is gathered from PONA data using the GC/MS technique. It is defined as the percent of aromatic type hydrocarbons determined on a molecular basis. Aromaticity as described herein represents the percent carbon in aromatic rings or the ratio of aromatic carbons to the total number of carbons (14). It can be determined by proton NMR or carbon 13 NMR methods. Aromaticity data were chosen for duplicate independent analysis since NMR is less dependent on the instrument, operator, and method than GC/MS. Aniline point measurements were made using the ASTM D 611 standard method.

The correlation between different analysis methods can be seen in Figures 2 and 3. The aromatic content and aromaticity data are in good agreement and have a linear correlation coefficient of 0.958. The aniline point data show greater spread (Figure 2) which could be due to the fact that aniline point is not an absolute parameter but only provides a measure of aromatics. As well, aniline point is known to give poor accuracy in the analysis of heavy fuels. The correlation coefficient for the aniline point data is 0.928.

Figure 3 is the regression plot of the FIA and aromatic content data. It shows a positive linear correlation with a correlation coefficient of 0.963. However, the method cannot provide data for some heavy fuels due to incomplete separation in column chromatography.

Figure 4 compares the aromaticity data from two independent laboratories. The slight variation is due to the difference in data manipulation methods used by the two laboratories. Laboratory 1 used

the Brown and Ladner method which assumes that the paraffinic hydrogen to carbon ratio is exactly 2.0 (15). Laboratory 2 took the assumption that the hydrogen to carbon ratio is larger than 2.0 and also incorporated corrections associated with other physical properties such as density and refractive index (16). The combined data show good agreement with a correlation coefficient of 0.971.

The physical and chemical properties of all the test fuels are reported in Table 2. The correlation between physical properties, e.g. fuel density, and aromatic properties was also studied as illustrated in Figure 5. Aromaticity and density exhibit a good linear relation with a correlation coefficient of 0.942. Aniline point data show wide variation which can be attributed to the reasons previously discussed.

Significant improvement can be seen in aniline point data correlation when it is related to the K factor of the fuels. K factor, also known as the Watson characterization factor, is defined as

$$K = \frac{(T_{b,R})^{1/3}}{s}$$

where $T_{b,R}$ = molal average boiling point, ^{o}R

s = specific gravity at 60/60 F (17).

K factor is the most widely used index of composition in the characterization of petroleum crude oils.

From Figure 6, the improved correlations are 0.979 and 0.963 for aromaticity-K factor and aniline point-K factor respectively. The improvement is due to the incorporation of boiling points rather than considering only one parameter: density (specific gravity). K factor is the most promising parameter for refinery use since it can be easily calculated from the boiling points and specific gravity data, which are readily available from fact sheets. As part of this research study, correlations are being developed to use K factor in place of fuel aromaticity to predict fuel performance.

Effect of fuel aromatics on soot production.

The effects of fuel aromatic compounds on combustion processes have been widely studied and are well documented in the literature. The impact of aromatics on residential oil combustion, especially on the increased generation of incomplete combustion products (e.g. particulates, carbon monoxide and hydrocarbons) have been examined under the research program described herein. Discussion in this paper is limited to soot production.

In the literature on solid particle emissions from combustion processes measurements for parameters such as smoke, particulates,

opacity and soot are reported based on the specific methods and instrumentation used. Particulates, which are generally defined for regulatory purpose as "any material with the exception of water that collects on a filter operated in an air-diluted exhaust stream" require multi-step, time consuming and expensive operations. Soot or carbon is defined as the nonvolatile portion of particulates and can be measured by thermogravimetric analysis or by the removal of condensed hydrocarbons from the particulates. Commercial smoke meters provide smoke opacity or transmittance readings and smoke testers such as Bosch and Bacharach (ASTM smoke number) offer smoke numbers. Although these methods all measure some sort of "unburnt combustion solids", conversion between the various methods is difficult if not impossible. Attempts at this have been made by Homan(17) who reports conversion factors among 11 smoke measurements; Alkidas(18) reported on the relationship between smoke measurements and particulates.

In this study, solid particles from furnace exhaust are measured with a Celesco smoke opacity meter and a Bacharach smoke number tester. The calibration of the smoke meter, and correlation with particulate mass concentration, has been carried out and reported elsewhere (20). Analytical data are reported in terms of percent opacity for ease of discussion; each reading represents opacity per transient phase or per cycle. For cyclic operations, data reported is the mean of a 5 cycle test.

The analytical precision of the data from opacity measurements of all test fuels has been discussed in a previous publication(12). Each value represents the mean of data from a minimum of 3 runs, with precision expressed as the coefficient of variation. For regular commercial No 2 fuels, transient emissions show variation of less than 7%. Heavy and highly aromatic fuels which usually experience combustion problems, show poor precision with errors usually higher than 20%. The error increases with decreasing oil quality. The regression plots in this paper show data from both a wide range of fuels. The errors associated with the lower grade fuels (usually on the right hand of the graph) are much larger than for the better quality oils (data on the left hand side).

The precision of the data is also affected by the run type. Transient opacity readings from cyclic operations show better precision than for cold start trials. This is a direct reflection of the effect of oil temperature on combustion. Cold start operations are subject to cold fuel and environment, whereas the subsequent cyclic starts experience more favourable conditions. For example, even though for all the experiments reported herein the fuel tank temperature was maintained at 15°C, the oil temperature at the nozzle adapter at the beginning of a cold start averaged 17 - 20 °C as compared to 40 - 75 °C for cyclic runs.

Opacity readings from cold start and cyclic transient phases from combustion tests of 22 fuels are reported in Table 4. Figure 7 graphically compares cold start and cyclic data. Aromaticity, being the most reliable among 4 different parameters, is used as the measure of fuel aromatic components. The current data indicate an

exponential increase in smoke opacity at cold start ignition for an increase in aromatic components. The breakaway point at 45% aromaticity suggests the upper limit which the fuels can tolerate without excessive emission levels. Opacity readings normally observed from domestic furnaces firing with commercial No. 2 fuels are 1.5% to 2.5% at the cold start transient phase. Cyclic operations generate much lower smoke due to a more favourable combustion environment. The effect of aromatics during normal furnace on/off operation is less pronounced even when oils with considerably high aromatic content are used. The average opacity per cyclic start for commercial furnace fuels is between 0.3% to 0.7%. The worst case observed (1.8% opacity) is for fuel with aromaticity of 59%.

From these observations, it appears that aromaticity is the prime factor causing soot production from residential burners. In reality, the observed combustion characteristics including gaseous and particulate emissions and burner ignition behaviour are caused by several physical and chemical properties, interrelated in a complex manner. For example, the breakaway point at 45% aromaticity, as seen in Figure 7, coincides with the following breakaway points in the applicable plots: 60% aromatic content, 4 c St fuel viscosity and cetane index of 25. Results describing the overall effects of aromatics, viscosity, and other physical and chemical properties on soot production have been reported elsewhere (18). It should be noted that in the opacity - aromaticity regression plots data from fuels with viscosity higher than 3.5 c St are omitted in order to try and isolate viscosity effects. It is impossible to totally isolate the effect of any one parameter on combustion performance, however a general indication of its importance may be drawn.

The research program described in this paper is continuing with the objective of incorporating all of the significant fuel oil properties into a mathematical model which predict combustion performance based on oil properties.

ACKNOWLEDGEMENTS

The authors express their appreciation to D.B. Barker and T.G. Sellers for their technical assistance and Mr. R. Lafleur and Dr. B. Glavincevski and for fuel analysis data. Thanks are also due to the Canadian oil companies who contributed test fuels for this program.

REFERENCES

1. Pelham, R.O. and Moriarty, R.D., Oil & Gas Journal, May, 65-77 (1985).
2. Schrepfer, M.W., Arnold, R.J., Stansky, C.A., Oil & Gas Journal, January, 79-93 (1984).

3. Alberta Energy and Resources, "Report ENRI/19-1", Edmonton, Alberta, Canada (1982).
4. Canadian National Energy Board, "Canadian Energy Supply and Demand 1983-2005", September 1984.
5. Steere, D.E. and Nunn, T.J., "SAE Technical Paper Series No. 790922 ", October 1979.
6. Brown, T.D. and Hayden, A.C.S.,CANMET Report ERP/ERL 78-24(CF), (1978).
7. Brown, T.D. and Hayden, A.C.S., CANMET Report ERP/ERL 78-02(CF), (1978).
8. Herlan, A., Combustion and Flame, 31,297-307 (1978).
9. Zahavi, E., Gal-Or, B. and Burcat, A., J. Inst. Energy, 28-40, March 1982.
10. Willis, D.J., "Institute of Mechanical Engineers Conference Publications" Paper C71, (1983).
11. Mill, G.A., Howarth, J.S., Howard, A.G., J. Inst. Energy. 57, (1984).
12. Lee, S.W. and Hayden, A.C.S., "ASHRAE Transactions" 86, (1986).
13. Ozobko, R.S., Clugston, D.M., Furimsky, E., Anal. Chem. 53:183 - 187 (1981)
14. King, P.J. and Sagarra, A., in "Modern Petroleum Technology", Hobson, G.D. and Phol, W. Eds. 4th publication. Institute of Petroleum. Applied Science Publication Service. (1973).
15. Brown, J.K, and Ladner, W.R., Fuel, 39, 87-96 (1960).
16. Glavincevski, B., Personal communication, (1985).
17. Watson, K.M. and Nelson, E.F., Ind. and Eng. Chem.,25, 880 - 887 (1933).
18. Homan, H.S., "SAE Technical Paper Series No. 850267", March 1985.
19. Alkidas, A.C., "SAE Technical Paper Series No. 840412", March 1984.
20. Lee, S.W. and Hayden, A.C.S., "ASHRAE summer meeting, Portland, Oregon." June 1986. Submitted for presentation.

Table 1. Aromatic Properties of Fuels.

Fuel	FIA %			MS %				Aromaticity %		Aniline point
	A	O	S	P	O	N	A	Laboratory1	Laboratory2	°C
C	45	3	53	24	0	34	42	31	31	45
D	na	na	na	29	0	38	33	24	22	60
E	23	11	66	32	0	43	25	21	19	61
F	na	na	na	21	0	26	42	42	44	31
L	38	1	61	29	0	36	35	21	27	55
M	71	1	28	15	0	20	65	40	48	26
N	29	1	70	33	0	37	30	16	22	57
O	78	2	21	10	0	14	76	51	59	5
P	78	1	22	13	0	13	74	48	54	7
Q	28	1	71	32	0	41	27	15	19	61
R	20	0	82	37	0	40	23	9	16	56
V	32	1	31	31	0	46	28	14	17	46
W	30	1	70	33	0	42	30	15	22	50
X	42	1	57	27	2	28	48	32	42	29
Y	55	2	44	23	1	30	50	34	43	36
Z	34	1	66	31	0	46	27	18	21	57
AA	33	1	67	28	0	51	26	18	23	56
BB	45	4	52	31	0	35	39	28	38	41
CC	59	1	39	25	0	27	54	36	44	30
DD	69	3	28	19	0	21	64	46	53	14
EE	62	2	36	14	0	17	68	45	49	25
FF	31	2	67	35	1	35	29	20	25	56

A, O, S denotes aromatics, olefins, saturates
P,O, N,A denotes paraffins, olefins, naphthenes, aromatics
na denotes not available

Table 2. Physical and Chemical Properties of Fuels.

Fuel	Density kg/l 15°C	Viscosity c St @ 40°C	Heat of combustion MJ/Kg	Simulated distillation °C 5%	°C 95%	Flash point °C	Pour point °C	Refractive index
C	0.88	2.91	44.8	160	387	62	-39	1.50
D	0.86	3.04	46.2	188	357	64	-29	1.48
E	0.86	3.26	46.8	211	351	88	-26	1.48
F	0.92	3.42	44.6	189	421	67	-52	1.49
L	0.86	2.68	44.0	190	404	62	-18	1.49
M	0.93	3.60	42.9	221	359	114	-13	1.53
N	0.85	2.09	44.3	196	357	62	-30	1.47
O	0.95	2.82	42.4	179	309	87	-24	1.55
P	0.94	2.82	43.2	184	316	101	-27	1.54
Q	0.85	2.59	45.5	172	363	63	-29	1.47
R	0.80	1.28	46.2	121	220	48	-51	1.45
V	0.84	1.74	45.3	94	414	11	-60	1.47
W	0.84	1.88	45.3	134	356	21	-36	1.47
X	0.86	1.35	44.2	127	376	10	-60	1.51
Y	0.91	3.26	43.7	207	380	70	-33	1.52
Z	0.87	4.09	44.8	204	378	72	-33	1.49
AA	0.88	5.12	44.7	211	386	74	-42	1.49
BB	0.88	2.65	44.5	206	332	73	-24	1.50
CC	0.90	2.70	43.9	213	329	78	-36	1.51
DD	0.94	2.77	42.7	224	330	83	-27	1.54
EE	0.92	2.90	43.2	185	380	65	-51	1.53
FF	0.86	2.52	45.1	200	325	70	-30	na

* na denotes not available

Table 3. Correlation of Fuel Properties and Particulate Emissions.

Fuel	Aroma-ticity%	Aromatic content%	Analine point°C	Diaromatics %(GC/MS)	K factor	Opacity% (cs)	Opacity% (cy)	Smoke # (cs)	Smoke # (cy)
C	31	42	45	12	11.29	1.3	0.7	6	6
D	22	33	60	12	11.56	1.6	0.5	8	6
E	19	25	61	6	11.64	1.8	0.6	7	6
F	44	42	31	12	11.01	1.5	2.2	9	7
L	27	35	55	13	11.45	1.9	1.3	7	7
M	* 48	65	26	19	10.81	* 52.3	1.8	>9	7
N	22	30	57	8	11.55	0.7	0.2	6	6
O	59	76	5	44	10.46	16.8	1.9	>9	7
P	54	74	7	30	10.62	9.1	2.1	8	7
Q	19	27	61	5	11.68	1.6	0.4	7	6
R	16	23	56	3	11.79	0.3	0.1	6	4
V	17	28	46	2	11.54	1.6	1.2	8	7
W	22	30	50	5	11.58	2.0	0.6	7	6
X	42	48	29	18	11.21	2.1	1.8	7	6
Y	43	50	36	22	11.03	10.4	1.2	>9	7
Z	* 21	27	57	7	11.52	* 2.4	1.0	>9	6
AA	* 23	26	56	6	11.43	*14.8	0.6	9	5
BB	38	39	41	13	11.22	3.0	1.2	8	6
CC	44	54	30	19	11.01	5.0	2.3	8	7
DD	53	64	14	34	10.61	15.4	1.8	>9	7
EE	49	68	25	na	10.81	20.9	2.9	>9	7
FF	25	29	57	10	11.57	2.3	0.6	5	4

cs denotes cold start
cy denotes cyclic start

- data not used in regression plots as fuel viscosity was higher than 3.6 c St.

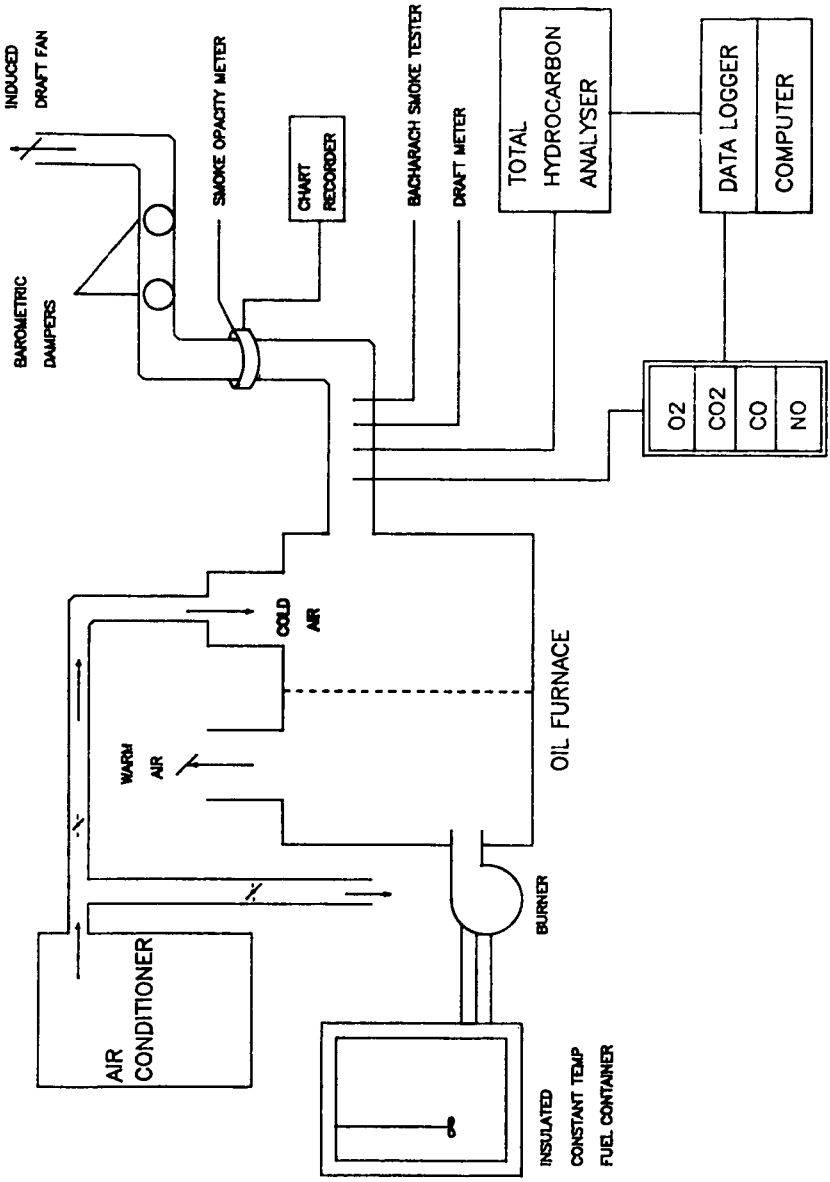

Figure 1. Schematic of the laboratory equipment facility used in the fuel quality evaluation experimental program.

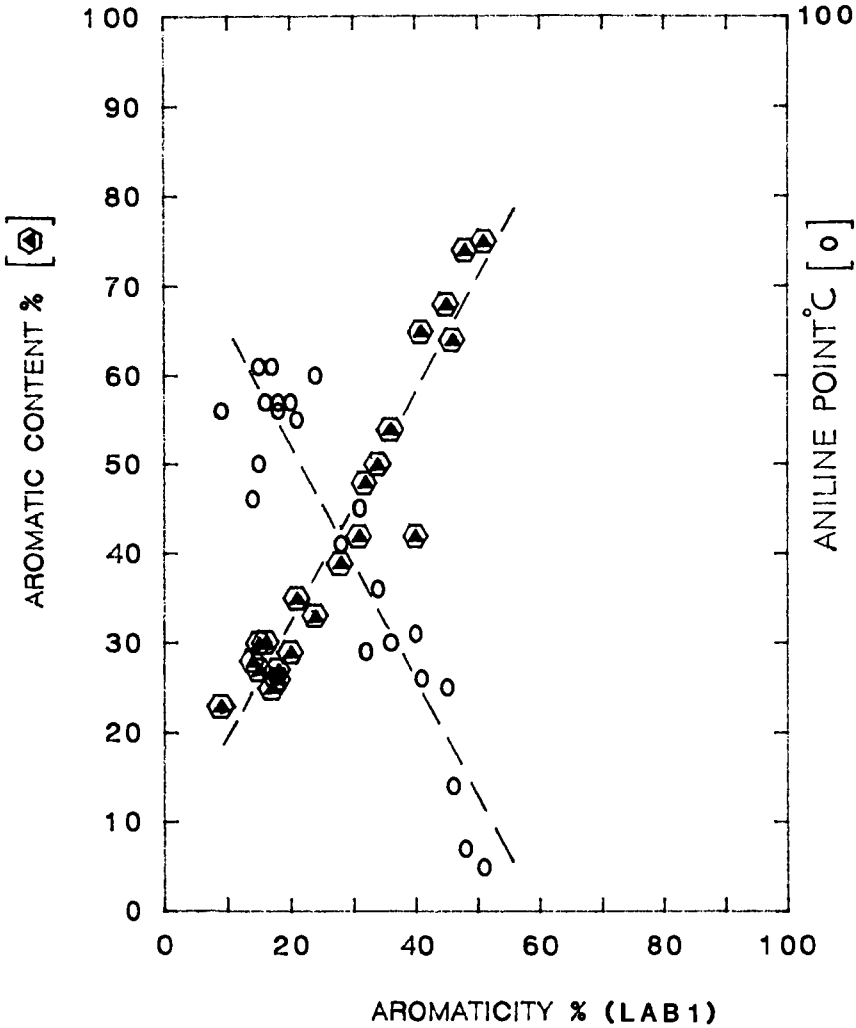

Figure 2. Comparison of fuel aromatic data as determined by three different analytical techniques.

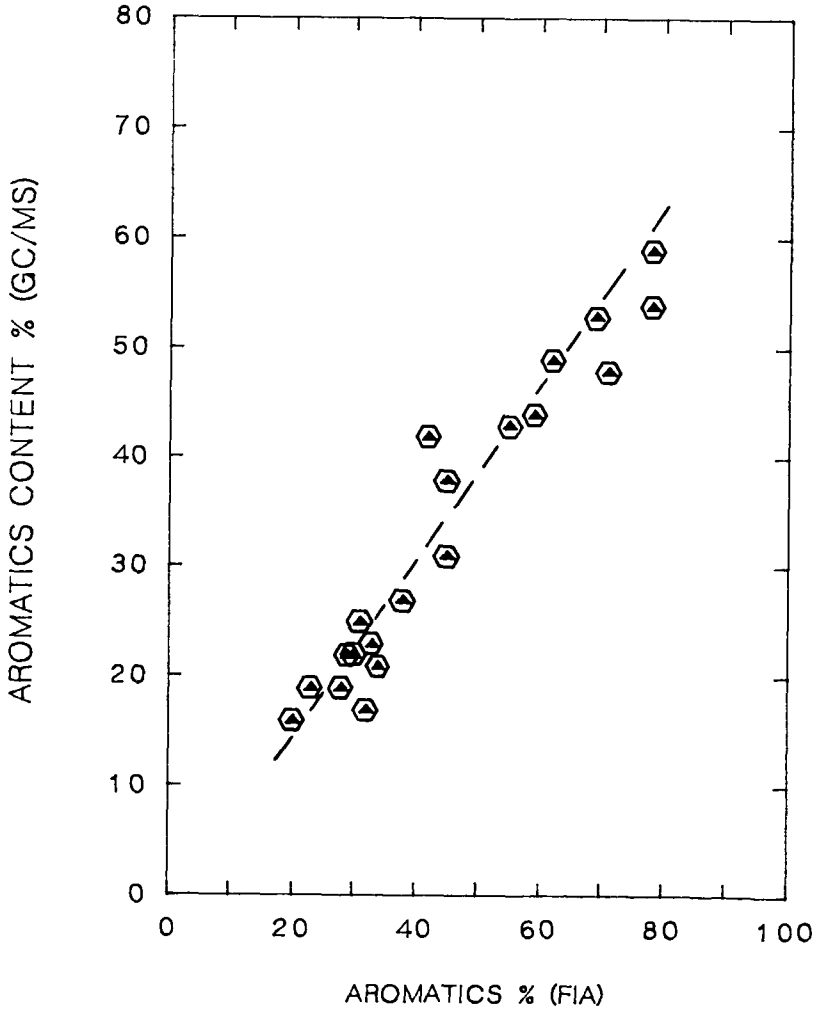

Figure 3. Correlation between fuel aromatic data as determined by GC/Ms method and FIA method.

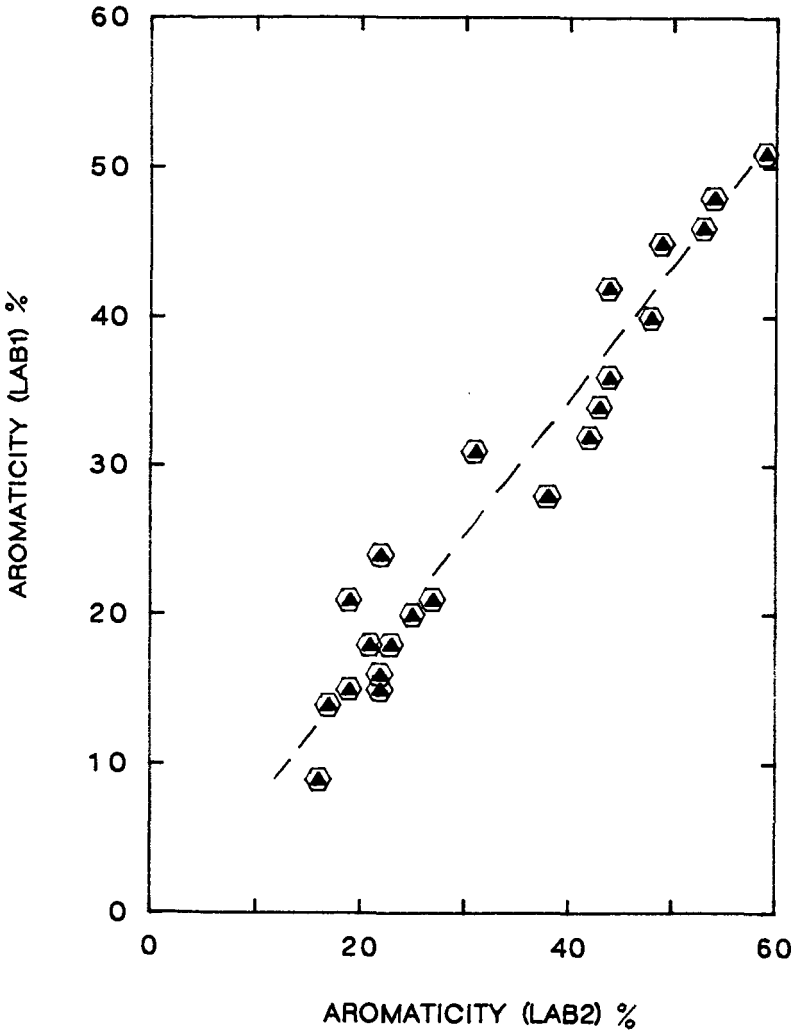

Figure 4. Comparison of fuel aromatic data as determined by two independent laboratories using PNMR technique.

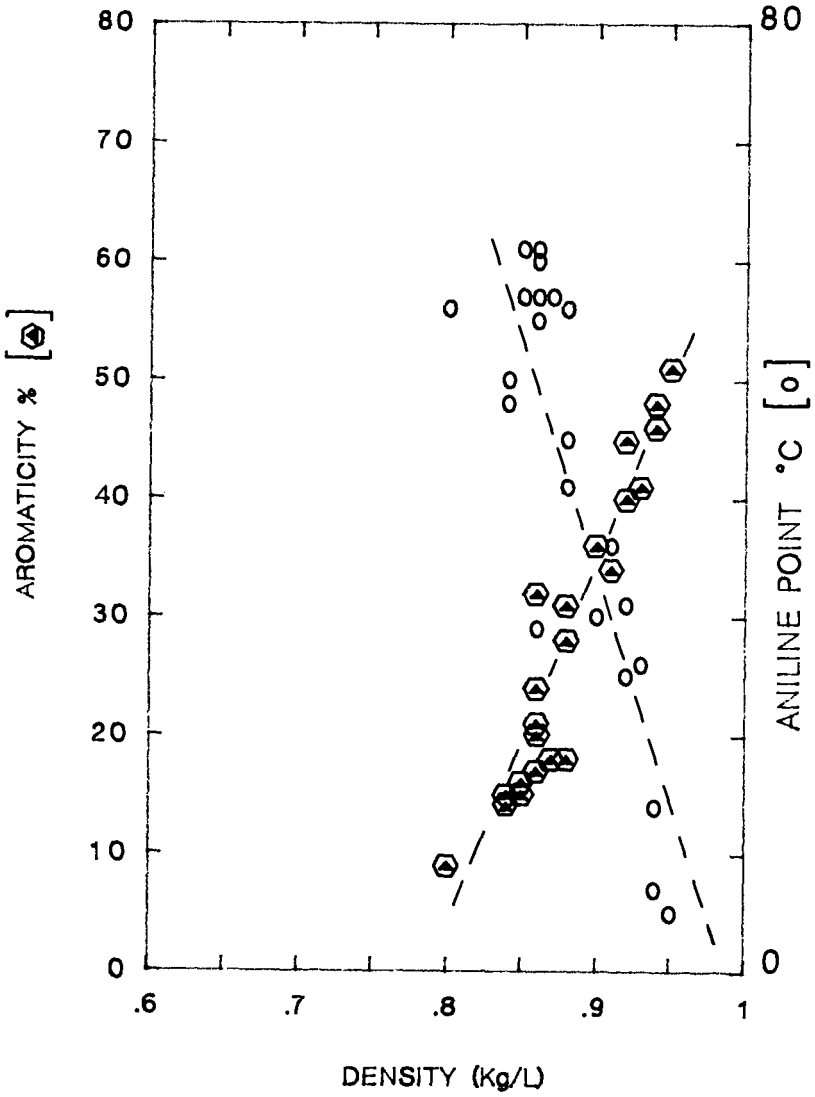

Figure 5. Correlations between fuel density and fuel aromatic data as determined by PNMR and aniline point determination techniques.

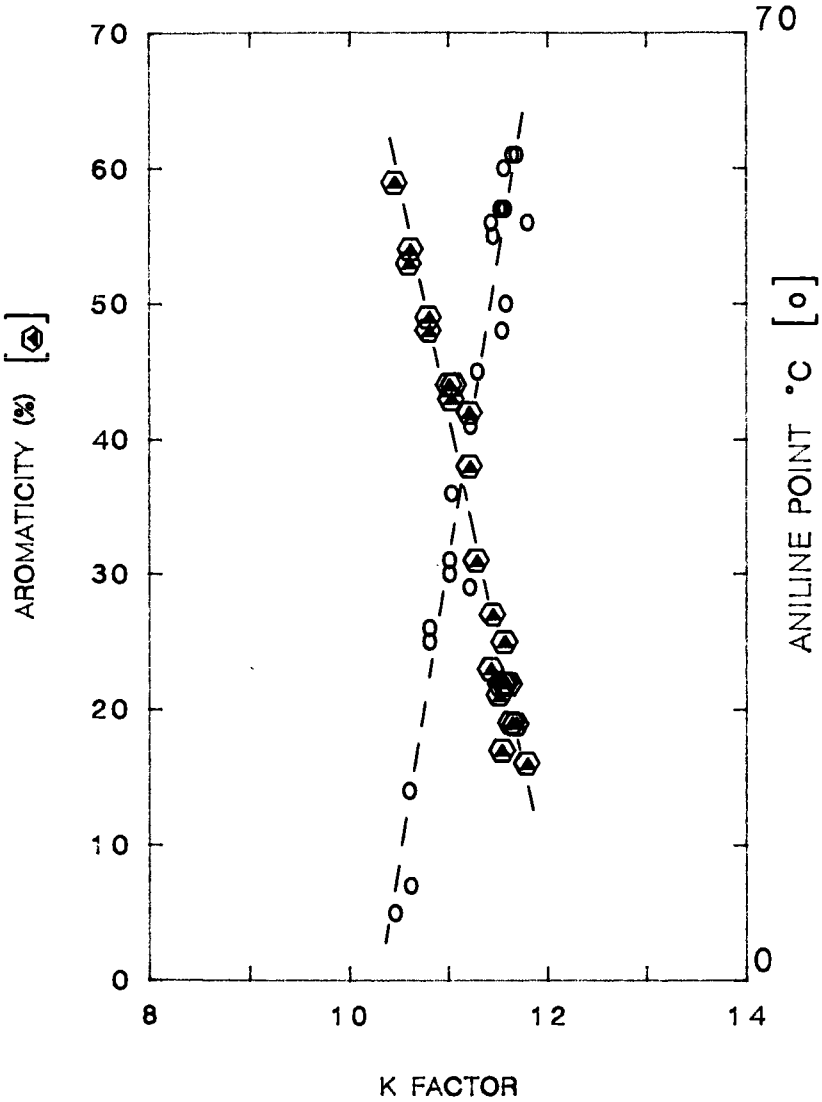

Figure 6. Correlations between Watson K factor and fuel aromatic data as determined by PNMR and aniline point determination techniques.

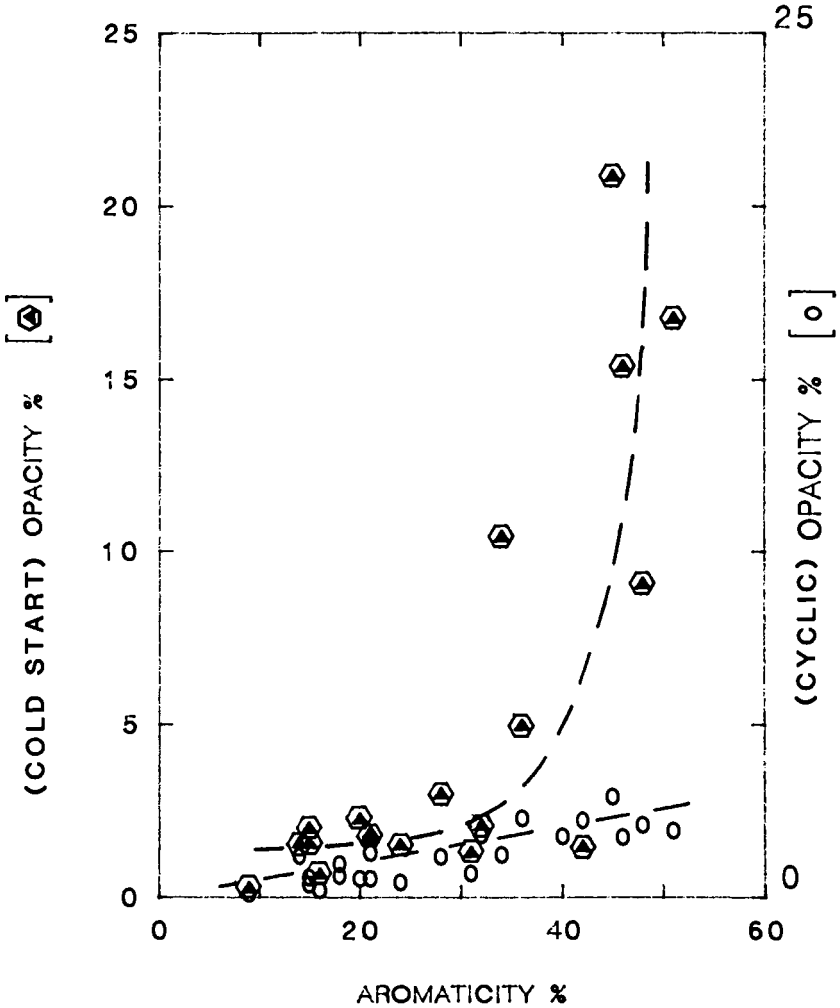

Figure 7. Correlations between fuel aromaticity and transient smoke opacity from cold start and cyclic operations.

IDENTIFICATION OF ORGANIC COMPOUNDS IN THE BITUMEN OF CHATTANOOGA OIL SHALE

Chris W. McGowan, Barbara E. Greenwell, David J. Crouse, Richard Markuszewski*, John J. Richard* and Michael J. Sepaniak**

*Dept. of Chemistry, Tennessee Tech University, Cookeville TN 38505
**Ames Laboratory, Iowa State University, Ames, IA 50011
**Dept. of Chemistry, University of Tennessee, Knoxville TN 37996

ABSTRACT

The bitumen of Chattanooga oil shale has been extracted with benzene. The benzene-soluble material was separated into acid, base and neutral fractions with ion exchange chromatography. This separation scheme has been used extensively to separate the organic material in Green River oil shale. The acid fraction was esterified with BF_3/MeOH. A large portion of the acid fraction was not esterified and this material was considered to be phenolic. The bases were separated into two fractions using alumina. The esters, the two base fractions and the total neutral fraction were analyzed using gas chromatography coupled to mass spectrometry. Two series constituting the methyl esters of normal carboxylic acids and carboxylic acids containing one double bond were identified. No homologous series were indicated in the base fraction. The base fraction was highly aliphatic. The major components in the neutral fractions were two series constituting normal and isoprenoid alkanes. A series of cycloalkanes and a series of alkenes were also indicated. The analysis scheme employed functions well for the separation and identification of aliphatic materials.

INTRODUCTION

Several cores of Chattanooga Shale from Tennessee have been extracted with benzene. The benzene-soluble bitumens have been further separated into acid, base and neutral fractions (1). In that study, the bitumen was dissolved in benzene and the acid fraction was absorbed on IRA 904 anion exchange resin. The acids were stripped from the resin by Soxhlet extraction with five percent acetic acid in benzene. In a similar fashion, the bases were absorbed on A-15 cation exchange resin and stripped by Soxhlet extraction with five percent isopropyl amine in benzene. The unabsorbed material constituted the neutral fraction. This separation scheme was adapted from the scheme proposed by Jewell et al. (2) and has been used to separate organic material associated with Green River oil shale (3,4,5). This scheme has been very successful in separating the mostly aliphatic material in Green River oil shale. Chattanooga oil shale, however, has been shown to be highly aromatic (6). The work presented in this paper was performed to identify components of the bitumen of Chattanooga oil shale and to make a comparison of the results to corresponding results for Green River oil shale.

Cooper (7) has extracted a Chattanooga oil shale outcrop in Texas and identified the presence of normal carboxylic acids from C_8 to C_{28} with a maximum at C_{16}. The ratio of even numbered carboxylic acids to odd numbered acids was measured at 1.56. Leddy et al. (8) extracted Antrim oil shale (a similar formation of the same age in

Michigan) with toluene and identified a series of normal alkanes and porphyrins.

EXPERIMENTAL

The acid fractions were esterified using boron trifluoride in methanol as described by McGowan and Diehl (9). Approximately 0.1-g samples of the acid fraction were boiled for five minutes in five mL of 14 percent boron trifluoride in methanol. The esters were extracted with two five-mL portions of pentane. Not all of the organic material was extracted into pentane. The base fraction was placed on an activated alumina column and eluted with hexane followed by benzene thus producing two fractions. The neutral fraction was not separated further.

The esters, the total base fraction and the neutral fraction were initially separated by gas chromatography on a six-foot, 1/8-in Tenax column which was temperature programmed from 100°C to 350°C with a flame ionization detector (FID). The esters the two base fractions and the neutral fraction were later separated on a 30-meter DB-5 fused silica capillary column which was temperature programmed from 50°C to 310°C with FID detection. Finally the separation was performed using the capillary column coupled to a mass spectrometer. A Finnegan 4000 GC/MS system was used. Mass spectra were recorded for the major peaks in each fraction.

RESULTS AND DISCUSSIONS

The pentane-insoluble organic matter remaining after the esterification process represented a highly polar material. This material was considered to be phenolic. However highly polar esters could also have been present. The presence of inorganic salts in the residue and the high volatility of the produced esters made quantitation of this polar material difficult. Attempts were made to quantitate the amount of weak acids (phenols) in the acid fraction by extraction of the carboxylic acids with $NaHCO_3$ solutions and back extraction after acidification. The extracted materials and residues were very gelatinous and difficult to work with. No conclusive results were obtained. This material was not analyzed further.

The gas chromatograms resulting from the DB-5 column and flame ionization detector for the esters, the hexane-soluble base fraction and the neutral fraction appear in Fig. 1. Three homologous series account for all of the major peaks in the esters of the acid fraction. One of the series was composed of normal alkanes ranging from C_{15} to C_{40} with a maximum at C_{24}. The alkanes were absorbed by the polyvinyl benzene portion of the ion exchange resin and later stripped by the acetic acid/benzene solvent. The major series in the ester fraction was composed of the methyl esters of normal carboxylic acids. Normal saturated carboxylic acids from C_6 to C_{26} were identified with a maximum at C_{16}. There was a definite predominance of the even numbered carboxylic acids to the odd numbered carboxylic acids. The methyl esters of the even numbered normal acids constituted 36 percent of the fraction while the methyl esters of the odd numbered normal acids constituted only five percent. A second series was composed of the methyl esters of normal carboxylic acids containing one double bond. Unsaturated acids from C_{10} to C_{20} were identified with a maximum at C_{18}. The

position of the double bond was not identified in this study. However, the mass spectrum of the methyl ester of the C_{18} unsaturated acid was almost a perfect match with the library generated mass spectrum for methyl oleate. Although not as pronouced as for the saturated acids, there was also a definite predominance of the even numbered unsaturated acids to the odd numbered unsaturated acids. The methyl esters of the even numbered unsaturated acids constituted eleven percent of the fraction while the methyl esters of the odd numbered unsaturated acids constituted four percent. Methyl esters of isoprenoid carboxylic acids were not identified. Methyl esters of aromatic carboxylic acids were not identified.

No clear homologous series of bases were identified. No base was unambiguously identified. The mass spectrum of most the components of the base fraction indicated the presence of alkyl amines. Alkyl amines from C_{15} to C_{26} containing from zero to three degrees of unsaturation were indicated. Five components had mass spectra which indicated highly aromatic systems. One of these was tentatively identified as a C_{18} quinoline (10).

The major series in the neutral fraction was composed of normal alkanes ranging from C_{12} to C_{31} with a maximum at C_{17}. A second homologous series was composed of isoprenoid alkanes ranging from C_{15} to C_{25} with a maximum at C_{19}. Both phytane and pristane were identified. Two other homologous series, together equal in concentration to the isoprenoid series, were composed of hydrocarbons containing one degree of unsaturation. The mass spectra of these compounds indicated a series containing rings and a series containing double bonds. A C_{18} alkane containing a cyclohexyl ring was identified. Cycloalkanes from C_{15} to C_{22} were indicated with a maximum at C_{18}. A C_{17} alkene was identified. Alkenes from C_{13} to C_{20} were indicated with a maximum at C_{17}. Two other homologous series, in very low concentration, were indicated by the gas chromatograms but were not identified by mass spectrometry. There was no even to odd predominance in either of the alkane series, the cycloalkane series or the alkene series. No aromatic compounds were indicated as major components of the neutral fraction.

The major compounds identified in this study were essentially the same as the major compounds identified in Green River oil shale (11,12,13,14,15). The notable exceptions were the presence of isoprenoid carboxylic acids and dicarboxylic acids in Green River oil shale; and the presence of unsaturated carboxylic acids and alkenes in Chattanooga oil shale. The presence of unsaturated acids and alkenes was unexpected and has not been noted previously for Chattanooga oil shale. Unsaturated essential fatty acids, such as oleic acid, were probably present at the time of deposition of both Chattanooga and Green River oil shale. However the conditions of lithification have apparently destroyed the double bonds in the case of Green River oil shale while preserving the double bonds in the case of Chattanooga oil shale.

The major components identified in each fraction in this study were aliphatic in nature. Only a few aromatic bases were indicated. The infrared spectra of each fraction (1) indicated the presence of aromatic material. The separation scheme employed in this study including the fractionation, derivatization and gas chromatography

did an excellent job of identifying aliphatic material. While this scheme works well in identifying the primarily aliphatic components in Green River oil shale, the scheme falls short in identifying all the major components of Chattanooga oil shale. The aromatic material present in Chattanooga oil shale was not identified. Some of the aromatic material may have been present in the pentane-insoluble portion of the esterified acids. It is possible that the aromatic material in Chattanooga oil shale is present primarily in the kerogen and not in the soluble bitumen. However this seems unlikely.

CONCLUSIONS

A series of normal alkanes and a series of normal carboxylic acids have been identified in the acid fraction of the bitumen of Chattanooga oil shale. An unexpected series of normal carboxylic acids containing one double bond has also been identified. There was a definite predominance of even numbered acids to odd numbered acids. The base fraction was primarily aliphatic. A series of normal alkanes, a series of isoprenoid alkanes and a series of cycloalkanes have been identified in the neutral fraction. An unexpected series of alkenes was also identified. The separation scheme employed does not identify any aromatic materials as major components of the bitumen.

ACKNOWLEDGEMENTS

The work at Ames Laboratory was supported by the Assistant Secretary for Fossil Energy. Ames Laboratory is operated for the U. S. Department of Energy by Iowa State University under Contract No. W-7405-Eng-82.

REFERENCES

1. McGowan, C.W., Leimer, H.W. and Kerr, C.P., "Characterization of Organic Material in Chattannoga Oil Shale and Shale Oil," Synthetic Fuels From Oil Shale And Tar Sands, Institute of Gas Technology, Chicago, 229, 1983.

2. Jewell, D.M., Weber, J.H., Bunger, J.W., Plancher, H. and Latham, D.R., Ion Exchange, Coordination and Adsorption Chromatographic Separation of Heavy End Petroleum Distillates," Anal. Chem., 44, 1391, 1972.

3. Chong, S-L., Cummins, J.J. and Robinson, W.E., "Fractionation of Soluble Extracts Obtained from Kerogen Thermal Degradation with CO and H_2O," Am. Chem. Soc. Div. Fuel Chem. Preprints, 21, 265, 1976.

4. Chong, S-L., Cummins, J.J. and Robinson, W.E., "Alkanes Obtained by Thermal Conversion of Green River Oil-Shale Kerogen Using CO and H_2O at Elevated Pressure," Isr. J. Technol., 17, 36, 1979.

5. Chong, S-L. and McKay, J.F., "Investigation of Organic Products from the Thermal Treatment of Green River Oil Shale with Methanol and Water," Am. Chem. Soc. Div. Fuel Chem. Preprints, 29, 26, 1984.

6. Miknis, F.P. and Smith, J.W., "NMR Survey of United States Oil Shales," Org. Geochem., 5, 193, 1984.

7. Cooper, J.E., "Fatty Acids in Recent and Ancient Sediments and Petroleum Reservoir Waters," Nature, 193, 744, 1962.

8. Leddy, D.G., Sandel, V.R., Swartz, G.L., Kenny, D.H., Gulick, W.M. and El Khadem, H.S., "Chemical Composition of Antrim Shales in the Michigan Basin," Report, FE-2346-89, NTIS, 1980.

9. McGowan, C.W. and Diehl, H., "The Oxidation of Green River Oil Shale with Perchloric Acid. Part II - The Analysis of Oxidation Products," Fuel Process. Technol., 10, 195, 1985.

10. Simoneit, B.R., Schnoes, H.K., Haug., P. and Burlingame, A.L., "High-Resolution Mass Spectrometry of Nitrogenous Compounds of the Colorado Green River Formation," Chem. Geol., 7, 123, 1971.

11. Cummins, J.J. and Robinson, W.E., "Normal and Isoprenoid Hydrocarbons Isolated from Oil Shale Bitumen," J. Chem. Data, 9, 304, 1964.

12. Gallegos, E.J., "Identification of New Steranes, Terpanes and Branched Paraffins in Green River Oil Shale by Combined Capillary Gas Chromatography and Mass Spectrometry," Anal. Chem., 43, 1151, 1971.

13. Anderson, P.H. and Parker, P.L., "Fatty Acids in Sedimentary Rocks," Carnegie Inst. Wash. Yearbook, 61, 181, 1962.

14. Haug, P., Schnoes, H.K. and Burlingame, A.L., "Isoprenoid and Dicarboxylic Acids Isolated from Colorado Green River Oil Shale," Science, 158, 772, 1967.

15. Lawlor, D.L. and Robinson, W.E., "Fatty Acids in Green River Formation Oil Shale," Am. Chem. Soc. Div. Petrol. Chem. Preprints, 10, 5, 1965.

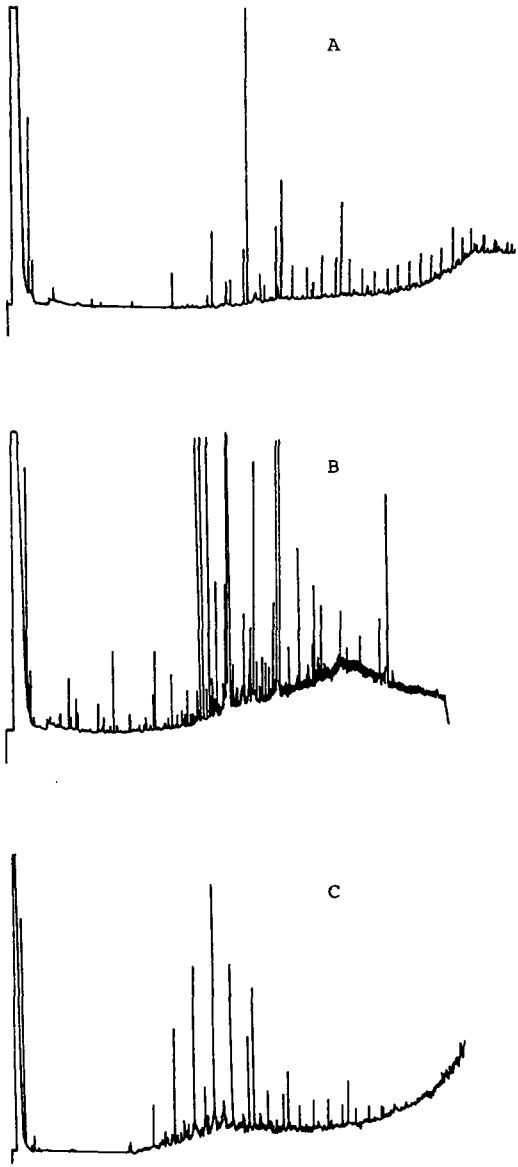

Fig. 1. Gas chromatograms of A. methyl esters of acid fraction B. hexane-soluble fraction C. neutral fraction

SOLVENT SWELLING OF COAL AND COAL MACERALS

David M. Bodily, Jyi-Perng Wann and Vance Kopp

Department of Fuels Engineering, University of Utah
Salt Lake City, Utah 84112

INTRODUCTION

Coal is composed of organic macerals, inorganic mineral matter, pores and pore-filling fluids. Coal normally displays the properties of an amorphous solid, but under appropriate conditions, coal displays both plastic and elastic behavior(1-3). A model to describe the structure of theorganic constituents of bituminous coal is that of a branched/crosslinked polymer. There is no repeating monomer unit, but a unit structure which is covalently bonded by bridging groups. The unit structures are composed of condensed-ring aromatic groups of from 2-4 rings, with molecular weights of around 300. The aromatic rings are substituted by naphthenic rings, alkyl groups and phenolic groups. The bridging groups contain C-O and C-C bonds which are broken during depolymerization and other liquefaction processes. The unit structures cluster in groups which give rise to X-ray diffraction patterns similar to those observed for graphite. The three-dimensional arrangement of the structural units produces a significant micropore volume. In addition to the covalent bridges, polar interactions also serve as crosslinks.

The condensed-ring aromatic units are rigid, but the covalent bridges should provide some flexibility. However, the bonding within clusters of unit structures and the polar interactions reduce the mobility of the coal units and under normal conditions, coal is a glass. At temperatures in the softening range, covalent bonds in the bridging groups are broken and the polar interactions disrupted, providing fluidity to the coal mass. When contacted at room temperature with a suitable polar solvent, coals swell and exhibit plastic and elastic properties(1-3). Under these conditions, the polar bonds are broken and the solvent acts as a plasticizer for the macromolecular network of the coal. Coal passes through a similar state in both carbonization and liquefaction processes, with the solvent being either added vehicle oil or decomposition products of the coal itself. Solvents with Hildebrand solubility parameters in the range of 9-15 $(cal/cm3)1^{/2}$ are effective in swelling coals and, in some cases, inducing spontaneous fracturing(4). The interaction of coal with organic solvents is of interest because of the potential for reacting swollen coals under relatively mild conditions and because of the potential for chemical comminution and chemical cleaning of coals. Changes in the physical properties of coals in the presence of organic solvents are discussed in this paper.

EXPERIMENTAL

Four coals from the Pennsylvania State University Coal Sample Bank and five bituminous coals from Utah were studied. The coals included one anthracite and samples rich in sporinite, resinite, vitrinite and semifusinite. The Utah coals cover a range of response in flotation experiments from easily and quickly floated to difficult to float.

The method of Green et al.(5) was used to measure the swelling properties of the coals. The coal sample was centrifuged in a narrow tube. Solvent is added and the coal is allowed to swell. After

equilibrium is achieved, the coal and solvent are again centrifuged. The increase in height of the column of coal is taken as the volumetric swelling of the coal. This method is reported to be more reliable than gravimetric methods and does not require corrections for pores.

Surface areas of coals and solvent-treated and heat-treated coals were measured by carbon dioxide adsorption at -77°C. The samples were placed in a vacuum system and any solvent was removed. The amount of CO_2 adsorbed was determined as a function of the pressure and the Dubinin-Polanyi equation was used to determine the surface area/pore volume[6]. X-ray diffraction measurements were performed at room temperature after solvents were removed at lower temperatures. The assignment of the 002 peak in the diffraction pattern was by comparison with the diffraction pattern of graphite.

Maceral fractions were prepared by the density gradient centrifugation method of Dyrkacz and Horwitz(7). The coal was ground in a fluid energy mill to an average particle diameter of several microns. The sample was then introduced into a density gradient of CsCl in water in a centrifuge and dispersed throughout the gradient. The gradient is displaced from the centrifuge and fractions of different density collected. The sample is recovered and a plot of yield versus density provides a density distribution for the sample. Fractions of similar density were combined for further measurements.

RESULTS AND DISCUSSION

The swelling ratio for coal PSOC-297 is shown in figure 1 as a function of the solubility parameter of the solvent used to cause swelling. This coal is 63% vitrinite and 16% sporinite. The swelling behavior is similar to that observed for the other bituminous coals, although the magnitude of the swelling varies from sample to sample. The swelling is expected to be a maximum for solvents that have solubility parameters similar to that of the coal. The curve shows two maxima. Pyridine causes the most swelling of the solvents tested. The effectiveness of pyridine in swelling the coals is thought to be due to the disruption of polar bonds between segments of the coal molecule, replacing them with H-bonds between the pyridine and the coal. The second maximum in the swelling curve is observed for THF as the solvent. The solubility parameter for coals is expected to be closer to that for THF than for pyridine. The less polar solvents may be causing the coal to swell within the constraints of the hydrogen bond crosslinks, without appreciably breaking the crosslinks.

The swelling is greatest for coals with higher vitrinite content among coals of similar rank. The coals with high inertinite and exinite contents show reduced swelling, although the behavior with regard to solubility parameter is qualitatively the same. The inertinite fraction is not expected to swell appreciably. The anthracite sample did not show any swelling in any of the solvents. The behavior of the anthracite and the inertinite fractions is expected to be similar. A separated sample of resinite showed high solubility in the more polar solvents. It is not certain whether a true solution was formed or if it was a gel or colloidal suspension. Swelling measurements could not be made on the resinite.

Swelling for the less-polar solvents does not appear to be the equilibrium swelling since the structure is constrained by the crosslinks and the less polar solvents are not strong enough to break these crosslinks. Samples were swollen with mixtures of THF and

cyclohexane. Swelling for the mixtures was intermediate between the values observed for the pure solvents. When the sample was swollen with THF and diluted with cyclohexane, the swelling remained near that of pure THF for dilutions up to 75% cyclohexane. Once the macromolecular network is expanded by the good solvent, the poorer solvent will maintain the swelling. Swelling would be expected to increase the pores in the coal structure. Surface areas for coals and swollen coals are shown in figure 2. The surface area is related to the pore volume. The surface area for non-swollen coals is 230-250 m^2/g. as measured at -77°C, for samples that are heat-treated up to 400°C. If the heat-treated samples are swollen in methanol and the solvent removed at low temperatures, the surface areas increase to 300-350 m^2/g. The polar solvent is more effective than temperature in causing the network to swell. If the sample is swollen and then heated to 100°C the macromolecular network relaxes and the surface area is similar to that for non-swollen coals. The coals with enhanced porosity show the same x-ray diffraction patterns as non-swollen coals. The solvent apparently does not disrupt the stacking of the condensed-ring aromatic structures in the coal.

CONCLUSIONS

The swelling of bituminous coals as a function of solubility parameter of the solvent shows two maxima. One is attributed to the solvation of the macromolecular network by a solvent with solubility parameter similar to the coal, increasing the hydrodynamic volume of the network. The other maxima is attributed to the breaking of hydrogen bonds that serve as crosslinks by polar solvents. The coal appears to be held in a constrained state by the polar crosslinks. Solvents are more effective in breaking these restrains than temperature. Porosity can be increased by swelling coals and removing the solvent at low temperatures. The coal network has considerable flexibility below 100°C, as evidenced by the relaxation of the induced porosity upon thermal treatment. Inertinite macerals and anthracites show little swelling. Vitrinites show high swelling and exinites show enhanced solubility.

ACKNOWLEDGMENTS

This work was supported by the U. S. Department of Energy, contract number DE-FG22-84PC70796.

REFERENCES

1. Green, T., Kovac., J., Brenner, D., and Larson, J., "The Macromolecular Structure of Coals", Coal Science, R. A. Meyers, ed., Academic Press, N. Y., 1982, p. 199.
2. Brenner, D., Fuel, 1985, 64, 167.
3. Larson, J. W., Preprints, Fuel Chem. Div., Am. Chem. Soc., 1985, 30(4), 444.
4. Keller, D. V., Jr., and Smith, C. D., Fuel, 1976, 55, 273.
5. Green, T. K., Kovac, J., and Larsen, J. W., Fuel, 1984, 63, 935.
6. Marsh, M., and Seimeniewska, T., Fuel, 1965, 44, 355.
7. Dyrkacz, G. R., and Horwitz, P., Fuel, 1982, 62, 3.

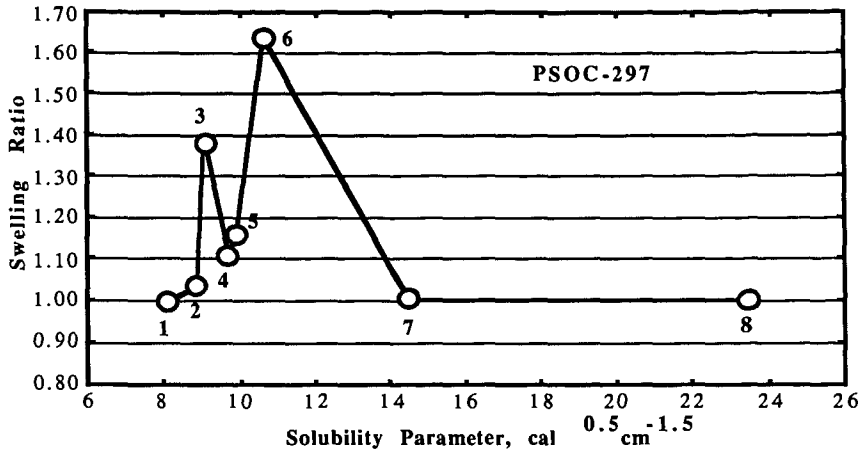

1 Cyclohexane
2 Toluene
3 Tetrahydrofuran
4 Dichloromethane
5 Acetone
6 Pyridine
7 Methanol
8 Water

Figure 1 Coal Swelling in Different Solvents

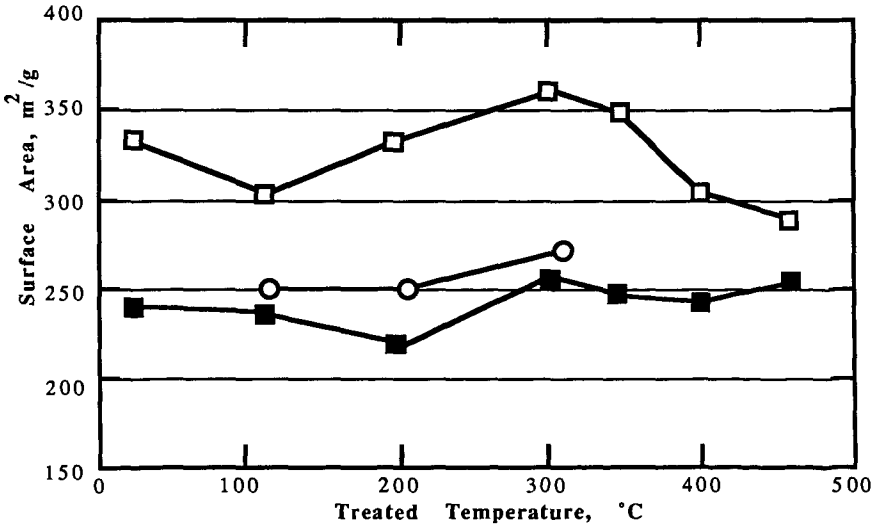

■ Non-swollen □ MeOH-swollen ○ MeOH-preswollen

Figure 2 Surface Area of Treated Coal

Coal Samples Available from the Premium Coal Sample Program

Karl S. Vorres and Stuart K. Janikowski

Chemistry Division, Building 211
Argonne National Laboratory
9700 South Cass Ave.
Argonne, IL 60439

INTRODUCTION

The purpose of the Premium Coal Sample Program (PCSP) is to provide the basic coal science research community with long term supplies of a small number of premium coal samples that can be used as standards for comparison and correlation. The premium coal samples produced from each coal and distributed through this program are chemically and physically as identical as possible, have well characterized chemical and physical properties, and will be stable over long periods of time. Coals are mined, transported, processed into the desired particle and sample sizes, and packaged into environments as free of oxygen as possible. Humidity is also to be controlled to keep the coals as pristine and in as stable a condition as possible.

There had been a feeling that such a program was needed for quite some time (1,2,3). Different authors and workers have expressed a concern over the difficulty in obtaining well selected, collected, prepared and characterized samples over a long period of time. The variation in properties through a coal seam over relatively short distances and the sensitivity of coal samples to oxidation in typical sample containers lead to difficulties in attempts to reproduce the work of other coal researchers. The PCSP is intended to relieve these concerns.

A number of steps are involved in the preparation and distribution of coal samples. These include selection, collection, transportation, preparation or processing (including mixing and packaging), storage, characterization, shipping and data dissemination. Each of these is necessary, and it one of the goals of the PCSP to provide the best quality possible in each of the steps to ultimately provide the best quality samples that can be distributed. Accordingly considerable care and planning has gone into each of the steps mentioned.

SAMPLE SELECTION

The support from the Chemical Sciences Division of the Office of Basic Energy Science will provide for a suite of eight samples. These samples are to provide as broad a range of representation as possible of U. S. coals. The choice of samples has involved a

consideration of the chemical composition, specifically the carbon, hydrogen, sulfur and oxygen contents to obtain representatives of the important ranges available. After consideration of the chemical composition, some specific coals were selected. These include a North Dakota lignite, Wyoming subbituminous, Illinois #6 high volatile bituminous, Upper Freeport medium volatile bituminous, Pocahontas low volatile bituminous, and a Pittsburgh #8 bituminous coal. Other coals are still under consideration for the remaining two samples.

SAMPLE COLLECTION

Sample collection must take place in an active commercial mine to assure the "freshest" coal possible. The collection is done under the supervision of at least one person from the U. S. Geological Survey. Either or both of Drs. Blaine Cecil and Ron Stanton supervise the collection of the whole seam or channel sample. For an underground sample, a continuous miner is used to expose a fresh seam face. When possible the miner is used to isolate a wedge shaped or rectangular block of coal. After roof bolting the floor around the sample is cleared and plastic sheets are put down to collect the actual sample. A three man crew from the Pittsburgh Testing Laboratory at Homer City, Pennsylvania led by David Allen uses hand picks to remove the sample. Coal is placed in double plastic bags in thinner seams (less than 5' thick), tied and taken to the surface for transfer to 55 gallon stainless steel drums. For thicker seams, the drums are taken directly into the mine, and the samples are shoveled carefully into the drums. Typical collection periods are 3-4 hours from the beginning of the collection to arrival of the sample at the surface.

A core sample was taken for the thick subbituminous sample. A contractor was obtained to provide three cores. A 3" core was taken for the USGS log, another 3" core was obtained to provide chunks of coal for long term storage, and a 6" core was used for the coal to be processed. Cores were rinsed and loaded into drums in the same manner as coal from thinner seams.

TRANSPORTATION

A refrigerated semi-truck is used to transport the sample to ANL for processing. The truck loads the empty drums, cylinders of argon used for purging and other necessary equipment at ANL. This load is taken to the mine site. At the mine the plastic bags of coal are dumped into the drums or the full drums are placed on the truck. The drums are purged with 10 or more volumes of argon gas to reduce the oxygen concentration in the drums to below 100 ppm. The load is then taken directly back to ANL for processing. Typically the sample arrives at ANL within 24 hours after being loaded on the truck. The truck temperature is kept at about 42 F en route.

PROCESSING

A unique facility has been built at ANL to process the coal samples. It is a large glove box about 12' tall, 5' wide and 40 feet long. There are 70 pairs of long rubber gloves in the walls of the box to permit manipulation of the sample and equipment during the processing. The oxygen concentration is maintained below 100 ppm during the processing through the use of a catalytic system to combine hydrogen with impurity oxygen.

At ANL the truck is unloaded and drums are taken to the processing facility with a forklift, weighed and placed in groups of three into an initial airlock. After purging the airlock, the drums are opened, and rolled on casters to a hydraulic drum dumper. The dumper picks the drums up and pours the contents into a crusher. The coal is broken into pieces no larger than 1/2" thick. The crushed coal passes through a chute to a vibrating lift which raises the coal to the top of the box for feeding to a pulverizer. Initially the pulverizer grinds the coal so that the particles pass through a 20 mesh screen. The ground coal is accumulated in a Littleford blender with a 2000 liter capacity. This will hold one ton of coal. After the entire batch has been ground it is then thoroughly mixed in the blender. Special studies were carried out to establish the mixing characteristics with coal samples and set the required duration of mixing. The mixed coal is moved from the blender with a tubular conveyor to either a discharge chute used to fill 5 gallon pails for transfer to the initial airlock for regrinding to pass a 100 mesh screen or to fill 5 gallon borosilicate glass carboys for long term storage. Intermittently portions of the sample are conveyed to an ampoule filler-sealer. Here amber borosilicate vials are filled with either 10 grams of -20 mesh material or 5 grams of -100 mesh material. A hydrogen-oxygen torch is used at stoichiometric flame conditions (controlled with a gas mass flow controller) for the sealing.
In processing,it is planned to prepare 5,000 of the 10 gram ampoules of -20 mesh material and 10,000 of the 5 gram ampoules of -100 mesh material. About 80% of the coal is stored in carboys which can be used later to fill additional ampoules when the supply is depleted.

STORAGE

The ampoules and carboys are kept in a separate storage room at about 72 F. This room is usually dark.

CHARACTERIZATION

The samples are characterized for three purposes. The first purpose is homogeneity determination. Initially, samples taken during the filling of the pails, carboys and ampoules are placed in holders for irradiation in the University of Illinois TRIGA reactor. The disintegration rates of induced Na, K and As are measured for bituminous coals, while the Na, As, La and Sc were used for the subbituminous coal due to the limited amount of K. The rates are compared for the different samples to establish the

homogeneity of the samples. The second purpose for characterization is the establishment of the analytical qualities of the coal. Samples are then analyzed in an interlaboratory program that is ongoing. Information on the program is available from the Program Manager. Additioal participation is possible. Standard ASTM methods or known variations of these are used. The analyses include the ultimate (C,H,N,S), proximate (volatile matter, fixed carbon, ash and moisture), calorific or Btu values, sulfur forms, major and minor elements in the ash, and equilibrium moisture. Maceral analysis and vitrinite reflectance are also carried out. For bituminous coals the free swelling index and Gieseler plasticity are also determined. The third type of analysis is used to establish the stability of the samples. The Gieseler plasticity is used as a sensitive indicator of oxidation for the bituminous samples. This test is done for the initial coals and is repeated periodically to establish the constancy of the values. For non-bituminous coals other techniques are being used and developed. The slurry pH is used to establish the oxidation which results in conversion of pyrite to sulfate.

AVAILABLE COAL SAMPLES

1. The first sample is an Upper Freeport sample collected near Homer City Pennsylvania in January 1985. This is a medium volatile bituminous coal from a 4' thick seam at the point of collection. The sample characterization is continuing. The preliminary values are: (as received basis)

carbon:	74-75%
hydrogen:	4-5%
total sulfur:	2-3%
ash:	12-13
moisture	1-2%

These samples are available in 5 grams of -100 mesh or 10 grams of -20 mesh material.

2. The second sample, a subbituminous coal from the Wyodak seam, was collected about six miles northeast of Gillette, Wyoming in October, 1985. The seam is about 120' thick at the point of collection. In this case the sample for processing consisted of a 6" core through the entire seam. The preliminary analysis of the sample on an as-received basis is:

carbon:	63-64%
hydrogen:	4-5%
sulfur:	0.4-0.6%
moisture:	28-30%
ash:	6-7%

Due to the high moisture content of this sample, it is being offered only in -20 mesh size, in 5 and 10 gram ampoules.

3. The third sample is a high volatile bituminous coal, from the Illinois #6 or Herrin seam, and was collected about 60 miles southeast of St. Louis in December, 1985. The 55 gallon drums

used for transporting the samples were taken into the mine since the seam thickness was about 7'. The preliminary analytical values on this coal (on an as-received basis) are:

carbon:	61-62%
hydrogen:	4-5%
sulfur:	4-5%
ash:	15-16
moisture:	9-10

This material is being offered in 5 grams of -100 mesh and 10 grams of -20 mesh coal.

4. The fourth coal is a Pittsburgh #8 seam sample from about 60 miles south and west of Pittsburgh, Pennsylvania. This was collected in March, 1986. The seam was about 6' thick at the collection point. The sample drums were taken into the mine to facilitate the loading and purging of the drums on the surface. This sample is being offered in ampoules of 5 grams of -100 mesh and 10 grams of -20 mesh material. The preliminary analytical data for the as-received samples were not available at the time of the writing.

SAMPLE AVAILABILITY

Samples are available to researchers upon completion of an order form. These forms are available from the Program Manager, Dr. Karl S. Vorres, at the address given in the heading, or by calling (312) 972-7374, or FTS 972-7374. The order forms accompany the periodic Product Announcements. These announcements briefly describe the sample in terms of its source and type of coal. When available, initial analytical data is included. Individuals may request that they be placed on the mailing list to receive these announcements by writing the Program Manager, indicating their address, telephone number and research interests. Upon receipt of the order and payment in the Assistant Controller's office, the orders are transmitted to the Program Manager for packing and shipping. A nominal replacement charge, currently $1.60 per gram, is made for the samples. An additional charge is made for foreign shipment to defray the added shipping charges. Samples are normally sent by United Parcel Service. Samples are shipped in specially designed corrugated cardboard cartons with foam padding above and below the ampoules, and an air space around the outside of them.

Samples are available in reasonable quantities. The Program Manager reserves the right to limit quantities in order to provide a continuing supply to all workers in the field over a decade or more.

USERS ADVISORY COMMITTEE

A Users Advisory Committee serves to provide a range of comments and suggestions on the Program to maximize its value to the users community. The individuals come from a range of backgrounds to

permit a variety of input on the many aspects of the sequence of events from the sample selection through distribution. The initial Committee included: Drs. Blaine Cecil of the U. S. Geological Survey, Marvin Poutsma of Oak Ridge National Laboratory, Ronald Pugmire of the University of Utah, William Spackman of Pennsylvania State University, Irving Wender of the University of Pittsburgh, Randall Winans and John Young of Argonne National Laboratory. The committee does rotate after a period of time. Newcomers to the group are: John Larsen of Lehigh University and Leon Stock of the University of Chicago. The Program Manager is deeply appreciative of the counsel and suggestions given by this group.

CURRENT RESEARCH

A wide range of programs is making use of the samples. Some examples include: new methods for direct determination of oxygen and organic sulfur in the coal matter, new methods of characterization using inverse chromatography, solvent swelling studies, reactions of organic sulfur species in the coal. A number of proposals to different funding agencies have specified that the investigators were planning to use these samples in their work.

ACKNOWLEDGMENTS

The authors gratefully acknowledge the support of the U. S. Department of Energy, Chemical Sciences Division of the Office of Basic Energy Science. In addition the assistance of many individuals who have contributed to the design and construction of the processing facility and the ongoing operations is appreciated. Joseph Gregar contributed to the design and development of the long term storage in glass carboys. Allan Youngs has helped with solutions to many of the mechanical problems that have occurred in the course of operation. F. Gale Teats carried out much of the construction of the processing facility. Peter Lindahl of the Analytical Chemistry Laboratory has coordinated the analytical effort. Many additional individuals have given time and energy in different aspects of the program and each one merits an expression of appreciation, but space will not permit a complete listing.

REFERENCES

1. R. C. Neavel, in "Coal Structure", Ed. M.L. Gorbaty and K. Ouichi, Adv. in Chem. Ser. 192, Am. Chem. Soc. (1981) p.1, from ACS/CSJ Chemical Congress, Honolulu, 1979.

2. I. Wender, International Energy Agency Working Party on Coal Technology, Luxembourg, (1979).

3. "Coal Sample Bank Workshop" report, GRI and USDOE, Atlanta (1981).